Transect NOG-01B[1]

Expedition 325 Scientists[2]

Chapter contents

Introduction

During Integrated Ocean Drilling Program (IODP) Expedition 325, cores were recovered from 10 holes (4 sites) at Noggin Pass, comprising transect NOG-01B (Holes M0052A–M0058A) (Fig. F1), with an average transect recovery of 42.57% of the drilled length. Water depths ranged from 42.27 to 167.14 m (lowest astronomical tide) and were taken from tidally corrected EM300 multibeam bathymetry data. Existing data sets were evaluated prior to arrival at each site, and drilling targets and their respective coordinates were chosen from within the agreed area approved by the IODP Environmental Protection and Safety Panel.

Hole M0052A

Operations

Transit to transect NOG-01B and waiting on weather

The *Greatship Maya* departed transect RIB-02A Site 3 (Hole M0051A) at 1645 h on 23 March 2010 and arrived at transect NOG-01B at 0910 h on 24 March.

Site 6, Hole M0052A

After going onto dynamic positioning at 0910 h, the vessel moved slowly onto station at Site 6 (Hole M0052A), completing the maneuver at 1120 h. Following an assessment of weather conditions at 1145 h, the vessel moved 500 m seaward of M0052A to wait on weather in deeper water. Operations continued to wait on weather on 25 March.

At 0655 h on 26 March the supply boat *Acheron* arrived alongside. Because of high winds and sea swell, it was not safe to conduct a boat-to-boat transfer of equipment. At 0745 h both vessels departed NOG-01B Site 6 to transit to calmer waters inside Flora Passage, arriving at 1100 h. Following a successful transfer, the *Greatship Maya* departed Flora Passage at 1120 h and arrived back at transect NOG-01B Site 6 at 1645 h, where it continued to wait on weather. At 1900 h permission was given for coring operations to start, and the seabed transponder was deployed at 1930 h. American Petroleum Institute (API) pipe was run between 2045 h and 2250 h, after which a downpipe camera survey was conducted. At 2355 h, the first extended nose corer run commenced (Table T1).

[1] Expedition 325 Scientists, 2011. Transect NOG-01B. *In* Webster, J.M., Yokoyama, Y., Cotterill, C., and the Expedition 325 Scientists, *Proc. IODP,* 325: Tokyo (Integrated Ocean Drilling Program Management International, Inc.). doi:10.2204/iodp.proc.325.106.2011
[2] **Expedition 325 Scientists' addresses.**

doi:10.2204/iodp.proc.325.106.2011

The run was halted after 1.4 m because of a very hard lithology, and the core was recovered. However, on recovery the liner was found to be crushed and the bit damaged. During recovery the API drill string came out of the hole because of vessel heave, and so Hole M0052A was terminated at 1.4 meters below seafloor (mbsf).

Sedimentology and biological assemblages

Hole M0052A consists of one lithostratigraphic unit.

Unit 1: Sections 325-M0052A-1X-1 to 1X-2, 41 cm: muddy *Halimeda* sand

Unit 1, spanning Sections 325-M0052A-1X-1, 0 cm, to 1X-2, 41 cm, consists of unconsolidated muddy lime sand with abundant *Halimeda* segments (Fig. F2). Bioclasts of mollusks, corals, and larger foraminifera are common. *Halimeda* segments are most abundant in interval 325-M0052A-1X-1, 0–31 cm. Well-preserved specimens of *Amphistegina* and *Alveolinella* are common in muddy very coarse sand from interval 325-M0052A-1X-2, 30–35 cm.

The corals are fragments of *Seriatopora, Goniopora, Montipora, Porites,* and Agariciidae (Fig. F3).

Physical properties

A total of 1.30 m of core was recovered from Hole M0052A, which was drilled to 1.40 m drilling depth below seafloor (DSF-A) (92.86% recovery). This equated to one core comprising three recovered sections. Physical property data from this hole are summarized in Table T2.

Density and porosity

In Hole M0052A, whole-core bulk density multisensor core logger (MSCL) measurements taken offshore on Core 325-M0052A-2X range from 1.85 to 2.23 g/cm^3 (Fig. F4). Overall, bulk density values are relatively stable downcore. Two discrete samples obtained from this hole during the Onshore Science Party showed moderately high porosities (47% and 42%), grain densities of 2.78 g/cm^3 for both samples, and bulk densities of 1.95 and 2.04 g/cm^3, respectively (Fig. F5).

P-wave velocity

There are no *P*-wave velocity data for Hole M0052A from either the MSCL or discrete measurements.

Magnetic susceptibility

In Hole M0052A, magnetic susceptibility values obtained by offshore measurement on the MSCL range from 3.16×10^{-5} to 6.06×10^{-5} SI (Fig. F4). Values downcore are relatively consistent.

Electrical resistivity

Whole-core, noncontact resistivity measurements on Hole M0052A cores range from 1.12 to 1.40 Ωm (Fig. F4). Similar to the other measurements, there is no evident downhole trend.

Digital line scans and color reflectance

Cores from Hole M0052A were digitally scanned and, where appropriate, measured for color reflectance. Only 1.3 m was measured for this borehole. Color reflectance in Hole M0052A varies between 44.06% and 66.39% (Fig. F6). The values obtained show higher dispersion in areas of muddy sand with *Halimeda* sp. A zone at 0.7 m CSF-A shows more consistent discrete measurements. These coincide with submassive corals with a relatively homogeneous coloration. The bottommost 10 cm of the measured section corresponds to coarse lime sand, showing higher reflectance values. The values observed for a* are, in general, negative, indicating a dominance of green coloration rather than red. The values for b* are always positive, indicating the presence of the color yellow.

Paleomagnetism

Measurements of low-field and mass-specific magnetic susceptibility (χ) were performed on samples taken from the working half of the recovered core. Positive low susceptibilities occur throughout the core, ranging from 0.03×10^{-8} to 1.13×10^{-8} m^3/kg. The arithmetic mean of the magnetic susceptibility of the core is 0.58×10^{-8} m^3/kg, indicating the presence of paramagnetic and/or ferromagnetic minerals.

Hole M0052B

Operations

Site 6, Hole M0052B

Coring (standard rotary corer) recommenced at 0115 h on 27 March 2010 at the same location as Hole M0052A (Table T1). The first core was recovered at 0200 h. The bit was found to be cracked, and the hole collapsed back to 1 mbsf. Coring continued for another three runs until 0430 h. However, weather conditions and large sea swells caused the bit to bounce on the bottom of the hole, as well as dynamic positioning deviation. At 0430 h the barrel became stuck in the bottom-hole assembly (BHA) and could not be recovered without tripping the API

pipe, so Hole M0052B was terminated at 6.9 mbsf. The barrel was recovered at 0745 h, and the bit was found to be bent and catching on the BHA landing ring.

Hole M0052B

Hole M0052B is divided into two lithostratigraphic units.

Unit 1: Section 325-M0052B-1R-1, 0–17 cm: muddy *Halimeda* sand

The uppermost Unit 1, consisting only of interval 325-M0052B-1R-1, 0–17 cm, is composed of unconsolidated muddy *Halimeda* sand containing common bioclasts of mollusks, larger foraminifera, echinoids, and corals. The muddy, very coarse sand from interval 325-M0052B-1X-1, 10–15 cm, contains well-preserved specimens of *Amphistegina, Alveolinella,* and *Sphaerogypsina*. Coral fragments include *Seriatopora* and encrusting Agariciidae.

Unit 2: Sections 325-M0052B-1R-1, 17 cm, to 3R-1, 5 cm: pebbles of corals, mollusks, and bioclastic packstone

The lowermost Unit 2, spanning Sections 325-M0052B-1R-10, 17 cm, through 3R-1, consists of pebbles of coral, mollusks, and bioclastic packstone associated with coarse to very coarse lime sand (Fig. F7). Some coral clasts are covered with thin encrusting nongeniculate coralline algae. Other bioclasts include *Halimeda* and larger foraminifera.

Larger coral pebbles are mainly submassive to massive fragments of *Isopora, Acropora, Porites,* Agariciidae, and Faviidae. Smaller fragments include *Montipora*(?), *Isopora, Acropora, Porites, Seriatopora,* and Agariciidae.

Physical properties

A total of 0.46 m of core was recovered from Hole M0052B, which was drilled to 6.90 m DSF-A (6.67% recovery). Only one core recovered from Hole M0052B was long enough to be measured on the multisensor core logger (MSCL) (>15 cm). Data from this core are summarized in Table T2.

Density and porosity

In Hole M0052B, whole-core MSCL measurements taken on Core 325-M0052B-1R range from 1.06 to 1.98 g/cm^3 (Fig. F8). No obvious downcore trend in the gamma density data set exists. One core plug was obtained from this hole, with moderately high porosity (48%), grain density of 2.80 g/cm^3, and bulk density of 1.95 g/cm^3 (Fig. F9). The discrete bulk density measurement agrees well with the MSCL bulk density measurement.

P-wave velocity

There are no *P*-wave velocity data for Hole M0052B either from the MSCL or from discrete measurements.

Magnetic susceptibility

In Hole M0052B, magnetic susceptibility values obtained offshore by measurements on the MSCL range from 1.79×10^{-5} to 4.32×10^{-5} SI (Fig. F8). Values tend to decrease downcore.

Electrical resistivity

Whole-core noncontact resistivity measurements on Hole M0052B cores range from 0.96 to 1.49 Ωm (Fig. F8). Similar to the gamma density, no downhole trend is evident.

Digital line scans and color reflectance

Cores from Hole M0052B were digitally scanned and, where appropriate, measured for color reflectance. Color reflectance in Hole M0052B ranges from 51.24% to 69.91% (Fig. F10), although only 40 cm was measured for this hole. The last section of this borehole (Section 325-M0052B-3R-1) was not measured for color reflectance because it was mainly composed of pebbles, corals, mollusks, and bioclastic packstone. The values in the uppermost 17 cm correspond to an interval of muddy *Halmeida* sp. sand.

Chronology

This hole has one calibrated radiocarbon age of 14 calibrated years before present (cal y BP; years before 1950 AD) from Core 325-M0052B-1R (Fig. F11). Limited recovery beneath this 14 cal y BP core indicates that this hole probably only contains material from the last deglaciation.

Hole M0052C

Operations

Site 6, Hole M0052C

At 0815 h on 27 March 2010, API pipe was run in at the same location as for Hole M0052B. Open-hole coring to 6.9 mbsf commenced at 0915 h (Table T1). At 1020 h, the first standard rotary corer core was recovered. On recovering the second core at 1130 h, the bit was found to be missing, and the hole had to be terminated at 8.8 mbsf. Tripping the API pipe began at 1140 h and was completed at 1330 h. The bottom-hole assembly and API standard rotary corer sys-

tems were checked while the *Greatship Maya* moved to a new location at Site 6.

Sedimentology and biological assemblages

Hole M0052C contains a single lithostratigraphic unit.

Unit 1: Section 325-M0052C-1R-CC: coralgal boundstone and grainstone

Unit 1, consisting only of Section 325-M0052C-1R-CC, is composed of fragments of coralgal boundstone and grainstone with bioclasts of corals (including one solitary coral), mollusks, nongeniculate coralline algae, and echinoids (Fig. **F12**).

The only large coral is a finely branched to submassive base of an *Acropora*(?) or *Porites*(?) colony. Fragments include *Acropora, Isopora, Seriatopora, Porites*(?), *Heliopora coerulea,* and a large ahermatypic coral.

Physical properties

A total of 0.10 m of core was recovered from Hole M0052C, which was drilled to a depth of 8.80 m DSF-A (5.26% recovery). There was insufficient recovery from Hole M0052C for multisensor core logger measurements or discrete samples to be taken. As such, the petrophysics data set for the hole is limited to color reflectance spectrophotometry and digital line scanning. This data are summarized in Table **T2.**

Digital line scans and color reflectance

The core from Hole M0052C was digitally scanned and measured for color reflectance. Only two discrete measurements of color reflectance spectrophotometry were taken for Hole M0052C. Their values for L* were 73.61% and 75.14%. Because of the small number of values, results were not plotted for this borehole. This section is mainly composed of granules and pebbles of corals.

Chronology

This hole has one calibrated radiocarbon age of 17 cal y BP from Core 325-M0052C-1R (Fig. **F13**). Limited recovery beneath this 17 cal y BP core indicates that this hole probably only contains material from the last deglaciation.

Hole M0053A

Operations

Site 6, Hole M0053A

API pipe started being run in Hole M0053A at 1400 h on 27 March 2010 with the intent to use the HQ coring system. Operations halted between 1510 and 1530 h to make repairs to the elevator. Between 1725 and 1800 h, operations stopped because of a squall passing through the area. Between 1800 and 1900 h, the dies on the roughneck were checked prior to running the bumper sub and lowering the seabed template to ~10 m below the sea surface. At 2010 h, the API string was lowered to the seabed and the bumper sub heave was monitored. The heave was not sufficient, possibly because of soft sediment, so a 3 m pup was added. The bumper sub appeared to compensate, and at 2130 h the seabed template was lowered to the seabed. However, at 2210 h, the bumper sub stopped compensating. At 2300 h, the decision was taken to abandon HQ coring and return to API pipe.

The seabed template was recovered between 2300 and 0030 h on 28 March and the bumper sub between 0030 and 0110 h. Additional API pipe was run between 0110 and 0120 h. The first extended nose corer core was recovered at 0210 h (Table **T1**) (all future runs, with the exception of Run 26, used the standard rotary corer core barrel). Between 0520 and 0550 h on 28 March, operations stopped while the latch head assembly was changed, and between 1330 and 1350 h, coring operations again stopped because of heavy rain obscuring the driller's view of the derrick. Coring then continued for another 17 runs until the hole was terminated at 0250 h on 29 March at 37.3 mbsf, with an average recovery of 32.7%.

At 0300 h on 29 March, the API pipe was tripped to just above the seabed, and a downpipe camera survey was conducted. This operation was completed by 0335 h, with the camera being left in the pipe for the vessel move 66 m to the next site. The seabed transponder was recovered at 0355 h, and the vessel began the move to Site 7 (Hole M0054A) at 0410 h.

Sedimentology and biological assemblages

Hole M0053A is divided into 10 lithostratigraphic units.

Unit 1, interval 325-M0053A-1X-1, 0–13 cm: unconsolidated muddy *Halimeda* sand

The uppermost Unit 1, consisting only of the uppermost interval 325-M0053A-1X-1, 0–13 cm, is composed of unconsolidated muddy *Halimeda* sand (Fig. **F14**). Bioclasts include corals, mollusks, larger foraminifera, and encrusting foraminifera (including *Homotrema rubrum*). Some bioclasts have brown or black staining.

The only large coral is a long *Pocillopora* branch. Fragments include *Seriatopora, Pocillopora, Montipora*(?), *Tubipora musica,* and *Heliopora coerulea.*

Unit 2: interval 325-M0053A-1X-1, 13–106 cm: coralgal boundstone with *Halimeda*

Unit 2, spanning interval 325-M0053A-1X-1, 13–106 cm, consists of coralgal boundstone associated with *Halimeda* sand (Fig. F15). The boundstone is broken into angular to subangular lithoclasts up to pebble size. Massive corals are dominant. Nongeniculate coralline algae exist only as thin encrusting forms. Spaces around boundstone clasts are filled with *Halimeda* sand with bioclasts of corals, mollusks, and larger foraminifera. Some bioclasts are stained black. Well-preserved specimens of *Amphistegina, Alveolinella, Heterostegina,* and Soritinae are common in muddy gravels from interval 325-M0053A-1X-1, 60–65 cm.

Larger corals are submassive to massive *Montipora*(?), *Goniopora*(?), *Porites,* Faviidae, and *Tubipora musica*.

Unit 3: Sections 325-M0053A-1X-CC through 2R-CC: lime sand and granules

Unit 3, spanning Sections 325-M0053A-1X-CC through 2R-CC, consists of lime sand and granules, probably produced by drilling disturbance. The sand and granules appear to have originated in the coralgal boundstones above (Unit 2) or below (Unit 4) this unit. Bioclasts of corals, mollusks, and *Halimeda* are present.

All corals are small fragments of *Seriatopora, Porites, Isopora,* Acroporidae, and Agariciidae.

Unit 4: Sections 325-M0053A-3R-CC through 10R-CC: coralgal boundstone

Unit 4, spanning Sections 325-M0053A-3R-CC through 10R-CC, is a coralgal boundstone consisting of corals with thin to thick crusts of nongeniculate coralline algae (Figs. F16, F17). Bioclasts of mollusks and *Halimeda* are present. Corals are bioeroded, with borings and constructional voids partly filled with unconsolidated silt-sized to fine-grained lime sand.

Corals are dominated by massive *Isopora* (Fig. F18) and medium-thickness branching (possibly corymbose?) *Acropora,* Faviidae (possibly *Leptoria*(?)) (Fig. F19), and some *Seriatopora*. Associated corals include *Pocillopora,* encrusting *Montipora, Porites*(?), Faviidae, Fungiidae, and *Tubipora musica*. Fragments include *Isopora, Seriatopora, Pocillopora, Montipora*(?), *Porites*(?), *Tubipora musica,* and Acroporidae.

Unit 5: Sections 325-M0053A-11R-1 through 17R-1: coralgal-microbialite boundstone

Unit 5, spanning Sections 325-M0053A-11R-1 to 17R-1, 21 cm, consists mainly of microbialites. Corals are covered by thin to thick nongeniculate coralline algal crusts which are, in turn, encrusted by microbialites (Fig. F20). Nongeniculate coralline algae volumetrically fill less space than microbialites and corals. Microbialites have laminated fabrics, and depressions in the microbialites are filled with bioclastic packstone rich in *Halimeda* segments (Figs. F21, F22). Some corals are bioeroded. Borings and constructional voids in the microbialite are occasionally filled with unconsolidated very fine sand-sized internal sediment.

Dominant corals in the abundant and diverse coral assemblage are massive *Isopora* and medium-thickness branching (possibly corymbose?) *Acropora*. The main associated corals are *Montipora,* fine branching and corymbose *Acropora,* Pocilloporidae, Faviidae, and *Tubipora musica*. Fragments include *Acropora, Seriatopora, Montipora, Porites,* Faviidae, and *Tubipora musica*.

Unit 6: Sections 325-M0053A-17R-CC through 21R-1: microbialite boundstone

Unit 6, spanning Sections 325-M0053A-17R-CC through 21R-1, is dominated by microbialite (Fig. F23) in which corals and nongeniculate coralline algae are much less common than in the previous coralgal-microbialite boundstone (Unit 5). Some microbiolite pieces have depressions filled with bioclastic packstone containing *Halimeda* segments (Figs. F24, F25). Some constructional voids are filled with unconsolidated very fine sand-sized internal sediment.

Corals are less abundant than in the overlying Unit 5. Most are branching *Acropora, Porites, Montipora*(?), *Seriatopora,* massive *Platygyra* (Fig. F26), and Agariciidae. The main associated corals are *Acropora, Seriatopora,* submassive *Cyphastrea,* and *Tubipora musica*. Fragments include *Acropora, Porites*(?), *Montipora*(?), and *Tubipora musica*.

Unit 7: Sections 325-M0053A-21R-CC through 23R-CC: coralgal-microbialite boundstone

Unit 7, spanning Sections 325-M0053A-21R-CC through 23R-CC, consists of pebble-sized or smaller angular to subangular lithoclasts of coralgal-microbialite boundstone with coarse lime sand. Bioclasts (mostly mollusks and corals) are rare in the sand and likely to be derived from the boundstone.

The only large coral is a submassive *Montipora*. Other corals are fragments of *Porites*(?), branching *Acropora, Cyphastrea, Pavona,* and *Porites* or *Montipora*.

Unit 8: Sections 325-M0053A-24R-CC through 25R-CC: unconsolidated sand and granules

Unit 8, spanning Sections 325-M0053A-24R-CC through 25R-CC, consists of unconsolidated sand and granules. Bioclasts include corals, nongeniculate coralline algae (branching species), *Halimeda,* larger foraminifera, and echinoids. Lithoclasts of gray bioclastic packstone are present. Occasional well-preserved or fragmented specimens of *Amphistegina* are present in muddy coarse sands from interval 325-M0053A-24R-CC, 6–11 cm.

The only corals are small fragments, including branching *Seriatopora, Acropora,* and *Tubipora musica,* and pieces of *Montipora* or *Porites*.

Unit 9: Sections 325-M0053A-26X-CC through 29R-CC: packstone and lime sand

Unit 9, spanning Sections 325-M0053A-26X-CC to 29R-CC consists of unconsolidated lime sands with variously sized bioclasts. Intervals 325-M0053A-26X-CC through 27R-CC, 1–33 cm, are composed of consolidated bioclastic packstone and unconsolidated lime sand (Figs. **F27, F28**). The packstone consists of bioclasts of *Halimeda* and mollusks, but most bioclasts are too small to be identified. The lower part of Unit 9 (interval 325-M0053A-27R-CC, 33 cm, to Section 29R-CC, 2 cm), consists of unconsolidated lime sand with gravel-sized bioclasts of corals, *Halimeda,* and less abundant larger foraminifera and mollusks. Some coral branches are covered with thin encrusting nongeniculate coralline algae. Occasional well-preserved or fragmented specimens of *Amphistegina* are present in gravelly coarse-grained sands from interval 325-M0053A-27R-1, 40–45 cm.

Small coral fragments are restricted to Sections 325-M0053A-26X-CC and 27R-1, as are fine-branching *Acropora* and Pocilloporidae, with a few pieces of *Montipora* or *Porites*.

Unit 10: Sections 325-M0053A-30R-1 through 33R-CC: dark gray sand with corals

The lowermost Unit 10, spanning Sections 325-M0053A-30R-1 through 33R-CC, consists of coarse to very coarse lime sand with coral clasts and larger foraminifera (Fig. **F29**). The lime sand is partly lithified in interval 325-M0053A-31R-10, 1–6 cm, where grayish lithoclasts may be derived from older limestones with gray to black staining. Large *Operculina* tests occur in interval 325-M0053A-33R-1, 0–5 cm. Medium to coarse sands from interval 325-M0053A-30R-1, 15–20 cm, contain abundant abraded or fragmented specimens of *Baculogypsina, Calcarina, Amphistegina,* and *Operculina*. Fragmented specimens of *Operculina,* Elphidiidae, *Amphistegina,* and *Baculogypsina* are common in medium to coarse sands from interval 325-M0053A-32R-1, 20–25 cm. Fragmented specimens of *Operculina, Amphistegina, Alveolinella,* and *Baculogypsina* are common in gravelly medium to coarse sands from interval 325-M0053A-33R-CC, 5–10 cm.

The only large coral is a massive *Galaxea* in Core 325-M0053A-31R (Fig. **F30**). Fragments include *Seriatopora,* foliaceous Pectiniidae(?), and an ahermatypic coral.

Physical properties

Hole M0053A was cored to a total depth (TD) of 37.30 m DSF-A, of which 12.18 m was successfully recovered (32.65% recovery). Physical property measurements taken on this core are summarized in Table **T2.**

Density and porosity

Multisensor core logger bulk density varies from 1.01 to 2.34 g/cm^3 in cores from Hole M0053A (Fig. **F31**). Cores recovered from this hole have an average length of 0.34 m and are frequently biscuited or rubbly, making it difficult to comment on downhole trends. The only exception to this is Section 325-M0053A-1R-1, which shows an increase in bulk density downsection. Eighteen discrete samples were taken from this hole for moisture and density measurements (Fig. **F32**).

Grain density varies between 2.72 and 2.80 g/cm^3, and bulk density varies between 1.94 and 2.38 g/cm^3 (Fig. **F32**). Results for porosity and bulk density are difficult to compare with lithology. There is principally coralgal and coralgal-microbialite boundstone between 4 and 23 m CSF-A, with porosity varying between 21% and 48%. The three discrete samples taken between 25 m CSF-A and TD have high porosity (lime sand zone with a porosity ranging from 36% to 47%).

P-wave velocity

P-wave velocity measurements taken on whole cores offshore yielded data in the uppermost 1 m and bottommost 7 m of the hole. Values range from 1525 to 1830 m/s (Fig. **F31**). As with other holes, those values close to the velocity of seawater should be treated with caution because data quality may have been compromised by poor core quality. The data set is patchy, and it is therefore impossible to comment on trends. However, four discrete samples were measured using the *P*-wave logger. Values from these dominantly microbialite boundstone samples range from 3434 to 3973 m/s (mean values for resaturated

samples) (Fig. F33). A plot of moisture and density bulk density versus discrete *P*-wave velocity indicates that velocity increases with increasing sample density (Fig. F33B).

Magnetic susceptibility

The range of magnetic susceptibility values for Hole M0053A is -1.64×10^{-5} to 69.26×10^{-5} SI (Fig. F31). Magnetic susceptibility is elevated, compared to the rest of the hole, in an interval from ~16 to 22 m CSF-A, with values in the range of 5×10^{-5} to 20×10^{-5} SI. This interval roughly corresponds to the presence of an a interval of microbialite boundstone. There is also a magnetic susceptibility peak at 5.31 m CSF-A (69.26×10^{-5} SI).

Electrical resistivity

Noncontact electrical resistivity measured on whole cores in Hole M0053A is variable, ranging from 0.52 to 31.28 Ωm (Fig. F31). Similar to the other multisensor core logger measurements, it is difficult to assess whether any genuine downhole trends occur in this hole because of the sporadic occurrence of data (a consequence of recovery and core length).

Digital line scans and color reflectance

Cores from Hole M0053A were digitally scanned and, where appropriate, cores were measured for color reflectance. Hole M0053A, in general, yielded highly dispersed values in each section with some variations in the range of reflectance values with hole depth (Fig. F34). Color reflectance in Hole M0053A varies between 35.96% and 79.95% for L*. The presence of heterogeneous material in this hole makes it difficult to relate the color reflectance measurements to the sediment without analyzing each measurement individually. The dispersion of the reflectance measurements in the uppermost 1 m of the hole is due to variable composition in this area of lime sand mud, boundstone, and lime pebbles. The range of color reflectance in this top part of the hole covers a wide range from 35.96% to 69.24%. The presence of a massive coral and a coralgal boundstone at ~3 m CSF-A creates a less dispersed pattern for the reflectance measurements (L*). From 4 to 23 m CSF-A, the alternation of heterogeneous lithologies within the coralgal, coralgal-microbialite, and microbialite boundstone units creates a highly scattered data set. A slightly negative downhole trend is also observed. A grainstone unit at 26.6 m CSF-A gives a consistent measurement of color reflectance parameters followed by more dispersed values due to the presence of coarse to very coarse lime sand. At 28 m CSF-A, a section of dark gray coarse lime sand gives a consistent measurement for L*. From 28 m CSF-A to TD, this dark gray coarse lime sand and a massive *Cyphastea* sp. present high dispersion in the reflectance values. No large variations in color indexes are evident. Values of a* are low but mainly positive (red color), and values of b* are always positive (yellow color). The a*/b* ratio indicates a variation in trend between the uppermost (0–25 m CSF-A) and lower (25–37 m CSF-A) parts of the hole.

Thermal conductivity

For Hole M0053A, three measurement points were taken, giving thermal conductivity values ranging from 0.94 to 1.15 W/(m·K) (Fig. F35).

Paleomagnetism

Measurements of low-field and mass-specific magnetic susceptibility (χ) were performed on samples taken from the working half of the recovered core (Fig. F36). Positive susceptibilities range from 0.01×10^{-8} to 14.69×10^{-8} m^3/kg with an arithmetic mean of 3.61×10^{-8} m^3/kg, indicating the presence of paramagnetic and/or ferromagnetic minerals. Higher values of magnetic susceptibility are concentrated largely in the stratigraphic interval between 13 and ~22 mbsf. In addition, negative susceptibilities concentrated in two main intervals (0–9 mbsf and 23 mbsf to TD) (diamagnetic) were recorded with an arithmetic mean of -0.46×10^{-8} m^3/kg.

Chronology

Two calibrated radiocarbon ages (17 cal y BP, Core 325-M0053A-3R; 20 cal y BP, Core 9R) (Fig. F37) and one U-Th age (24 cal y BP, Core 25R) (see Table T10 in the "Methods" chapter) are consistent with their stratigraphic positions. The U-Th age is only slightly affected by corrections for initial ^{230}Th (the seawater correction makes the age 0.4 k.y. younger). This hole recovered material from the Last Glacial Maximum, as well as the early deglacial. This hole is noteworthy in that it appears to have substantial recovery from the Last Glacial Maximum, with Cores 325-M0053A-10R through 25R being bracketed by 20 and 24 cal y BP ages.

Hole M0054A

Operations

Site 7, Hole M0054A

The *Greatship Maya* was on station over Hole M0054A at 0425 h on 29 March 2010, and the seabed transponder was deployed. The downpipe camera survey began at 0440 h but took until 0530 h to

complete, as an additional API pipe had to be run in, requiring recovery and redeployment of the camera system. Time was needed to repair hydraulic fluid leaks on the roughneck and to conduct maintenance on the main power pack. After lowering the seabed template, seabed was tagged at 1515 h, followed by washing down to set the API pipe in the hole. HQ coring commenced at 1600 h and continued until 0425 h on 30 March (Table T1).

The hole was terminated at 0425 h at a depth of 18.72 mbsf after three consecutive runs recovered no material. It was considered necessary to recover the bottom-hole assembly to deck, where it was discovered that 60 cm of cored material had become wedged in the bottom-hole assembly and was preventing the barrel from latching. The average recovery for Hole M0054A was 23.98%.

Sedimentology and biological assemblages

Hole M0054A is divided into three lithostratigraphic units.

Unit 1: Sections 325-M0054A-1R-1 to 2R-1, 6 cm: modern reef pebbles

The uppermost Unit 1, spanning Sections 325-M0054A-1R-1 to 2R-1, 6 cm, consists of fragments of corals, mollusks, and branching species of nongeniculate coralline algae. Some coral clasts are encrusted by thin nongeniculate coralline algae. Coral fragments include *Acropora, Stylophora, Platygyra, Montipora,* and *Porites*.

Unit 2: Sections 325-M0054A-2R-1, 6 cm, through 3R-1: coralgal boundstone

Unit 2, spanning Sections 325-M0054A-2R-1, 6 cm, through 3R-1, consists of coralgal boundstone. Corals are dominated by branching forms, and the tips of some coral branches have thick crusts of with nongeniculate coralline algae (Fig. F38). Unconsolidated fine lime sand with bioclasts partly to fully fills constructional voids.

Corals are dominated by fine branching *Seriatopora* (Fig. F38) and fine branching (corymbose?) *Acropora*. Associated corals are *Tubipora musica* and massive *Favia* and *Galaxea fascicularis* (Fig. F39). Fragments include foliaceous *Montipora,* branching *Acropora* and *Stylophora,* massive *Porites,* solitary Fungiidae, and *Tubipora musica*.

Unit 3: Section 325-M0054A-4R-1: coralgal-microbialite boundstone

The lowermost Unit 3, consisting only of Section 325-M0054A-4R-1, is composed of coralgal-microbialite boundstone (Fig. F40). Corals are covered with nongeniculate coralline algae, which in turn are encrusted with microbialites. Microbialites have laminated and, rarely, thrombolitic fabrics.

The dominant coral is fine branching *Seriatopora* (Fig. F40) with associated branching *Acropora* and encrusting *Porites*(?) or *Montipora*(?).

Physical properties

Hole M0054A was cored to a total depth of 18.72 m DSF-A, of which 2.23 m was successfully recovered (11.91% recovery). Table T2 summarizes physical property data for this hole.

Density and porosity

Multisensor core logger (MSCL) bulk density in Hole M0054B varies from 1.01 to 2.22 g/cm^3 (Fig. F41). The cores recovered that were sufficiently long (>15 cm) to be logged on the MSCL were composed of rubble, and as such, it is likely that bulk density data underestimates the actual values of the core material. Two discrete samples were available for measurement from Hole M0054A (Fig. F42). Bulk densities for these samples are 2.22 and 2.42 g/cm^3. The corresponding porosities are 35% and 20%, and grain densities were 2.85 and 2.76 g/cm^3, respectively. As expected, bulk densities given by discrete samples are higher than values from core logging.

P-wave velocity

As a result of the quality of recovered cores for Hole M0054A, *P*-wave velocity MSCL data for whole cores are not available (Fig. F41). However, two discrete samples were taken and measured, giving values of 2994 and 3890 m/s (mean resaturated values) (Fig. F43). These are appropriate values for well-lithified porous formations such as these microbialite boundstone samples. The small data set makes it difficult to comment on trends.

Magnetic susceptibility

Magnetic susceptibility measurements for Hole M0054A vary from 0.21 × 10^{-5} to 43.95 × 10^{-5} SI, with no obvious downhole trend (Fig. F41). The maximum magnetic susceptibility was reached at 11.12 m CSF-A.

Electrical resistivity

Noncontact resistivity measured on whole cores ranges from 0.93 to 66.18 Ωm (Fig. F41). Overall, resistivity decreases with depth in Hole M0054A. However, owing to the quality of the core measured, it would be wise to treat this data set with caution.

Digital line scans and color reflectance

Cores from Hole M0054A were digitally scanned, and, where appropriate, cores were measured for color reflectance. Color reflectance in Hole M0054A varies from 39.63% to 77.13% for L* (Fig. F44). Approximately 4.5 m (from ~11 to 15.5 m CSF-A) of sediment was measured for Hole M0054A. The scattered nature of color reflectance values in these cores is due to the presence of variable lithologies within the same section (e.g., fragments of mollusks and corals, pebbles, and coralgal boundstone). The last section of this borehole corresponds to a coralgal-microbialite boundstone unit. This lithostratigraphic unit shows different colorations, and in general, as observed in previous boreholes, it shows a lack of consistency between measurements in the same section. No trends were detected in the color indexes a* and b* or in the a*/b* ratio. Values of a* were low but mainly positive (red coloration), and values of b* were always positive (yellow color).

Thermal conductivity

One thermal conductivity value of 1.055 W/(m·K) was measured for Hole M0054A at 27.6 mbsf.

Paleomagnetism

Measurements of low-field and mass-specific magnetic susceptibility (χ) were performed on all samples taken from the working half of the recovered core (Fig. F45). Positive low susceptibilities occur, with an arithmetic mean of 5.26×10^{-8} m^3/kg. Core susceptibilities range from 1.56×10^{-8} to 12.73×10^{-8} m^3/kg, indicating the presence of paramagnetic and/or ferromagnetic minerals. Higher values in magnetic susceptibility are mainly concentrated in the stratigraphic interval below ~13 mbsf to the base of the core. Two negative susceptibilities at 9.42 and 12.99 mbsf have values of -2.81×10^{-8} and -0.06×10^{-8} m^3/kg.

Hole M0054B

Operations

Site 7, Hole M0054B

Operations in Hole M0054B commenced at 0545 h on 30 March 2010 following recovery of the blocked bottom-hole assembly (BHA) that led to the termination of Hole M0054A. The HQ pipe was run down the API string, tagging the bottom of the borehole at 0830 h. The first core was recovered at 0915 h and consisted of wash material from the caving of Hole M0054A (Table T1). Coring then continued until 1910 h, when Core 325-M0054B-12R was recovered and the total depth of 33.2 mbsf was achieved. The average recovery for Hole M0054B was 29.63%

Following recovery of this core, the drill floor was prepared for wireline logging operations. Through-pipe gamma logging started at 2330 h and was completed at 0145 h on 31 March. The HQ string was tripped to swap the BHA with a shoe to allow the open-hole logging sondes to be run. At 0315 h, a hydraulic fluid leak occurred, which delayed the tripping of the HQ string. At 0520 h, tripping recommenced, and the HQ BHA was recovered to deck at 0645 h. Following removal of the crossover sub from the top drive, half an API pipe was run in and the crossover reattached. At 0815 h, the HQ string was run back into the hole, and flushed with mud and water. At 1530 h, the HQ string was put into heave compensation. At 1600 h, the conductivity sonde was run, followed by the acoustic borehole image (1745 h), optical borehole image (1900 h), spectral gamma (2145 h), sonic (2330 h), magnetic susceptibility (0110 h on 1 April), Idronaut (0155 h) and caliper (0240 h) sondes. By 0335 h, all wireline tools were recovered to the deck and the logging rooster box was demobilized.

At 0530 h, tripping of the HQ string commenced and continued until 0800 h, followed by tripping of the HQ pipe to just above the seabed to allow deployment of the downpipe camera for posthole survey. Tripping was interrupted by a further hydraulic fluid leak on the iron roughneck from 0840 until 0855 h, when tripping recommenced. By 0920 h, the API pipe was positioned just above the seafloor, and the seabed template was lifted to 7 m above the seafloor to allow the camera survey to commence. At 0940 h, the camera was deployed. It is thought that the camera was caught on the steps inside the bumper sub, blowing the bulb and making it impossible to complete the survey.

The camera was recovered to deck by 1000 h. The remaining API pipe was tripped until the bumper sub was level with the drill floor for inspection by 1120 h. By 1140 h, the seabed frame had been lifted to 20 meters below sea level (mbsl) and the seabed transponder recovered to allow transit to the next hole. At 1200 h, the vessel commenced transit to Hole M0055A.

Sedimentology and biological assemblages

Hole M0054B is divided into four lithostratigraphic units.

Unit 1: Sections 325-M0054B-1W-CC through 8R-2: microbialite boundstone

The lowermost Unit 1, spanning Sections 325-M0054B-1W-CC through 8R-1, consists of microbialite boundstone (Fig. F46) containing relatively low proportions of coral. Coralline algae occur as thick crusts over the corals and as thinner foliose plants (Fig. F47). Microbialites are usually dark colored and laminated (Fig. F48). Some reach several centimeters in thickness, grow in several phases (Fig. F49), and develop microdome shapes. Microbialite is structureless at contacts with coral and coralline algae. *Halimeda*-rich internal sediment is trapped in microbialites or accumulated as packstone (Fig. F50) within the boundstone. Digitate growths may occur on the upper surfaces of microbialite crusts. All components of the boundstone are bioeroded by bivalves and sponges (Fig. F51).

The dominant corals are encrusting, platy, or submassive *Montipora* (Fig. F46) and *Porites* (Fig. F52), although their relative proportions cannot be estimated because they are often indistinguishable in small exposures. Associated corals are massive *Isopora,* fine-branching *Acropora, Stylophora,* Pocilloporidae, *Tubipora musica* (Fig. F53), and (in Section 325-M0054B-8R-2) submassive to massive Faviidae, including *Cyphastrea* (Fig. F54).

Unit 2: interval 325-M0054B-9R-1, 0–69 cm: lime sand with *Halimeda*

Unit 2, consisting of interval 325-M0054B-9R-1, 0–69 cm, is composed of medium to coarse lime sand and pebbles rich in *Halimeda,* plus mollusk, coral, and coralgal fragments. Although some downhole contamination may have occurred, the scarcity of fragments of overlying facies suggests that the lime sand is an original uncontaminated deposit. Well-preserved specimens of *Amphsitegina* are present but rare in very coarse sand from interval 325-M0054B-9R-1, 45–50 cm.

Two large corals, a massive *Porites* with black growth bands (Fig. F55) and a branching (corymbose) *Acropora* (Fig. F56) are present near the top of the interval. Fragments include *Acropora, Seriatopora,* and *Tubipora musica*.

Unit 3: Sections 325-M0054B-9R-1, 69 cm, through 10R-1: rudstone

Unit 3, spanning Sections 325-M0054B-9R-1, 69 cm, through 10R-1, consists mainly of dark gray rudstone (Fig. F57). The major components are *Halimeda,* gastropods, bivalves, larger foraminifera, coral fragments, and coral coated by coralline algae.

A fragment of boundstone containing medium-thickness branching *Acropora* forms the top of the unit. Other corals include branching *Acropora,* massive *Porites,* and *Seriatopora* fragments.

Unit 4: Sections 325-M0054B-11R-1 through 12R-1: lime sand with larger foraminifera

The lowermost Unit 4, spanning Sections 325-M0054B-11R-1 through 12R-1, consists of medium to coarse lime sand and pebbles rich in fragments of larger foraminifera, *Halimeda,* mollusks, coral, and bryozoans. The sand is dark colored because of the presence of black grains. The scarcity of fragments from the overlying Unit 3 suggests this lime sand represents an original uncontaminated deposit. Medium to coarse sands from interval 325-M0054B-12R-1, 10–15 cm, commonly include fragmented specimens of *Calcarina, Operculina,* and *Amphistegina*.

There are few recognizable corals apart from occasional fragments of Acroporidae and Pocilloporidae (including *Seriatopora*) and a small piece of the fragmenting fungiid *Diaseris contorta*.

Physical properties

Hole M0054B was cored to a total depth (TD) of 33.20 m DSF-A, of which 8.25 m was successfully recovered (29.63% recovery). Petrophysical data from these cores are summarized in Table T2.

Density and porosity

Multisensor core logger (MSCL) bulk density varies from 1.02 to 2.37 g/cm^3 in cores from Hole M0054B (Fig. F58). The cores are characterized by biscuited and rubbly sections, which compromise the quality of the whole-core MSCL measurements. This quality is reflected in fluctuating bulk density values. Measurements for moisture and density were taken on eight discrete samples between 15 and 31 m CSF-A in Hole M0054B (Fig. F59). Porosity increases with depth from 25% to 49%, as the lithologies change downhole from a microbialite boundstone to lime pebbles to lime sand to a rudstone unit at the base of the measured interval. Grain density varies between 2.74 and 2.82 g/cm^3, whereas bulk density for the samples falls within the range of 1.91 to 2.34 g/cm^3. Discrete bulk density measurements display good agreement with the higher MSCL bulk density values.

P-wave velocity

Successful *P*-wave velocity MSCL measurements are limited to the bottommost two cores in Hole

M0054B. Values range from 1502 to 1678 m/s (Fig. F58). The proximity of these values to the velocity of seawater (1500 m/s) suggests that core quality issues (see "Physical properties" in the "Methods" chapter) may have compromised the data quality. Four core plugs were taken from Hole M0054B and measured with the *P*-wave logger. Data for these samples range from 3538 to 4093 m/s (mean resaturated values). This fits well with the samples being composed mainly of microbialite boundstone (Fig. F60A). In discrete samples measured from Hole M0054B, no clear correlation between *P*-wave velocity and bulk density exists (Fig. F60B).

Magnetic susceptibility

Hole M0054B magnetic susceptibility values range from -1.09×10^{-5} to 22.91×10^{-5} SI (Fig. F58). The lower end of this range dominates in the bottom third of the hole (from ~21 m CSF-A to TD). From ~15 to 21 m CSF-A, a zone of higher magnetic susceptibility exhibits obvious variation downhole, but no evidence for a systematic trend exists. This relative high coincides with the microbialite boundstone unit.

Electrical resistivity

Hole M0054B noncontact resistivity measurements fall between 0.56 and 25.28 Ωm (Fig. F58). The highest resistivity values are encountered from 15 to 22 m CSF-A. The downhole trend is very similar to that encountered in the magnetic susceptibility data set, with higher values in the interval from 15 to 21 m CSF-A and lower values below 21 m CSF-A.

Digital line scans and color reflectance

All cores from Hole M0054B were digitally scanned, and, where appropriate, cores were measured for color reflectance. The dispersed trend obtained for color reflectance measurements in Hole M0054B is consistent with the dispersion in Hole M0054A. This consistency is in keeping with the close proximity of these two holes. Hole M0054B has higher recovery than Hole M0054A. However, only a small region of the cores overlap and can be compared. Color reflectance in Hole M0054B varies between 40.12% and 79.36% for L* (Fig. F61). The composition of Hole M0054B from 11 to 20 m CSF-A is mainly a microbialite boundstone unit that is coincident with a relatively similar composition (i.e., coralgal microbialite boundstone) in Hole M0054A below 14 m CSF-A. As with Hole M0054A, measurements taken in this unit show a highly dispersed pattern (40.12% to 79.36% for L*). Values of a* and b* for microbialite are always positive. At 24.3 m CSF-A, the presence of a rudstone unit is coincident with a narrowing of the range of L* (54.81%–62.09%). Values from 27.24 m CSF-A to TD are dispersed because of the presence of medium to coarse pebbles. This bottom of the borehole shows mainly negative a* values.

Paleomagnetism

Measurements of low-field and mass-specific magnetic susceptibility (χ) were performed on samples taken from the working half of the recovered core (Fig. F62). Positive susceptibilities were recorded in samples throughout much of the core, ranging from 0.01×10^{-8} to 15.25×10^{-8} m^3/kg. The arithmetic mean of the positive measurements from the core is 4.71×10^{-8} m^3/kg, indicating the presence of paramagnetic and/or ferromagnetic minerals. Higher values in magnetic susceptibility are mainly concentrated in the stratigraphic interval from the top of the core to 21.71 mbsf. Susceptibility measurements of the core from 21 mbsf to TD show a negative (diamagnetic) portion ranging from -0.04×10^{-8} to -0.36×10^{-8} m^3/kg with an arithmetic mean of -0.23×10^{-8} m^3/kg.

Chronology

Two calibrated radiocarbon ages (13 cal y BP, Core 325-M0054B-1W; 18 cal y BP, Core 3R) (Fig. F63) and one U-Th age (20 cal y BP, Core 4R) (see Table T10 in the "Methods" chapter) are consistent with their stratigraphic positions. The U-Th age is unaffected by corrections of initial ^{230}Th. This hole recovered material from the Last Glacial Maximum interval, as well as the early deglacial. This hole has a substantial amount of recovery from the Last Glacial Maximum interval and potentially older Pleistocene because there are eight cores below Core 325-M0054B-4R, which is dated to 20 cal y BP.

Downhole measurements

Hole M0054B represented the first hole where geophysical wireline operations could be performed in a HQ ("logging") hole. It was therefore possible to run the high-priority imaging tools (see "Downhole logging" in the "Methods" chapter for information on the HQ logging set-up and logging tool details). Geophysical wireline logging operations were completed in Hole M0054B to a maximum depth of 33.23 m wireline log matched depth below seafloor (WMSF) with the ANTARES Spectral Natural Gamma Probe (ASGR) sonde. However, open-hole measurements were only made between ~17.52 and 26.02 m WMSF at the largest interval. Recovery in Hole M0054B was just over 29.63%; therefore, as continuous measurements, the downhole logging data can be used to fill in data gaps where there is an absence of core or low

core recovery. Chronologically, the following tools were run:

1. ASGR 256 (through API [conductor pipe] and HQ pipe),
2. Induction Conductivity Probe (DIL45) (conductivity in open hole),
3. Acoustic Borehole Televiewer (ABI40) (acoustic imaging tool)
4. Optical Borehole Televiewer (OBI40) (optical tool),
5. ASGR 256 (Spectral Gamma Ray in open hole),
6. Sonic (communication issues experienced, resulting in 50% data loss),
7. EM51 (magnetic susceptibility in open hole),
8. IDRONAUT (borehole fluid analyzer), and
9. Caliper (CAL3) (borehole diameter).

Hole stability was relatively poor, and consequently there was some hole infilling during wireline operations, reducing the section available for open-hole logging.

Two logging units can be identified in the measured section of Hole M0054B (Fig. **F64**):

1. Unit I (17.52–22.36 m WMSF; Cores 325-M0054B-7R through 9R) is characterized by relatively high total gamma ray (TGR) counts ranging from 33 to 40.5 cps. Conductivity is relatively low in Unit I, ranging between ~40 and 181 mmho, although conductivity gradually increases toward the base of this unit. Magnetic susceptibility wavers around 0.7 mSI throughout the unit, and the caliper shows the borehole to be in gauge throughout. Acoustic images provide virtual hardness visualization, and within Unit I the large majority of the formation appears "hard." The acoustic data provide a virtual borehole view (Fig. **F65**), which clearly shows the quality of the borehole. Optical images also show some of the main cavities in the borehole wall. However, data are of low quality because of the amount of suspended sediment in the borehole fluid. Lithostratigraphic units identified within this logging unit include (coral)algal/microbialite boundstone (Sections 325-M0054B-5R-1 through 8R-1) followed by lime sand (with Halimeda) unit (Section 9R-1), and finally rudstone (Section 9R-1, 69 cm, and below). Clearly the boundstones lend themselves to aiding borehole stability; hence, the borehole is in gauge throughout this logging unit.
2. Unit II (22.36–32.99 m WMSF; Cores 325-M0054B-10R through 12R) is defined by lower TGR counts compared with Unit I, with values ranging from ~14 to 20 cps. Conductivity values are consistently high in the unit, with values consistently around 380 mmho. There is a minor decrease in magnetic susceptibility compared with Unit I, with values around 0.6 mSI. The caliper data indicate that the hole width is greater than the upper unit. Hole diameters ranging from 12 to 16 cm were measured, indicating two main areas of hole washout and probable hole instability at 22.82 and 23.70 m WMSF. Acoustic images clearly show a major change in lithology with a shallowly dipping boundary at 22.36 m WMSF. The borehole wall exhibits lower "hardness" in the acoustic image throughout this logging unit, and the traveltime image shows an elevated number of cavities and borehole wash-outs. Lithostratigraphic units encountered in this logging unit include dark gray rudstone (Section 325-M0054B-10R-1) that passes into lime sand (with large benthic foraminifera) unit.

Lithostratigraphic and logging unit boundaries do not perfectly concur. Coring and wireline logging use different methods of measuring depth, so further work will be needed to integrate wireline logging and core data. However, the current "raw" relationships can be seen on Figure **F66.**

Hole M0055A

Operations

Site 5, Hole M0055A

The *Greatship Maya* was on station at Site 5, Hole M0055A, at 1230 h on 1 April 2010, and the seabed transponder was deployed. Once completed, the seabed template was lowered to ~10 m off the seabed and API pipe was run to just above the seabed. The downpipe camera survey was conducted by 1530 h, and the API pipe tagged the seabed at 1545 h. By 1620 h, the API pipe had been washed down 2 m. The API pipe was then disconnected and set on elevators on the drill floor. Following this, HQ rods were run, tagging the bottom (3.29 mbsf) at 1920 h. HQ coring operations continued until 0555 h on 2 April, when the hole was terminated at 31.29 mbsf with an average recovery of 35% (Table **T1**).

The HQ rods were tripped by 0805 h, and the API pipes were clear of the seabed by 0845 h. The seabed template was lifted above the seabed, and the seabed transponder was recovered. The *Greatship Maya* departed Hole M0055A at 0920 h.

Sedimentology and biological assemblages

Hole M0055A is divided into five lithostratigraphic units.

Unit 1: 325-M0055A-1R-1, 0–40 cm: unconsolidated mud with sand

The uppermost Unit 1, consisting of interval 325-M0055A-1R-1, 0–40 cm, is composed of unconsolidated mud with sand that includes some bioclasts (e.g., *Halimeda,* coral, and small benthic foraminifera). Well-preserved specimens of small benthic foraminifera (e.g., Miliolida and *Cibicidoides*) are common in mud from interval 325-M0055A-1R-1, 10–15 cm. Larger foraminifera and planktonic foraminifera are not present. There are no visible corals.

Unit 2: Sections 325-M0055A-1R-1, 40 cm, through 4R-2: coralgal-microbialite boundstone

Unit 2, spanning Sections 325-M0055A-1R-1, 40 cm, to 4R-2, 150 cm, consists of coralgal-microbialite boundstone (Figs. **F67, F68**) in which corals are covered with nongeniculate coralline algae or microbialite. Most nongeniculate coralline algae are thick encrusting forms. Locally, microbialite has a laminated fabric. Corals are bioeroded, and borings are partly to fully filled with fine sand. Depressions and spaces between coralgal-microbialite frameworks are filled with unconsolidated or consolidated calcareous sand with bioclasts of *Halimeda,* coral, and nongeniculate coralline algae.

A diverse coral assemblage is dominated by several branching *Acropora* species (Figs. **F69, F70**) to the base of Section 325-M0055A-3R-1. The remainder of the interval is dominated by massive *Isopora* (Fig. **F71**), *Porites,* and Faviidae (Fig. **F72**); large *Tubipora musica* (Fig. **F73**); submassive *Goniopora*(?); and branching Pocilloporidae, including *Stylophora*(?) and *Seriatopora*. Visible fragments are scarce but include Acroporidae and *Tubipora musica*.

Unit 3: Section 325-M0055A-5R-1: coralgal boundstone

Unit 3, consisting only of Section 325-M0055A-5R-1, is coralgal boundstone containing corals thickly but irregularly encrusted by nongeniculate coralline algae (Fig. **F74**). Some corals are bioeroded, and the borings are filled with consolidated or unconsolidated sediment. Spaces within the coralgal framework are filled with multigenerational consolidated sediments rich in bioclasts of *Halimeda,* coral, and mollusks (Fig. **F75**).

Dominant corals are massive *Porites* (Fig. **F76**) with some massive Faviidae (Fig. **F77**), branching Acropora, and encrusting *Montipora*(?).

Unit 4: Sections 325-M0055A-5R-2 through 6R-CC: coralgal boundstone with grainstone

Unit 4, spanning Sections 325-M0055A-5R-2, 0 cm, through 6R-CC, is composed entirely of coralgal boundstone in which corals are thickly covered with nongeniculate coralline algae (Fig. **F78**). Nongeniculate coralline algae are volumetrically more important than corals. Coral skeletons may be diagenetically altered into calcite (Fig. **F79**). Cavities are filled with bioclastic grainstone/packstone rich in corals, mollusks, *Halimeda,* and nongeniculate coralline algae fragments. The cavity walls have brown staining throughout the unit (Fig. **F80**). These features indicate possible subaerial exposure and subsequent meteoric diagenesis before deposition of the grainstone/packstone filling.

The few corals present are diagenetically altered and difficult to identify. They include branching Pocilloporidae (Fig. **F81**) and Acroporidae (including possibly corymbose *Acropora*) and an unidentified massive coral.

Unit 5: Sections 325-M0055A-7R-1 through 10R-1: grainstone

The lowermost Unit 5, spanning Sections 325-M0055A-7R-1 through 10R-1, consists mainly of bioclastic grainstone with pale brown staining. The grainstone contains abundant bioclasts of *Halimeda,* mollusks, and corals (Fig. **F82**). The corals are diagenetically altered, possibly indicating subaerial exposure. Recognizable corals include pebbles of Acroporidae at the top of the unit and larger pieces of massive Faviidae and one piece of *Porites* lower in the unit.

Physical properties

Hole M0055A was cored to a total depth of 31.29 m DSF-A, of which 10.00 m was successfully recovered (35% recovery). Petrophysical data are summarized in Table **T2.**

Density and porosity

Bulk density multisensor core logger (MSCL) measurements vary from 1.00 to 2.41 g/cm^3 in cores from Hole M0055A (Fig. **F83**). Despite core recovery being relatively high in comparison with other holes and the fact that core length is also higher (average = 0.76 m), the quality of the bulk density data is not very good because core quality is poor (see **"Physical properties"** in the "Methods" chapter), with many of the cores composed of either biscuited or very

fragmented material. Overall, no evidence for a downhole trend or any intervals where data are significantly different exists. Twelve measurements were taken on discrete samples (Fig. F84), with bulk density data ranging from 1.95 to 2.44 g/cm^3. Figure F84 illustrates the fact that poor core quality leads to an underestimate of bulk density from the MSCL measurement. As in Hole M0053A, coralgal-microbialite and coralgal boundstone units dominate between 4 and 16 m CSF-A, and the porosity varies between 13% and 48%. Grain density for these discrete samples varies between 2.66 and 2.83 g/cm^3.

P-wave velocity

MSCL *P*-wave velocity data are only available for the first core in Hole M0055A, and values range from 1510 to 1647 m/s (Fig. F83). As with many of the other holes, these values are very close to the velocity of seawater, which may be indicative of poor core quality giving an underestimate of the actual core density. Six core plugs were taken from Hole M0055A cores and were measured with the *P*-wave logger. Velocities measured on these samples range from 3591 to 4256 m/s (Fig. F85A). In discrete samples measured from Hole M0055A, *P*-wave velocity exhibits no correlation with bulk density (Fig. F85B).

Magnetic susceptibility

The top of Hole M0055A (Section 325-M0055A-1R-1) can be distinguished from the remainder of the hole by elevated magnetic susceptibility values reaching a maximum of 395.32 × 10^{-5} SI (Fig. F83). This section corresponds to a lithostratigraphic unit composed of unconsolidated mud and sand. From Section 325-M0055A-2R-1 to total depth, values remain in the range of –1 × 10^{-5} to 10 × 10^{-5} SI.

Electrical resistivity

Noncontact resistivity, measured on whole cores, is highly variable and ranges from 0.33 to 77.41 Ωm (Fig. F83). Despite the questionable core quality (see "Physical properties" in the "Methods" chapter), the quality of some of the data is good, with smooth curves being evident in downcore sections. The central portion of this hole yields higher resistivity values than the top and bottom intervals (a similar trend to the magnetic susceptibility data). This central interval, between ~6 and ~17 m CSF-A, corresponds to the dominantly coralgal-microbialite and coralgal boundstone units.

Digital line scans and color reflectance

Cores from Hole M0055A were digitally scanned and, where appropriate, measured for color reflectance. Hole M0055A has a range of reflectance from 46.36% to 83.07% for L* (Fig. F86). In the upper sections (3.30–4.10 m CSF-A), values evolve from lower reflectance to higher reflectance downhole because of changes in lithology from lime mud to sandy mud and then to boundstone pebbles. From 6.30 to 16.71 m CSF-A, values obtained for reflectance are dispersed. This dispersion appears to be related to the presence of a coralgal-microbialite boundstone unit with heterogeneous color. In this area, some measurements indicate a high value for red color (11.14 m CSF-A) coincident with the presence of *Tubipora* sp. The last two sections measured (top depths of 19.5 and 22.5 m CSF-A) correspond to grainstones with *Halimeda* sp.

Paleomagnetism

Measurements of low-field and mass-specific magnetic susceptibility (χ) were performed on samples taken from the working half of the recovered core (Fig. F87). Positive low susceptibilities occur for most of the core, ranging from 0.06 × 10^{-8} to 11.64 × 10^{-8} with an arithmetic mean value of 2.14 × 10^{-8} m^3/kg, indicating the presence of paramagnetic and/or ferromagnetic minerals. In addition, two negative susceptibilities were measured at 16.31 and 28.31 mbsf with values of –0.39 × 10^{-8} and –0.35 × 10^{-8} m^3/kg, respectively.

Chronology

Two calibrated radiocarbon ages (14 cal y BP, Core 325-M0055A-1R; 23 cal y BP, Core 4R) (Fig. F88) and one U-Th age (25 cal y BP, Core 5R) (see Table T10 in the "Methods" chapter) are consistent with their stratigraphic positions. The U-Th age is only slightly affected by corrections for initial ^{230}Th (the seawater correction makes the age 1.0 k.y. younger). This hole recovered material from the Last Glacial Maximum, as well as the early deglacial. This hole has a substantial amount of recovery from the Last Glacial Maximum and potentially older material because there are five cores below Core 325-M0055A-5R, which is dated to 25 cal y BP.

Hole M0056A

Operations

Site 5, Hole M0056A

The *Greatship Maya* transited slowly to Site 5 (Hole M0056A), 66 m away from Hole M0055A, with the seabed template suspended in the water column. At 0935 h on 2 April 2010 the seabed transponder was deployed, and at 0945 h the template was lowered over Hole M0056A to 72 mbsl. Between 0955 and

1035 h, the API pipe and seabed template were lowered to just above the seabed, at which point the downpipe camera survey was conducted. The seabed template was lowered onto the seabed, and the API pipe tagged bottom at 1120 h. The API was then washed in 1.3 m. At 1230 h, the API pipe was broken and the elevators set on the slips prior to running HQ rods.

Coring operations started when the HQ rods tagged bottom at 1415 h and continued until 2100 h, when the HQ crossover and saver sub had to be replaced following failure of a weld. Coring restarted at 2140 h and continued until 0635 h on 3 April, when the hole was terminated at 41.29 mbsf with an average recovery of 30.8% (Table T1). The HQ rods were tripped by 0840 h and the top drive reconnected to the API pipe. The seabed template and API pipe were lifted to ~9 m above the seabed, and a downpipe camera survey was conducted. At 0935 h, the API pipe was tripped back to the bumper sub, and the seabed template was lifted into the moonpool in preparation for transit. At 1040 h, the seabed transponder was recovered, and the *Greatship Maya* departed Site 5 at 1050 h.

Sedimentology and biological assemblages

Hole M0056A is divided into four lithostratigraphic units.

Unit 1: Sections 325-M0056A-1R-1 to 2R-1, 127 cm: coralgal boundstone

The uppermost Unit 1, spanning Sections 325-M0056A-1R-1 to 2R-1, 127 cm, unconformably overlies Unit 2 and is coralgal boundstone composed mainly of corals thickly covered with encrusting nongeniculate coralline algae (Fig. F89). In situ fruticose (shrubby branched) nongeniculate coralline algae occur in interval 325-M0056A-2R-1, 87–94 cm (Fig. F90). The uppermost part (~110 cm) of Unit 1 is stained brown. Cavities with brown-stained walls occur throughout Unit 1 and are partly filled with unconsolidated sand dominated by *Halimeda* segments. Interval 325-M0056A-2R-1, 76–95 cm, contains cavities filled with gravelly internal sediment (Figs. F91, F92).

The upper part of Unit 1 is dominated by abundant encrusting *Montipora* colonies (Fig. F90) and possibly some encrusting *Porites*(?). This pattern transitions into dominance by massive Faviidae (e.g., *Cyphastrea*) (Fig. F93), submassive *Porites,* corymbose(?) *Acropora,* and encrusting *Montipora*(?) lower in the unit (intervals 325-M0056A-1R-2 through 2R-1).

Unit 2: Sections 325-M0056A-2R-1, 127 cm, to 7R-1, 47 cm: packstone with grainstone interlayers

Unit 2, spanning Sections 325-M0056A-2R-1, 127 cm, to 7R-1, 47 cm, unconformably underlies the coralgal boundstone of Unit 1. Unit 2 is packstone composed mainly of bioclasts of coral, *Halimeda,* nongeniculate coralline algae, and mollusks (Fig. F94). Dissolved segments of *Halimeda* create moldic porosity in some places, especially in intervals 325-M0056A-4R-1, 20–60 cm, and 4R-1, 60–65 cm, and Section 7R-1, 47 cm (Fig. F95). Cobble-sized lithoclasts of coralgal boundstone occur in some places, especially interval 325-M0056A-4R-1, 132–140 cm. Grainstone interlayers occur in two places: intervals 325-M0056A-4R-1, 108–141 cm, and 5R-1, 46–55 cm. The packstone in interval 325-M0056A-3R-1, 10–26 cm, has brown staining.

Coral dissolution increases in severity with increasing depth in this unit, and few corals are identifiable, apart from Section 325-M0056A-5R-1, which contains several encrusting to massive *Porites* and Faviidae. Identifiable corals include a few pieces of *Porites, Montipora*(?), Acroporidae, Agariciidae, and Fungiidae.

Unit 3: Sections 325-M0056A-7R-1, 47 cm, to 10R-1, 16 cm: coralgal-microbialite boundstone

Unit 3, spanning Sections 325-M0056A-7R-1, 47 cm, to 10R-1, 16 cm, is composed mainly of coralgal-microbialite boundstone (Fig. F96) in which thick microbialites with laminated fabrics cover corals. The corals also appear to be diagenetically altered (Figs. F97, F98). Nongeniculate coralline algae are a minor component. Depressions in microbialite surfaces are filled with bioclastic packstone containing *Halimeda* segments and molluscan shells (Fig. F99). Dissolution cavities filled by light gray, consolidated silt-sized internal sediment occur throughout Unit 3.

There are almost no corals in the uppermost and lowermost sections of Unit 3. Altered corals in the middle of Unit 3 are mainly encrusting *Porites*(?) or *Montipora*(?), with a few massive Faviidae (Fig. F100) and *Porites*(?).

Unit 4: Sections 325-M0056A-10R-1, 16 cm, through 16R-CC: packstone

The lowermost Unit 4, spanning Sections 325-M0056A-10R-1, 16 cm, to 16R-CC, 7 cm, consist of bioclastic packstone composed mainly of bioclasts rich in *Halimeda* segments (Fig. F101). Corals are

common in Cores 325-M0056A-11R through 13R. Other bioclasts include nongeniculate coralline algae and mollusks. A grainstone interlayer occurs near the base of Hole M0055A in interval 325-M0055A-14R-1, 25–40 cm. Many bioclasts have dissolved, creating moldic porosity (Figs. F101, F102). Dissolution cavities may be filled with consolidated, gray, silt-sized internal sediment (Fig. F103).

Corals are diagenetically altered and vary in identity and abundance. Massive *Porites* and *Galaxea* are common in Sections 325-M0056A-13R-1, 13R-CC, and 15R-CC. Scarce corals in Sections 325-M0056A-11R-1 and 14R-1 are mainly encrusting *Montipora*(?), *Porites,* and Faviidae; other fragments include *Isopora* and Agariciidae.

Physical properties

Hole M0056A was cored to a total depth of 41.29 m DSF-A, of which 12.73 m was successfully recovered (30.83% recovery). Table T2 summarizes the physical property data for this hole.

Density and porosity

Multisensor core logger bulk density in Hole M0056A cores varies from 1.00 to 2.52 g/cm^3 (Fig. F104). Similar to Hole M0055A, gamma density data quality is compromised by the fragmented nature of much of the recovered core, yielding data which often zig-zags down section. As such, it is extremely difficult to identify any downhole patterns. Measurements taken on 10 discrete samples (Fig. F105) indicate a range of porosity from 18% to 42% and variation in grain density from 2.68 to 2.79 g/cm^3. As expected, bulk density from the discrete samples is at the high end of the range given by the multisensor core logger measurements, with values falling between 2.02 to 2.42 g/cm^3.

P-wave velocity

There are no whole-core *P*-wave velocity data available for Hole M0056A. However, three discrete samples were taken from the hole for measurement on the *P*-wave logger. These samples have *P*-wave velocities in the range of 3715 to 4168 m/s (mean resaturated values) (Fig. F106A). These values are appropriate for well-lithified porous formations such as these. With this limited data set, no clear relationship exists between bulk density and velocity (Fig. F106B).

Magnetic susceptibility

Magnetic susceptibility values in Hole M0056A range from -1.22×10^{-5} to 308.18×10^{-5} SI, with the majority of values falling in the range of -1×10^{-5} to 5×10^{-5} SI. Two magnetic susceptibility highs occur at 26.14 m CSF-A (308.18×10^{-5} SI) and 29.22 m CSF-A (36.63×10^{-5} SI) (Fig. F104). Both of these highs occur within the packstone unit. No obvious downhole trends exist.

Electrical resistivity

Hole M0056A appears to identify a series of packages with decreasing resistivity downhole (Fig. F104). The most obvious of these packages can be observed in Cores 325-M0056A-1R, 4R, 8R, and 9R. Overall, electrical resistivity measurements range from 0.58 to 38.20 Ωm, and no obvious downhole trend exists.

Digital line scans and color reflectance

Cores from Hole M0056A were digitally scanned, and, where appropriate, cores were measured for color reflectance. Color reflectance in Hole M0056A shows no obvious trend with depth. Values are highly scattered for all sections. L* varies between 51.4% and 80.83% (Fig. F107). The first two sections measured (0–7 m CSF-A) are the ones with largest range of reflectance values. They correspond to the coralgal boundstone unit and bioclastic packstone interval. The range for L* narrows downsection, with values constrained between 60% and 80%, with the exception of two outliers with lower reflectance. The heterogeneity of the recovered core, in terms of both lithology and degree of fragmentation, makes it impossible to identify any pattern without a more detailed examination of the data. No relevant trends were found in the color indexes (a* and b*).

Paleomagnetism

Measurements of low-field and mass-specific magnetic susceptibility (χ) were performed on samples taken from the working half of the recovered core (Fig. F108). Positive susceptibilities were recorded in the majority of samples, ranging from 0.01×10^{-8} to 3.68×10^{-8}, with an arithmetic mean of 0.91×10^{-8} m^3/kg, indicating the presence of paramagnetic and/or ferromagnetic minerals. In addition, nine negative susceptibilities (diamagnetic) were measured, present in two main intervals from 0 to 6 mbsf and 26 to 37 mbsf, ranging from -0.13×10^{-8} to -1.92×10^{-8}, with an arithmetic mean of -0.67×10^{-8} m^3/kg.

Chronology

Two calibrated radiocarbon ages (34 cal y BP, Core 325-M0056A-2R; 39 cal y BP, Core 5R) (Fig. F109) and one U-Th age (84 cal y BP, Core 13R) (see Table T10 in the "Methods" chapter) are consistent with their stratigraphic positions. The U-Th age is only slightly affected by corrections for initial ^{230}Th (the seawater correction makes the age 0.5 k.y. younger).

Therefore, this hole recovered material older than the Last Glacial Maximum from marine isotope Stages 5a and 3. It is likely that this hole may also have recovered material from marine isotope Stage 4 between Cores 325-M0056A-5R and 13R.

Hole M0057A

Operations

Site 2, Hole M0057A

At 1125 h, the seabed transponder was deployed, and by 1140 h the *Greatship Maya* had settled on station at Site 2, Hole M0057A. The transponder on the seabed template was changed prior to lowering the template to ~35 m below the sea surface. At 1135 h, API pipe was run to just above the seabed, and a downpipe camera survey was conducted. Further API pipe was then run, tagging the seabed at 1400 h. The API pipe was then set on the elevators and disconnected from the top drive at 1430 h in preparation for running HQ pipe. The seabed was tagged with the HQ pipe at 1520 h, and coring operations began (Table **T1**).

After Run 3 the hole was caving, possibly because of the string swabbing the hole. Coring operations continued after hole conditioning until 2325 h, when there was a twist off between the crossover sub and the top HQ pipe. Between 2325 h on 3 April and 0100 h on 4 April, the crossover sub was tripped out for repairs and the core barrel was recovered. On the next run, damage to the threads on two HQ rods was sustained while running a new rod in, and two rods were tripped to replace them. Coring then continued until 0440 h, when it was noted that mud was leaking from the repaired crossover sub/HQ pipe joint. To enable safe working on the joint, three HQ rods were tripped out. During the repair period, the hole collapsed. Open-hole drilling and flushing back down to the previously reached depth of 32.38 mbsf ran from 0610 to 0710 h, at which point coring operations restarted.

Operations were temporarily halted between 1040 and 1100 h because of a fire alarm caused by an oil leak dripping onto the exhaust pipe in the engine room. Operations then continued until 1230 h, when the hole was terminated at 41.78 mbsf with an average hole recovery of 45.5%. Between 1240 and 1520 h the HQ rods were tripped, followed by the API pipe. A problem with the iron roughneck delayed lifting of the seabed template, which was completed at 1730 h. The seabed transponder was recovered by 1750 h, and the template and drill floor were secured in preparation for transit to Site 8, Hole M0058A.

Hole M0057A

Hole M0057A is divided into six lithostratigraphic units.

Unit 1: Sections 325-M0057A-1R-1 to 7R-1, 35 cm: coralgal boundstone

The uppermost Unit 1, spanning Sections 325-M0057A-1R-1 to 7R-1, 35 cm, consists of coralgal boundstone with minor amounts of microbialite. The proportion of coral is relatively high (Fig. **F110**). Coralline algae occur mainly as thick crusts on top of corals (Fig. **F111**) and are intergrown with vermetids and encrusting foraminifera. In the uppermost Section 325-M0057A-1R-1, coralline algae occur occasionally as frameworks of thin foliose plants (Fig. **F112**). Microbialites are poorly developed and occur mainly as thin crusts with rough to digitate surfaces on coralline algae and corals (Fig. **F113**). Some bioclasts are trapped in the microbialite. Lithified internal sediments of *Halimeda*-rich packstone to rudstone have accumulated in pockets. All boundstone components are bioeroded by bivalves and sponges and contain worm tubes. Soft muddy sediment fills some bivalve borings. Larger foraminifera are absent from the sandy gravels in intervals 325-M0057A-5R-1, 70–75 cm, and 6R-1, 130–135 cm.

Encrusting to submassive *Porites* or *Montipora* (often indistinguishable) are common in the upper part of Unit 1. Massive colonies dominate in Section 325-M0057A-2R-1 (Fig. **F114**) and are increasingly abundant lower in Unit 1. Massive *Isopora* and branching *Acropora* dominate the middle of the unit (Figs. **F111, F115**). Associated corals are branching *Acropora* and *Pocillopora,* Faviidae (including *Favia*), and Poritidae (including *Goniopora*). Fragments include *Isopora,* branching *Acropora, Seriatopora, Stylophora*(?), Agariciidae, Faviidae, Pocilloporidae, and one piece that may be an octocoral(?) (Fig. **F116**).

Unit 2: Sections 325-M0057A-7R-1, 35 cm, through 8R-1: grainstone to rudstone (whitish)

Unit 2, spanning Sections 325-M0057A-7R-1, 35 cm, through 8R-1, consists of whitish grainstone to rudstone rich in *Halimeda,* with coral, mollusk, and coralline algal fragments (Fig. **F117**). Coral fragments, up to 14 cm in size, are encrusted locally by coralline algae (Fig. **F118**). The rudstone includes intraclasts of a *Halimeda* rudstone with a greenish muddy matrix that is pitted by bivalve borings infilled with fine-grained internal sediment. Moldic porosity, created by partial dissolution of originally aragonitic components, and geopetal infilling of larger voids occurs throughout the unit. Brown-stained, irregular sur-

faces within the grainstone suggest subaerial exposure and diagenetic alteration (Fig. F119).

Most corals are tilted or upside down and probably not in growth position. They include massive *Platygyra* (Fig. F120), massive *Montastrea curta* (Fig. F118), a solitary Fungiidae (Fig. F121), and some small coral fragments that include branching *Acropora*.

Unit 3: Sections 325-M0057A-10R-1 through 12R-CC: coralgal boundstone with rudstone/grainstone (yellowish)

Unit 3, spanning Sections 325-M0057A-10R-1 through 12R-CC, consists mainly of yellowish coralgal boundstone alternating with yellowish rudstone. Corals are covered by thick crusts of coralline algae. No microbialite is visible. Corals, mollusks, and *Halimeda* are the main components of the rudstone, and both corals and coralline algae are intensely bioeroded. Coral skeletons and other originally aragonitic components are extensively dissolved (Fig. F122). Many surfaces in both the boundstone and rudstone have reddish stains, and Section 325-M0057A-10R-1, 48 cm, contains the possible trace of a root (Fig. F123). Interval 325-M0057A-10R-CC, 4–8 cm, contains a spectacular cavity partially filled with small calcitic speleothems.

Although few corals are visible, large corals include massive *Montipora, Symphyllia* (Fig. F124), and *Acropora* associated with branching to submassive *Pocillopora, Acropora, Stylophora*(?), *Montipora, Favia,* and massive *Porites* (Fig. F125). Fragments include *Seriatopora*(?), *Acropora,* and *Isopora*.

Unit 4: Sections 325-M0057A-13R-1 to 14R-2, 50 cm: coralgal boundstone

Unit 4, spanning Sections 325-M0057A-13R-1 to 14R-2, 50 cm, consists mainly of a whitish coralgal boundstone. Thin encrusting corals are intergrown with crusts of coralline algae (Fig. F126) containing local concentrations of vermetid gastropods (Fig. F127). The internal sediment is packstone/grainstone to rudstone with grains composed of corals, mollusks, coralline algae, larger foraminifera, and *Halimeda*. The absence of fragments from overlying units suggests that the lime sand is an original uncontaminated deposit. Extensive partial dissolution of coral and other originally aragonitic components occurs throughout the interval.

Dominant corals are encrusting to massive *Montipora* (Fig. F126), Agariciidae, and possibly some *Porites*. Associated corals include *Cyphastrea* and *Leptoseris*. Fragments include *Acropora, Montipora,* and *Cyphastrea*.

Unit 5: Sections 325-M0057A-14R-2, 50 cm, through 15R-CC: coralgal boundstone (pinkish)

Unit 5, spanning Sections 325-M0057A-14R-2, 50 cm, through 15R-CC, consists of pink-colored coralgal boundstone with internal sediments of packstone to rudstone (Fig. F128). Corals are encrusted by thick coralline algal crusts. Corals, mollusks, and larger foraminifera are main components of the rudstone. Interval 325-M0057A-14R-2, 118–130 cm, contains a concentration of spicules (probably from octocorals). Corals and coralline algae are intensely bioeroded. Sponge borings filled with fine-grained sediments have been exposed by dissolution of the host coral (Fig. F129). Near the top of Unit 5, a brownish calcrete overprints large dissolution cavities in the packstone in interval 325-M0057A-14R-2, 50–85 cm (Fig. F130). Extensive dissolution of corals and other originally aragonitic components is common throughout the unit.

Dominant corals are encrusting to massive Acroporidae (*Acropora* or *Isopora*) (Fig. F129) and Agariciidae (including *Leptoseris*(?) and *Pachyseris*(?)) (Fig. F130).

Unit 6: Sections 325-M0057A-16R-1 through 16R-2: packstone to rudstone (pinkish)

The lowermost Unit 6, spanning Sections 325-M0057A-16R-1 through 16R-2, consists of pinkish packstone to rudstone (Fig. F131) with large coral fragments. The major components are fragments of corals, mollusks, and coralline algae. Interval 325-M0057A-16R-1, 50–64 cm, contains a concentration of spicules. Coral fragments and other major components are intensely bioeroded, and borings are filled with packstone. Coral skeletons and other originally aragonitic components are extensively dissolved. Dissolution surfaces within the packstone and the coral fragments have pinkish stains.

Corals are severely diagenetically altered. The only identifiable corals are encrusting to submassive Agariciidae (probably *Pachyseris*) (Fig. F132) and a single solitary Fungiidae.

Physical properties

Hole M0057A was cored to a total depth of 41.78 m DSF-A, of which 19.00 m was successfully recovered (45.48% recovery). A summary of the physical property data for this hole is given in Table T2.

Density and porosity

In Hole M0057A, gamma density varies from 1.00 to 2.38 g/cm^3 (Fig. F133). As with most other cores in this transect, gamma density data appears erratic, and a broad range of values is measured within any

one core. The reason for these erratic data is that core quality is poor as a result of biscuiting and fragmentation. Consequently, the majority of bulk density data underestimates bulk density at any given point. Discrete moisture and density measurements on 14 samples from Hole M0057A give bulk densities ranging in value from 2.08 to 2.49 g/cm^3 (Fig. F134). Overall, these values are at the high end of the range of multisensor core logger bulk density for this hole. Discrete samples are principally coralgal boundstone and a few rudstone samples, with a porosity varying between 14% and 39%. Grain density is between 2.67 and 2.75 g/cm^3 for all but two of the samples, which have a higher grain density (2.86 and 2.90 g/cm^3).

P-wave velocity

Because of core quality issues, there are no whole-core *P*-wave velocity data available for Hole M0057A. However, 11 discrete samples were taken from across the hole to be measured on the *P*-wave logger. Measurements yielded values ranging from 3022 to 5322 m/s (mean resaturated values) (Fig. F135A). These values are appropriate for well-lithified, porous formations such as these. There is a weak (general) positive linear relationship between bulk density and *P*-wave velocity (Fig. F135B).

Magnetic susceptibility

Hole M0057A has magnetic susceptibility values ranging from –1.27 × 10^{-5} to 27.09 × 10^{-5} SI. Downhole variation is obvious. The most notable feature is an interval of elevated magnetic susceptibility that increases from ~3 × 10^{-5} SI at 18 m CSF-A to 27.09 × 10^{-5} SI at 18.5 m CSF-A before falling quite dramatically to ~0 × 10^{-5} SI at 18.68 m CSF-A (Fig. F133). However, these values do not appear to be coincident with any significant lithostratigraphic features.

Electrical resistivity

Noncontact resistivity measured on whole cores in Hole M0057A is variable, ranging from 0.87 to 28.91 Ωm (Fig. F133). No systematic downhole trend is obvious from this data set, and certain cores (325-M0057A-2R, 3R, 10R, and 11R) clearly give erratic data, probably as a consequence of core quality (see "Physical properties" in the "Methods" chapter).

Digital line scans and color reflectance

Hole M0057A was one of the two boreholes with relatively high recovery for this transect. All cores were digitally scanned and, where appropriate, measured for color reflectance. Reflectance in Hole M0057A ranges from 38.56% to 83.03% with a homogeneous distribution and dispersion of the measurements with depth (Fig. F136). The interval from 0 to 6 m CSF-A presents a large range of values from 40.98% to 79.84% for L. The range of L* values then narrows to between 59.8% and 80.8%. This unit is largely composed of coralgal boundstone. These ranges of dispersion for L* are maintained throughout most of the hole because of the occurrence of corals within the coralgal boundstone The presence of a coralgal boundstone and packstone (to rudstone) unit below 35.4 m CSF-A makes reflectance values a bit higher than observed toward the top of the hole. Values for a* were mainly positive but close to zero, except for two outliers at 24.66 and 24.95 m CSF-A. These outliers are due to the presence of red stains detected in the cores, which are likely the result intense diagenesis of corals at these depths. The borehole exhibits high dispersion of data at all depths in all three parameters of color reflectance (L*, a*, and b*).

Paleomagnetism

Measurements of low-field and mass-specific magnetic susceptibility (χ) were performed on samples taken from the working half of the recovered core (Fig. F137). Positive susceptibilities were recorded in samples from much of the core, ranging from 0.02 × 10^{-8} to 4.00 × 10^{-8} m^3/kg, with an arithmetic mean of 0.95 × 10^{-8} m^3/kg, indicating the presence of paramagnetic and/or ferromagnetic minerals. In addition, 22 negative susceptibilities (diamagnetic) were recorded throughout the hole, ranging from –0.02 × 10^{-8} to –1.78 × 10^{-8}, with an arithmetic mean of –0.50 × 10^{-8} m^3/kg.

Chronology

A calibrated radiocarbon age (12 cal y BP, Core 325-M0057A-5R) (Fig. F138) and one U-Th age (old, Core 15R) (see Table T10 in the "Methods" chapter) are consistent with their stratigraphic positions. The assessment that the U-Th age is "old" is based on the [^{230}Th/^{238}U] being in excess of any possible closed-system scenario. Therefore, this hole recovered material from the middle portion of the deglaciation and may well have recovered material from before the Last Glacial Maximum.

Hole M0058A

Operations

Site 8, Hole M0058A

The *Greatship Maya* reached Site 8 at 1950 h on 4 April 2010, and the seabed transponder was deployed prior to the vessel settling on station over Hole M0058A by 2005 h. Between 2010 and 2240 h,

repairs on the roughneck and roughneck hydraulics were undertaken prior to running API pipe. The first run started at 0220 h on 5 April and coring continued for 15 runs; all runs were made with the extended nose corer with the exception of Run 5, which was made with the standard rotary corer (Table T1). Coring operations were going smoothly until problems with the power packs surging and cutting out caused operations to stop between 1035 to 1245 h and again between 1355 and 1425 h. The hole was terminated after Run 15 at 41.4 mbsf, with an average recovery of 82%.

At 1515 h, the power pack stalled, delaying tripping of the API pipe. All API pipe was on deck by 1845 h, and the drill floor and template were secured and ready for transit by 2105 h. At 2115 h, the *Greatship Maya* came off dynamic positioning, and it departed Site 8 (Hole M0058A) at 2130 h.

Transit to Townsville

The *Greatship Maya* departed the final site of transect NOG-01B at 2130 h on 5 April 2010 and arrived at the port of Townsville, Australia, at 1430 h on 6 April. Demobilization of the vessel and clearances of the containers by AQIS and Customs officials continued until 1130 h on 7 April, when all European Consortium for Ocean Research Drilling (ECORD) Science Operator (ESO) personnel and science party members departed the vessel.

Sedimentology and biological assemblages

Hole M0058A is divided into seven lithostratigraphic units.

Unit 1: Sections 325-M0058A-1X-1, to 3X-1, 141 cm: mud

The uppermost Unit 1, spanning Section 325-M0058A-1X-1 to Core 3X-1, 141 cm, consists of homogeneous green (6/10Y) mud without visible layering or signs of bioturbation (Fig. F139). Planktonic (?) and small benthic foraminifera are common. Sponge spicules are rare. The boundary between Unit 1 and the underlying fine to medium sands of Unit 2 is irregular and may be an erosional surface (Fig. F140). There are no corals in this unit (or in any other unit of Hole M0058A).

Unit 2: Sections 325-M0058A-3X-1, 141 cm, to 4X-1, 107 cm: fine to medium sand with larger foraminifera

Unit 2, spanning Sections 325-M0058A-3X-1,141 cm, to 4X-1, 107 cm, consists of fine to medium sand with abundant larger foraminifera. Planktonic foraminifera are absent. There is no layering and no signs of bioturbation. Interval 325-M0058A-4X-1, 0–10 cm, is an interlayer of mud containing small benthic foraminifera and, rarely, larger foraminifera (*Operculina*). Bioclasts are common in interval 325-M0058A-4X-1, 0–107 cm, and include bryozoans, coralline algae, serpulids, echinoids, *Halimeda,* mollusks, and larger foraminifera. Cemented lithoclasts of fine to medium sand occur in the lower part of Unit 2 (interval 325-M0058A-4X-1, 56–107 cm). One lithoclast is covered with nongeniculate coralline algae and serpulids. There are no corals.

Unit 3: Sections 325-M0058A-4X-1, 107 cm, through 6X-CC: fine to medium sand with granule-sized bioclasts and grainstones

Unit 3, spanning Sections 325-M0058A-4X-1, 107 cm, to 6X-CC, 1 cm, consists of fine to medium sand with granule- to pebble-sized bioclasts and pebble- to cobble-sized lithoclasts of brown grainstone (Fig. F141). Loose bioclasts in the sand include fragments of mollusks, bryozoa, coralline algae, echinoids, larger foraminifera, and serpulids. No planktonic foraminifera are visible. The grainstone is composed of fragments of *Halimeda,* coralline algae, larger foraminifera, and mollusk shells. Moldic voids in the grainstone may indicate partial dissolution of originally aragonitic components. There are no corals.

Unit 4: Sections 325-M0058A-7X-1 to 11X-2, 19 cm: mud

Unit 4, spanning Sections 325-M0058A-7X-1 to 11X-2, 19 cm, consists of homogeneous green (6/5GY-6/10Y-5/Y10) mud (Figs. F142, F143) with no signs of layering or bioturbation. Small benthic foraminifera occur throughout this unit and are very abundant in the uppermost interval 325-M0058A-7X-1, 0–1 cm. Planktonic foraminifera are present in Sections 325-M0058A-7X-3 through 8R-CC. In Section 325-M0058A-8X-2, there are well-preserved gastropod shells in two horizons: Sections 325-M0058A-8X-2, 30 cm, and 325-M0058A-8X-3, 8 cm. There are no corals.

Unit 5: Sections 325-M0058A-11X-2, 19 cm, to 11X-3, 48 cm: bioturbated mud

Unit 5, spanning Sections 325-M0058A-11X-2, 19 cm, to 11X-3, 48 cm, consists of dark green (4/10Y) bioturbated mud (Fig. F144). There is no visible layering. Small benthic foraminifera occur throughout this unit. No planktonic foraminifera are visible. There are no corals.

Unit 6: Sections 325-M0058A-11X-3, 48 cm, to 13X-1, 7 cm: fine to medium sand

Unit 6, spanning Sections 325-M0058A-11X-3, 48 cm, to 13X-1, 7 cm, consists of fine to medium dark green (4/10Y) sand containing bioclasts, with an interlayer of mud in Section 325-M0058A-12X-CC (Fig. F145). Larger foraminifera *Operculina* and small benthic foraminifera are common. Whereas other bioclasts are rare, they include planktonic foraminifera (usually with black-stained tests), mollusks, bryozoans, echinoids, and fragments of packstone. There are no corals.

Unit 7: Sections 325-M0058A-13X-1, 7 cm, through 15X-2: mud

The lowermost Unit 7, spanning Sections 325-M0058A-13X-1, 7 cm, through 15X-2, consists of green (6/10GY) mud. Benthic foraminifera are common throughout this unit. Planktonic foraminifera are rare in Core 325-M0058A-13X and absent from Cores 14X and 15X. Mollusk shells are rare. In the uppermost part of Unit 7, intervals 325-M0058A-13X-1, 7–73 cm, and 13X-1, 121–145 cm, have distinct 1–3 cm diameter burrows filled with fine to medium sand (Fig. F146). There are no corals.

Physical properties

Hole M0058A was cored to a total depth of 41.40 m DSF-A, of which 33.94 m were successfully recovered. This equates to 81.98% recovery, which is the best recovery for the holes in Expedition 325. Petrophysical data are summarized in Table T2.

Density and porosity

Multisensor core logger bulk density varies from 1.60 to 2.32 g/cm^3 in cores from Hole M0058A (Fig. F147). Unlike most other holes, the quality of the gamma density data for Hole M0058A is excellent as a consequence of good core quality (well-filled liners and saturated cores). Overall, bulk density increases downhole in the top 10 m CSF-A, coinciding with the upper lithostratigraphic mud and a lower fine to medium sand unit. Beyond this, bulk density is relatively constant. The corresponding range of bulk densities given by discrete samples is 1.57 to 2.62 g/cm^3, and the two downhole plots are in very close agreement (Fig. F148).

The cores are mainly composed of fine to medium lime muds. Porosity of the discrete samples ranges from very low (6%) to high (68%). The higher porosity values can be attributed to the presence of clays within the samples. Grain density varies between 2.70 and 3.73 g/cm^3.

P-wave velocity

Hole M0058A is the only hole that gives a complete record of *P*-wave velocity from whole-core multisensor core logger measurements (Fig. F147). Data values range from 1504 to 1739 m/s with two intervals identified as having higher *P*-wave velocity: ~5.6–7.2 m CSF-A and ~28.8–32.4 m CSF-A. The relatively low values for *P*-wave velocity are suggestive of underconsolidated material. A total of 35 discrete *P*-wave measurements were taken on samples from Hole M0058A. Many of these yielded poor data as a consequence of the sample being underconsolidated. Samples that gave good *P*-wave signals resulted in velocities ranging from 1508 to 2281 m/s (mean initial value) (Fig. F149A). One outlier value of 3673 m/s (mean resaturated value [not included in the data table]) corresponds to the only lithified sample (brown grainstone) measured in this hole (Sample 325-M0058A-4X-1, 97–99 cm), at 10.56 m CSF-A. In discrete samples from Hole M0058A, *P*-wave velocity plotted against bulk density identifies three groups (Fig. F149B).

Magnetic susceptibility

As already mentioned, Hole M0058A has the best core recovery and core quality of all the holes and, as such, yields some of the best magnetic susceptibility data. Values range from -0.22×10^{-5} to 52.74×10^{-5} SI, with zones of lower magnetic susceptibility giving values as high as ~8×10^{-5} SI (Fig. F147). Three clear zones of elevated magnetic susceptibility exist from ~6.5 to 10 m CSF-A (maximum value = 26.55×10^{-5} SI), ~26 to 32.5 m CSF-A (maximum value = 35.73×10^{-5} SI), and ~35.5 to 36.5 m CSF-A (29.74×10^{-5} SI). Preliminary comparison of this data set with the kappabridge data set (see "Paleomagnetism") suggest that there is very good agreement between the two.

Electrical resistivity

Electrical resistivity values measured on whole cores from Hole M0058A are within the limited range of 0.50 to 1.68 Ωm (Fig. F147), dominantly around 0.7 Ωm. Typically, resistivity values are affected by lithology, pore fluid, and salinity, as well as core liner saturation. However, in this hole there are no clear changes in resistivity coincident with lithostratigraphic unit boundaries. Instead, values are generally constant downhole and the data set is relatively complete (a testament to the good core quality).

Digital line scans and color reflectance

Hole M0058A had the best recovery of all holes cored during Expedition 325. All cores were digitally scanned and, where appropriate, measured for color

reflectance (Fig. F150). From 0 to 6.94 m CSF-A, the homogeneous green mud unit creates a slightly negative downhole trend in reflectance. Results are very consistent with depth until the bottom of this interval, where there is a larger data range owing to the presence of a fine to medium sand layer. An interval of fine to medium sand was measured from 8.75 to 10.23 m CSF-A and shows greater scatter in the reflectance data. Sections from 14.68 m CSF-A to total depth are mainly composed of a green mud unit showing a slight decrease in reflectance to 17.01 m CSF-A, followed by an increase in L* values to ~25.5 m CSF-A, where reflectance decreases again until it reaches a layer of medium fine sand at 28.85 m CSF-A (Fig. F150). This sand unit is easily detectable by higher scatter in the reflectance data set (28.85–31.22 m CSF-A). From 32.54 m CSF-A, another section of green mud unit gives more homogeneous reflectance values. A small sandy mud layer can be identified by the higher dispersion of the measurements, reaching peak reflectance at 35.75 m CSF-A. Another green mud unit from 35.48 to 38.28 m CSF-A shows a slight decrease in reflectance. Data scatter again shows the presence of sand at the bottom of the hole. Some trends observed in the L* data are also identifiable from a* or b* values because of a change in sediment color. A clear example of this correlation is the positive trend in a* from ~25.75 to 30 m CSF-A, which correlates with the medium fine sand layer at this depth. The values of the a*/b* ratio also show a similarity in trends with reflectance values, but the curves are smoother than for L*.

Thermal conductivity

A total of 29 measurements, one per section, were undertaken on full cores from Hole M0058A. Thermal conductivity values range from 0.967 to 1.237 W/(m·K). Variations in thermal conductivity with depth show no trend line (Fig. F151).

Data integration

Good agreement is observed between color reflectance, magnetic susceptibility data obtained with the MSCL, and the paleomagnetic discrete measurements (Fig. F152). These three measurements indicate the presence of potential cycles at the same depths, which are reflected in changes in the magnetic susceptibility or reflectance (L*) of the sediments. Hole M0058A is located at the fore reef slope; hence, changes in the coloration and magnetic susceptibility of the sediment might relate to variations in the contribution of calcium carbonate and terrigenous sediments from the adjacent shelf as sea levels oscillated over the last several glacial–interglacial timescales.

Paleomagnetism

Measurements of low-field or mass-specific magnetic susceptibility (χ) were performed on samples taken from the working half of the recovered core using both 1 cm^3 and standard paleomagnetic box samples (Fig. F153). Positive magnetic susceptibilities occur throughout the core, ranging from 4.50×10^{-8} to 277.78×10^{-8} m^3/kg, with an arithmetic mean value of 38.24×10^{-8} m^3/kg. Figure F153 shows two zones of high susceptibility with respect to the base values. The first zone is located between 8.63 and ~9.35 mbsf and the second between ~27 to 32.60 mbsf, with a maximum value of 277.78×10^{-8} m^3/kg, as mentioned above. These positive susceptibilities indicate the presence of ferromagnetic minerals.

Chronology

This hole has one radiocarbon date from Core 325-M0058A-4X that is older than the limit of the radiocarbon method (Fig. F154). Although this hole may have younger material in Cores 325-M0058A-1X through 4X, the rest of this hole is either older than 50 cal y BP or the material dated comprises reworked carbonate.

Transect NOG-01B summary

Sedimentology and biological assemblages

The uppermost parts of the seven holes in deeper water (Holes M0052A–M0052C, M0053A, M0054A and M0054B, and M0055A) contain mud and muddy sand (Fig. F155). Coralgal and coralgal-microbial boundstone units occur below the muds in these holes, and also below(?) the top of the recovered succession in the two holes in shallower water (Holes M0056A and M0057A). Coralgal boundstones are as thick as 4–15 m and are dominated by corals encrusted by coralline algae. Algal crusts often contain vermetid gastropods and the encrusting foraminifer *Homotrema rubrum*. Coralgal-microbial boundstone units are as thick as 10–16 m and contain thick crusts (as thick as several centimeters) of microbialite, in addition to corals and coralline algae. The main corals in these boundstones are diverse assemblages of branching *Acropora, Seriatopora,* massive *Isopora, Porites, Montipora,* Faviidae, and *Tubipora*.

Unconsolidated sands, as well as consolidated grainstone and rudstone units, lie below the two boundstone units in all but the three holes (M0052A–M0052C) in which drilling did not penetrate below the boundstone. The grainstones/rudstones are 4–13 m thick and composed of shell and skeletal fragments of coral, coralline algae, *Halimeda,* mollusks, and benthic foraminifera.

Although no material was recovered from beneath the grainstone/rudstone unit in Hole M0055A, three holes (M0053A, M0054A, and M0054B) have a lime sand interval below the lower grainstone/rudstone. In these holes, the downcore succession of unconsolidated and/or modern reef sediment, boundstones, grainstones/rudstones, and lime sand resembles the pattern observed along transect HYD-01C.

In contrast, the uppermost grainstone/rudstone units in Holes M0056A and M0057A overlie a long succession that includes boundstone, grainstone/rudstone, and packstone units. Coralgal boundstones, 12 m thick, are the dominant lithologies in Hole M0057A and include a thin interval of packstones in the lowest boundstone interval. In Hole M0056A, 8 m of coralgal-microbial boundstone overlies a 13 m thick succession of grainstones/packstones. No consistent pattern has yet been extracted in the succession of facies in these holes. The major corals observed in the deeper, older boundstones are encrusting submassive to massive *Montipora,* massive *Porites* and Faviidae, and occasional *Galaxea* or Agariciidae.

Three holes (M0055A, M0056A, and M0057A) contain packstone and grainstone lithologies, with calcrete features including brownish staining, undulating dissolution surfaces, and rhizoliths at the top of the uppermost grainstone rudstone unit and as layers separating intervals within the underlying boundstone. Obvious dissolution of constituents, especially originally aragonitic coral particles, has left moldic porosity, neomorphisms, and other dissolution features. These features are interpreted as several phases of emersion and weathering, including paleosol formation, within the recovered deposits.

Hole M0058A is the deepest hole of Expedition 325, beginning at 167 mbsl. Its 41.4 m length consists mainly of unconsolidated green mud with two intercalated units of fine to medium sand and a few grainstone units (Fig. **F147**). The three mud units in Hole M0058A are characterized by a lack of bedding. Small fragments of mollusk shells and small benthic foraminifera are scattered through the mud. Planktonic foraminifera are present only in Sections 325-M0058A-1X-2, 1X-7, 1X-8, 1X-11, and 1X-12, and there are occasional fragments of bryozoan colonies and clypeasteroid burrowing echinoids. Cores 325-M0058A-11X and 13X show clear signs of bioturbation. The upper sand/grainstone unit is at least 2 m thick and consists of fine to medium sand with fragments of well-cemented grainstone, mollusks, bryozoa, coralline algae, echinoids, larger foraminifera, and serpulids. The grainstone consists of shells and fragments of calcareous algae, larger foraminifera, and mollusks. The lower sand unit is ~7 m thick, consists of fine to medium sand, and is less distinct than the upper sand unit.

Table **T3** documents all the larger foraminifera described in this transect in association with hole, run, and depth (below seafloor).

Physical properties

Recovery at transect NOG-01B holes was much greater compared to the other transects visited during Expedition 325, with an average recovery of ~40%. Water depths and borehole depths reached in each hole from this transect are as follows:

Hole M0052A = 97.63 mbsl, 1.40 m DSF-A.
Hole M0052B = 97.63 mbsl, 6.90 m DSF-A.
Hole M0052C = 97.63 mbsl, 8.80 m DSF-A.
Hole M0053A = 97.87 mbsl, 37.30 m DSF-A.
Hole M0054A = 107.23 mbsl, 18.72 m DSF-A.
Hole M0054B = 107.23 mbsl, 33.20 m DSF-A.
Hole M0055A = 87.33 mbsl, 31.29 m DSF-A.
Hole M0056A = 81.22 mbsl, 41.29 m DSF-A.
Hole M0057A = 42.27 mbsl, 41.78 m DSF-A.
Hole M0058A = 167.14 mbsl, 41.40 m DSF-A.

Density and porosity

Bulk density was measured at transect NOG-01B using two methods: (1) gamma ray attenuation on a multisensor core logger (MSCL), which provides an estimate of bulk density from whole cores, and (2) discrete MAD samples measured with a pentapycnometer using 20 mm diameter plugs drilled from the working half of core sections and/or rock fragments, which provide grain density and porosity data. Because of the higher levels of recovery and core quality in this transect, one can have more confidence in the MSCL data. Bulk density values measured on whole cores range from 1 to 2.52 g/cm^3. Bulk densities measured on discrete samples vary between 1.57 and 2.62 g/cm^3. Plug porosity varies between 6% and 68% (Fig. **F156**), whereas grain densities varied between 2.66 and 3.73 g/cm^3. Some grain density values are <2.71 g/cm^3, the density for calcite. This could be due to an anomalous measurement and/or the presence of clays in the plugs. Across the transect, bulk density increases as porosity decreases (Fig. **F157**).

P-wave velocity

A cross-plot of velocity (from discrete samples) versus porosity (from discrete samples) for all sites shows primarily an inverse relationship (Fig. **F158**) between acoustic velocity (*P*-wave) and porosity. However, there is a secondary group of data with extremely high porosity and relatively low *P*-wave velocity related to the lime mud units recovered in

Hole M0058A. MSCL values acquired range from 1502m/s (Hole M0054A) to 1830 m/s (Hole M0053A). In Hole M0058A, because of the high recovery (~82%) and nature of the core, MSCL values and discrete measurements are in accord. For all other shelf edge fossil reef holes, much lower values have been recorded for coralgal and coralgal-microbialite boundstone units compared with discrete measurements on core plugs. Discrete *P*-wave velocity measurements range from 1508 m/s (Hole M0058A) to 5322 m/s (Hole M0057A).

Magnetic susceptibility

Magnetic susceptibility data from transect NOG-01A can be used with more confidence than at the previous transects. Over this transect, magnetic susceptibility ranges from -1.64×10^{-5} SI (Hole M0053A) to 395.32×10^{-5} SI (Hole M0055A). Small variations and trends are clearly visible in Hole M0054B between ~15 and 22 m CSF-A, and an almost continuous record is available for Hole M0058A.

Electrical resistivity

Obtaining reliable resistivity measurements on whole cores was much easier at this transect with improved recovery. As with all other measurements, Hole M0058A exhibits the most continuous and convincing record obtained with the MSCL during Expedition 325. This transect represents the location from where the best resistivity measurements were taken on cores. Over the entire transect, resistivity is variable, with both the lowest (0.33 Ωm) and the highest (77.41 Ωm) values recorded in Hole M0055A. Trends in the data are much more visible at this transect—with some small fluctuations in Hole M0055A.

Color reflectance

In transect NOG-01B, Holes M0052A–M0052C and M0053A were located in similar water depths and can be correlated. The same also applies for Holes M0054A and M0054B. Hole M0058A was located in the fore reef slope area. Boreholes M0052A and M0052B had low recovery, and reflectance measurements were consistent for both of them, exhibiting a similar range of reflectance values. Hole M0052C also had low recovery, and only two measurements (not plotted) of color reflectance were taken for this borehole. Recovery in Hole M0053A was higher (~33%), and the color reflectance values taken in the top few meters are consistent with other boreholes in transect NOG-01B at the same depth (Holes M0052A–M0052C). Recovery for Hole M0054A was low but relates well with values obtained for Hole M0054B, which is the neighboring borehole. Discrete measurements of reflectance values for all transect NOG-01B boreholes are represented in Figure **F159.** Boreholes have been plotted from shallower to deeper water (left to right) using the same depth scale. Reflectance shows consistent trends for holes located at the same water depth, indicating a possible correlation between them.

Paleomagnetism

Transect NOG-01B comprises 10 holes at 5 sites, and materials recovered were predominantly corals and calcareous sediments (with the exception of the mud-dominated fore reef slope Hole M0058A). The materials show mainly positive values of low-field and mass-normalized magnetic susceptibility. The arithmetic mean of these values indicates the presence of paramagnetic and/or ferromagnetic materials.

Most peaks in magnetic susceptibility are located at particular depth intervals. Peaks were observed between ~14 and 22 mbsf for Sites 6 and 7 (Holes M0052A–M0054B), associated with lithologic variations. At Sites 2 and 5 (Holes M0055A–M0057A), peaks were recorded at 2–3, 5, ~10, ~15, and ~18 mbsf. Most variations appear to be related to the occurrence of detrital magnetic materials from terrigenous or windblown volcanic sources. However, this cannot be fully quantified until further research is conducted (e.g., Curie experiments).

Magnetic susceptibility measured at these sites is stronger than at transects HYD-02A and HYD-01C, located further south. It is believed that this is related to the closer proximity of the modern reef systems and therefore a potential source of detrital magnetic materials. However, the Ribbon Reef transect (RIB-02A) shows average magnetic susceptibility values that are even higher than those measured at Noggin Pass (NOG-01B). These values suggest that the source of the magnetic minerals may be located north of the Great Barrier Reef or that the volume of magnetic mineral is directly related to the proximity to the mainland.

Further studies of ferromagnetic material will detect and define the magnetic properties and geomagnetic behavior. Further rock magnetic studies on these layers may provide information on the nature and processes that produced and drove these fluctuations in magnetic susceptibility. Environmental magnetic studies may reinforce the climatic origin of these layers and provide information on the volume, composition, and grain size of the magnetic component retained.

Geochemistry

Interstitial water

A total of 77 interstitial water samples from transect NOG-01B were obtained from Holes M0052A (4), M0053A (13), M0054A (4), and M0058A (56) and analyzed for cations and anions (Table T4). Parameters including pH, alkalinity, and concentrations of ammonium were measured during the offshore phase of the expedition, whereas the major cations and anions were measured during the Onshore Science Party. The geochemical constituents were all determined to be within the normal range for marine sediments. Hole M0058A consisted of fine to coarse sediments, unlike other holes, and therefore continuous interstitial water sampling was achieved.

There was no systematic vertical variation in the pH, alkalinity, and concentrations of chloride and bromide in Hole M0058A (Fig. F160). In contrast, variations in the concentrations of ammonia, magnesium, calcium, strontium, and sulfate were observed. Ammonia and strontium concentrations increased with depth from 0.1 to 2.2 mM and 90 to 451 µM, respectively, whereas opposite trends were observed in the other three parameters; as depth increased, concentrations of magnesium, calcium, and sulfate decreased from 53 to 34, 10 to 7, and 29 to 18 mM, respectively (Fig. F160).

The notable characteristic of interstitial water from Hole M0058A is that two large anomalies occur at 6–10 and 29–36 m CSF-A along the profiles of total iron and manganese concentration (Fig. F160). These anomalies may indicate discrete periods of terrestrial material input to the reef environment during the past. Further investigations are needed to fully understand the cause of these anomalies.

XRD results

The results of the semiquantitative HighScore mineral identification are presented in Tables T5 and T6 and in Figures F161 and F162. The average mineralogy for Hole M0058A is 54% carbonate (28% aragonite, 13% calcite, and 13% Mg calcite, with <1% other carbonates), 20% quartz (with <1% tridymite and cristobalite), 8% feldspars (dominantly albite, but also some alkaline feldspars), 13% clay minerals (dominantly kaolinite, 5.5%, and muscovite, 5%), 2% amphiboles and pyroxenes, and ~1% evaporite minerals, which are dominantly halite.

In the case of feldspar and clay mineral identification, where the major mineral of a group is absent, it is often the case that another mineral of that group is present. For example, albite is near ubiquitous but is not present in some samples. Where it is absent, another feldspar is often present in a similar amount to the nearby samples for albite (e.g., Sample 325-M0058A-2X-1, 8–9 cm) (Table T5). Similar apparent substitutions are observed for clay minerals; where muscovite is absent it is "replaced" by illite or another similar clay, and where kaolinite is absent it is "replaced" by nacrite or another similar clay. It is probable that these apparent substitutions have arisen from misidentification of mineral peaks by the HighScore analysis because of the varying chemical compositions of the minerals causing the position of the peaks to differ from those of the reference database and the "substituted" minerals having similar diffraction spectra. To simplify interpretation of the mineral data and to negate uncertainty arising from inaccurate identification of similar minerals, minerals have been grouped: all carbonates (aragonite, calcite, and Mg calcite are still considered separately), quartz (all SiO_2 polymorphs), all feldspars, muscovite and illite group clays, kaolinite group clays, and amphibole and pyroxene minerals.

Lithologically, Hole M0058A is composed of fine sand-silt units punctuated by two coarse-grained units at 8.7–9.9 mbsf (Sections 325-M0058A-4X-1 through 4X-CC) and 28.9–31.3 mbsf (Sections 11X-3 through 12X-CC; gray bands in Figures F161 and F162). Each of these coarse units lies above sections of no recovery. Here, the fine-grained units are referred to as the upper, middle, and lower fine-grained units and the coarse-grained units as the upper and lower coarse-grained units.

Mineral abundances

Mineral abundances for Hole M0058A are shown in Figure F161 and Tables T5 and T6. The abundance of carbonate in Hole M0058A varies from 28% to 76%. The upper fine unit has a carbonate percentage profile that changes from 65% to 31% carbonate from 0.04 to 8.68 mbsf, which is similar to the lower part of the middle fine-grained unit. The upper coarse unit has a carbonate percentage that is slightly higher than the lower coarse unit at 50%–60%. The carbonate percentage of the middle fine-grained unit increases rapidly from ~40% at 14.79 mbsf to a high of 60%–70% at 17.78 mbsf and then decreases from 76% at 24.38 mbsf to 28% at 28.18 mbsf. The lower coarse unit has a lower carbonate percentage that also decreases downcore from 48% to 30%. The lower part of the core has a high carbonate content, which decreases from 65%–75% to 50%–60% from 33.59 to 40.27 mbsf. The profile for the percentage of quartz (all polymorphs) shows opposite trends to that of percent carbonate. The covariation of quartz and carbonate abundance has a negative correlation (r = –0.86). The percentage of quartz in the upper fine-grained unit increases downward from 15% to

37% from 0.04 to 8.68 mbsf, and the upper coarse unit has a low quartz content of 13%–15%. The percentage of quartz in the middle fine-grained unit also decreases downhole from ~30% at 14.79 mbsf to 12% at 24.38 mbsf, and then increases to 34% at 28.18 mbsf. In contrast, the lower coarse unit has a higher quartz content that increases downcore from 17% to 38%. The lower part of the core has a relatively low quartz content that increases from 10% to 22% from 33.59 to 40.27 mbsf.

The percent clay data are variable and do not show a clear trend, although the coarse-grained units may have a slightly higher average clay content than the finer grained units: 17.0% ± 2.4% versus 12.9% ± 1.1% (at the 95% confidence interval).

The percent feldspar data are also variable but do show trends. The coarse-grained units have a higher feldspar content (12.2% ± 2.6%) versus 7.5% ± 1.0% for the fine-grained units (at the 95% confidence interval), and the fine-grained units show trends that closely approximate the trends in quartz content, especially in the upper and middle fine-grained units.

The percent amphiboles and pyroxenes data are sparser than the other mineral groups, with many samples not having any amphibole or pyroxene. A clear trend exists in the data with the greatest abundance of amphibole and pyroxene (as much as 9%) in the upper fine unit, lower abundance in the middle unit, and still lower abundance in the lower fine-grained unit.

Relative abundance ratios

Relative abundance ratios for Hole M0058A are shown in Figure **F162** and Table **T7.** The Mg calcite/calcite ratio is near constant in the fine-grained units (mean of 1.0 ± 0.2) but increases to mean ratios of 2.6 ± 0.3 in the lower coarse unit and is as high as 4.2 in the upper coarse unit.

The carbonate/SiO_2 ratio varies downcore in parallel with carbonate content and inversely to quartz content. Where feldspars are also included with SiO_2 for the ratio, the pattern is similar because of the covariation of quartz and feldspar content downcore. There is a rapid fall to ~1.4 at the top of the middle fine-grained unit. In the upper and middle fine-grained units, carbonate/SiO_2 decreases from 6.8 to ~0.85 (4.4 for the upper unit) immediately above the coarse-grained unit. The carbonate/SiO_2 ratio decreases continuously from the top of the upper fine-grained unit, but in the middle fine-grained unit it increases from 3.2 at 17.28 mbsf gradually to a 6.8 peak at 24.38 mbsf. The lower fine-grained unit has a carbonate/SiO_2 ratio of 6–8; the ratio decreases rapidly at ~38 mbsf to ~3 at the bottom of the recovered unit.

The aragonite/calcite (both calcite and Mg calcite) ratio shows an inverse relationship to the Mg calcite/calcite ratio downcore. The coarse-grained units have lower aragonite/calcite ratios with a mean of 0.6 ± 0.2 versus the mean for the fine-grained units of 1.2 ± 0.1. Although there is little variation in the aragonite/calcite ratio within the fine-grained units, subtle upward trends toward lower ratios exist in each of the upper, middle, and lower units.

The ratios of clay mineralogy ([illite, mica]/kaolinite) and siliciclastic composition (feldspars/SiO_2) are highly variable and display no clear trends downcore. However, there is a subtle increase in the (illite, mica)/kaolinite ratio between the middle and upper fine-grained units, which have means of 0.9 ± 0.2 and 1.7 ± 0.3, respectively.

Carbon content

The results for total organic carbon (TOC), total carbon (TC), and total inorganic carbon (TIC) are presented in Table **T8** and Figure **F163.** TC content ranges from 5.27 to 10.18 wt% (average = 8.75 wt%), TOC content ranges from 0.19 to 0.51 wt% (average = 0.29 wt%), and TIC content ranges from 4.89 to 9.96 wt% (average = 8.46 wt%).

Within the upper fine-grained unit, TC content ranges from 7.08 to 9.97 wt% (average = 8.72 wt%), TOC content ranges from 0.25 to 0.39 wt% (average = 0.33 wt%), and TIC content ranges from 6.49 to 9.58 wt% (average = 8.40 wt%). Within the middle fine-grained unit, TC content ranges from 5.27 to 10.18 wt% (average = 8.77 wt%,) TOC content ranges from 0.19 to 0.51 wt% (average = 0.28 wt%), and TIC content ranges from 4.89 to 9.96 wt% (average = 8.49 wt%). Within the lower fine-grained unit, TC content ranges from 7.74 to 10.10 wt% (average = 9.95 wt%), TOC content ranges from 0.21 to 0.42 wt% (average = 0.33 wt%), and TIC content ranges from 7.34 to 9.88 wt% (average = 9.62 wt%). The two coarse-grained units contain low TOC content with an average value of 0.25 wt%.

Chronology

The shallowest hole drilled on transect NOG-01B (Fig. **F155**), Hole M0057A (Site 2), was drilled into a feature at a 40 m water depth (lowest astronomical tide [LAT]), which returned an age of 12 cal y BP near the core top (Core 325-M0057A-5R) at 52 mbsl. Therefore, this hole seems to have recovered material from the middle of the last deglaciation. One further U-Th age determination on this hole was at-

tempted in Core 325-M0057A-15R. However, the sample did not yield an age interpretation because it was diagenetically altered. Nevertheless, it is likely that the lower cores of Hole M0057A do capture material from prior to the Last Glacial Maximum (LGM). Hole M0056A (Site 5) penetrated a feature at 82 mbsl and returned ages of 34 and 39 cal y BP from near the core top (Cores 325-M0056A-2R and 5R). These ages indicate that the hole recovered material that predates the LGM, probably from marine isotope Stage 3. The deeper portion of this hole yielded an older age of 84 cal y BP (Core 325-M0056A-13R) from 114 mbsl, indicating significant accumulation from 84 to 39 ka. Hole M0055A (Site 5) drilled into feature located slightly deeper, at 90 mbsl, than Hole M0056A. Hole M0055A returned an age of 14 cal y BP from the shallowest core (Core 325-M0055A-1R), suggesting accumulation during at least the early to middle portion of the last deglaciation. Two ages of 23 and 25 cal y BP were recovered deeper in this hole at 100–103 mbsl (Cores 325-M0055A-4R and 5R), indicating accumulation of LGM material at this site.

A deeper feature in 97 m water depth (LAT) was drilled by four holes (M0052A, M0052B, M0052C, and M0053A) at Site 6. The upper cores (325-M0052B-1R, 325-M0052C-1R, and 325-M0053A-3R) yielded ages of 17–14 cal y BP, suggesting that they span the early to middle portion of the deglaciation. Deeper in Hole M0053A, two ages of 20 and 24 cal y BP, at 106 and 123 mbsl, respectively (Cores 325-M0053A-9R and 25R), indicate substantial accumulation of material at Site 6 during the LGM. The deepest hole drilled on the shelf edge on transect NOG-01B (Hole M0054B at Site 7) penetrated a seabed feature at 116 m water depth (LAT). The upper cores of this hole yielded ages of 13, 18, and 20 cal y BP from 113, 119, and 123 mbsl (Cores 325-M0054B-1W, 3R, and 4R), respectively, indicating accumulation of material during the early and mid-deglaciation, whereas the cores below may represent material from the LGM. The last hole drilled (Hole M0058A at Site 8) at transect NOG-01B was on the fore reef slope sediments at 167 m water depth (LAT). The only sample analyzed for radiocarbon (Core 325-M0058A-4R) was beyond the limit of the radiocarbon method (Fig. **F154**). This indicates that the majority of Hole M0058A probably spans a significant period older than 50 cal y BP.

Downhole measurements

One hole (M0054B) was logged in transect NOG-01B. Despite having good core recovery (in Expedition 325 terms) (29.63%), the data set for this hole will be vastly improved by the inclusion of logging data from the suite of wireline tools deployed in the hole. The logging data provides a continuous downhole data set as well as allowing more precise core positioning within the hole.

Borehole geophysical instruments

The suite of downhole logging tools deployed at transect NOG-01B is as follows:

- The Optical Borehole Televiewer (OBI40).
- The Acoustic Borehole Televiewer (ABI40).
- The Hydrogeological probe (IDRONAUT).
- The Spectral Natural Gamma Probe (ASGR).
- The Induction Resistivity Probe (DIL45)-medium (ILM, 0.57 m) and deep (ILD, 0.83 m) investigation depths The Full Waveform Sonic Probe (SONIC).
- The magnetic susceptibility probe (EM51).
- The caliper probe (CAL3)–borehole diameter.

Preliminary results

Wireline logging operations at transect NOG-01B were performed in one HQ hole (M0054B). This provided the only opportunity to run both of the high-priority imaging tools in a "logging" hole. After completion of coring, ASGR logging through pipe was performed, and then the HQ drill string was pulled and the coring bit exchanged for an open-shoe casing to provide borehole stability in unstable sections and a smooth exit and entry of logging tools. In addition, seawater was pumped into the hole in order to try to displace the guar gum drilling mud and condition the hole for open-hole logging. The API conductor pipe and HQ drill string were sitting at ~17 m WMSF, and with a total hole depth of ~33 m WMSF open, leaving little margin for borehole infilling or collapse. With the exception of the ASGR through-pipe log, logging was obtained over a maximum interval of ~8.5 m. Borehole conditions were relatively hostile, and the lower portion of the hole began to infill. In order to record ultra-high-resolution geophysical downhole logging data, the acquisition was done in the rooster box, which is heave-compensated.

Two main logging units were identified in Hole M0054B (Fig. **F164**):

1. Unit I is characterized by relatively high total gamma ray and generally low conductivity, although there is a gradual increase in conductivity toward the base of this unit. Magnetic susceptibility wavers around 0.7 mSI throughout, and the caliper shows the borehole to be in gauge. Acoustic images provide virtual hardness visualization, and within Unit I the majority of the formation appears "hard." Lithostrati-

graphic units identified within this logging unit include (coral) algal-microbialite boundstone, lime sand (with Halimeda), and rudstone. Clearly, the boundstones lend themselves to providing more stable borehole conditions.

2. Unit II is defined by lower total gamma ray counts compared with Unit I and higher conductivity values. There is a minor decrease in magnetic susceptibility compared with Unit I, and caliper data indicate hole widening compared with the upper unit. Acoustic images clearly show a significant change in formation at a major shallowly dipping boundary. Lithostratigraphic units observed in this logging unit include dark gray rudstone, which passes downhole into lime sand (with large benthic foraminifera).

Further work will be needed to integrate the depth discrepancies shown between the logging and lithostratigraphic unit boundary depths.

References

Bronk Ramsey, C., 2009. Bayesian analysis of radiocarbon dates. *Radiocarbon,* 51(1):337–360. **http://digitalcommons.arizona.edu/restrictedobjectviewer?o=http://radiocarbon.library.arizona.edu/Volume51/Number1/0b094122-5128-4777-9edd-b4dad8f3864d**

Reimer, P.J., Baillie, M.G.L., Bard, E., Bayliss, A., Beck, J.W., Blackwell, P.G., Bronk Ramsey, C., Buck, C.E., Burr, G.S., Edwards, R.L., Friedrich, M., Grootes, P.M., Guilderson, T.P., Hajdas, I., Heaton, T.J., Hogg, A.G., Hughen, K.A., Kaiser, K.F., Kromer, B., McCormac, F.G., Manning, S.W., Reimer, R.W., Richards, D.A., Southon, J.R., Talamo, S., Turney, C.S.M., van der Plicht, J., and Weyhenmeyer, C.E., 2009. Intcal09 and Marine09 radiocarbon age calibration curves, 0–50,000 years cal BP. *Radiocarbon,* 51(4):1111–1150. **http://digitalcommons.arizona.edu/restrictedobjectviewer?o=http://radiocarbon.library.arizona.edu/Volume51/Number4/49691745-6a68-4e2c-a26f-08f0a16c1a53**

Publication: 16 July 2011
MS 325-106

Figure F1. Contour plot showing transect NOG-01B (Noggin Pass), Expedition 325. Sites 1–8 and Holes M0052A–M0058A are indicated. See Figure F2 in the "Expedition 325 summary" chapter for general location. EPSP = Environmental Protection and Safety Panel, GBRMPA = Great Barrier Reef Marine Park Authority.

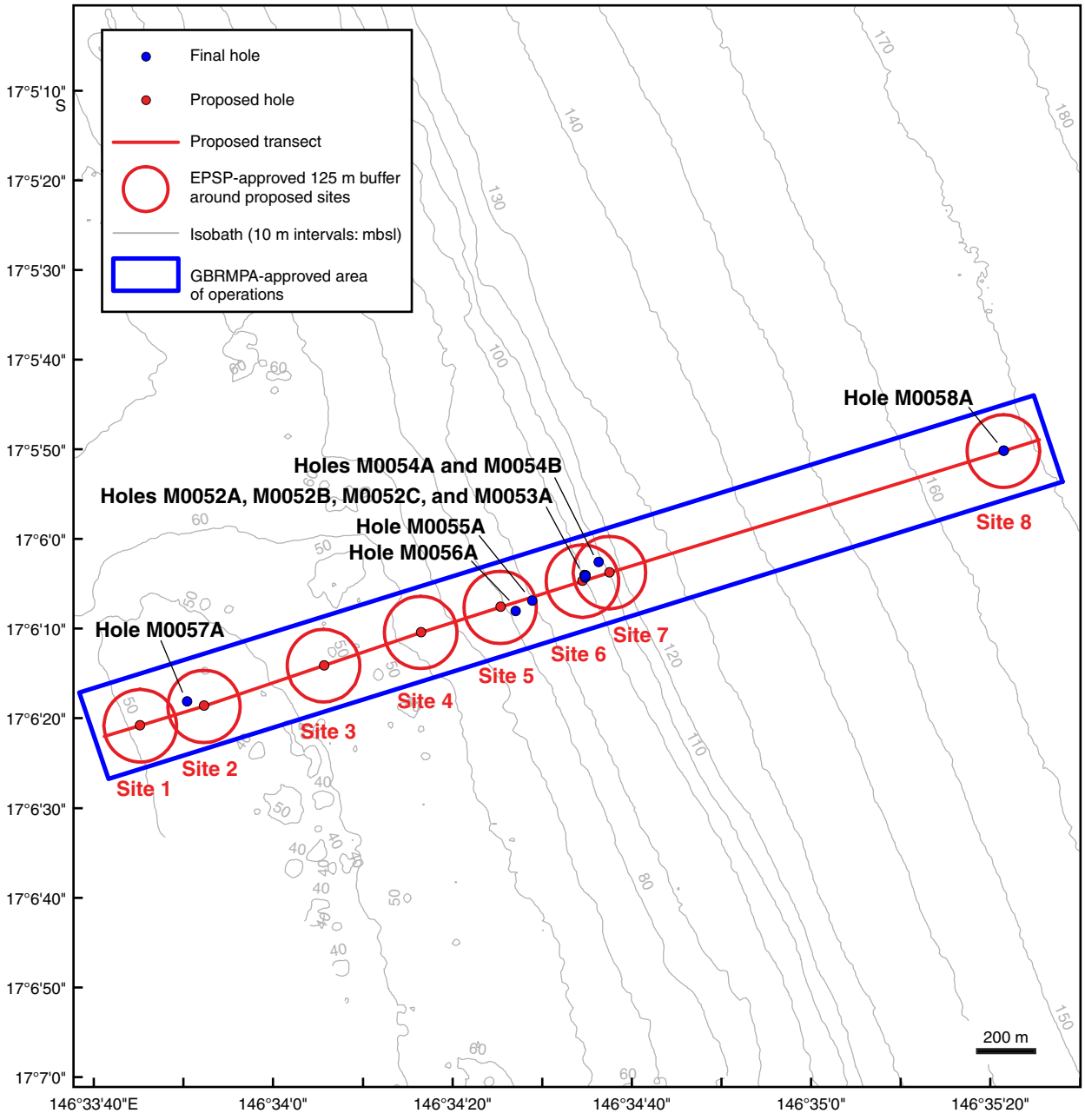

Figure F2. High-resolution line scan image of muddy lime sand with *Halimeda,* mollusks, benthic foraminifera, coral pebbles, and rare bryozoans (interval 325-M0052A-1X-2, 0–17 cm). Fragments of encrusting *Montipora* and fine branching *Seriatopora* are also present.

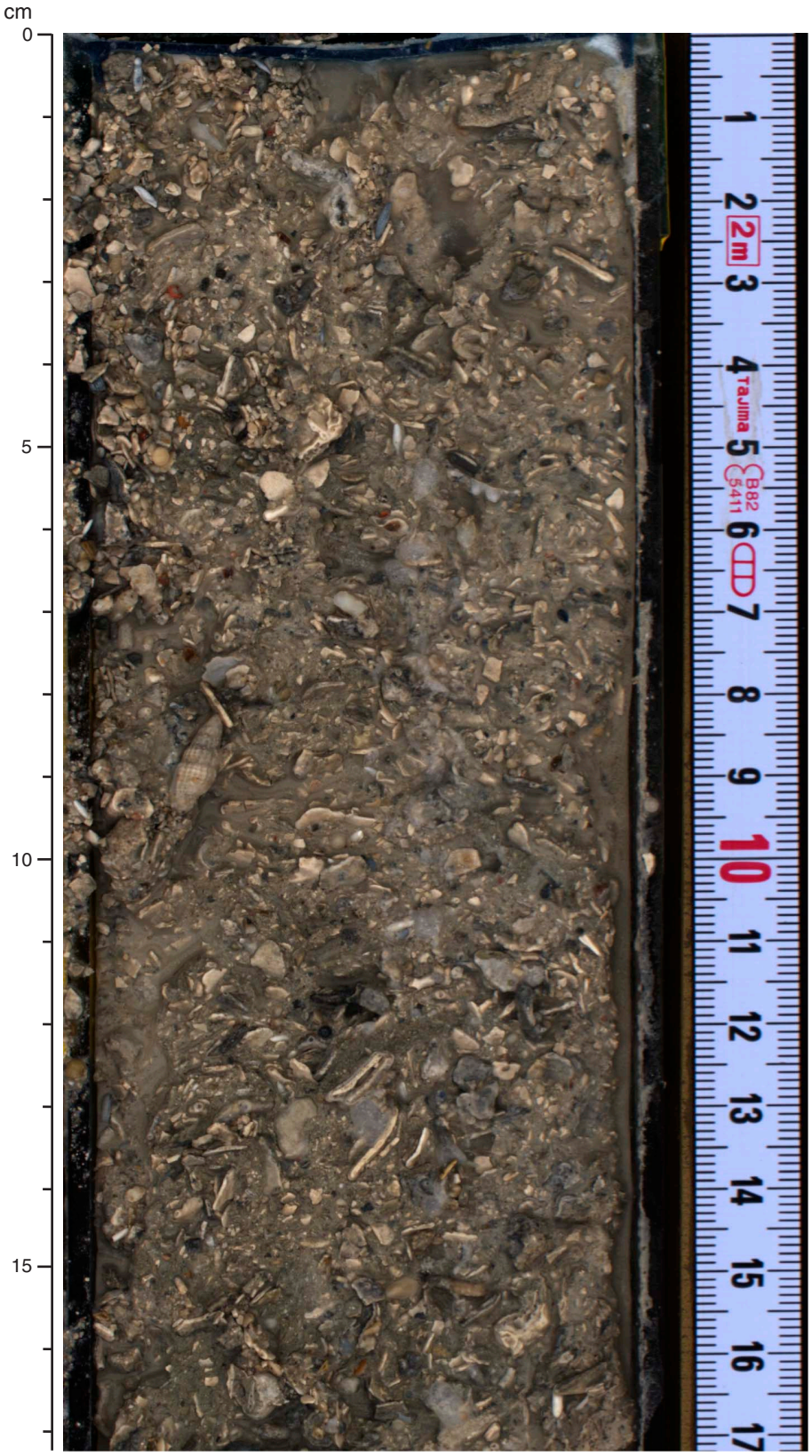

Figure F3. High-resolution line scan image of fragments of a massive *Goniopora* (interval 325-M0052A-1X-2, 41–53 cm).

Figure F4. Summary diagram showing data collected on whole cores using the MSCL, Hole M0052A.

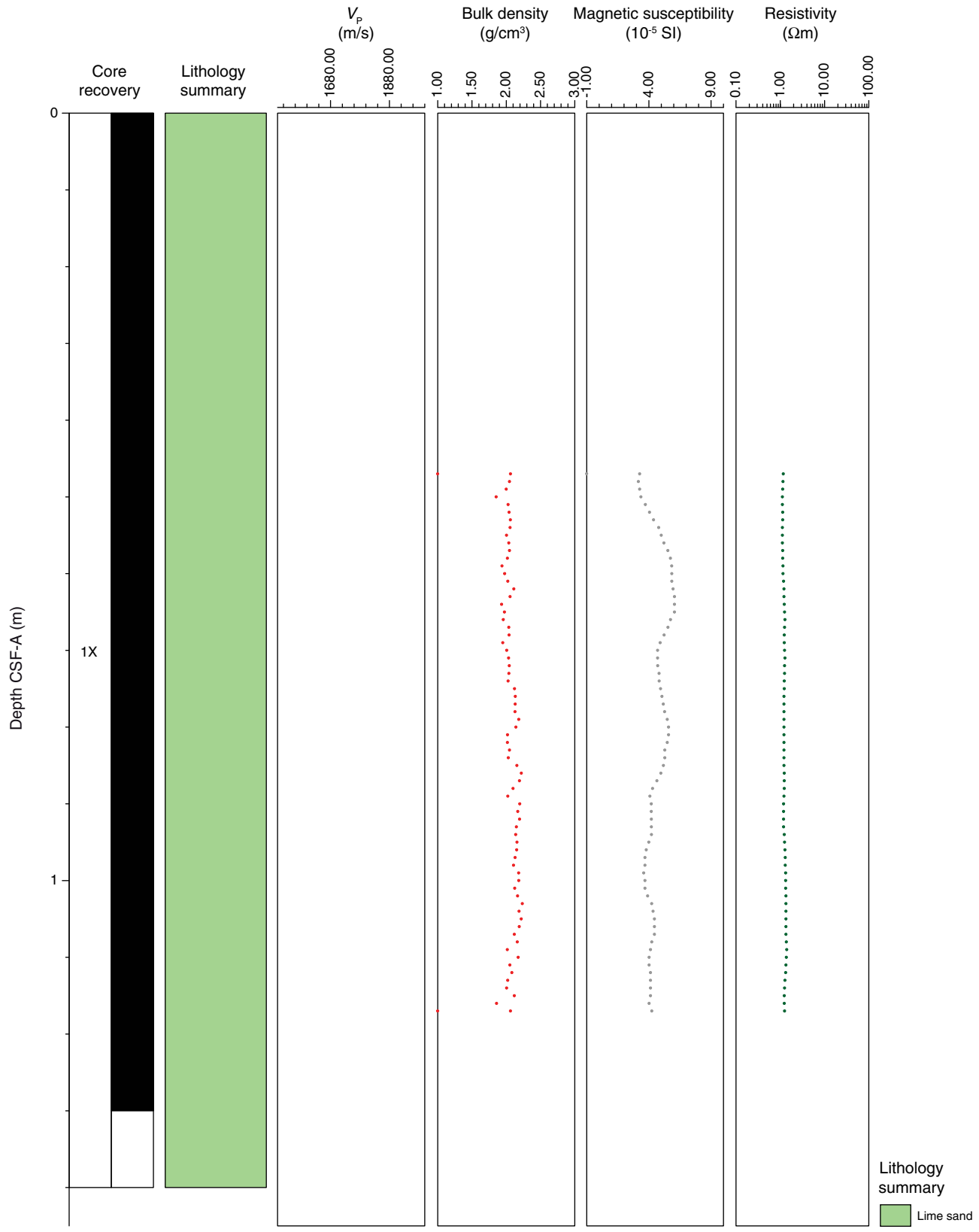

Figure F5. Petrophysical measurements obtained from discrete samples with a pycnometer, Hole M0052A. Bulk density measured on whole cores with the MSCL is shown in red on the bulk density plot.

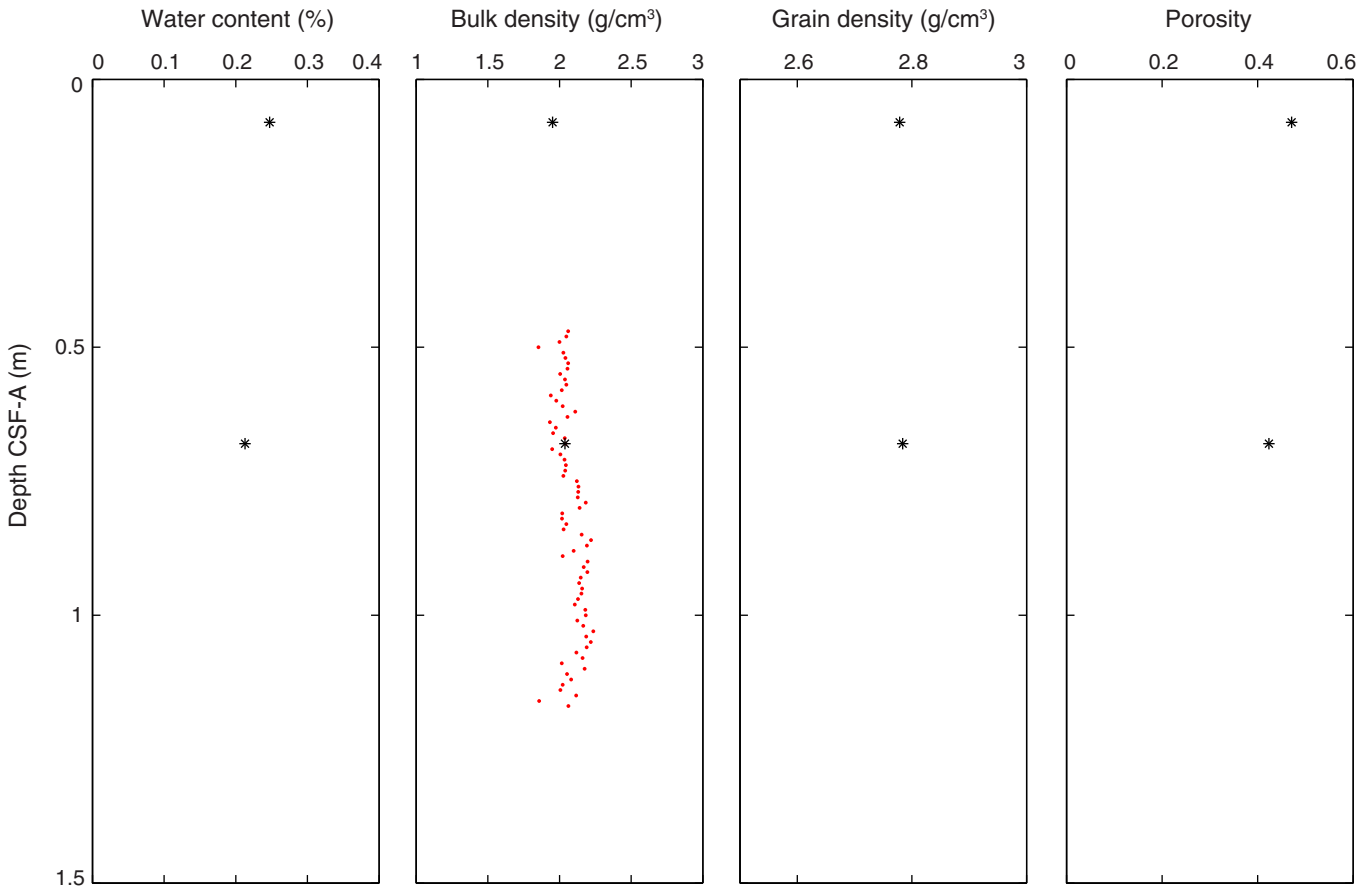

Figure F6. Values of reflectance (L*), green to red (a*), and blue to yellow (b*) indexes, along with ratio a*/b* for Hole M0052A.

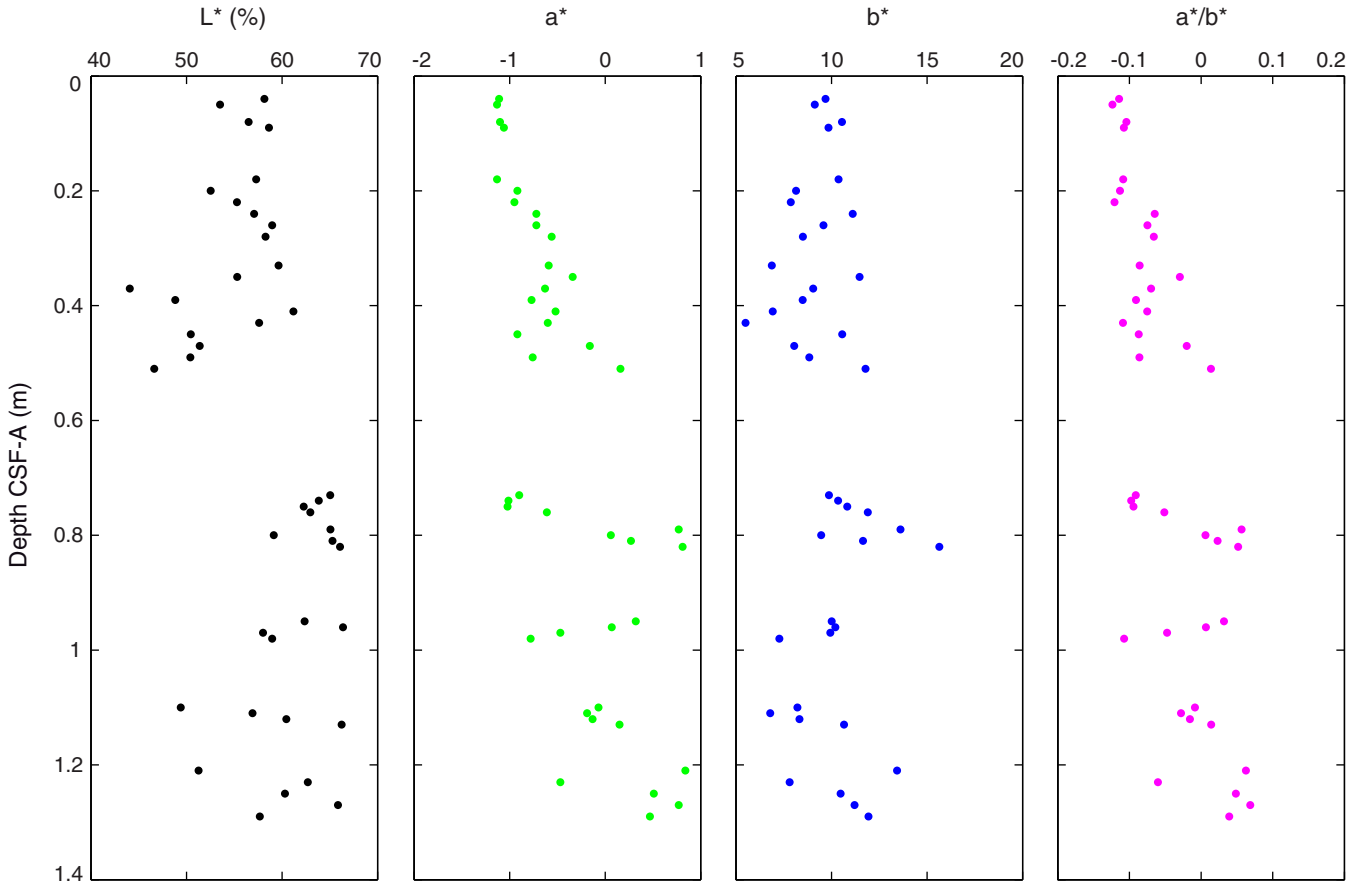

Figure F7. High-resolution line scan image of coarse to very coarse lime sand with pebbles of corals, *Halimeda,* mollusks, benthic foraminifera, and coralline algae (interval 325-M0052B-1R-1, 17–39 cm). Bioclastic packstone pebbles/granules are also present.

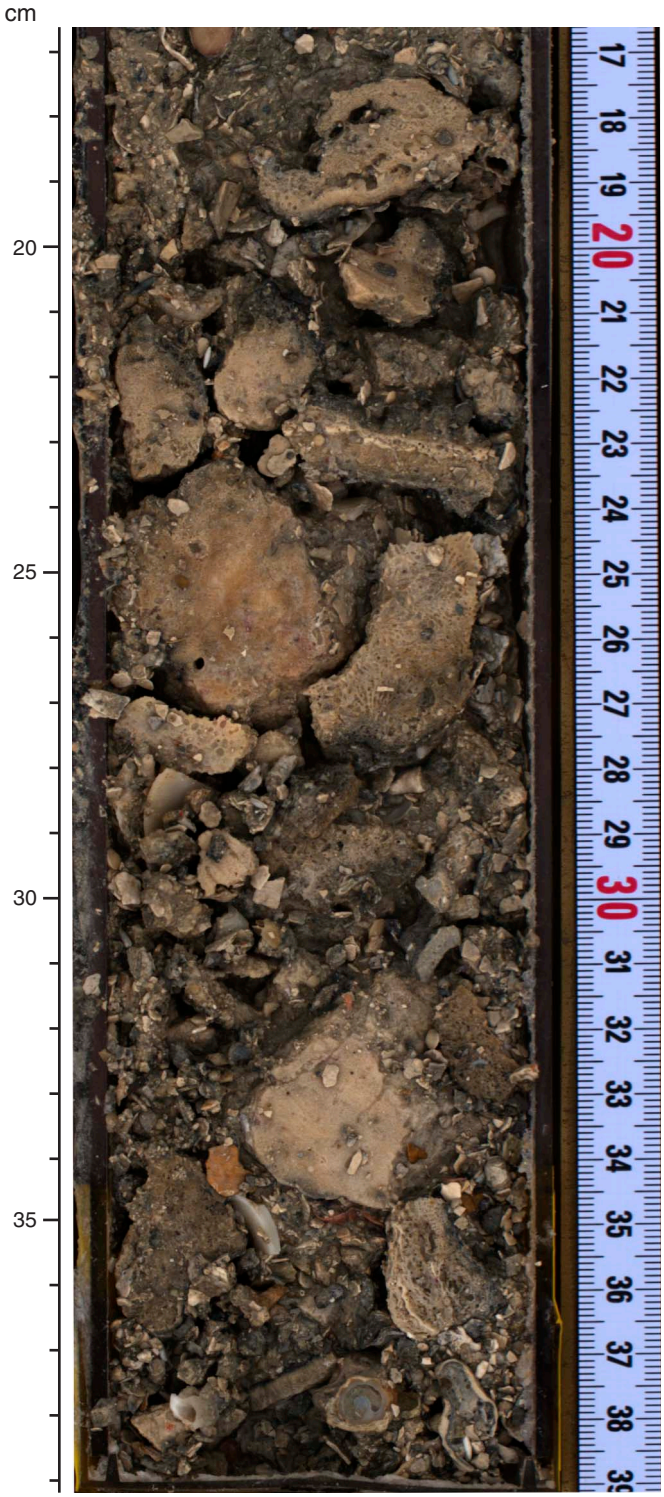

Figure F8. Summary diagram showing data collected on whole cores using the MSCL, Hole M0052B.

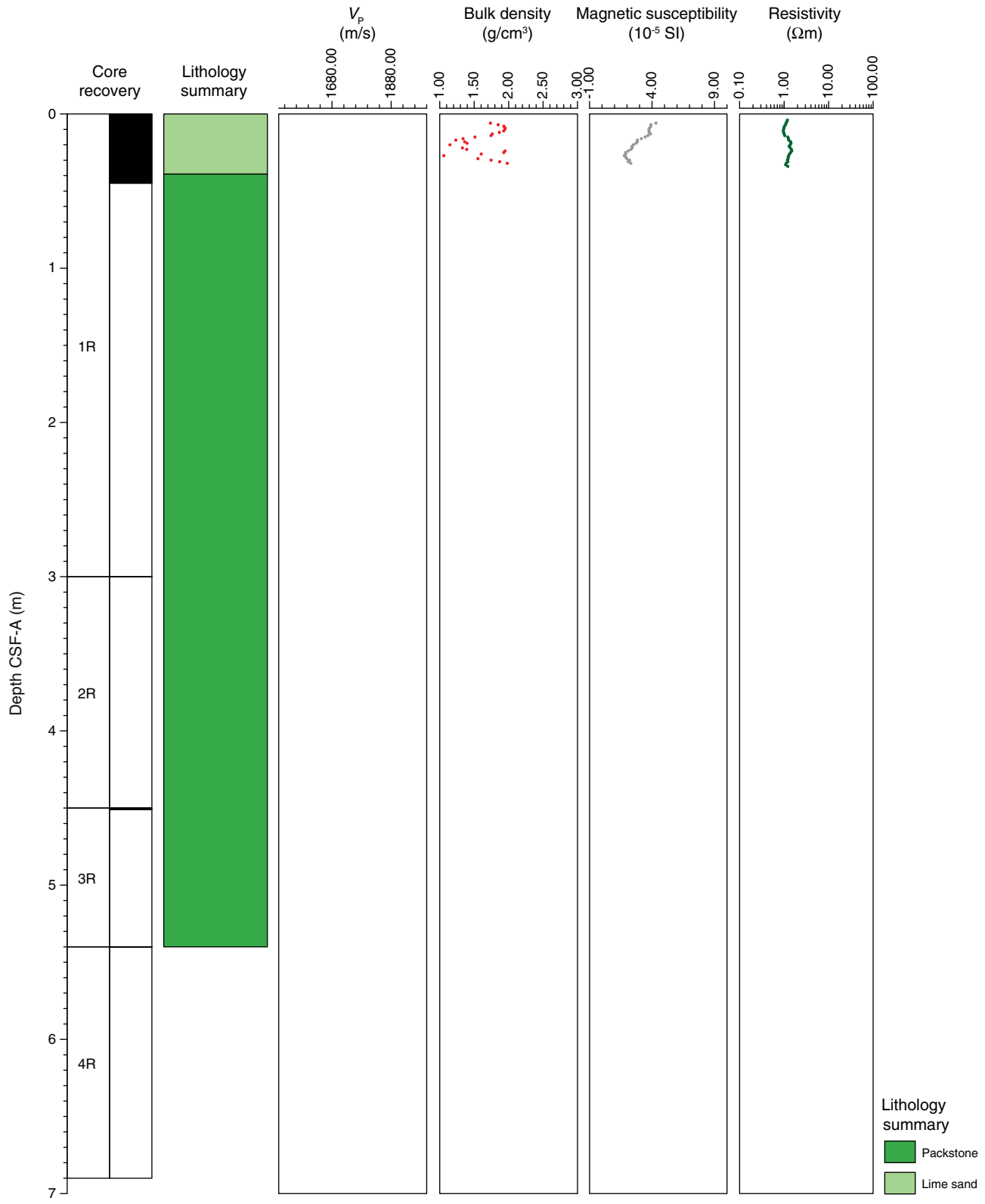

Figure F9. Petrophysical measurements obtained from discrete samples with a pycnometer, Hole M0052A. Bulk density measured on whole cores with the MSCL is shown in red on the bulk density plot.

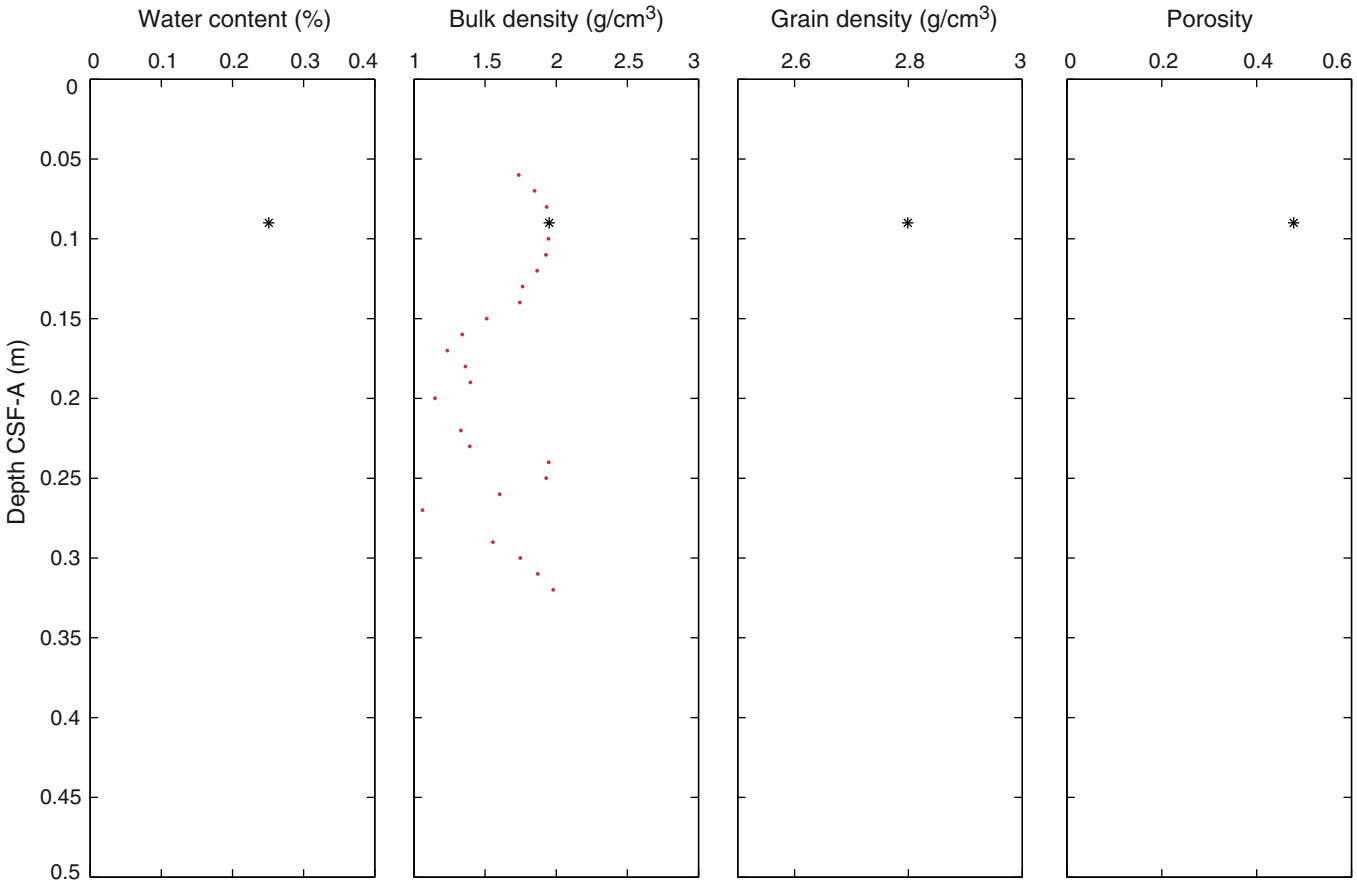

Figure F10. Values of reflectance (L*), green to red (a*), and blue to yellow (b*) indexes, along with ratio a*/b* for Hole M0052B.

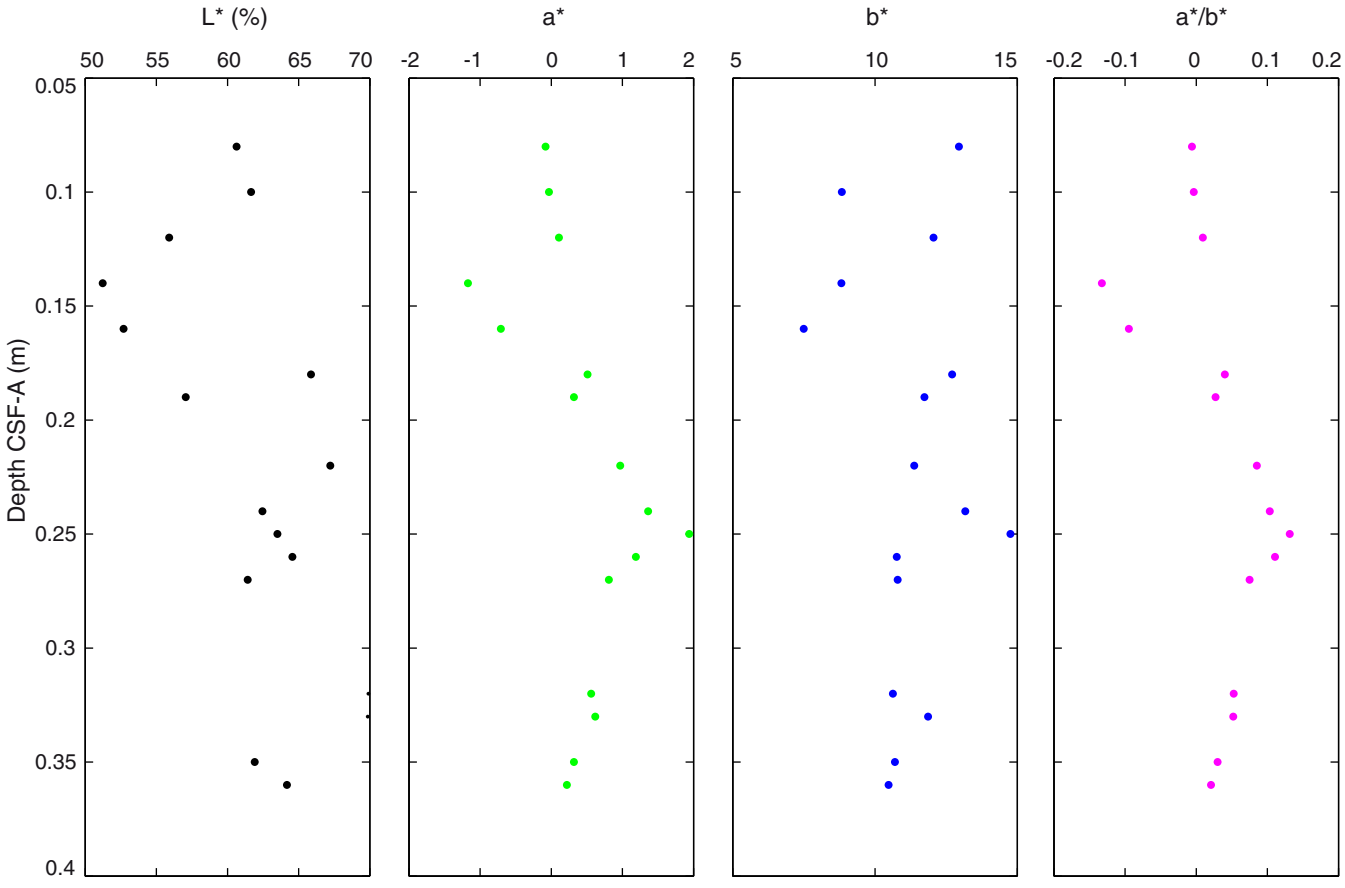

Figure F11. Preliminary chronology for Hole M0052B. Radiocarbon data are presented as graphs with the uncalibrated radiocarbon age and uncertainty shown as the red normal distribution on the ordinate axis and the probability distribution of the calibrated age shown in gray on the abscissa. The marine09 calibration curve is shown in blue. Horizontal bars indicate portions of the age distribution that are significant at the 95.4% confidence interval and the mean age (white circle ±1 standard deviation) used for the purposes of the preliminary dating. All ages are presented as thousands of calendar years BP (1950 AD). See Table **T10** in the "Methods" chapter. (See Bronk Ramsey [2009], as well as Bronk Ramsey [2010] at **c14.arch.ox.ac.uk/oxcal.html.**)

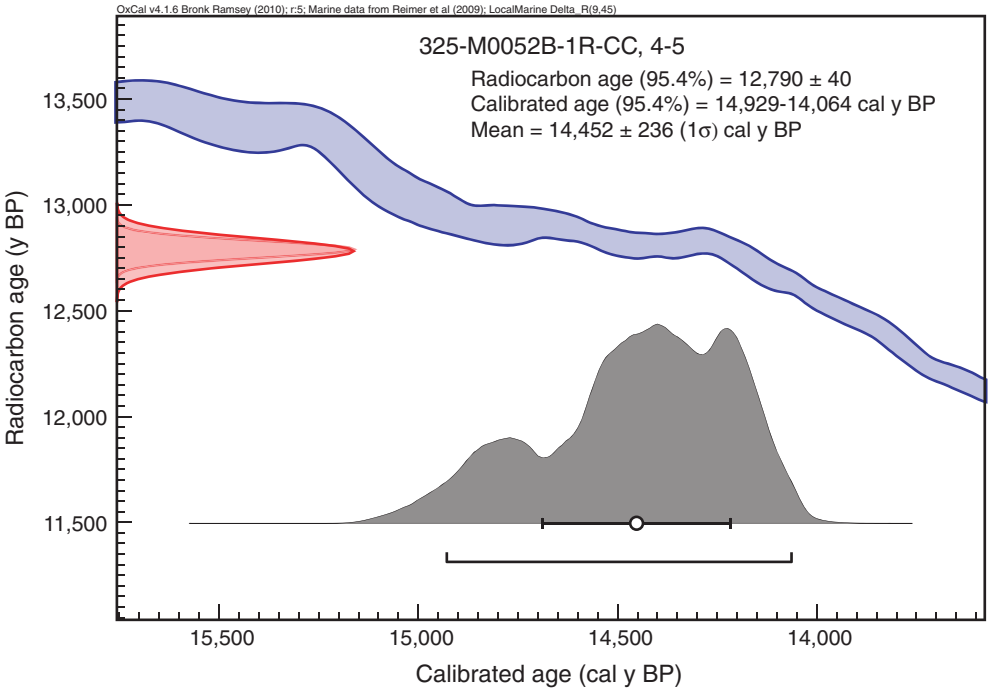

Figure F12. High-resolution line scan image of granules and pebbles of coral with coralline algal crusts and vermetids (interval 325-M0052C-1R-CC, 0–10 cm). Fragments of bioclastic grainstone are also present.

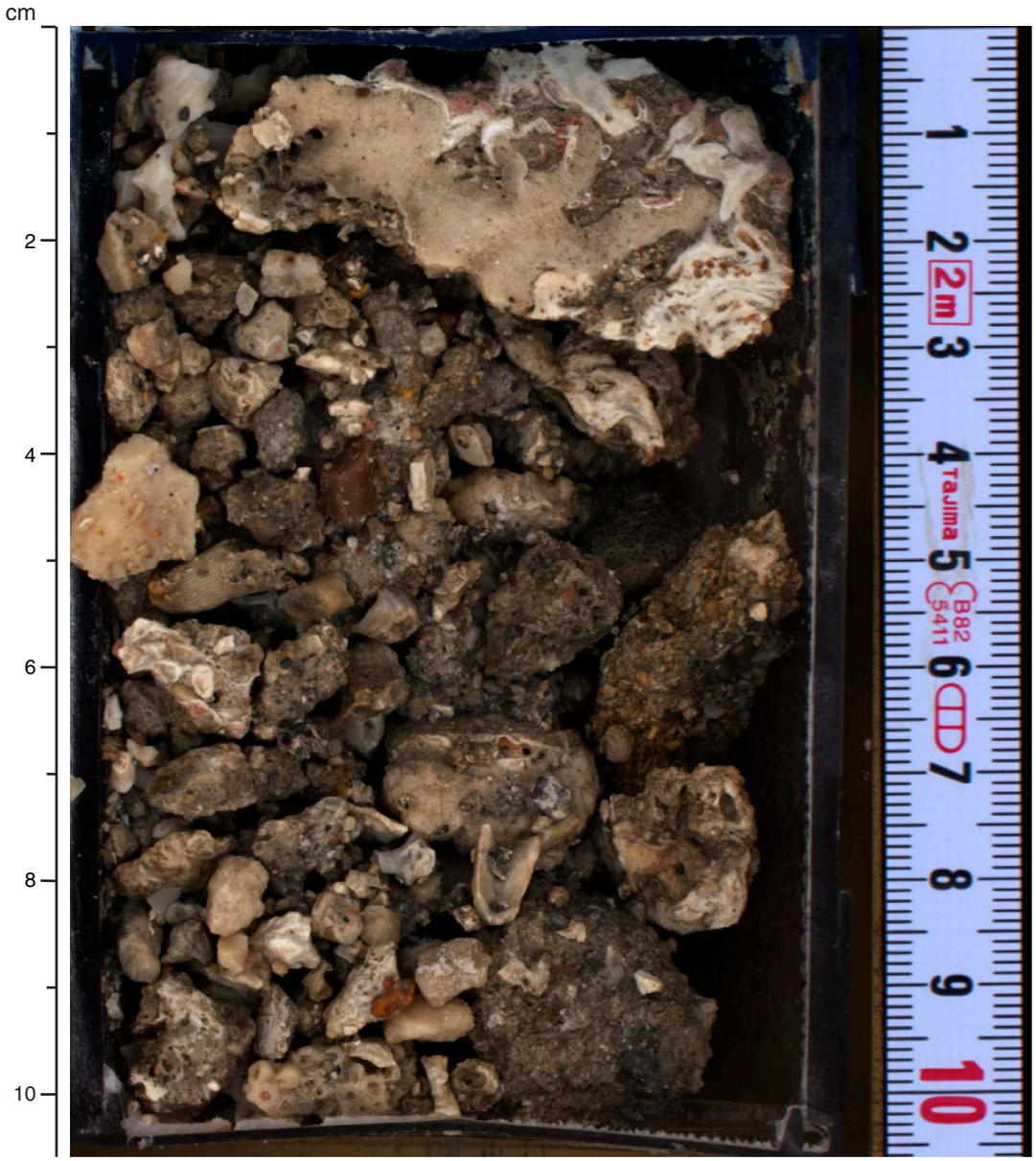

Figure F13. Preliminary chronology for Hole M0052C. Radiocarbon data are presented as graphs with the uncalibrated radiocarbon age and uncertainty shown as the red normal distribution on the ordinate axis and the probability distribution of the calibrated age shown in gray on the abscissa. The marine09 calibration curve is shown in blue. Horizontal bars indicate portions of the age distribution that are significant at the 95.4% confidence interval and the mean age (white circle ±1 standard deviation) used for the purposes of the preliminary dating. All ages are presented as thousands of calendar years BP (1950 AD). See Table **T10** in the "Methods" chapter. (See Bronk Ramsey [2009], as well as Bronk Ramsey [2010] at **c14.arch.ox.ac.uk/oxcal.html.**)

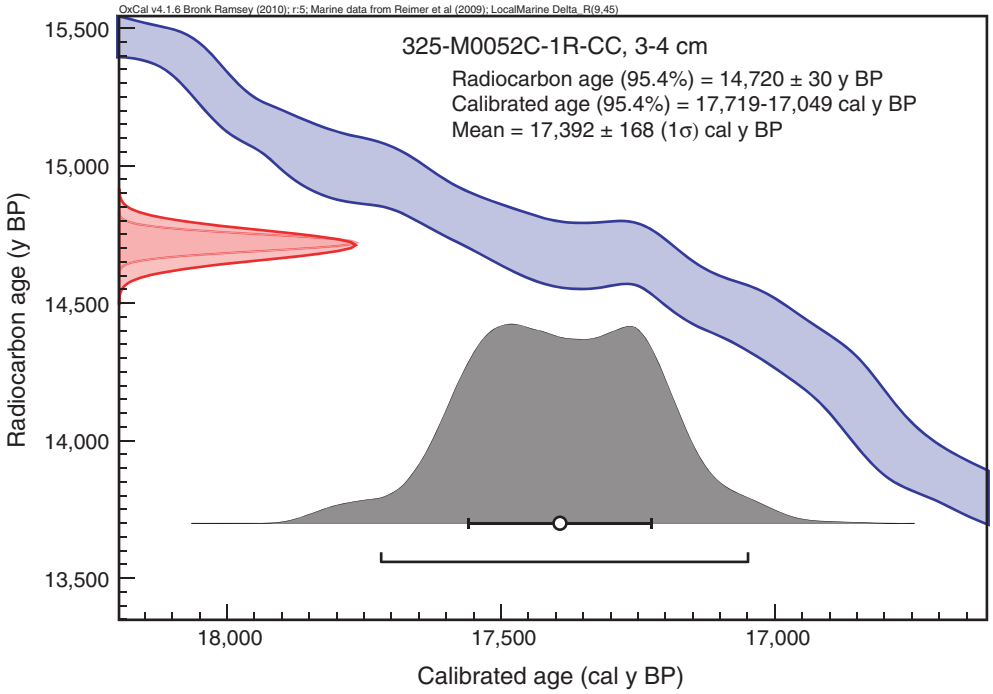

Figure F14. High-resolution line scan image of a muddy sand with *Halimeda,* benthic foraminifera, and mollusks (interval 325-M0053A-1X-1, 0–12 cm). Fragments of *Heliopora, Seriatopora,* encrusting *Montipora*(?), and *Pocillopora* are also visible.

Figure F15. High-resolution line scan image of coralgal boundstone containing submassive *Montipora*(?) with coralline algal crusts, *Halimeda* fragments, benthic foraminifera, and mollusks (interval 325-M0053A-1X-1, 15–33 cm).

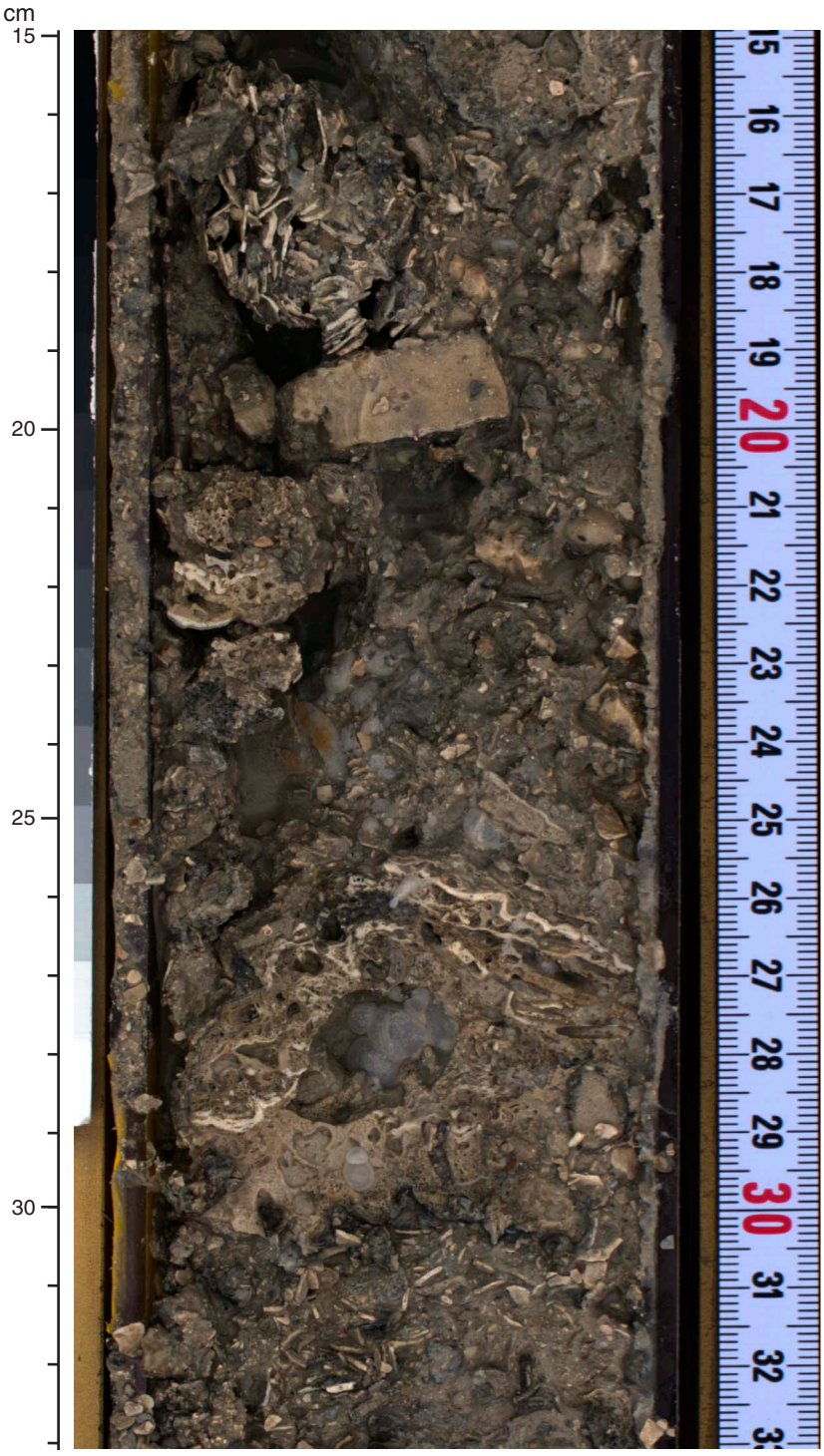

Figure F16. High-resolution line scan image of coralgal boundstone composed of encrusting *Montipora*(?) or *Porites*(?) and undetermined corals with thick coralline algal crusts (interval 325-M0053A-7R-1, 15–23 cm).

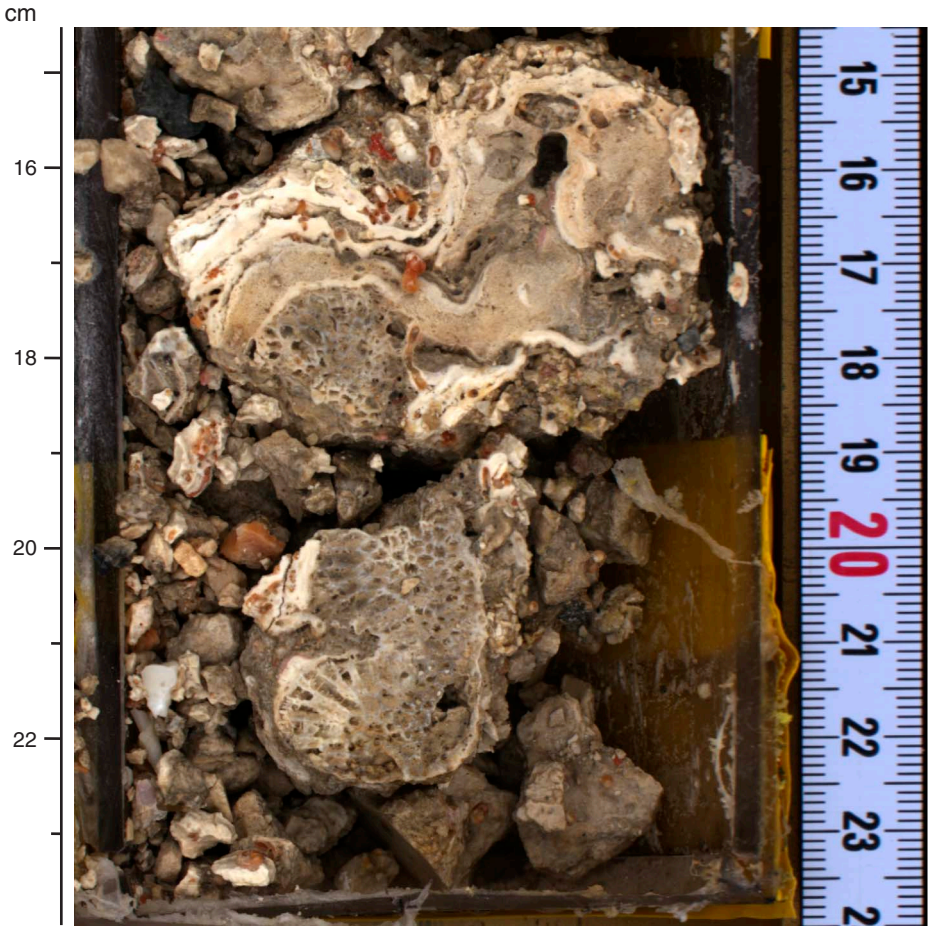

Figure F17. High-resolution line scan image of coralgal boundstone with intercalated intervals of bioclastic packstone (interval 325-M0053A-10R-1, 1–26 cm). Corals are corymbose(?) *Acropora,* fine branching *Seriatopora,* and submassive (?) *Montipora* encrusted by thick coralline algal crusts with vermetids and *Homotrema*. *Halimeda* plates are also visible.

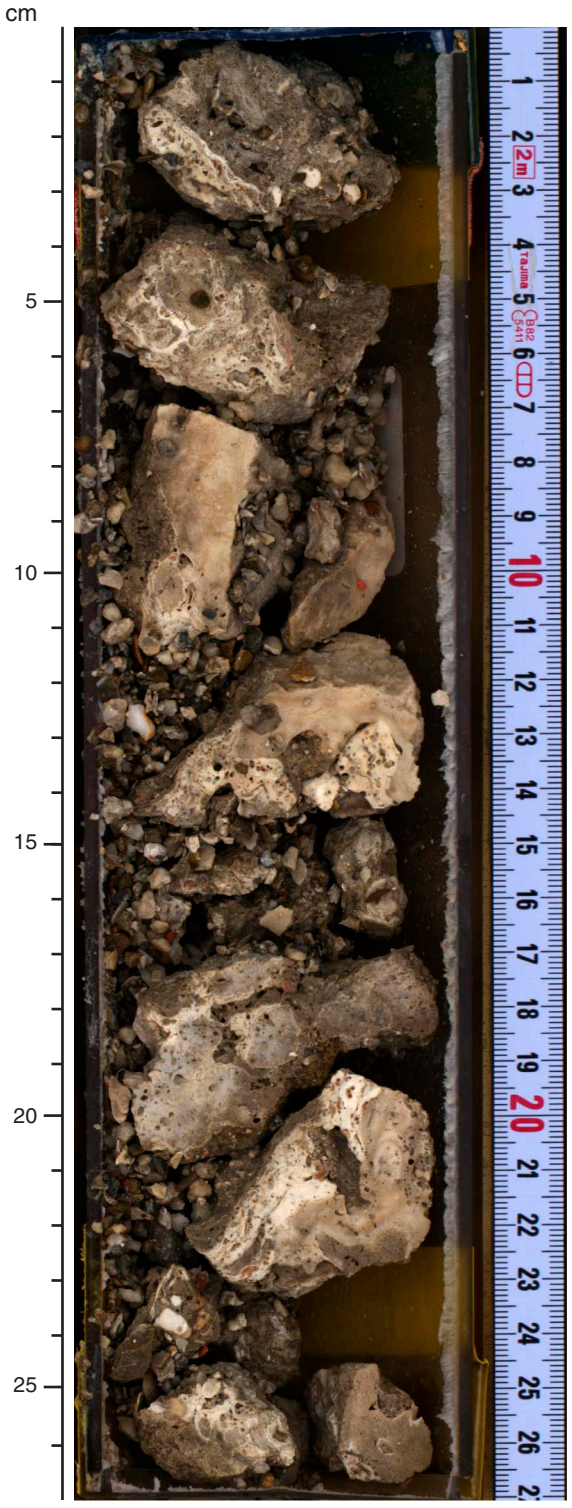

Figure F18. High-resolution line scan image of a massive *Isopora* colony (interval 325-M0053A-9R-CC, 1–12 cm).

Figure F19. High-resolution line scan image of a massive Faviidae colony (interval 325-M0053A-5R-1, 3–23 cm).

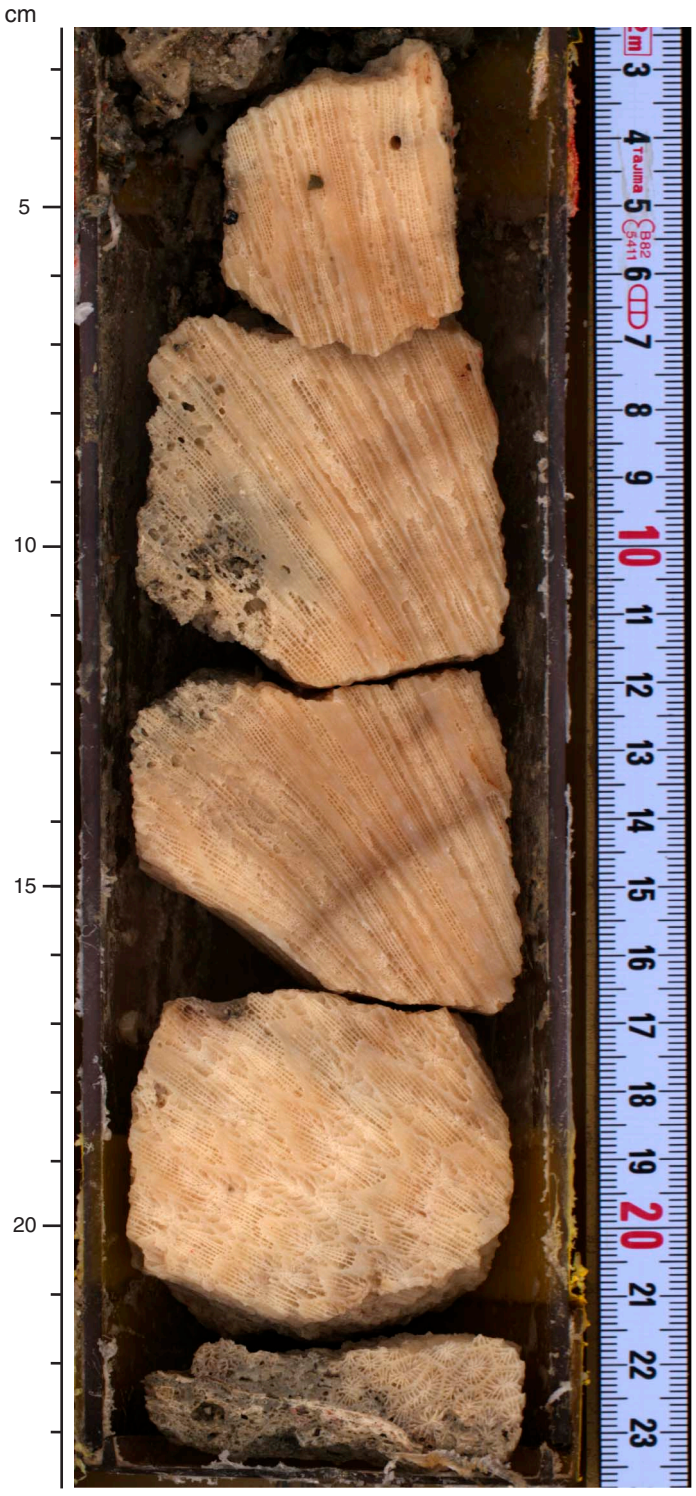

Figure F20. High-resolution line scan image of the base of a branching *Acropora* colony encrusted by coralline algae and microbialites (interval 325-M0053A-16R-1, 14.5–26.5 cm).

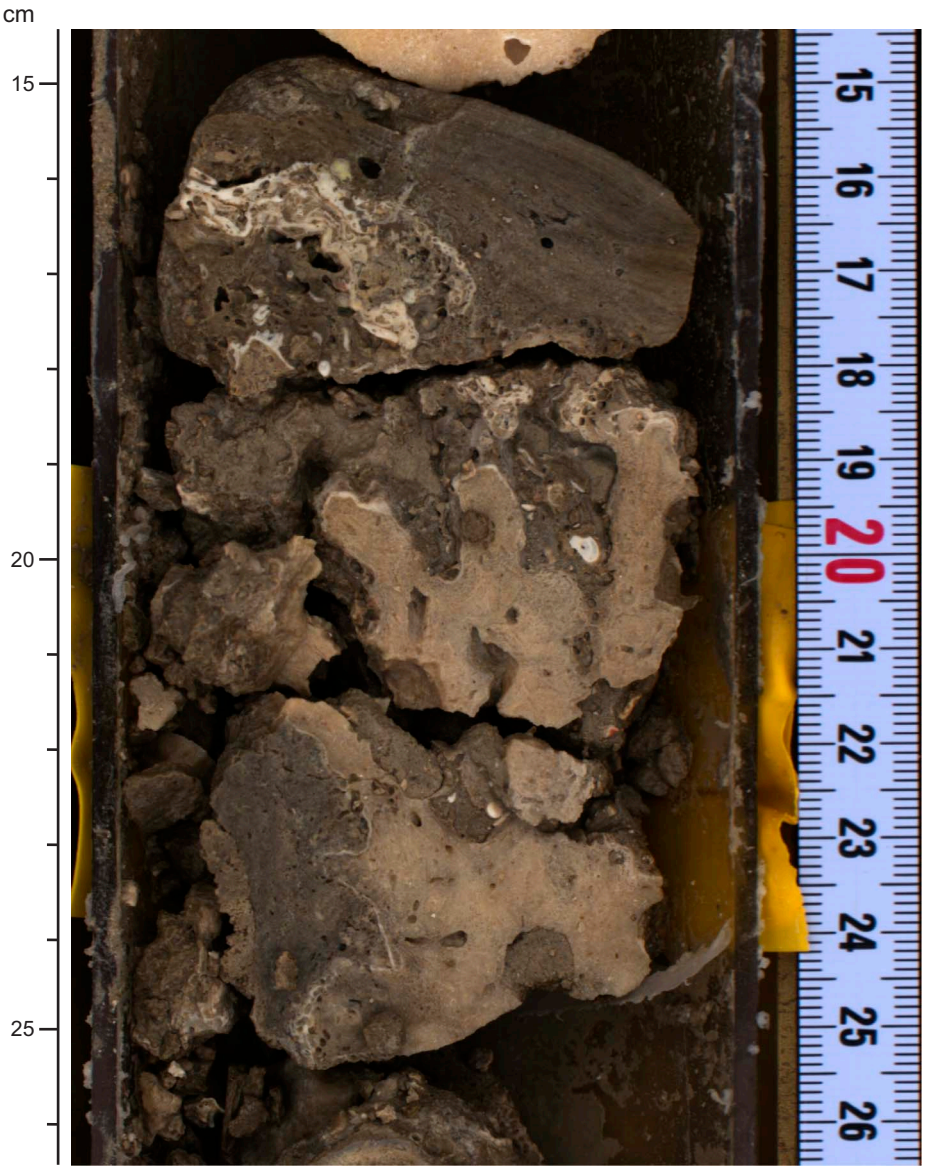

Figure F21. High-resolution line scan image of a coralline algal crust covered by laminated microbialite (interval 325-M0053A-16R-1, 38–44 cm).

Figure F22. High-resolution line scan image of *Halimeda* packstone infilling a framework of fine branching *Acropora*(?), encrusting *Montipora* or *Porites,* and coralline algal crust (interval 325-M0053A-15R-1, 12–19 cm).

Figure F23. High-resolution line scan image of a thick coralline algae crust covered by thick microbialite (interval 325-M0053A-18R-1, 10–18.5 cm).

Figure F24. High-resolution line scan image of microbialite boundstone alternating with unconsolidated, *Halimeda*-rich packstone (interval 325-M0053A-19R-1, 36–47 cm).

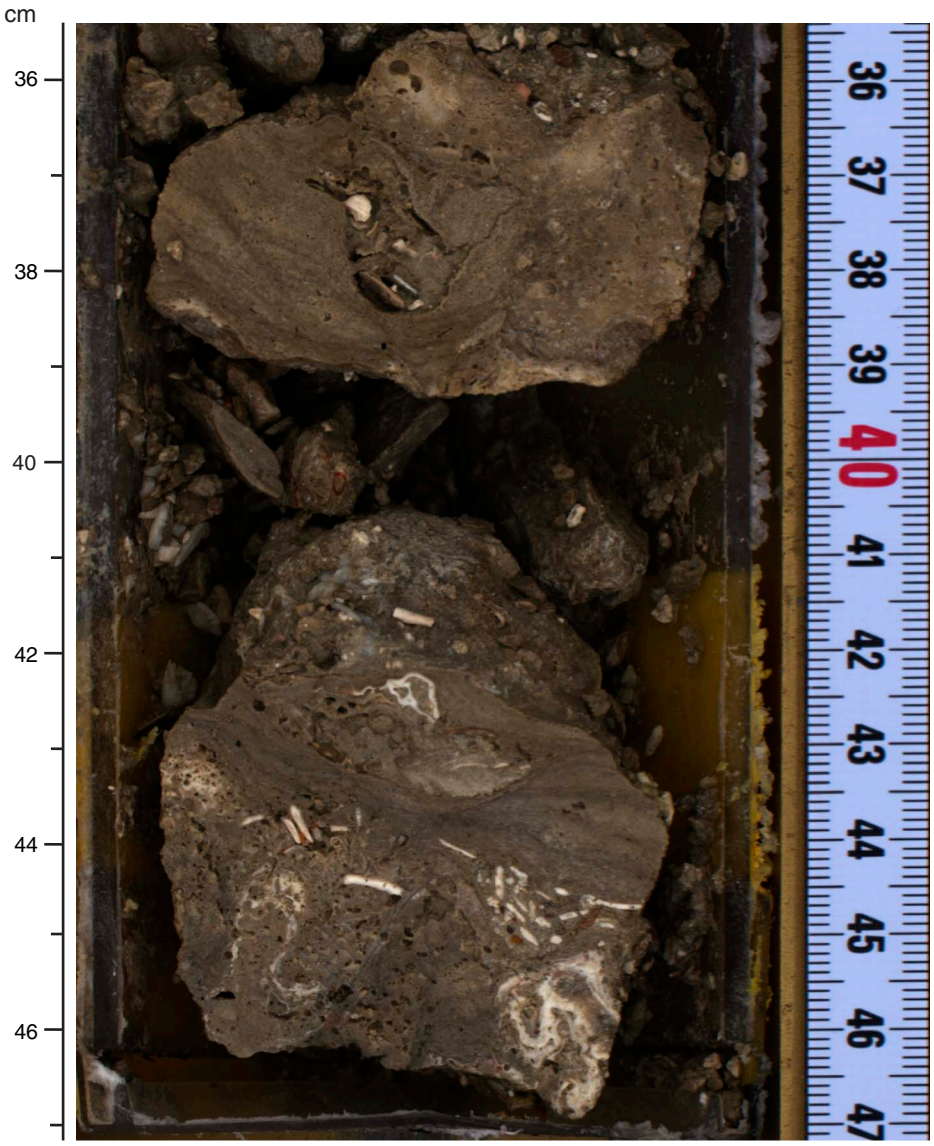

Figure F25. High-resolution line scan image of *Porites* or *Montipora* encrusted by thin coralline algae and thick microbialite (interval 325-M0053A-20R-CC, 5–13 cm).

Figure F26. High-resolution line scan image of alternating microbialites, coralline algal crusts, and massive *Platygyra* (interval 325-M0053A-21R-1, 3–20 cm).

Figure F27. High-resolution line scan image of grainstone to rudstone with coral, coralline algae, mollusks, larger foraminifera, and *Halimeda* (interval 325-M0053A-26X-CC, 4–10 cm).

Figure F28. High-resolution line scan image of grainstone to rudstone with coral, coralline algae, mollusks, larger foraminifera, and *Halimeda* (interval 325-M0053A-27R-1, 24–34 cm). Fragments include *Porites* or *Montipora* encrusting surfaces and a Pocilloporidae branch in the grainstone.

Figure F29. High-resolution line scan image of dark gray, coarse lime sand with corals (foliaceous Pectiniidae, fine branching coral, ahermatypic coral ?), larger foraminifera, and *Halimeda* (interval 325-M0053A-33R-1, 0–15 cm).

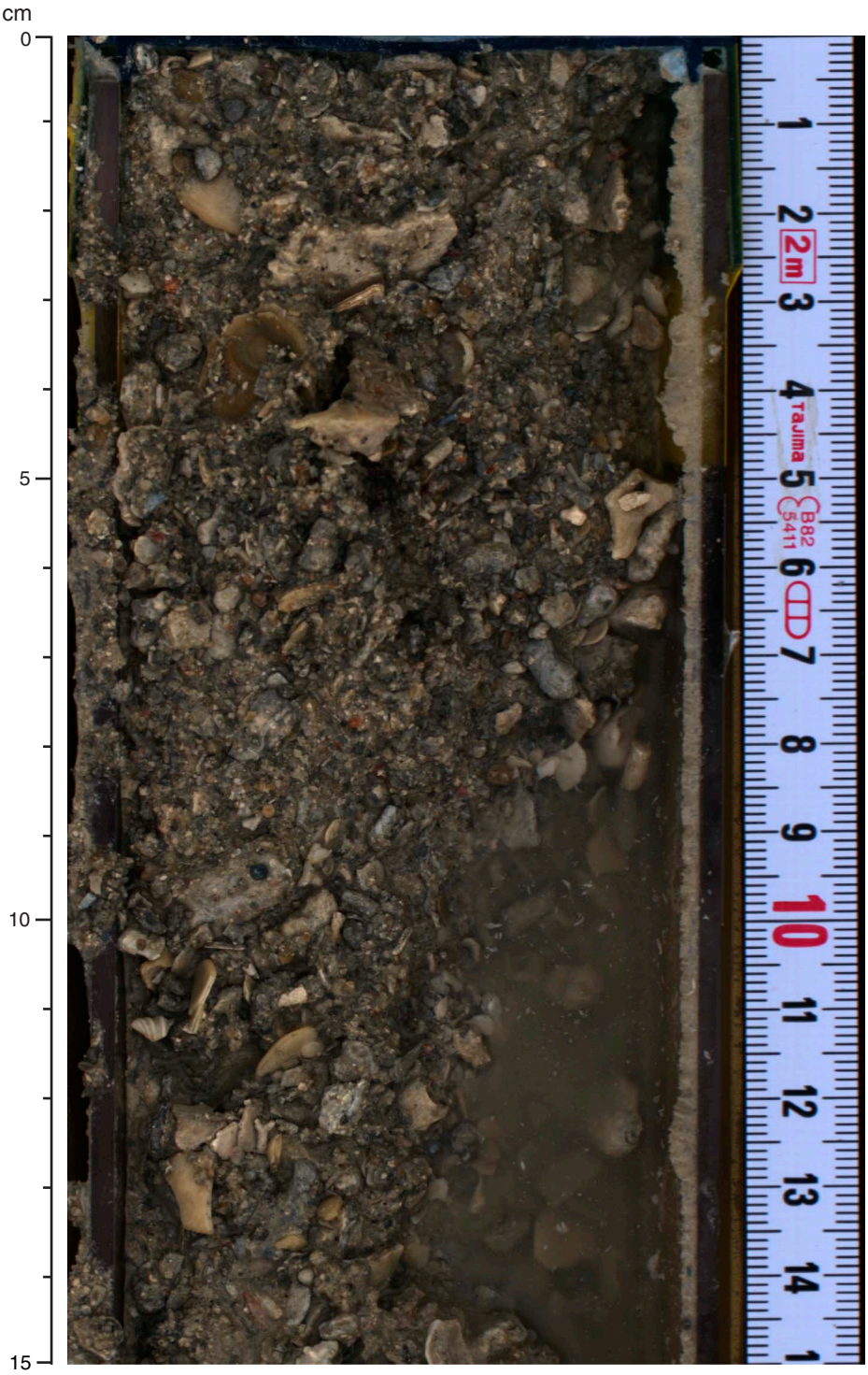

Figure F30. High-resolution line scan image of (from top): 0–7 cm, dark gray medium to coarse lime sand with corals (*Porites* or *Montipora* fragments) and larger foraminifera; 7–20 cm, massive *Cyphastrea;* and 20–30 cm, dark gray, medium to coarse sand with unidentified corals, mollusks, and larger foraminifera (interval 325-M0053A-31R-1, 0–30 cm).

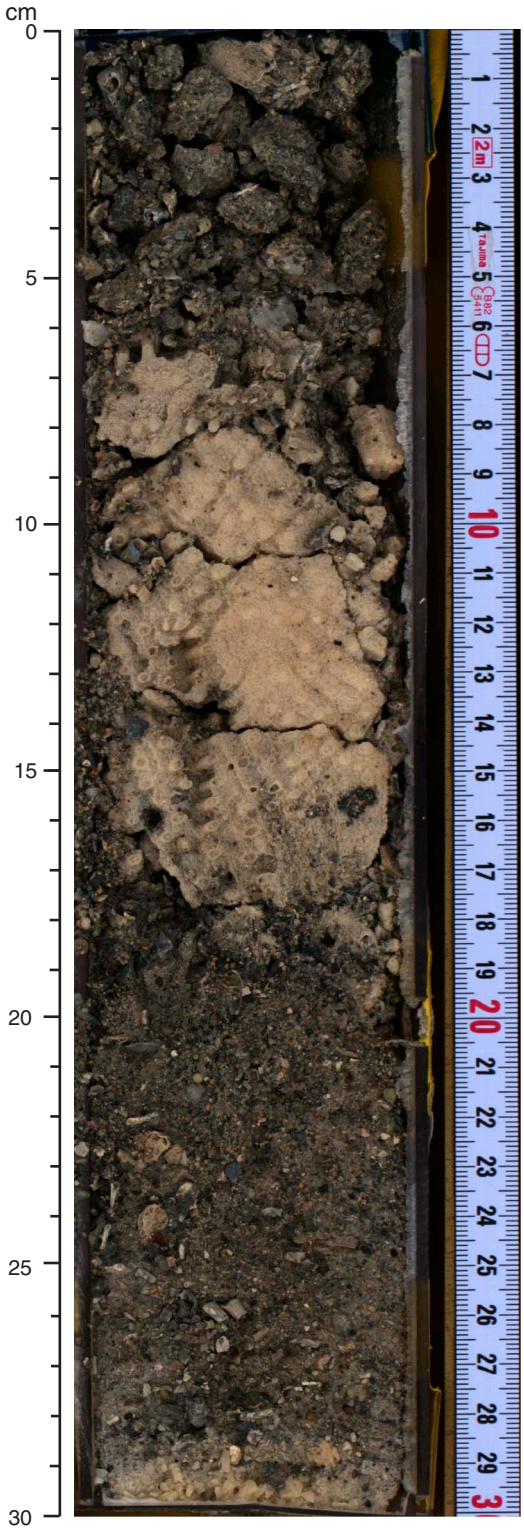

Figure F31. Summary diagram showing data collected on whole cores using the MSCL, Hole M0053A.

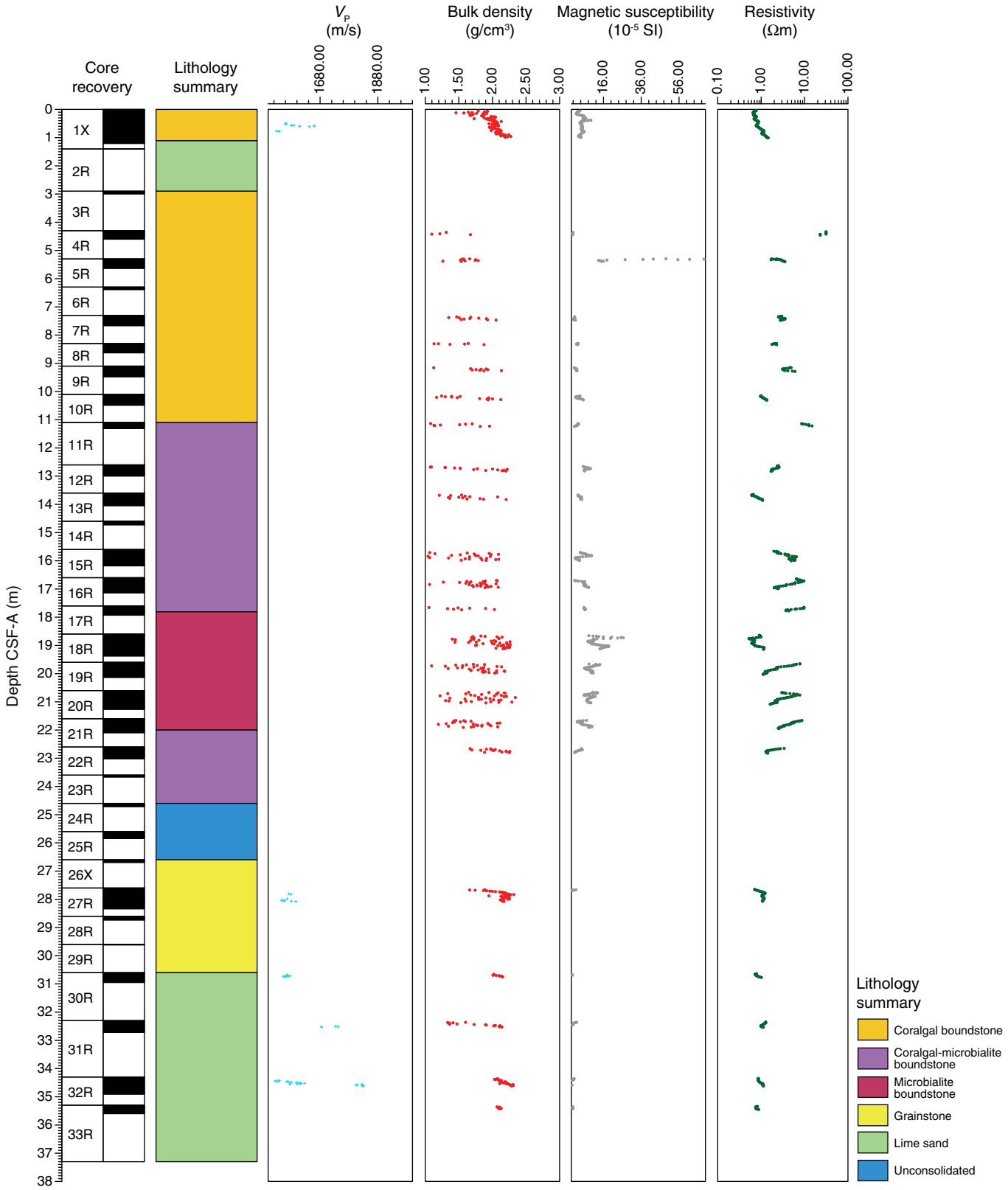

Figure F32. Petrophysical measurements obtained from discrete samples with a pycnometer, Hole M0053A. Bulk density measured on whole cores with the MSCL is shown in red on the bulk density plot.

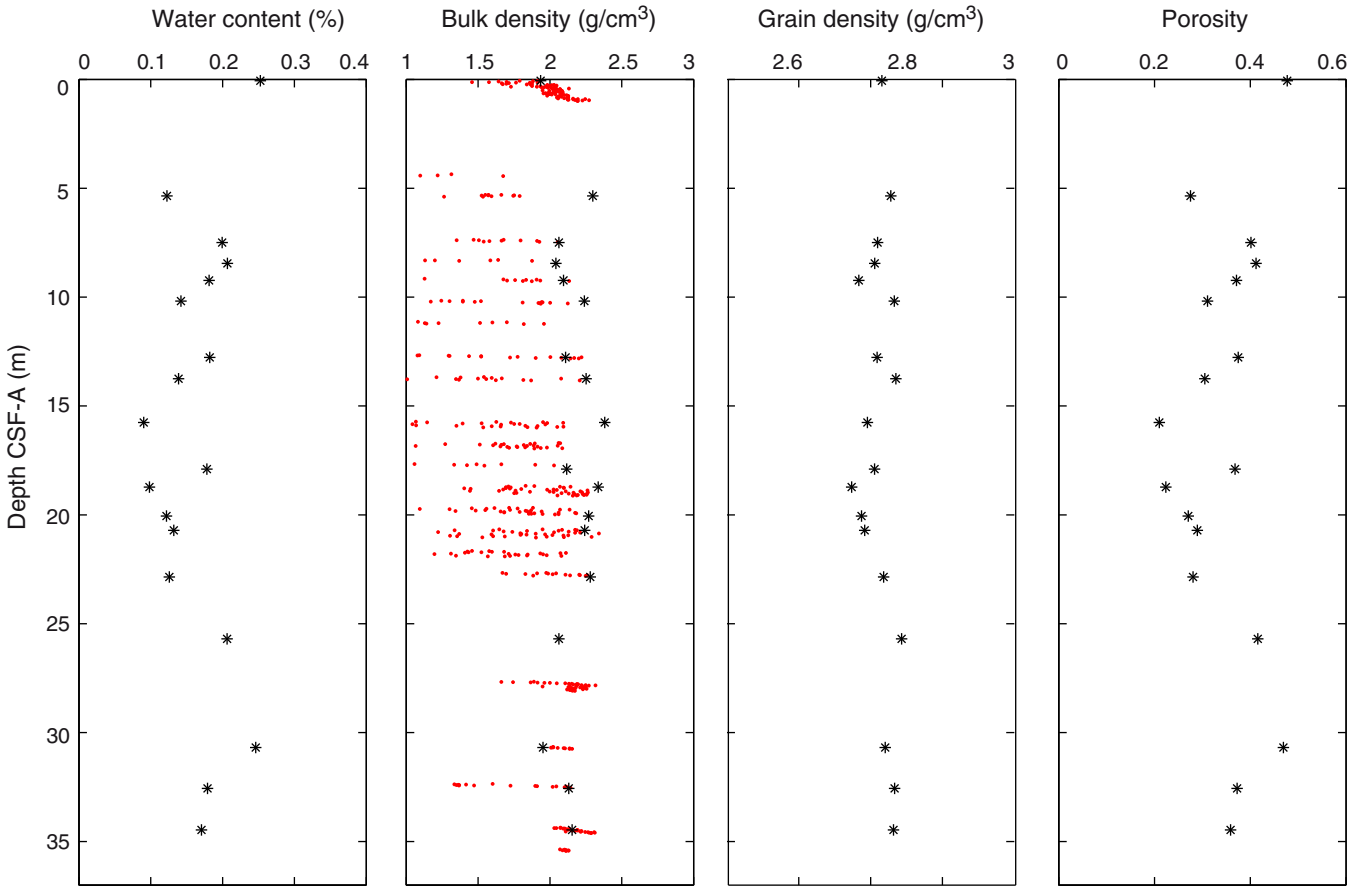

Figure F33. *P*-wave velocity data, Hole M0053A. **A.** Plot of initial, dry, and resaturated *P*-wave velocity measurements on discrete samples vs. depth. Three measurements were taken at each depth and are denoted by a dot. Average values are plotted as an open triangle. **B.** Plot showing discrete *P*-wave velocity vs. discrete bulk density.

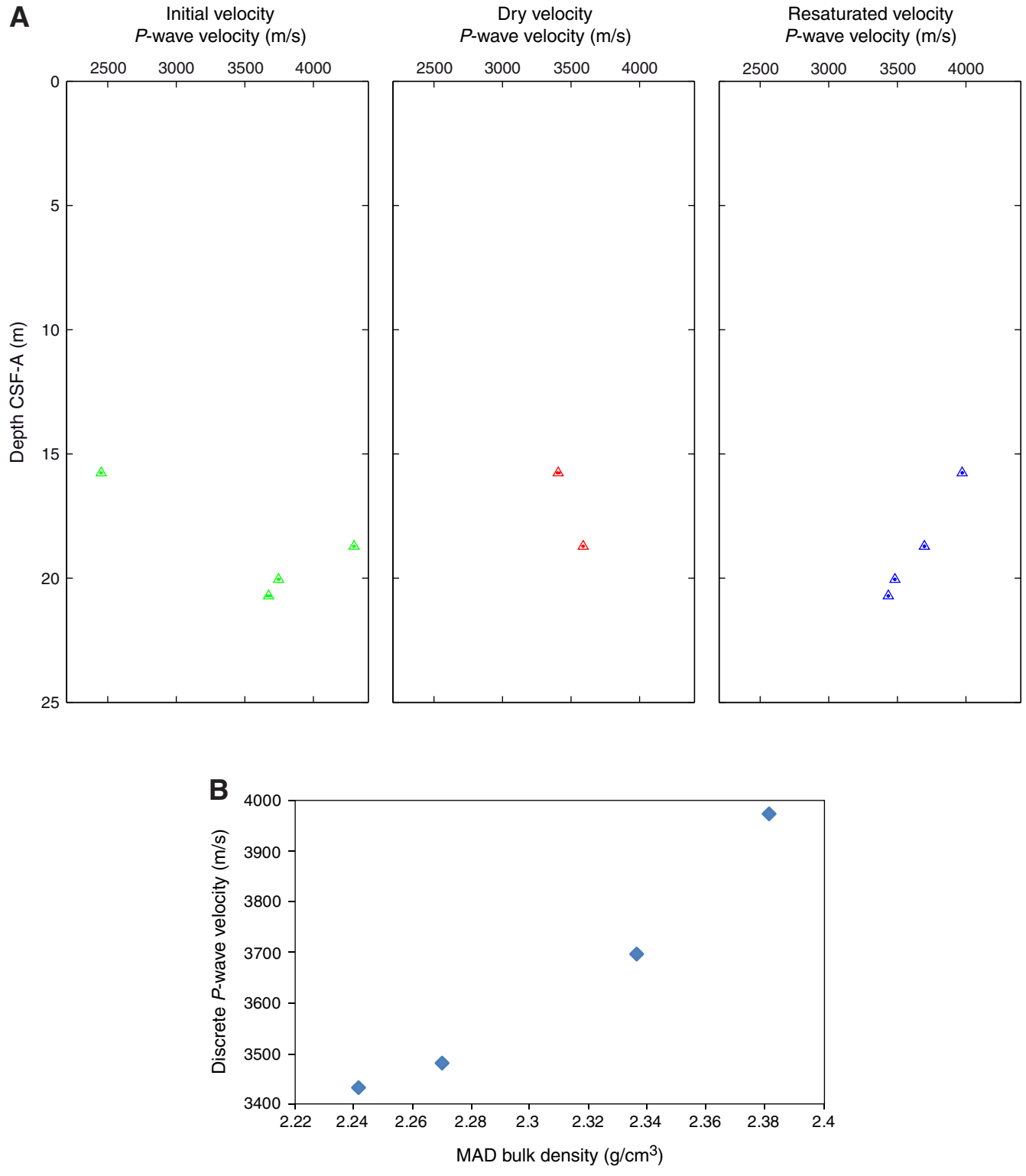

Figure F34. Values of reflectance (L*), green to red (a*), and blue to yellow (b*) indexes, along with ratio a*/b* for Hole M0053A.

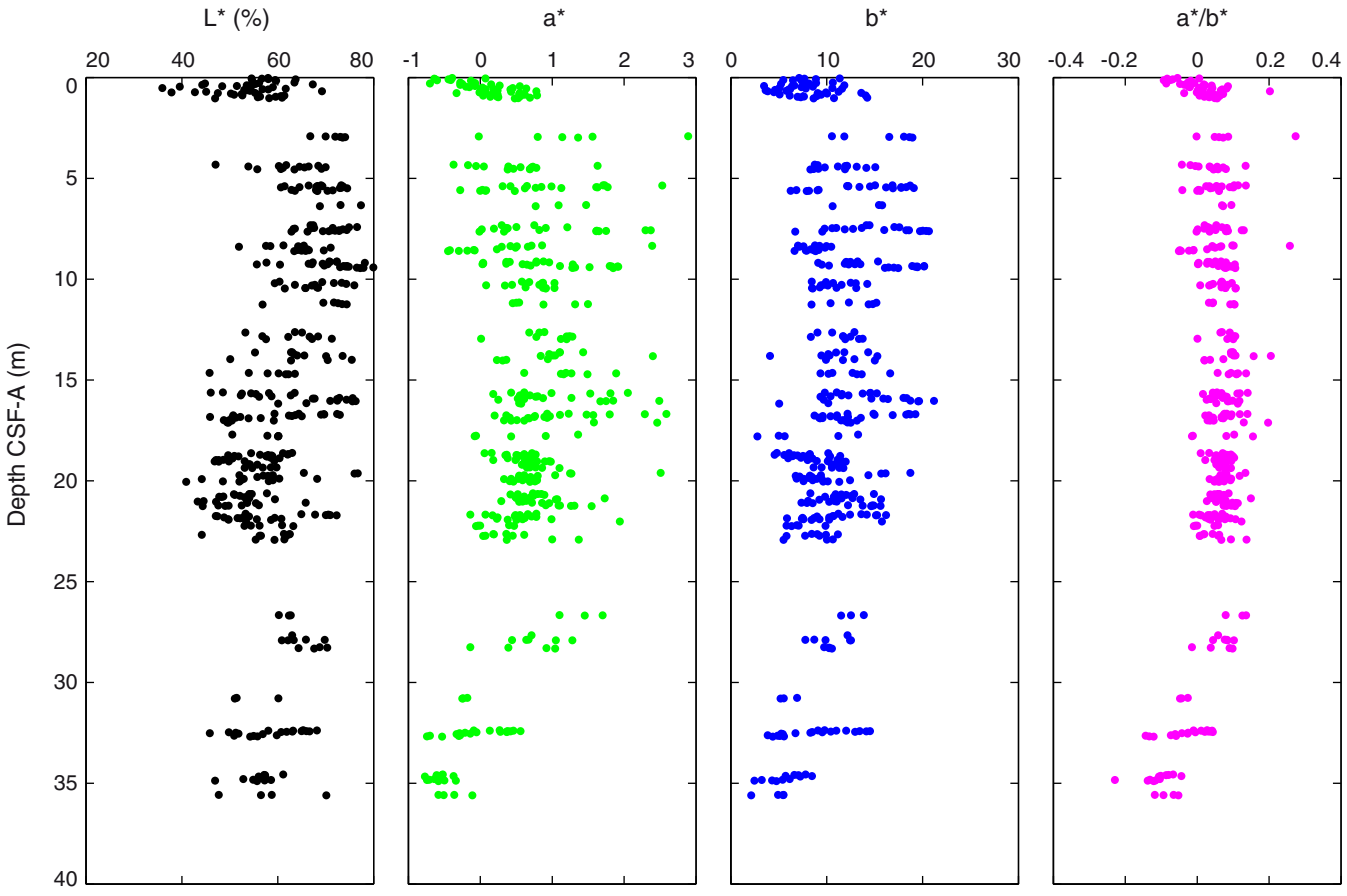

Figure F35. Plot of thermal conductivity vs. depth, Hole M0053A. Error bars indicate the standard deviation.

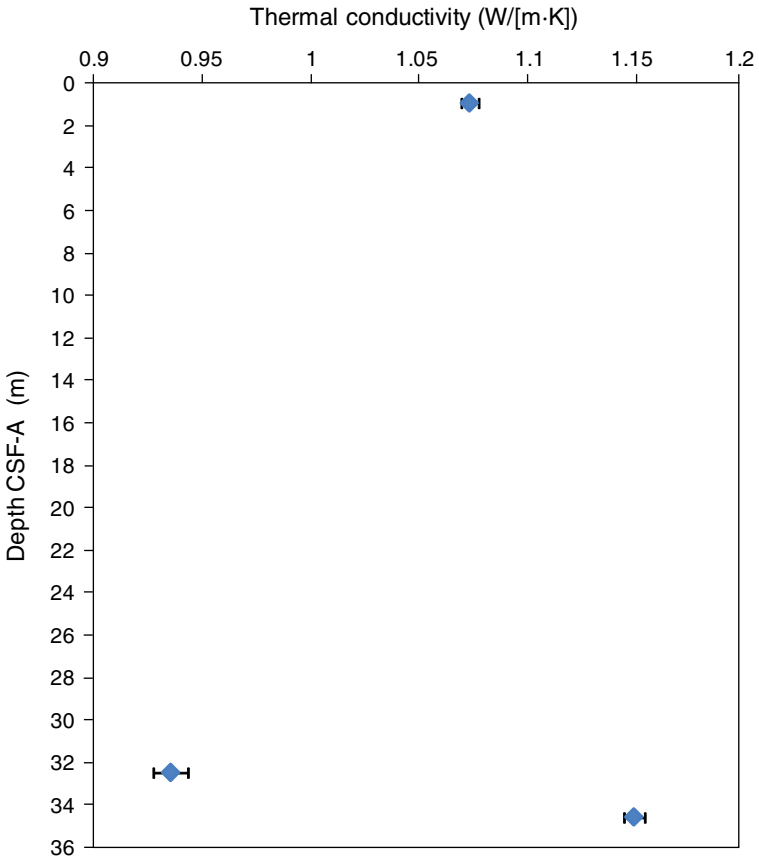

Figure F36. Magnetic susceptibility record for Hole M0053A. Water depth = 97.87 m (LAT).

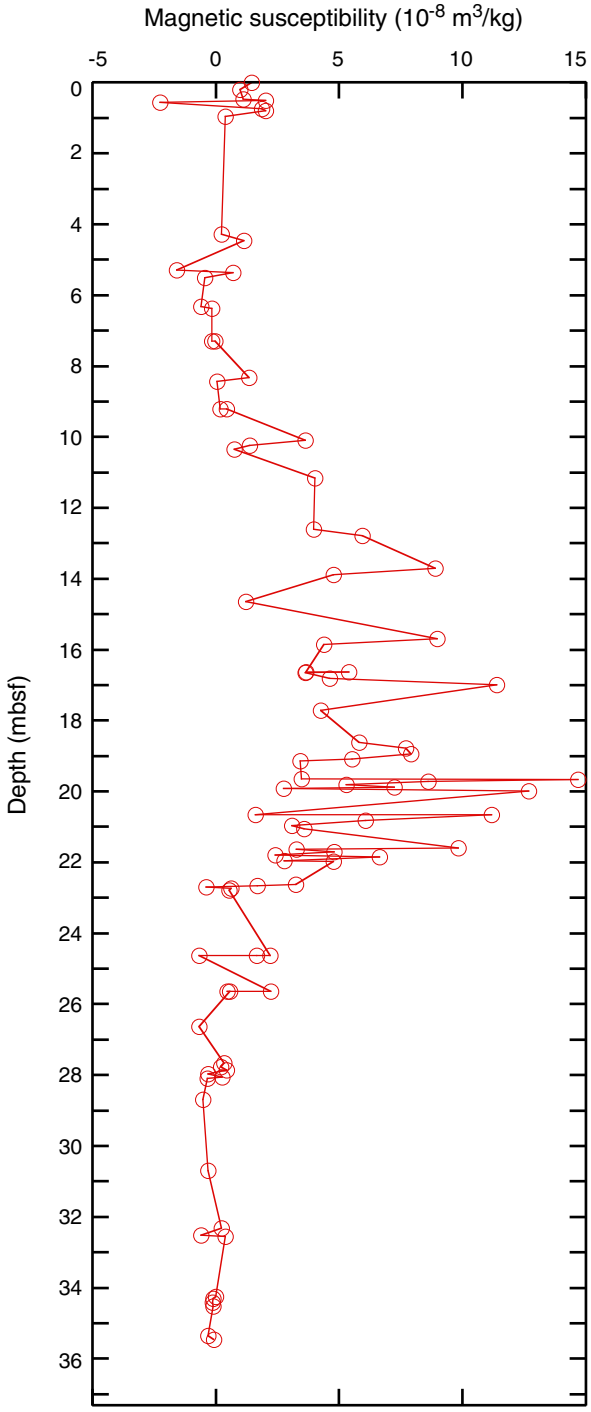

Figure F37. Preliminary chronology for Hole M0053A. Radiocarbon data are presented as graphs with the uncalibrated radiocarbon age and uncertainty shown as the red normal distribution on the ordinate axis and the probability distribution of the calibrated age shown in gray on the abscissa. The marine09 calibration curve is shown in blue. Horizontal bars indicate portions of the age distribution that are significant at the 95.4% confidence interval and the mean age (white circle ±1 standard deviation) used for the purposes of the preliminary dating. All ages are presented as thousands of calendar years BP (1950 AD). See Table **T10** in the "Methods" chapter. (See Bronk Ramsey [2009], as well as Bronk Ramsey [2010] at **c14.arch.ox.ac.uk/oxcal.html.**)

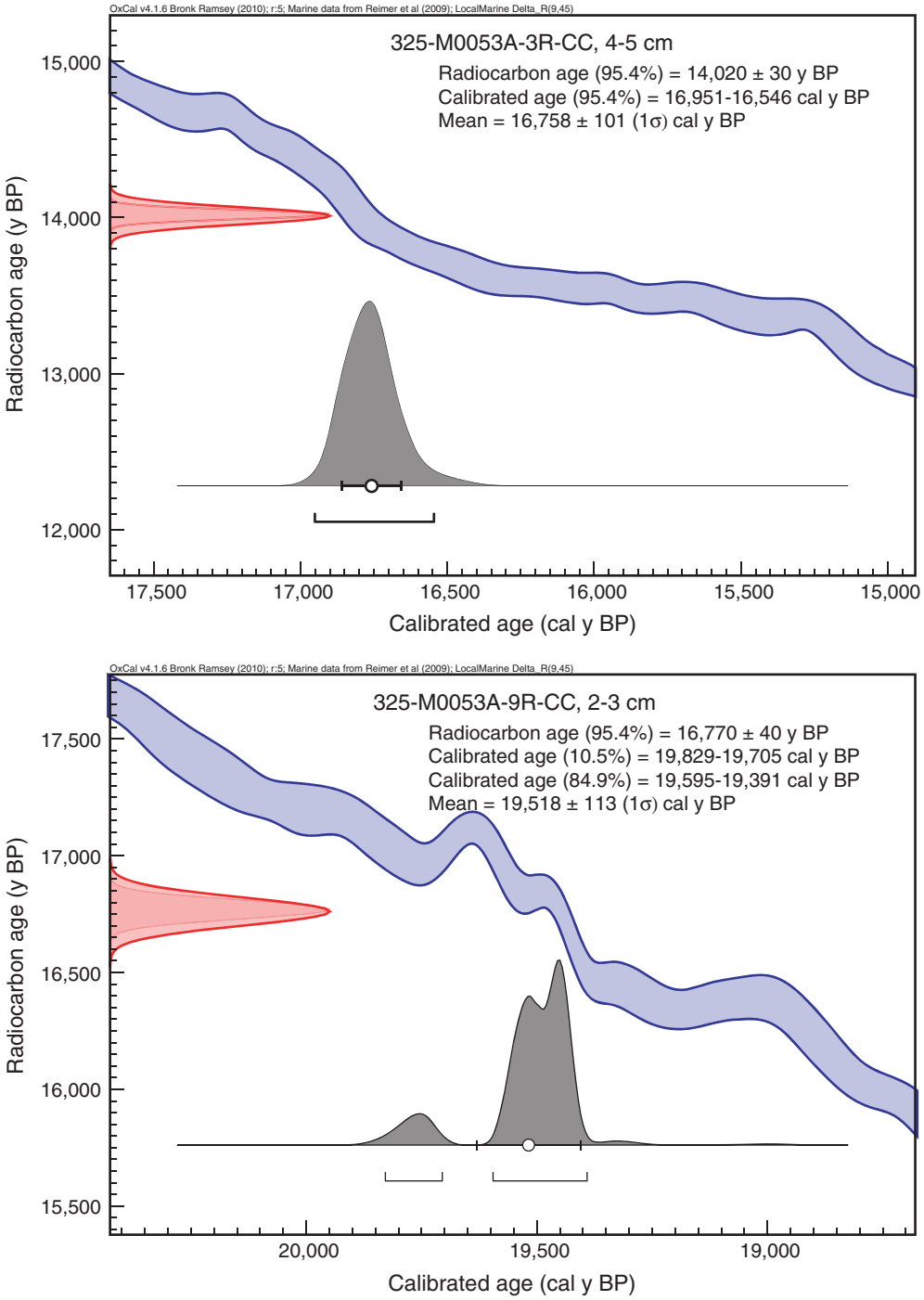

Figure F38. High-resolution line scan image of fine branching *Seriatopora* encrusted by thick coralline algae (interval 325-M0054A-3R-1, 49–59 cm).

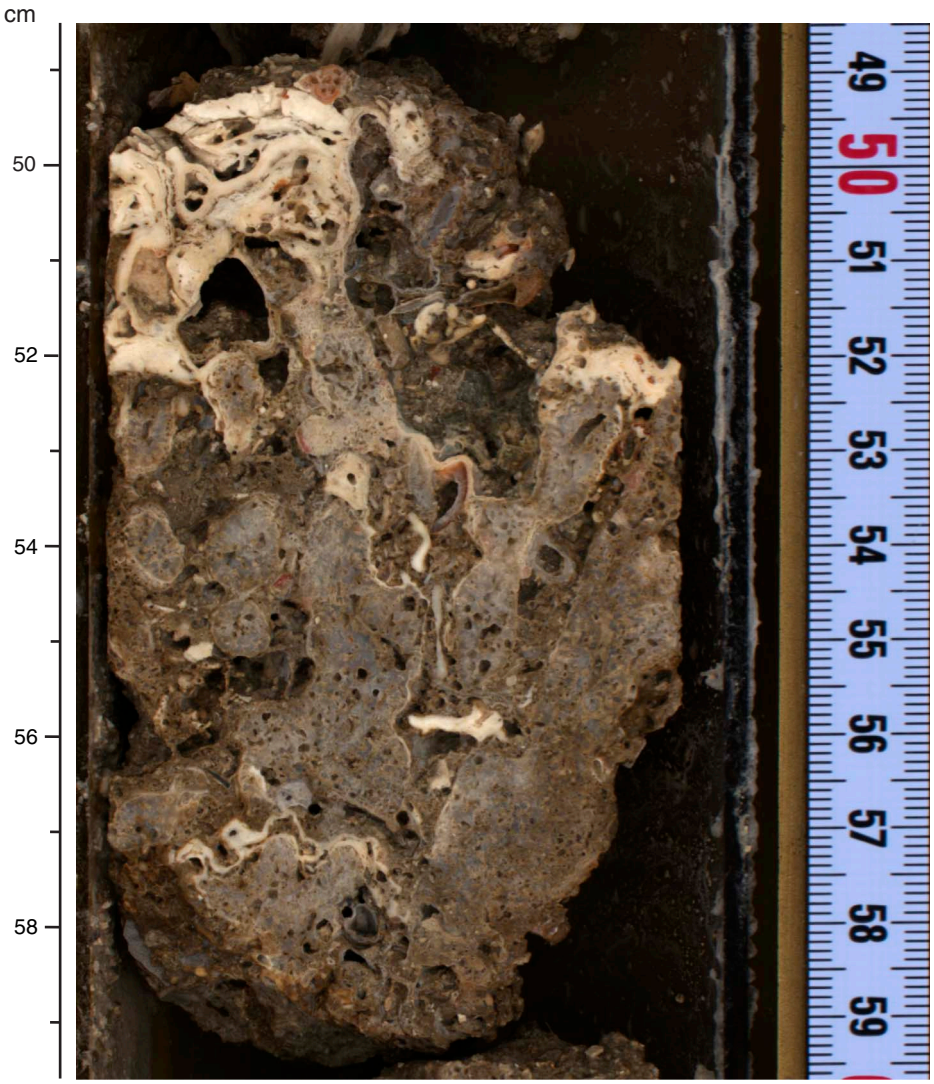

Figure F39. High-resolution line scan image of a massive *Galaxea fascicularis* (not in situ) and *Favia* encrusted by thin to thick coralline algae (interval 325-M0054A-2R-1, 21–31 cm). Internal sediment contains *Halimeda*.

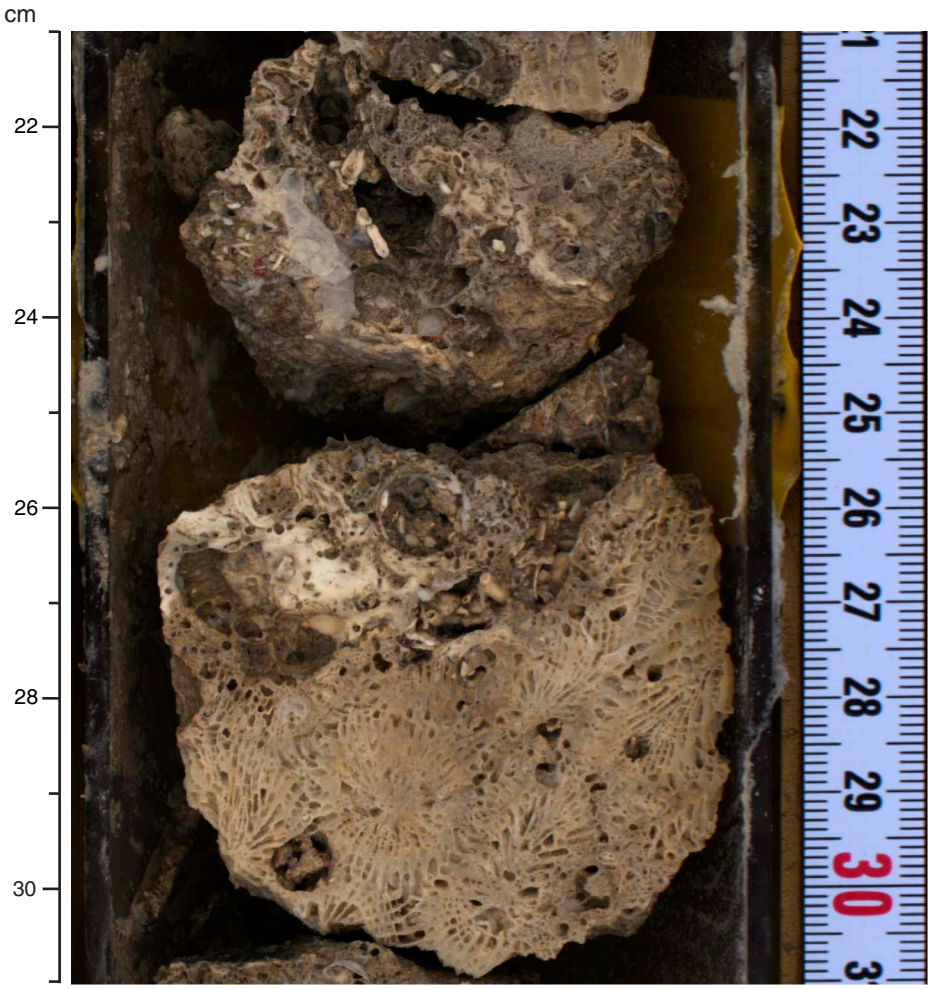

Figure F40. High-resolution line scan image of a coral framework of encrusting *Porites* or *Montipora,* fine to medium branching *Acropora* (not in situ), and fine branching *Seriatopora* (in situ?), encrusted by thin to thick coralline algae (interval 325-M0054A-4R-1, 7–32 cm).

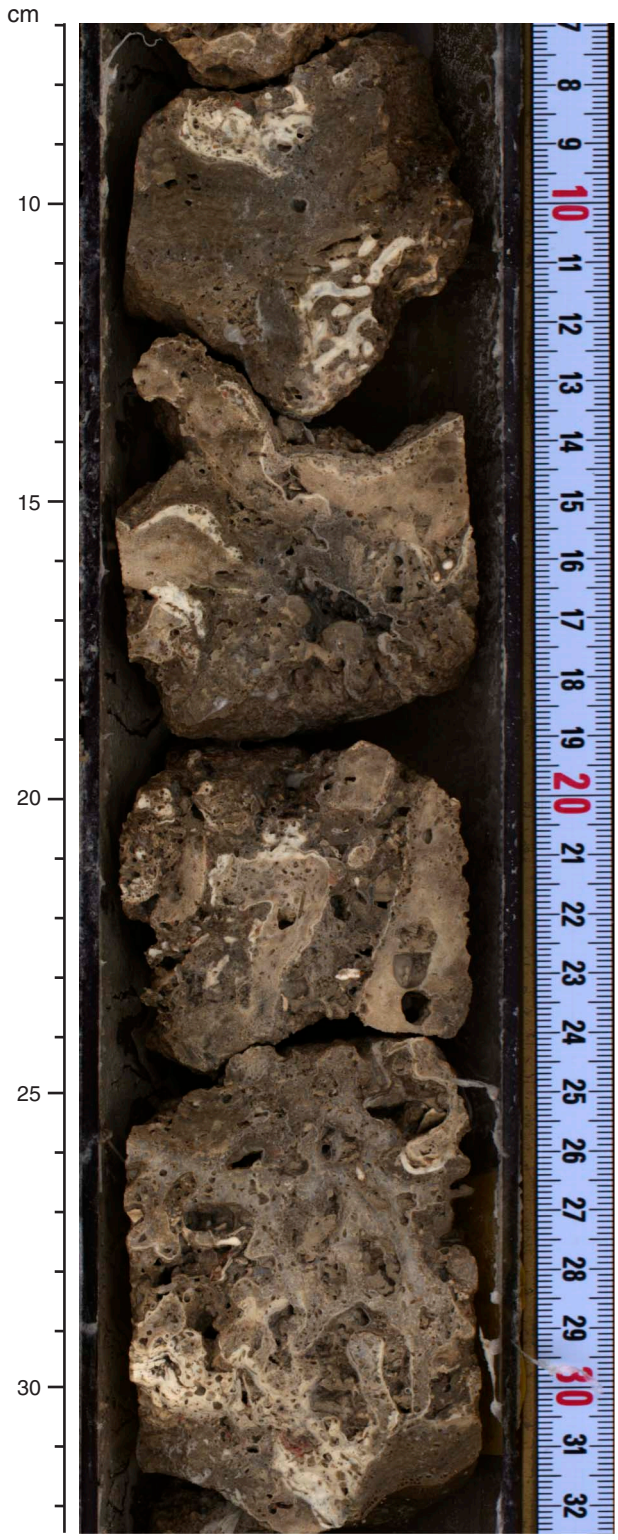

Figure F41. Summary diagram showing data collected on whole cores using the MSCL, Hole M0054A.

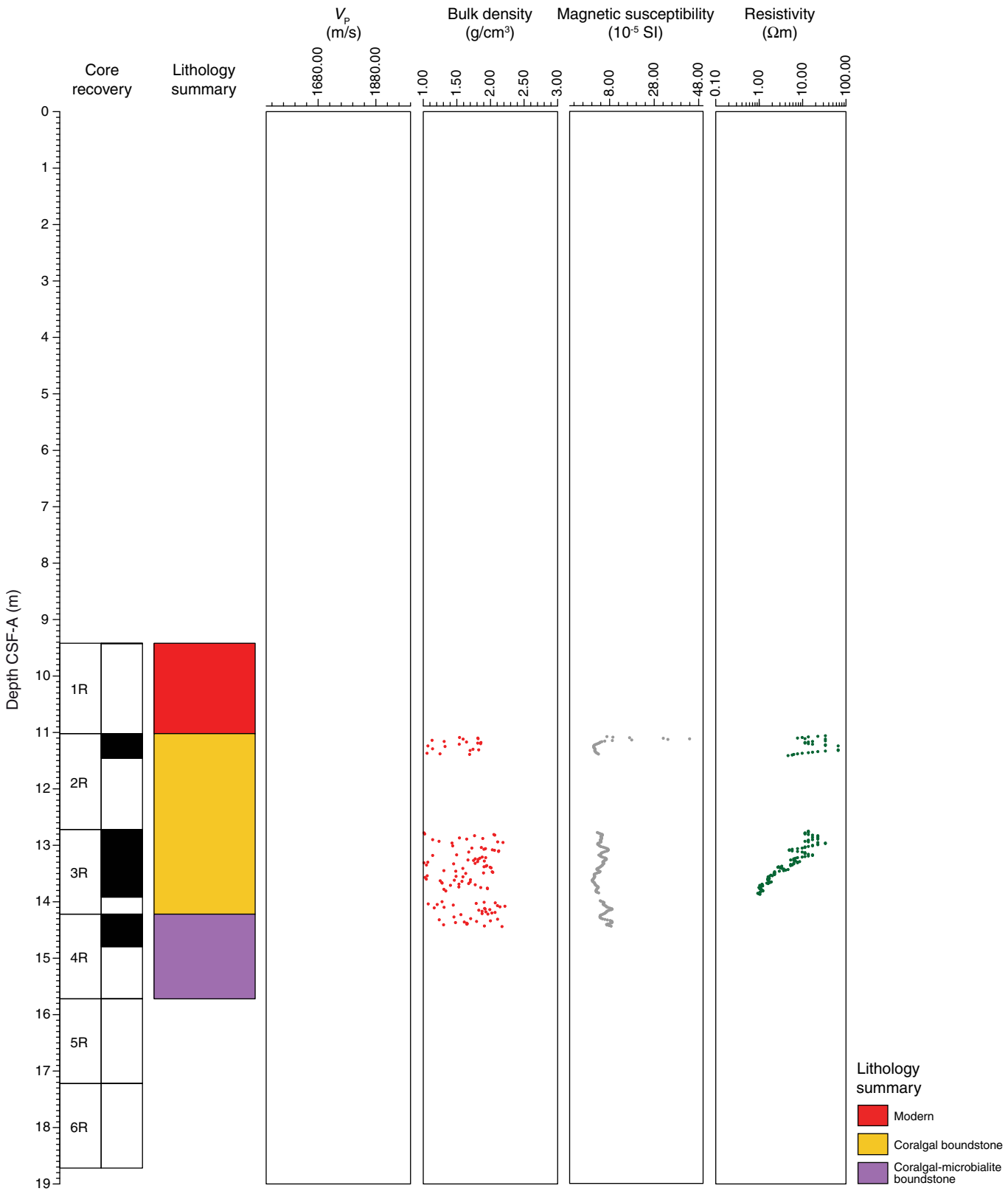

Figure F42. Petrophysical measurements obtained from discrete samples with a pycnometer, Hole M0054A. Bulk density measured on whole cores with the MSCL is shown in red on the bulk density plot.

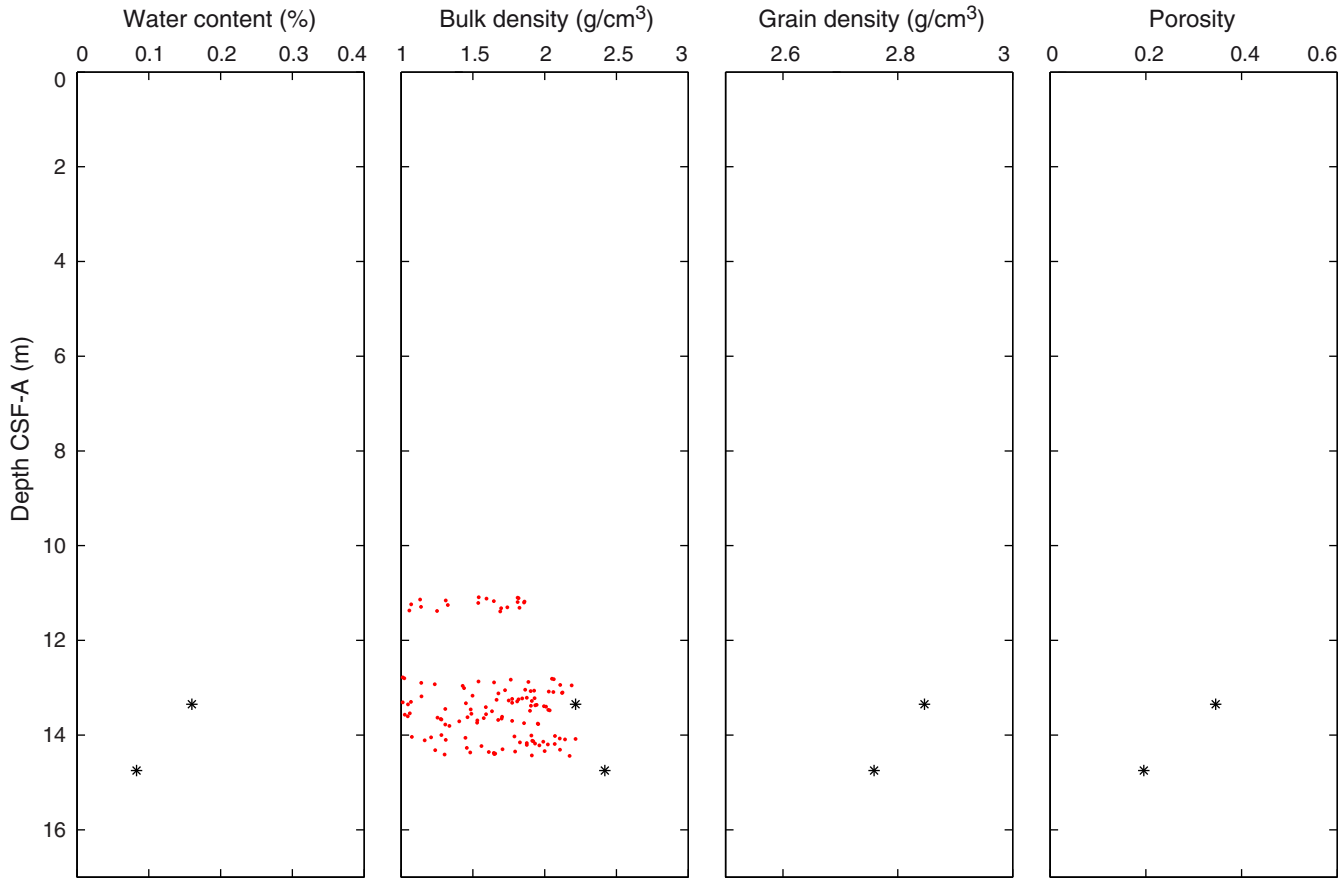

Figure F43. *P*-wave velocity data, Hole M0054A. **A.** Plot of initial, dry, and resaturated *P*-wave velocity measurements on discrete samples vs. depth. Three measurements were taken at each depth and are denoted by a dot. Average values are plotted as an open triangle. **B.** Plot showing discrete *P*-wave velocity vs. discrete bulk density.

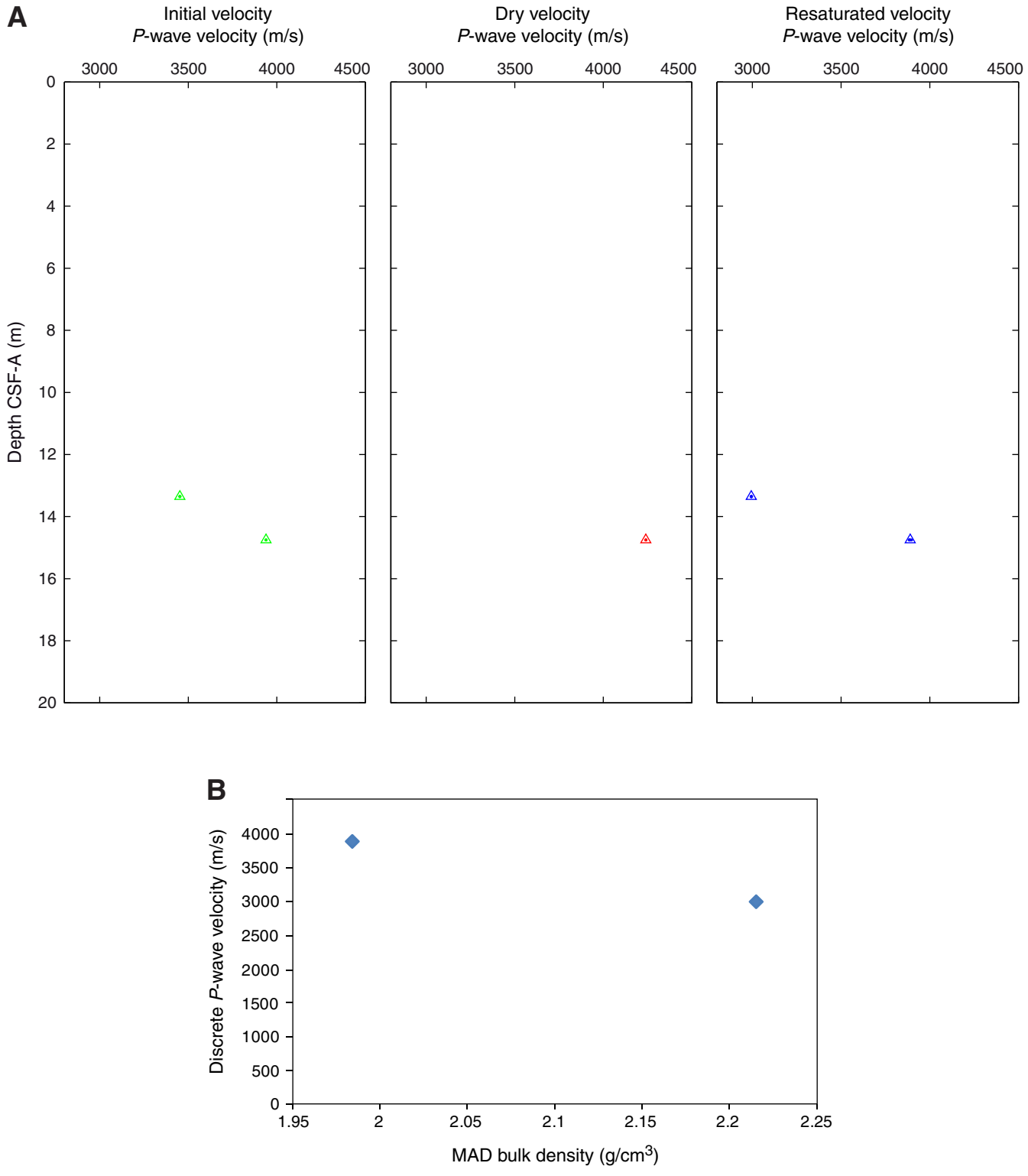

Figure F44. Values of reflectance (L*), green to red (a*), and blue to yellow (b*) indexes, along with ratio a*/b* for Hole M0054A.

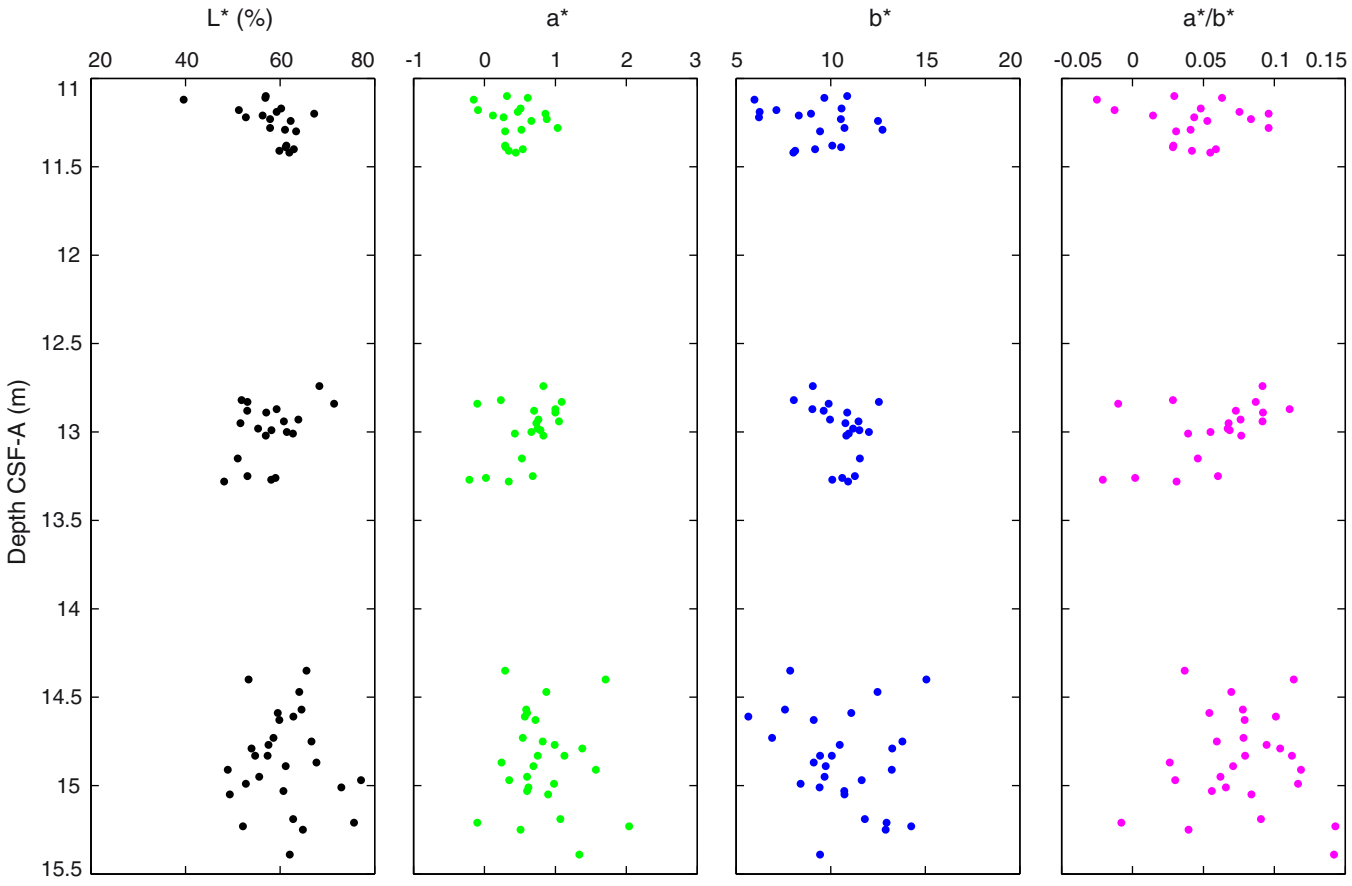

Figure F45. Magnetic susceptibility record for Hole M0054A. Water depth = 107.23 m (LAT).

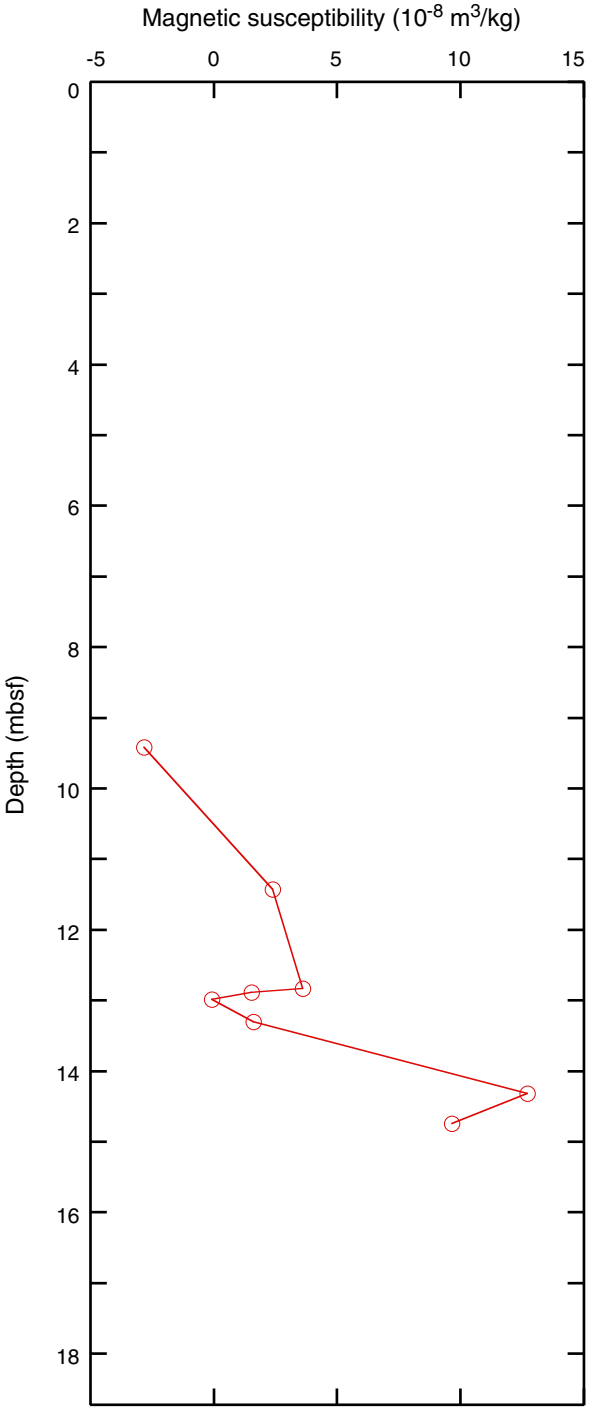

Figure F46. High-resolution line scan image of a framework of encrusting and submassive *Montipora* encrusted by thick coralline algae and laminated microbialite (interval 325-M0054B-4R-1, 20–40 cm).

Figure F47. High-resolution line scan image of an encrusting *Montipora*? (in situ?) and fine branching *Seriatopora* encrusted by thick coralline algae and microbialite (interval 325-M0054B-7R-1, 11–25 cm).

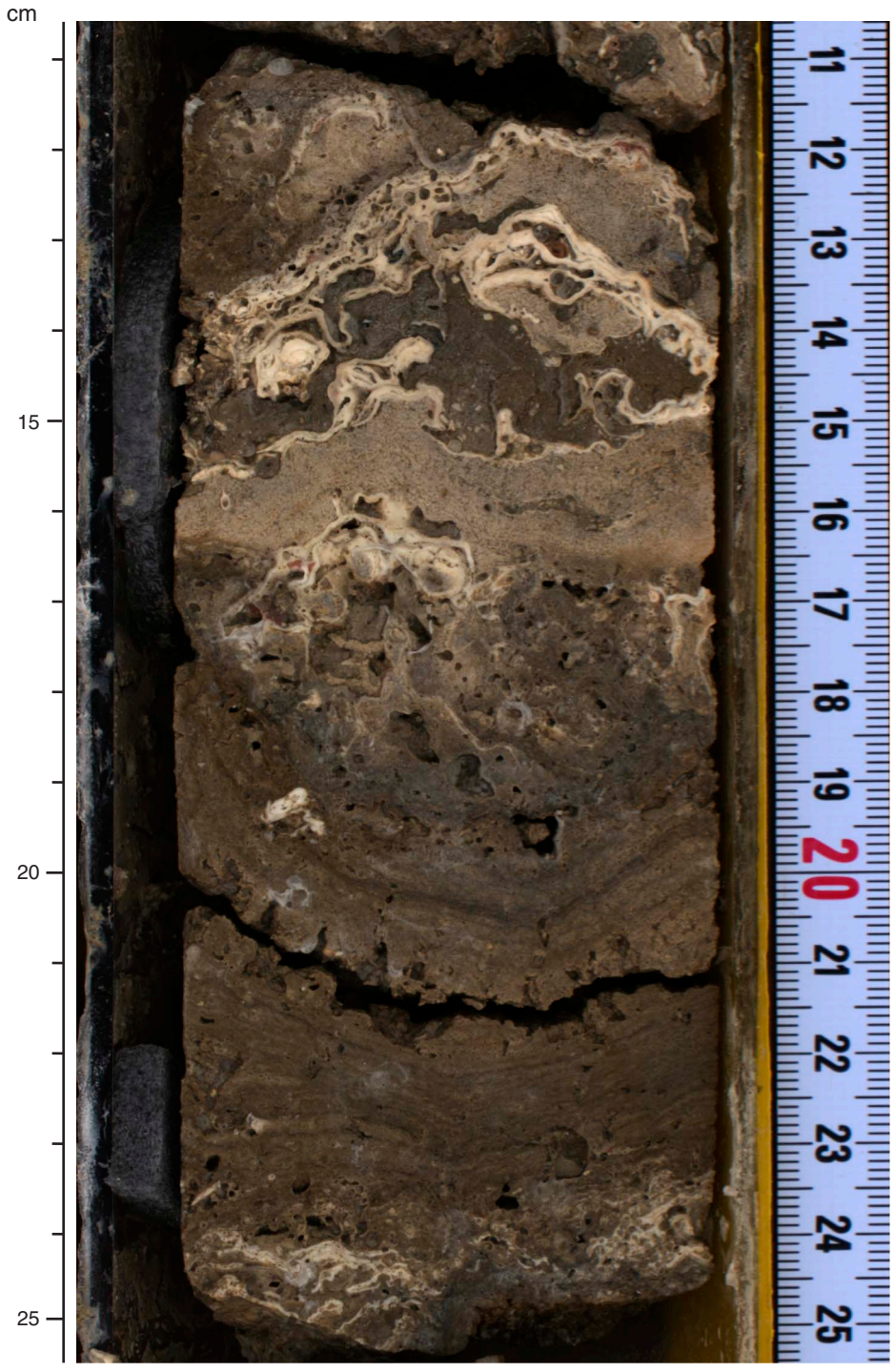

Figure F48. High-resolution line scan image of a bioeroded coral encrusted by thick coralline algae and well-laminated microbialite (interval 325-M0054B-7R-1, 95–104 cm).

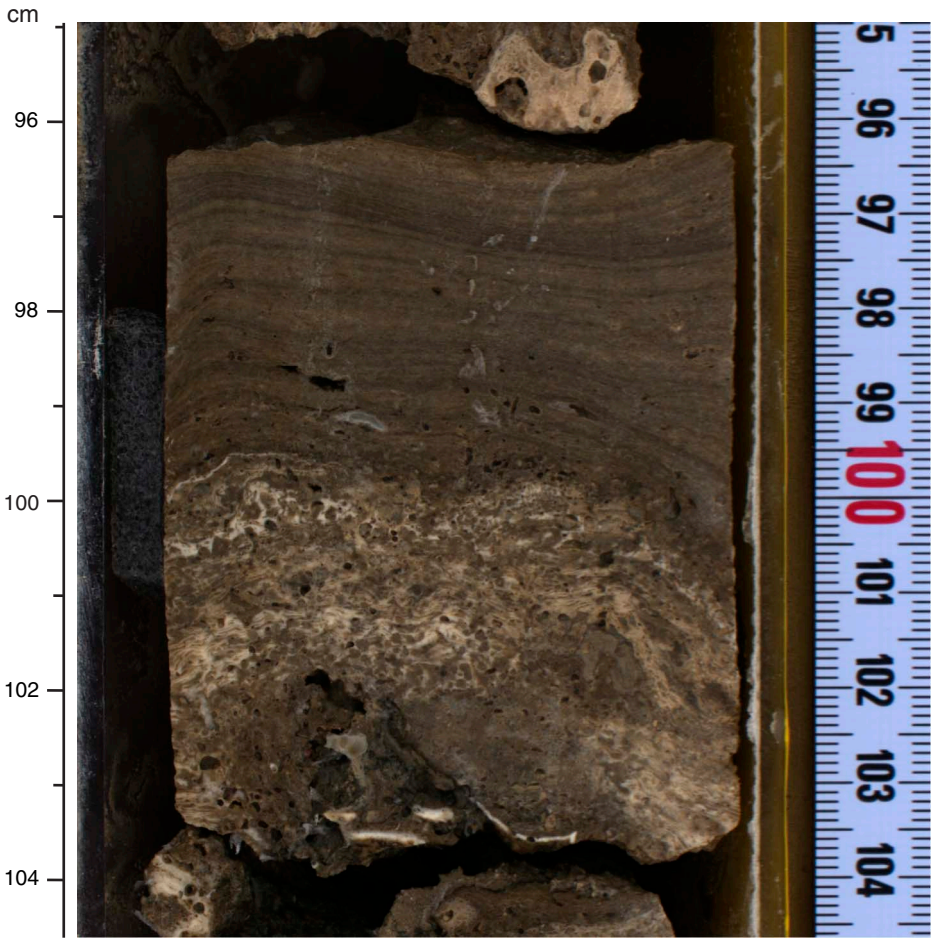

Figure F49. High-resolution line scan image of a highly altered coral framework encrusted by microbialites and infilled with *Halimeda*-rich internal sediment (interval 325-M0054B-8R-2, 39–58 cm). Microbialites show two phases of growth.

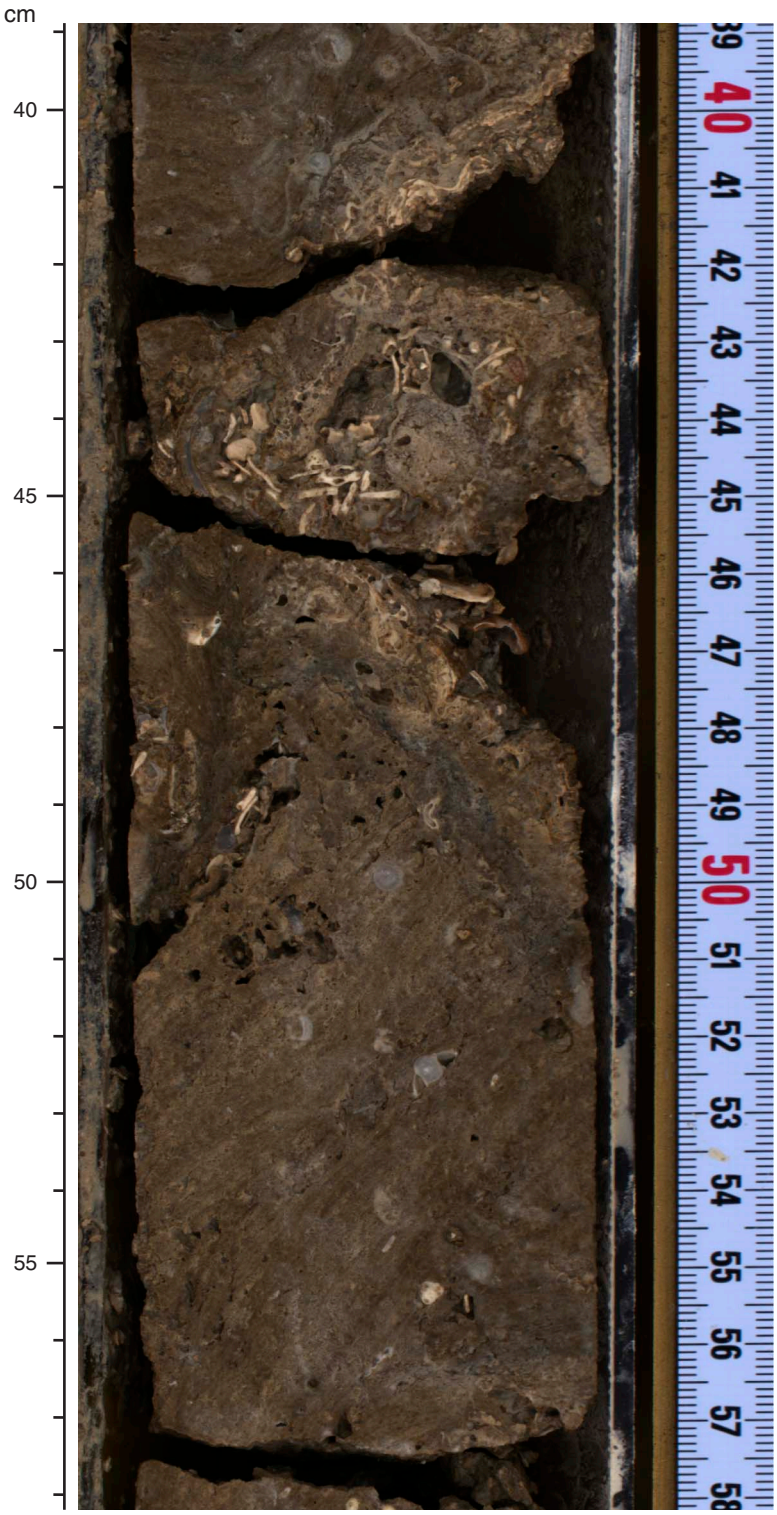

Figure F50. High-resolution line scan image of internal sediment composed of consolidated *Halimeda*-rich floatstone to rudstone (interval 325-M0054B-8R-1, 65–71 cm).

Figure F51. High-resolution line scan image of (at the base) a medium branching *Acropora* encrusted by thick coralline algae (interval 325-M0054B-7R-1, 41–55 cm). At the top, a very thin in situ encrusting coral (encrusted by microbialites) covers an algal crust.

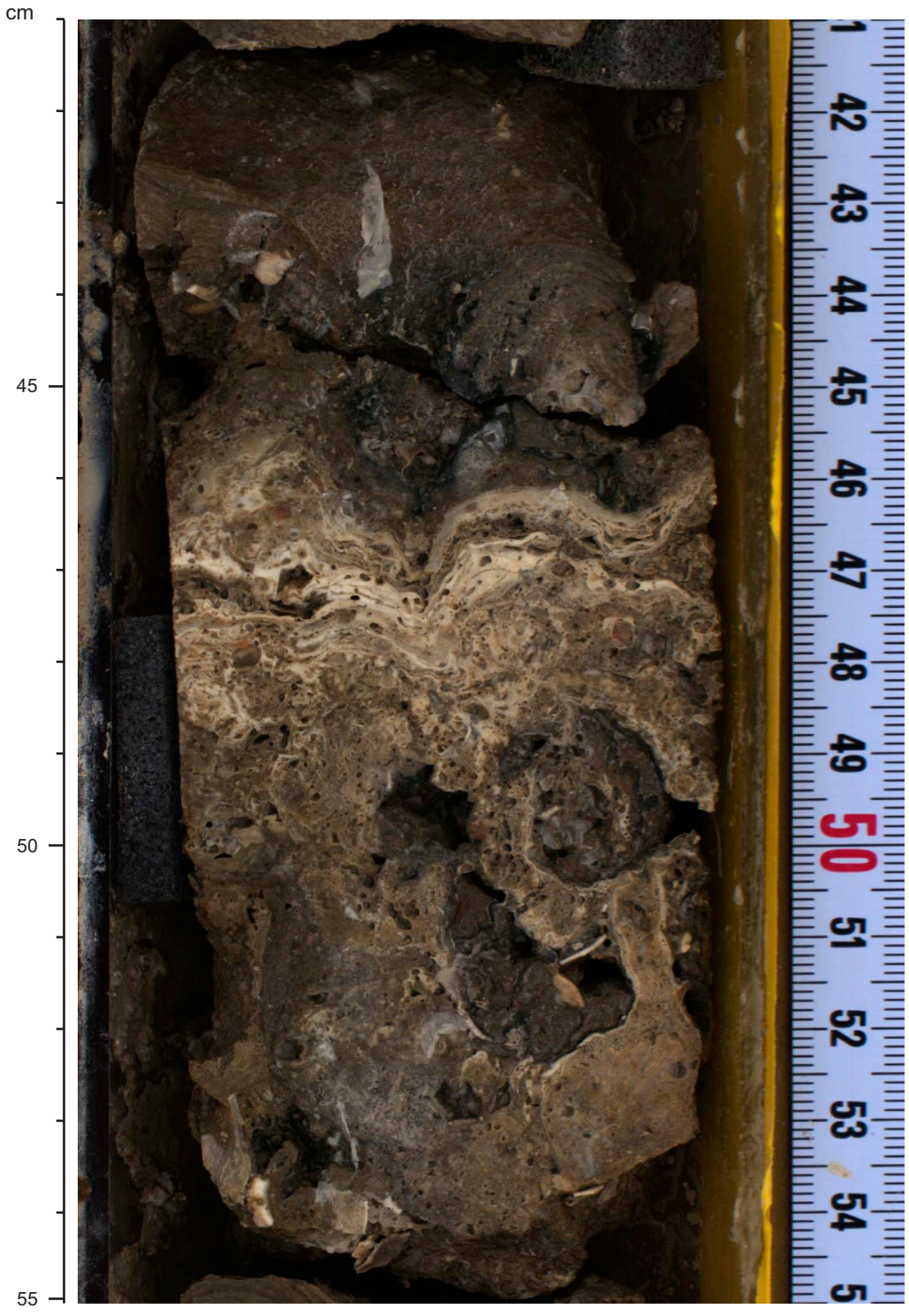

Figure F52. High-resolution line scan image of a framework of platy *Porites*(?) and fine branching *Acropora* encrusted by thick coralline algae and laminated microbialites (interval 325-M0054B-6R-1, 10–28 cm).

Figure F53. High-resolution line scan image of a massive *Tubipora musica* (in situ?) encrusted by thick coralline algae and laminated microbialites (interval 325-M0054B-6R-1, 66–83 cm).

Figure F54. High-resolution line scan image of a bioeroded framework of massive *Cyphastrea* and massive Faviidae encrusted by thick coralline algae and microbialites (interval 325-M0054B-8R-2, 65–80 cm).

Figure F55. High-resolution line scan image of a massive *Porites* (in situ?) (interval 325-M0054B-9R-1, 3–9 cm).

Figure F56. High-resolution line scan image of a medium branching corymbose *Acropora* (interval 325-M0054B-9R-1, 15–22 cm).

Figure F57. High-resolution line scan image of rudstone with *Halimeda,* mollusk fragments, and larger foraminifera (interval 325-M0054B-10R-1, 13–24 cm).

Figure F58. Summary diagram showing data collected on whole cores using the MSCL, Hole M0054B.

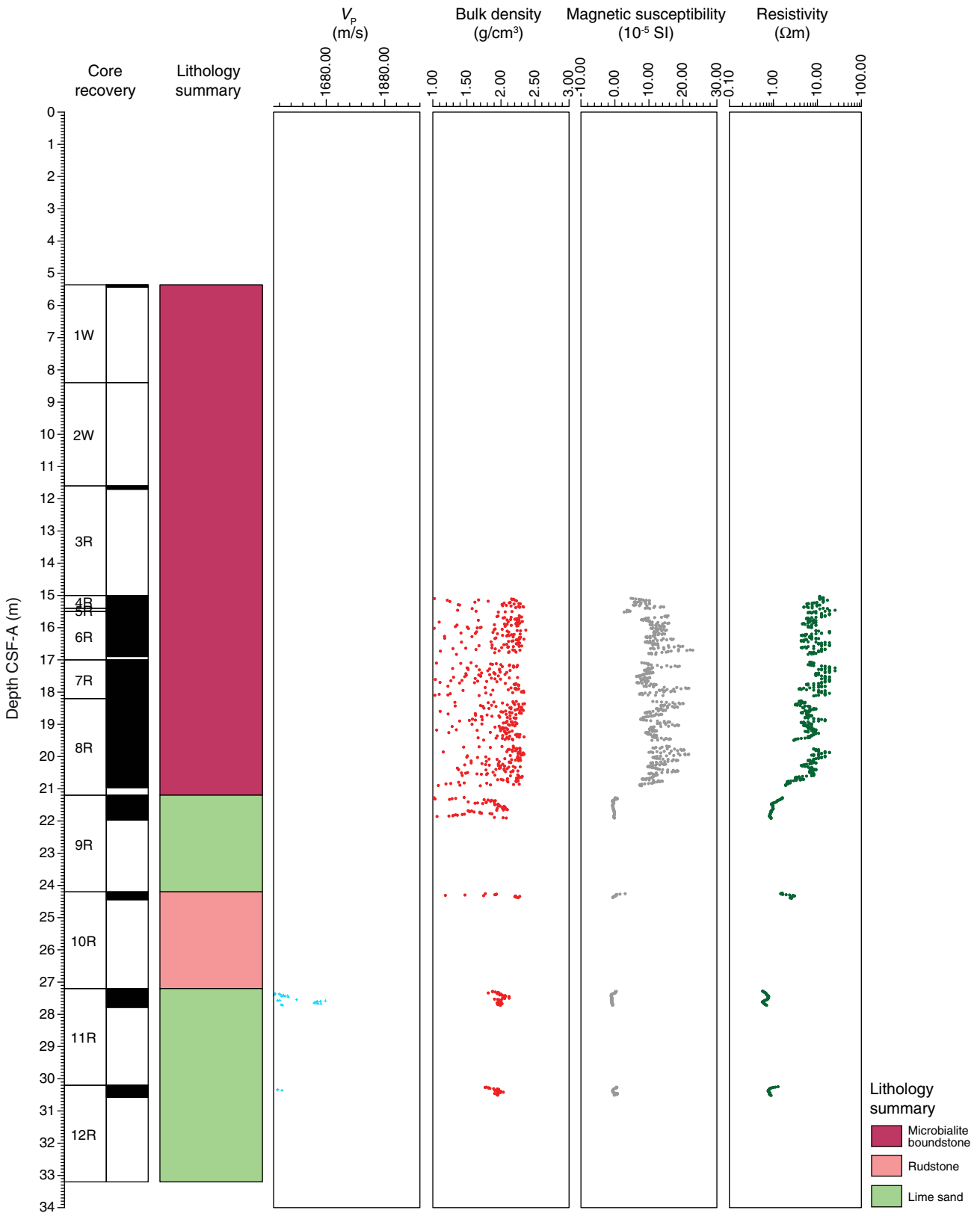

Figure F59. Petrophysical measurements obtained from discrete samples with a pycnometer, Hole M0054B. Bulk density measured on whole cores with the MSCL is shown in red on the bulk density plot.

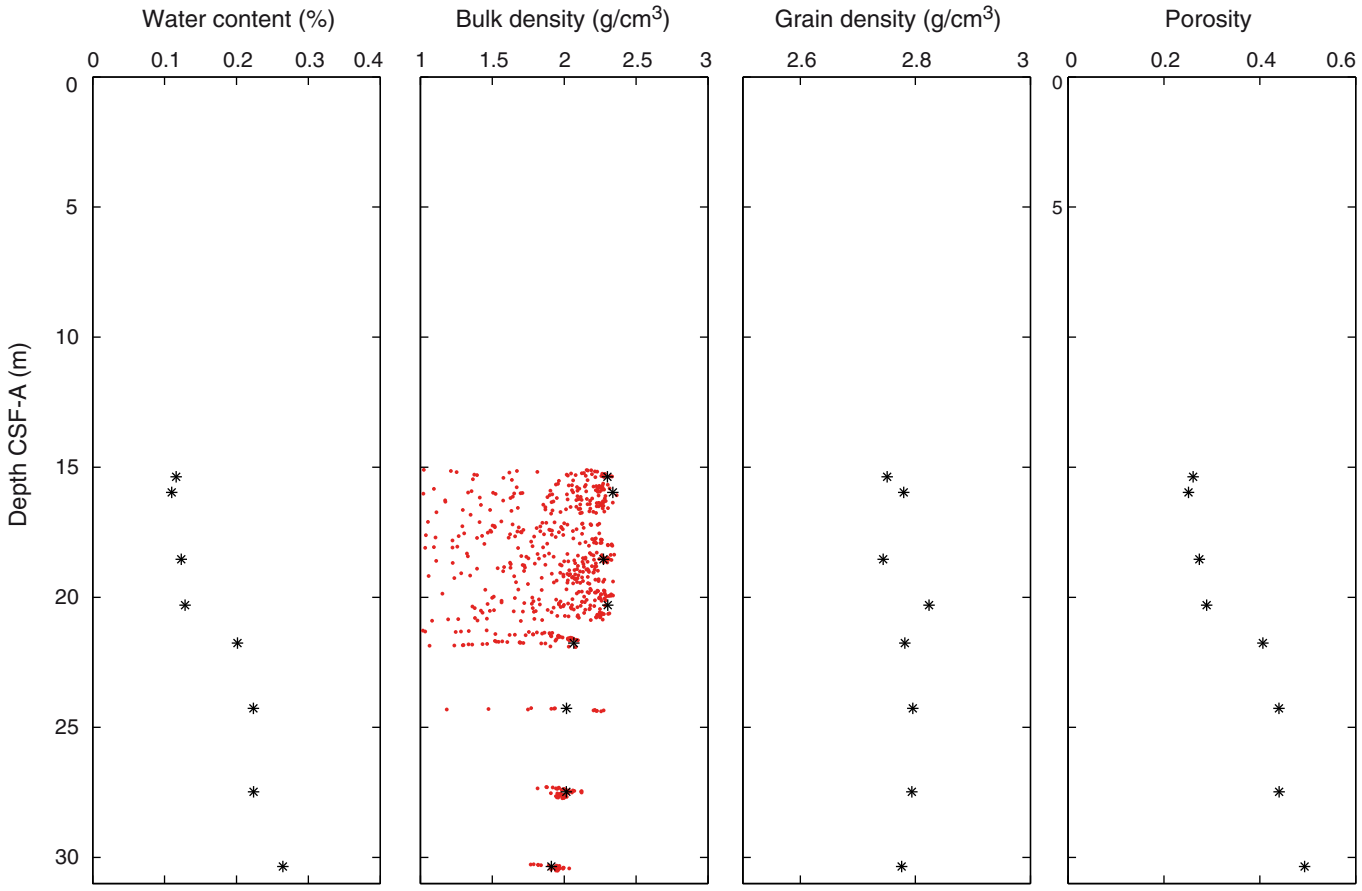

Figure F60. *P*-wave velocity data, Hole M0054BA. **A.** Plot of initial, dry, and resaturated *P*-wave velocity measurements on discrete samples vs. depth. Three measurements were taken at each depth and are denoted by a dot. Average values are plotted as an open triangle. **B.** Plot showing discrete *P*-wave velocity vs. discrete bulk density.

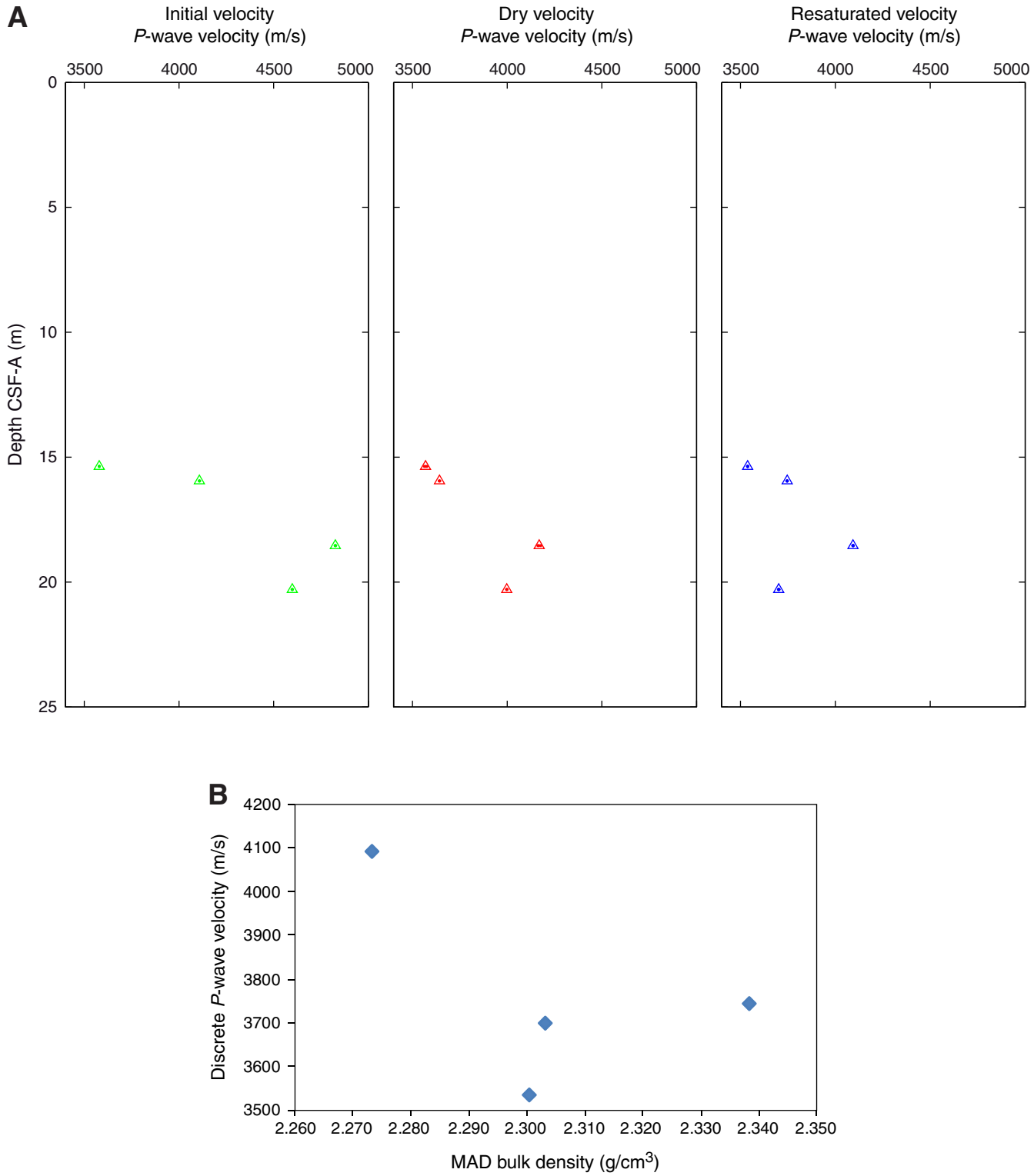

Figure F61. Values of reflectance (L*), green to red (a*), and blue to yellow (b*) indexes, along with ratio a*/b* for Hole M0054B.

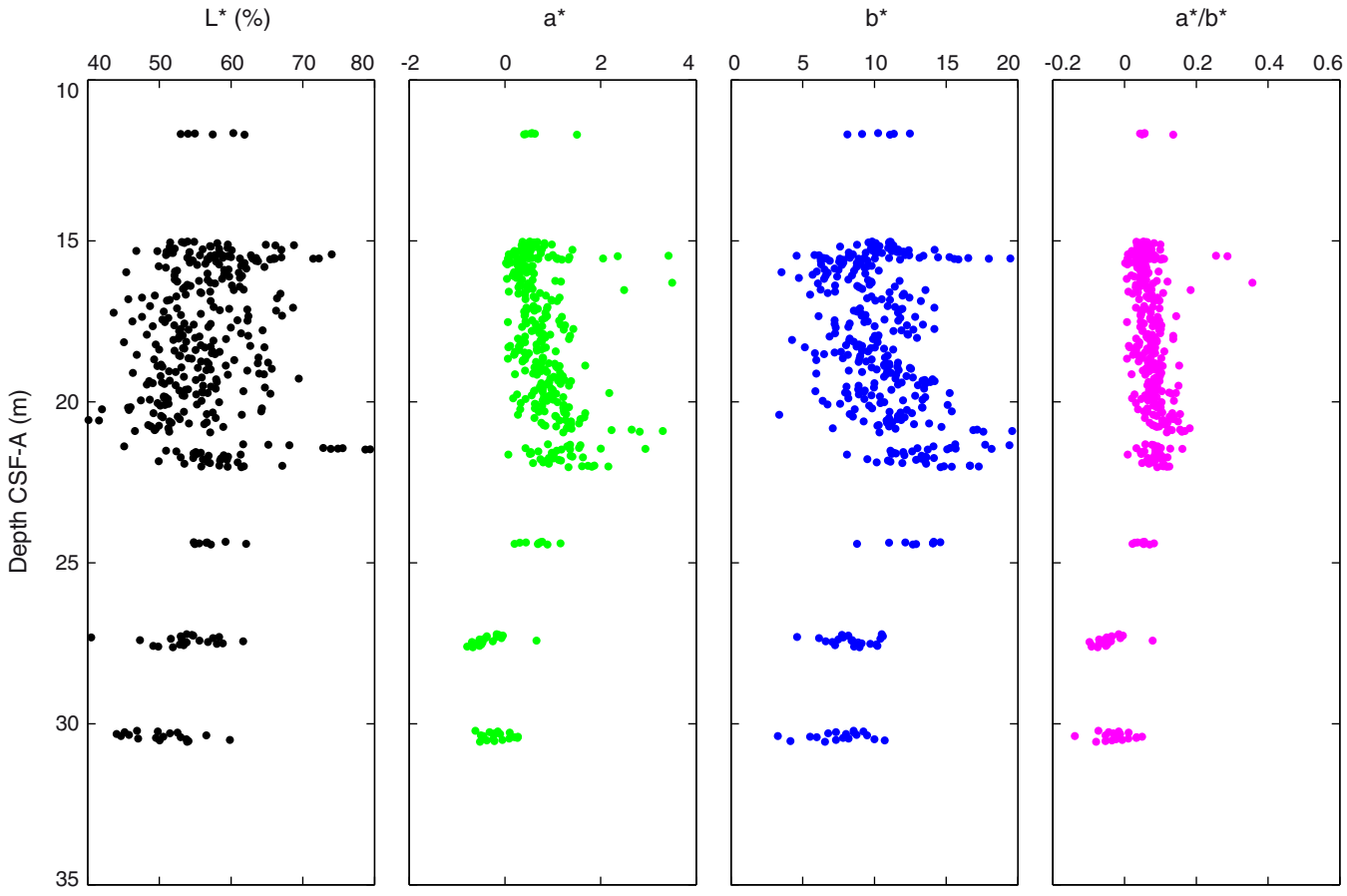

Figure F62. Magnetic susceptibility record for Hole M0054B. Water depth = 107.43 m (LAT).

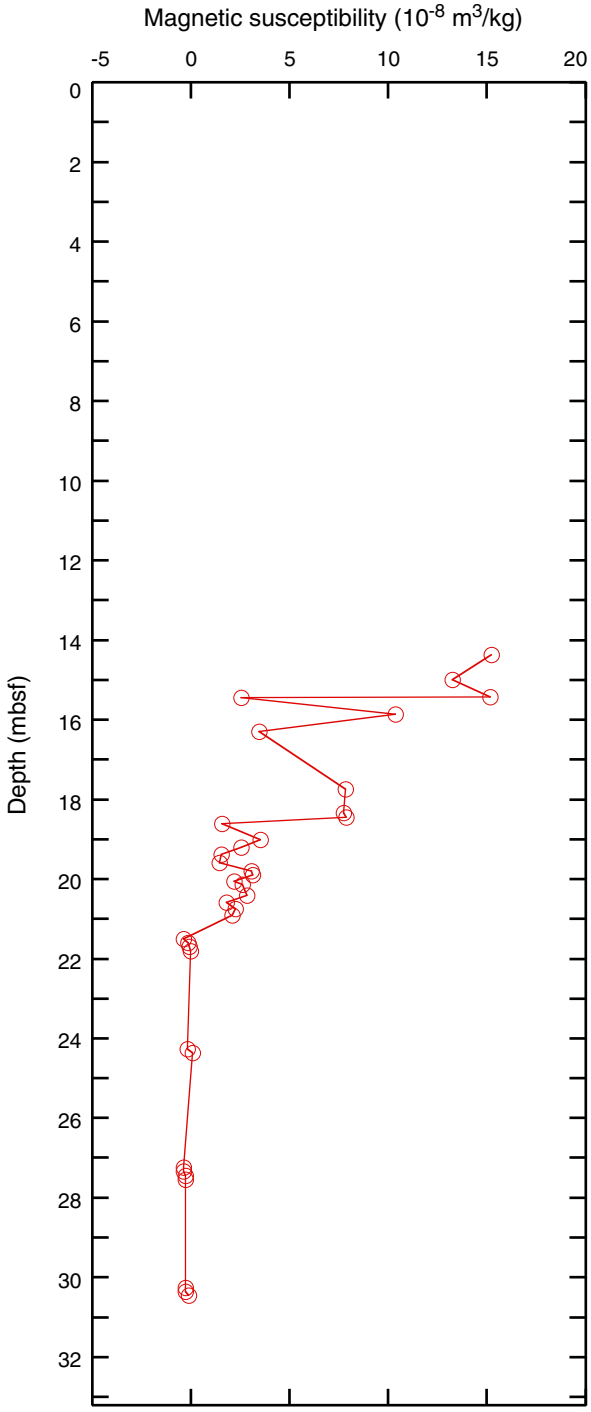

Figure F63. Preliminary chronology for Hole M0054A. Radiocarbon data are presented as graphs with the uncalibrated radiocarbon age and uncertainty shown as the red normal distribution on the ordinate axis and the probability distribution of the calibrated age shown in gray on the abscissa. The marine09 calibration curve is shown in blue. Horizontal bars indicate portions of the age distribution that are significant at the 95.4% confidence interval and the mean age (white circle ±1 standard deviation) used for the purposes of the preliminary dating. All ages are presented as thousands of calendar years BP (1950 AD). See Table **T10** in the "Methods" chapter. (See Bronk Ramsey [2009], as well as Bronk Ramsey [2010] at **c14.arch.ox.ac.uk/oxcal.html.**)

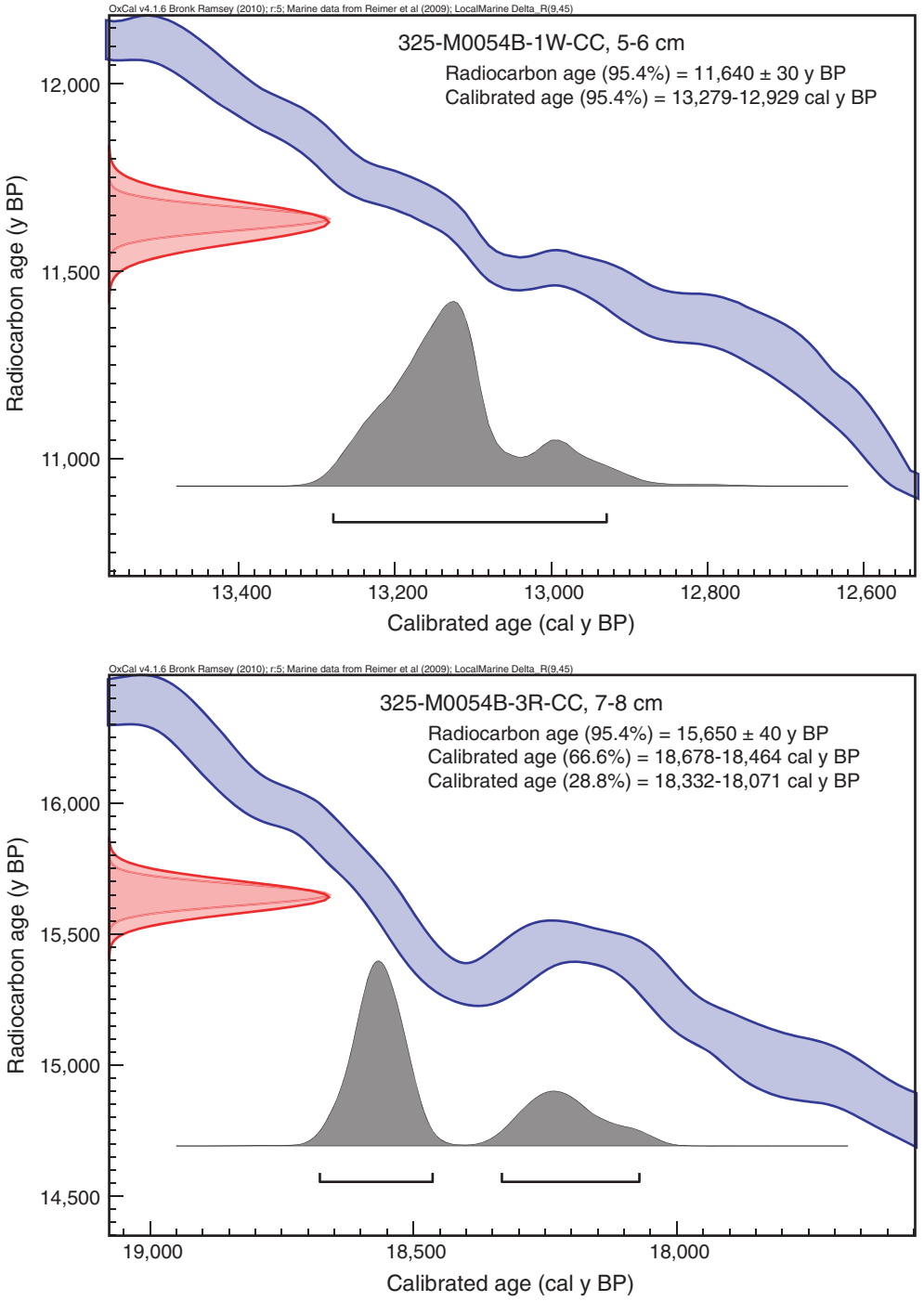

Figure F64. Composite of logging data, Hole M0054B. **A.** Through-pipe data. TGR = total gamma ray (raw), TP = through pipe. (This figure is also available in an **oversized format.**) (**Continued on next four pages.**)

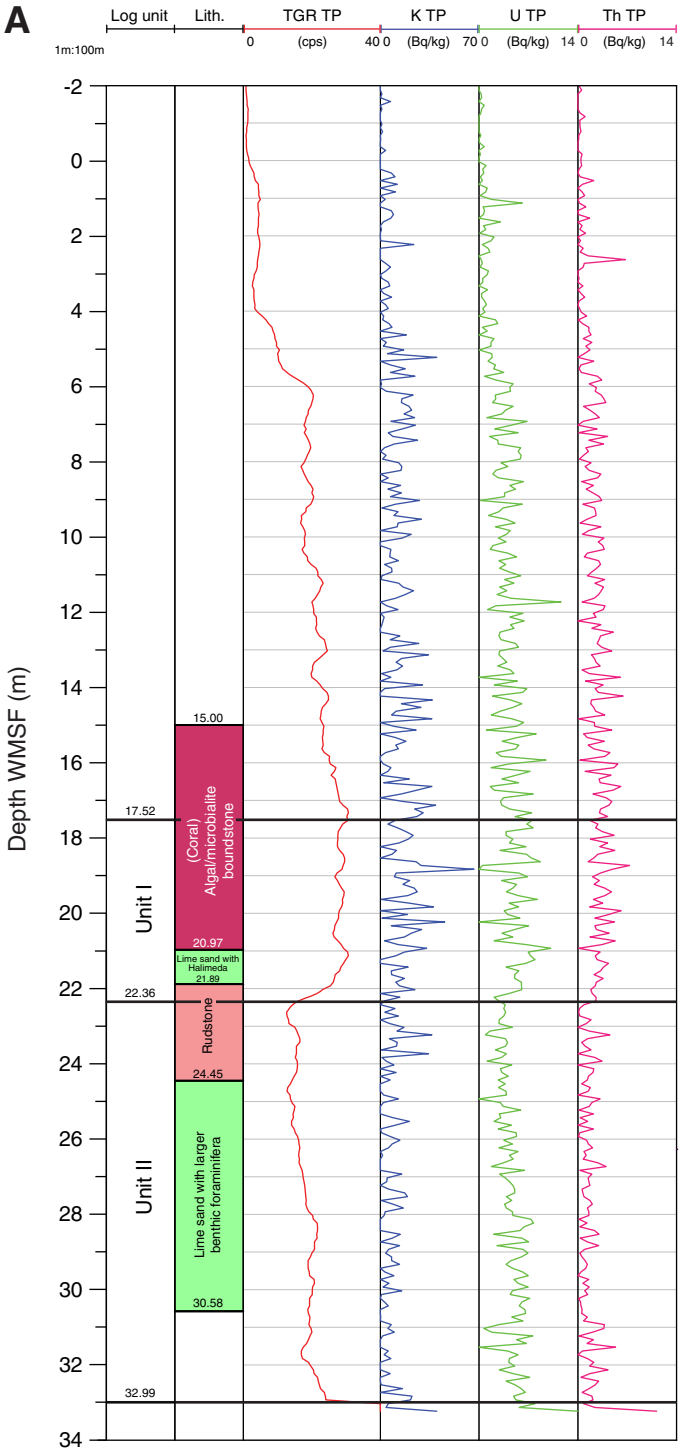

Figure F64 (continued). B. Conductivity and acoustic image data. ILD = deep conductivity, ILM = medium conductivity, OH = open hole. (**Continued on next page.**)

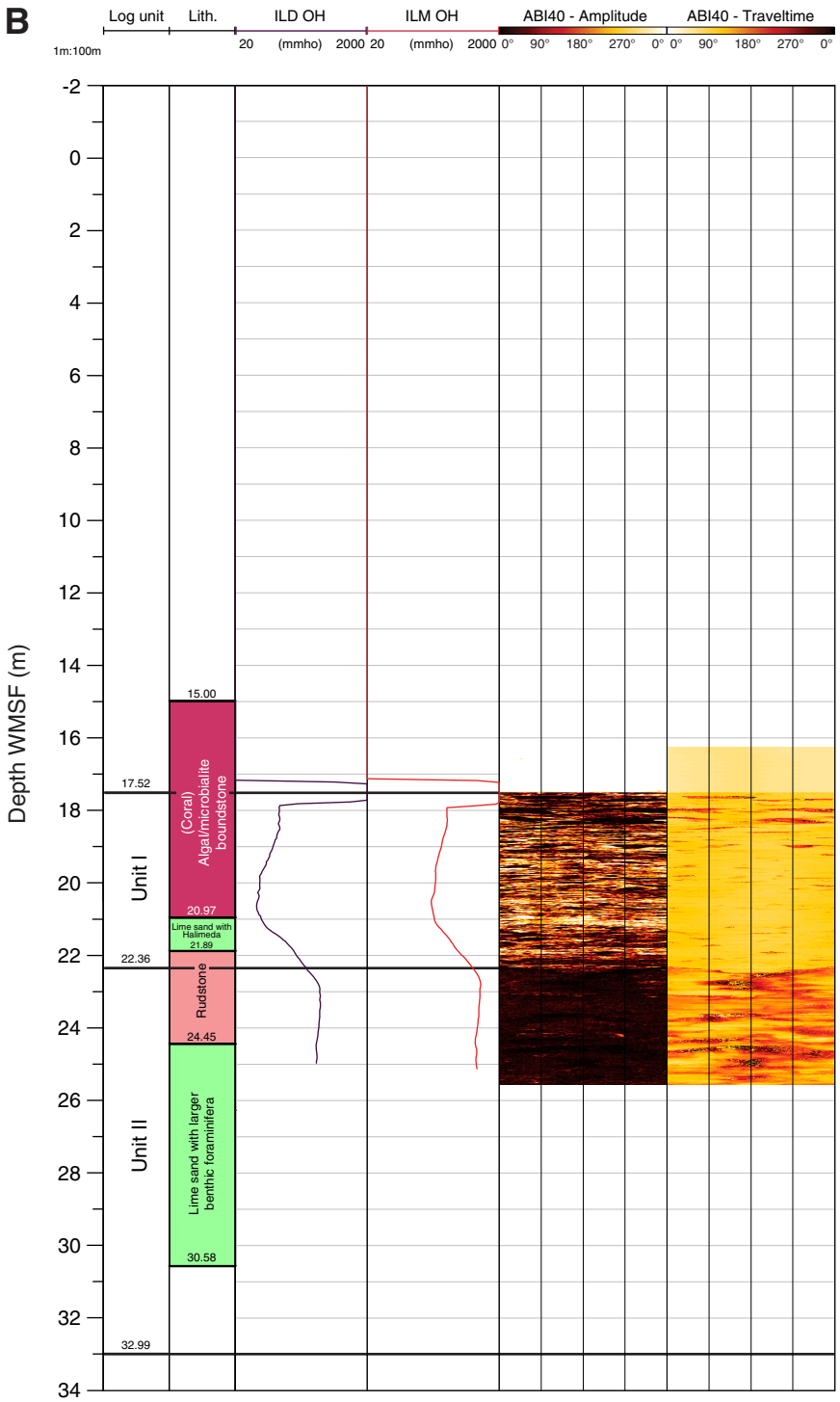

Figure F64 (continued). C. Optical image and open-hole gamma data. TGR = total gamma ray (raw), OH = open hole. (**Continued on next page.**)

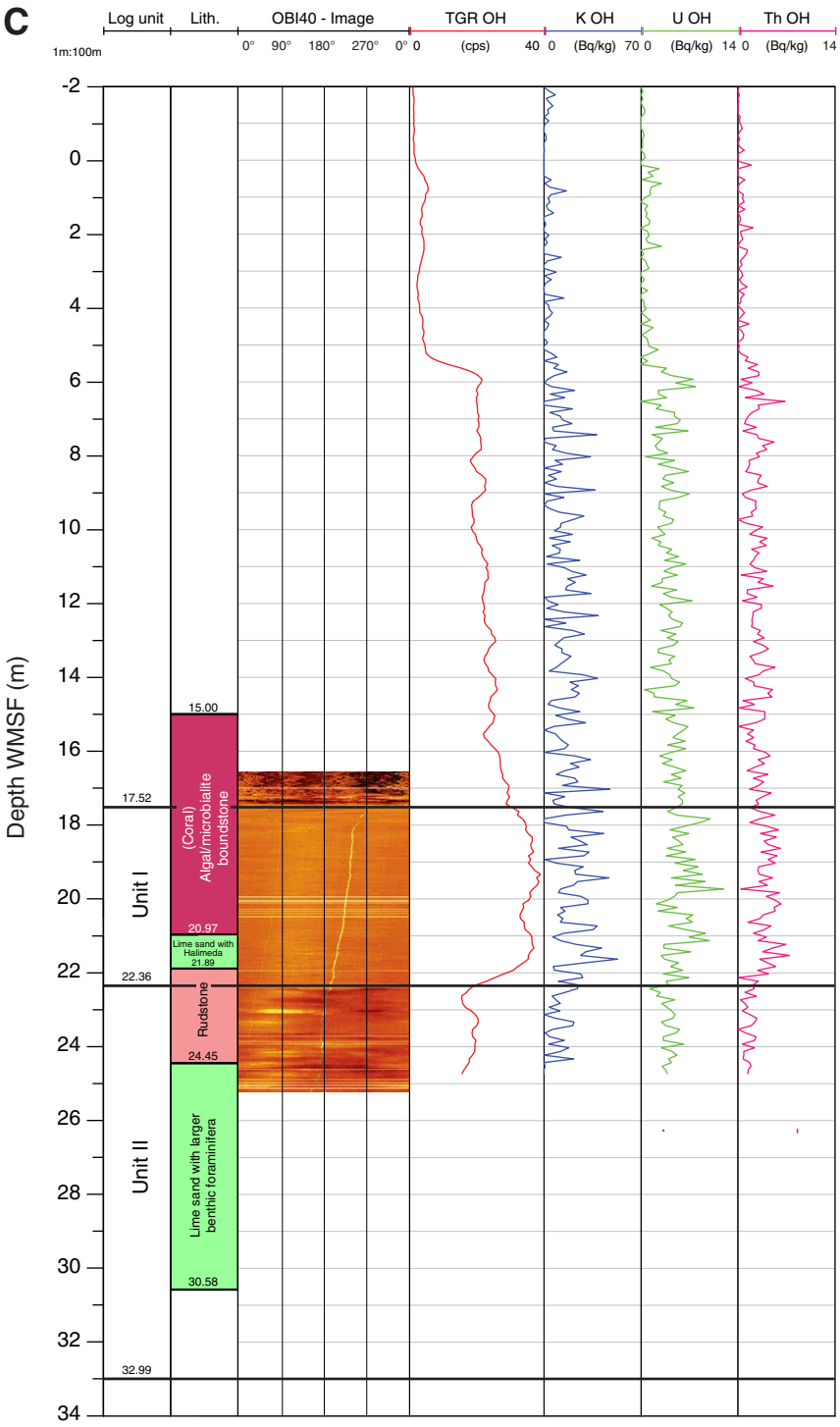

Figure F64 (continued). D. Sonic and EM51 data. RX1 = sonic waveforms for receiver 1, RX2 = sonic waveforms for receiver 2, V_P = *P*-wave velocity, IL = induction log, MSUS = magnetic susceptibility. (**Continued on next page.**)

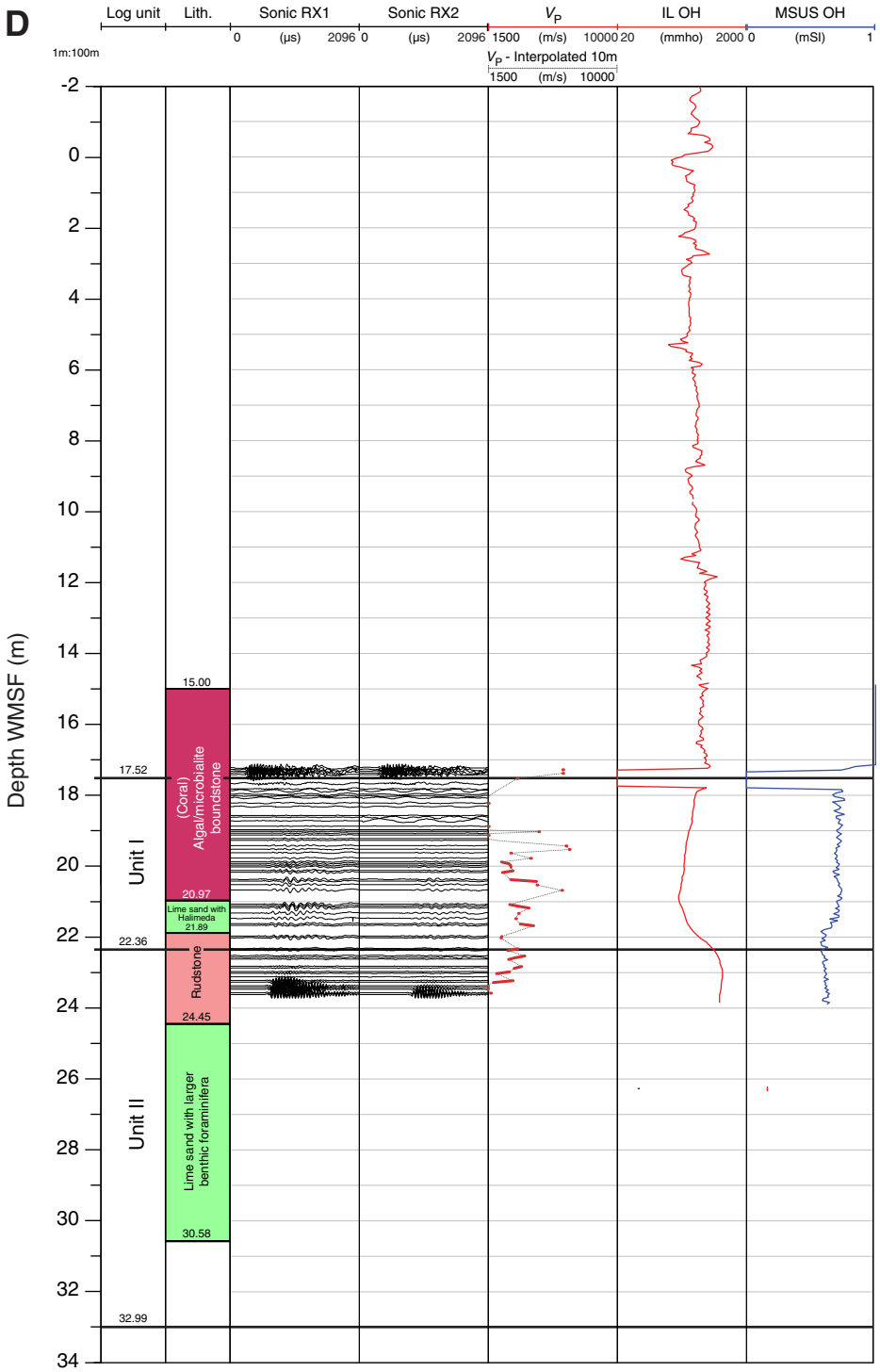

Figure F64 (continued). E. IDRONAUT and caliper data.

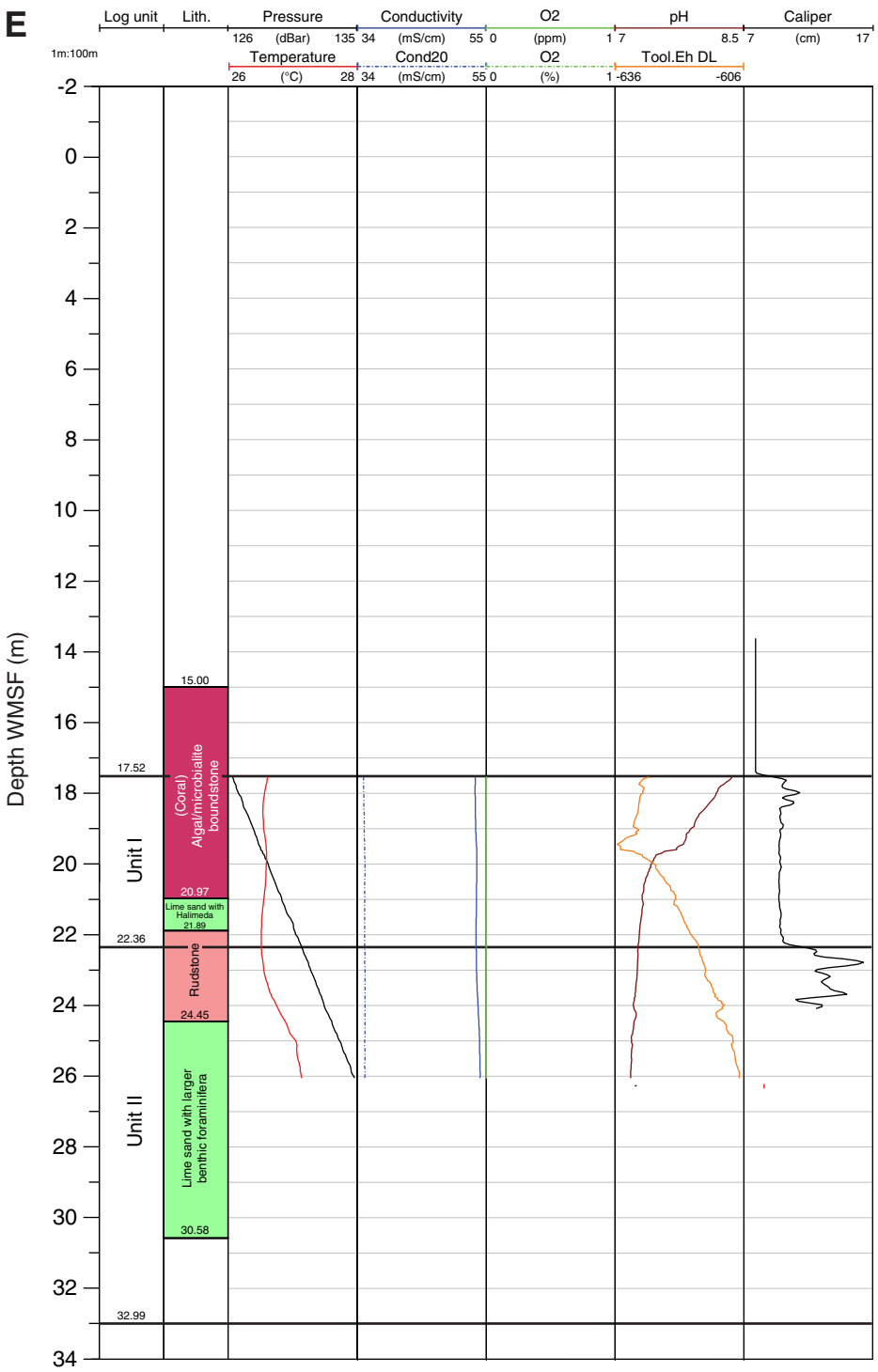

Figure F65. Composite illustrating the detail acquired by the ABI40 tool and 3D virtual borehole, Hole M0054B. 3D Borehole = 3D borehole visualization. ABI40 traveltime image is overlain by TGR, and OBI40 optical image is overlain by the caliper log.

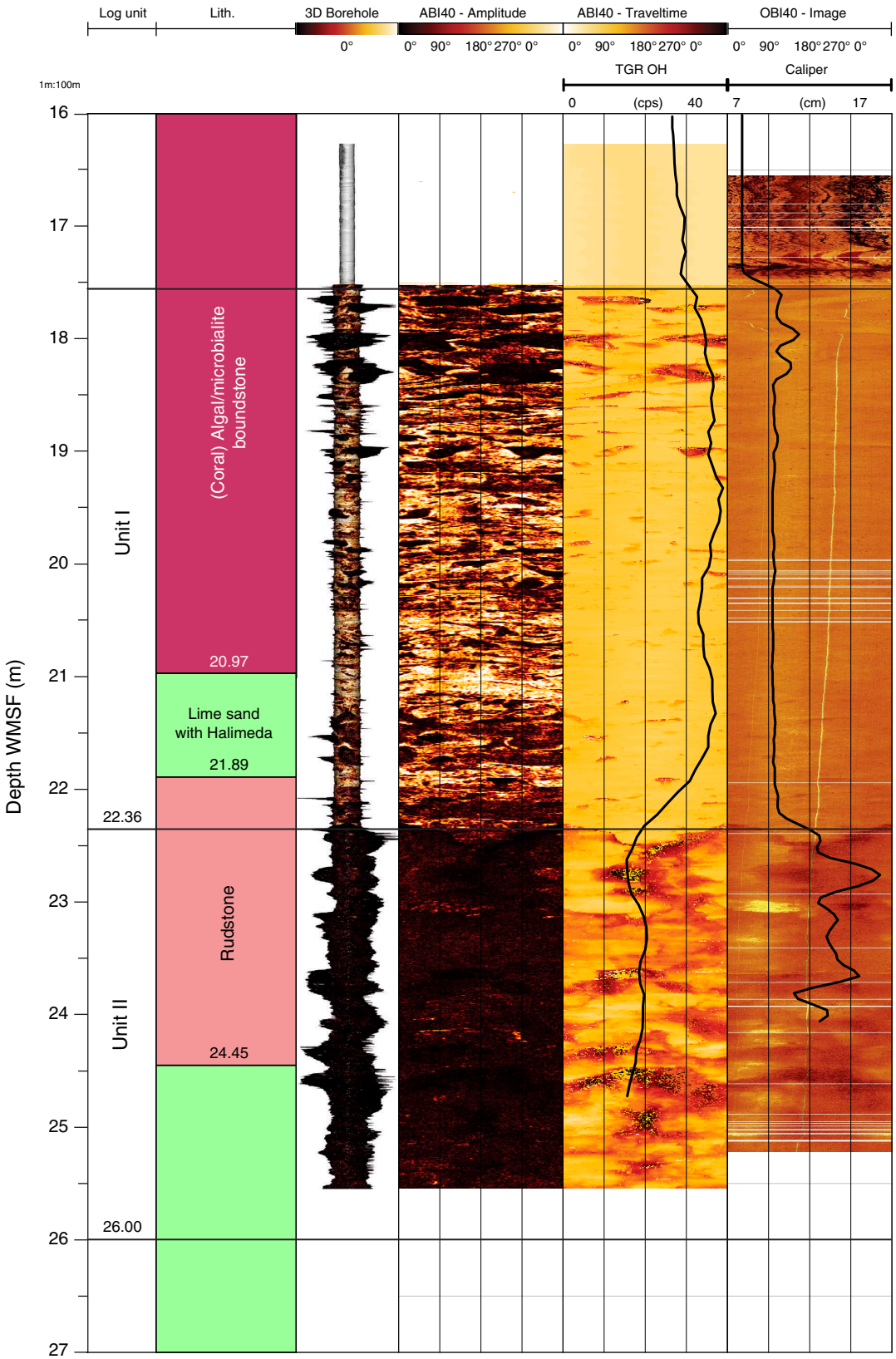

Figure F66. Composite showing core imagery alongside high-resolution borehole images, Hole M0054B. ABI40 traveltime image is overlain by TGR collected in open hole, OBI 40 optical image is overlain by the caliper log, and deep conductivity (ILD) log acquired with the DIL45 is overlain by the conductivity log acquired with the EM51. OH = open hole.

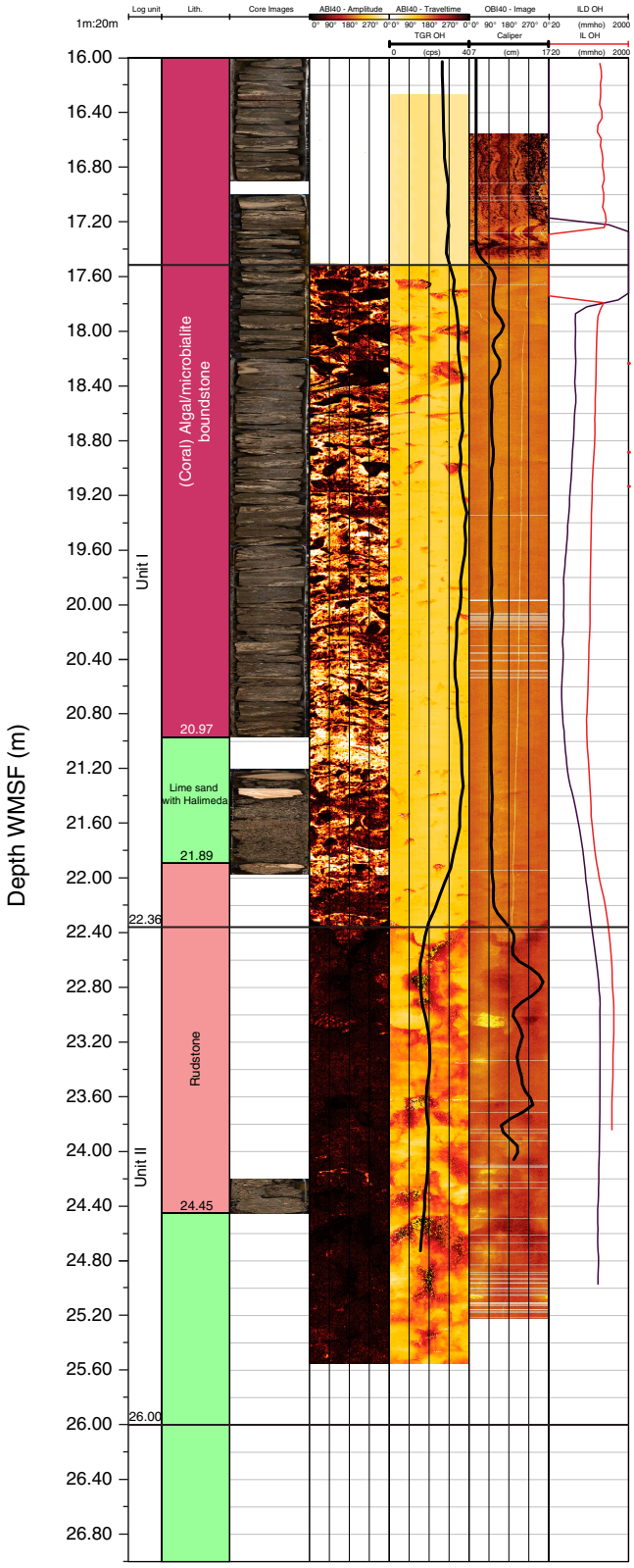

Figure F67. High-resolution line scan image of a robust branching *Acropora* and other Acroporidae encrusted by thick coralline algae with vermetids, gastropods, and nonlithified internal sediment (interval 325-M0055A-3R-1, 1–12 cm).

Figure F68. High-resolution line scan image of a medium branching *Acropora* encrusted by thick coralline algae (interval 325-M0055A-3R-1, 74–84 cm).

Figure F69. High-resolution line scan image of a medium branching *Acropora* (interval 325-M0055A-2R-1, 22–33 cm).

Figure F70. High-resolution line scan image of a medium branching *Acropora* encrusted by thick coralline algae (interval 325-M0055A-3R-1, 85–104 cm).

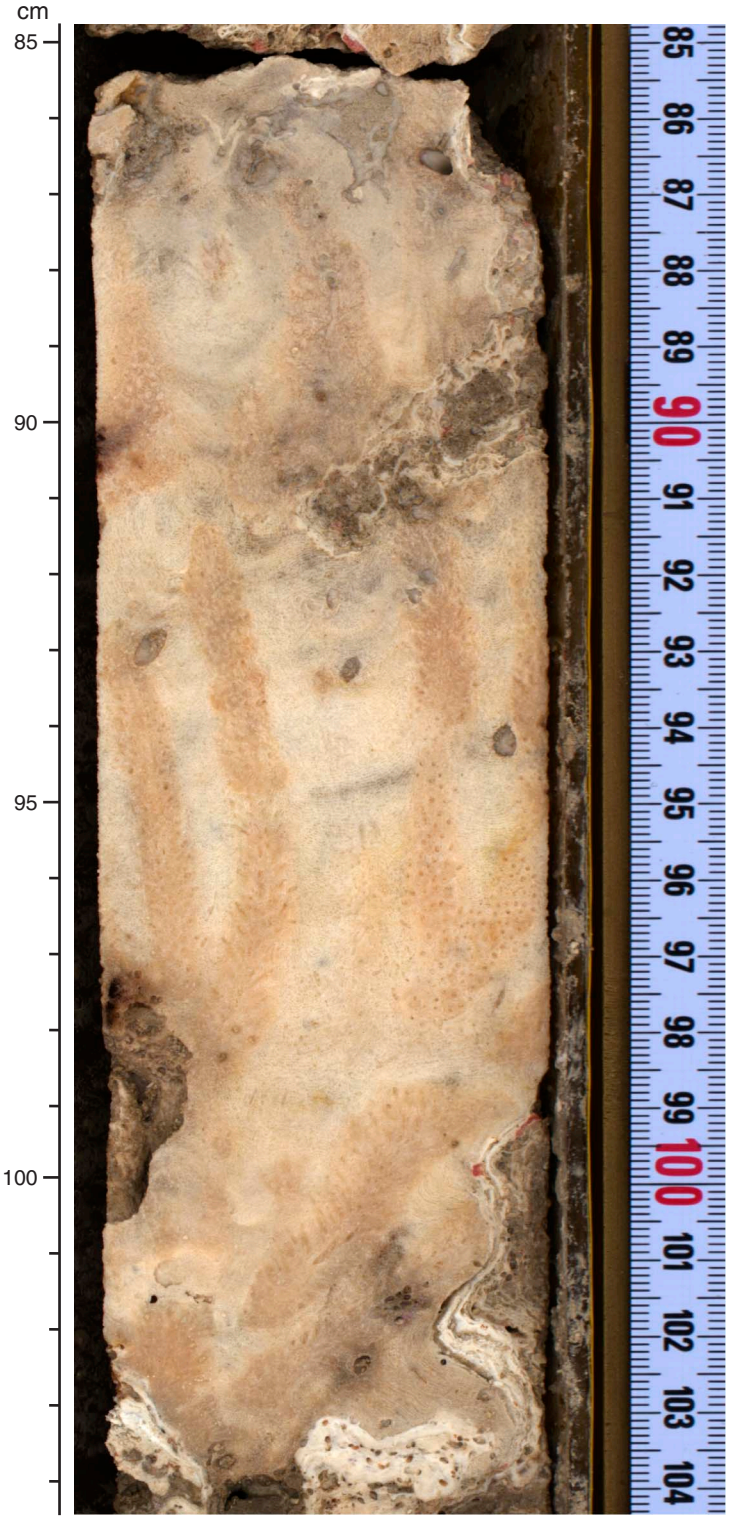

Figure F71. High-resolution line scan image of *Tubipora musica* and massive *Isopora* (in situ?) encrusted by thick coralline algae (interval 325-M0055A-4R-2, 24–35 cm).

Figure F72. High-resolution line scan image of a massive Faviidae (interval 325-M0055A-4R-2, 61–69 cm).

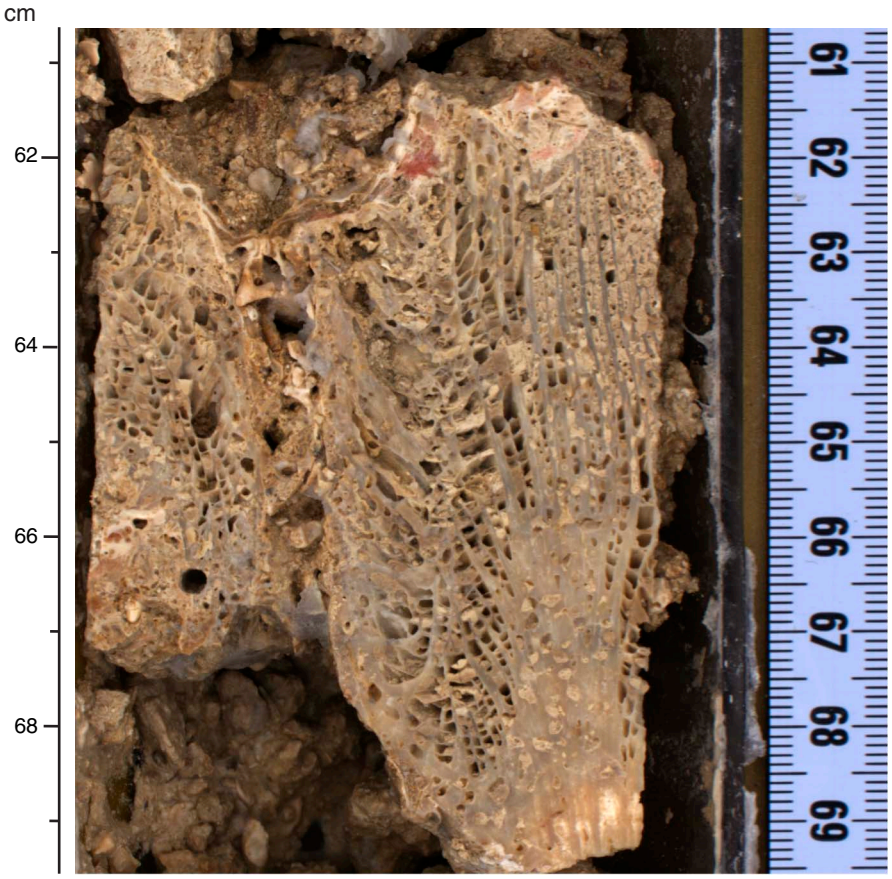

Figure F73. High-resolution line scan image of thick coralline algal crusts with vermetid gastropods underlying *Tubipora musica* covered by laminated microbialite (interval 325-M0055A-4R-1, 47–68 cm).

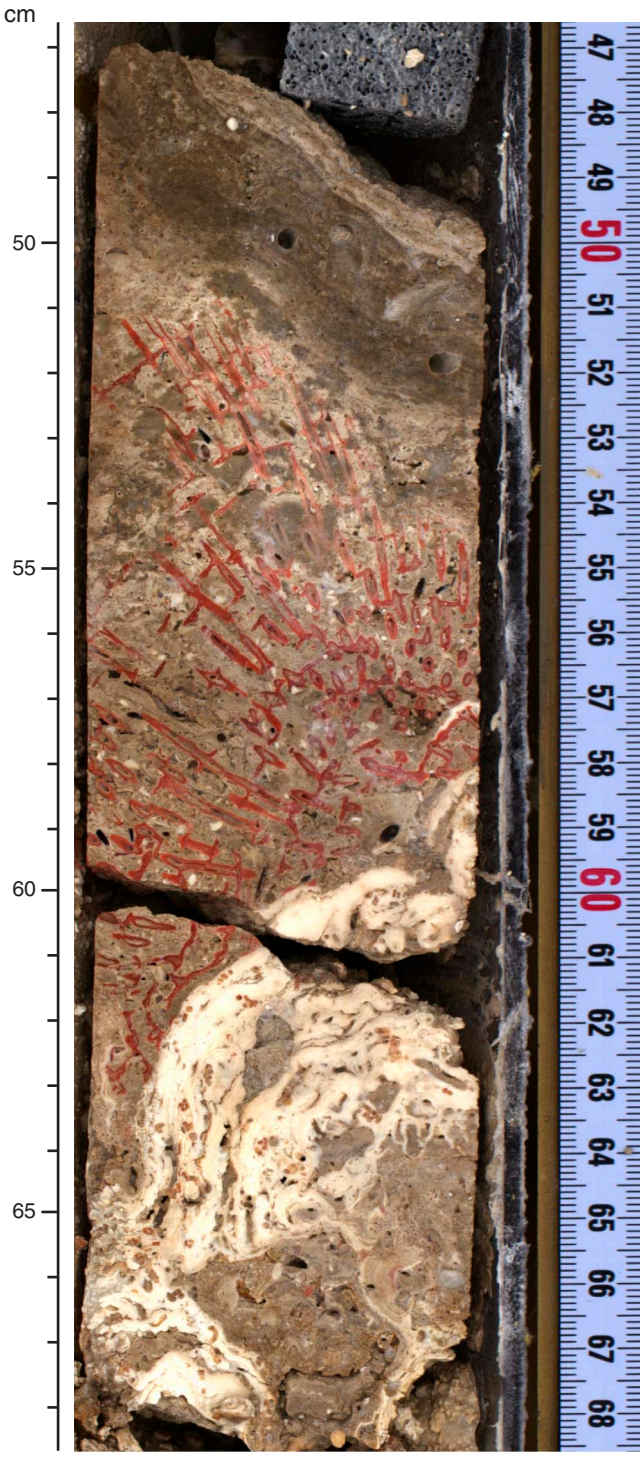

Figure F74. High-resolution line scan image of thick coralline algal crusts beneath a massive *Porites* (in situ?) (interval 325-M0055A-5R-1, 53–78 cm).

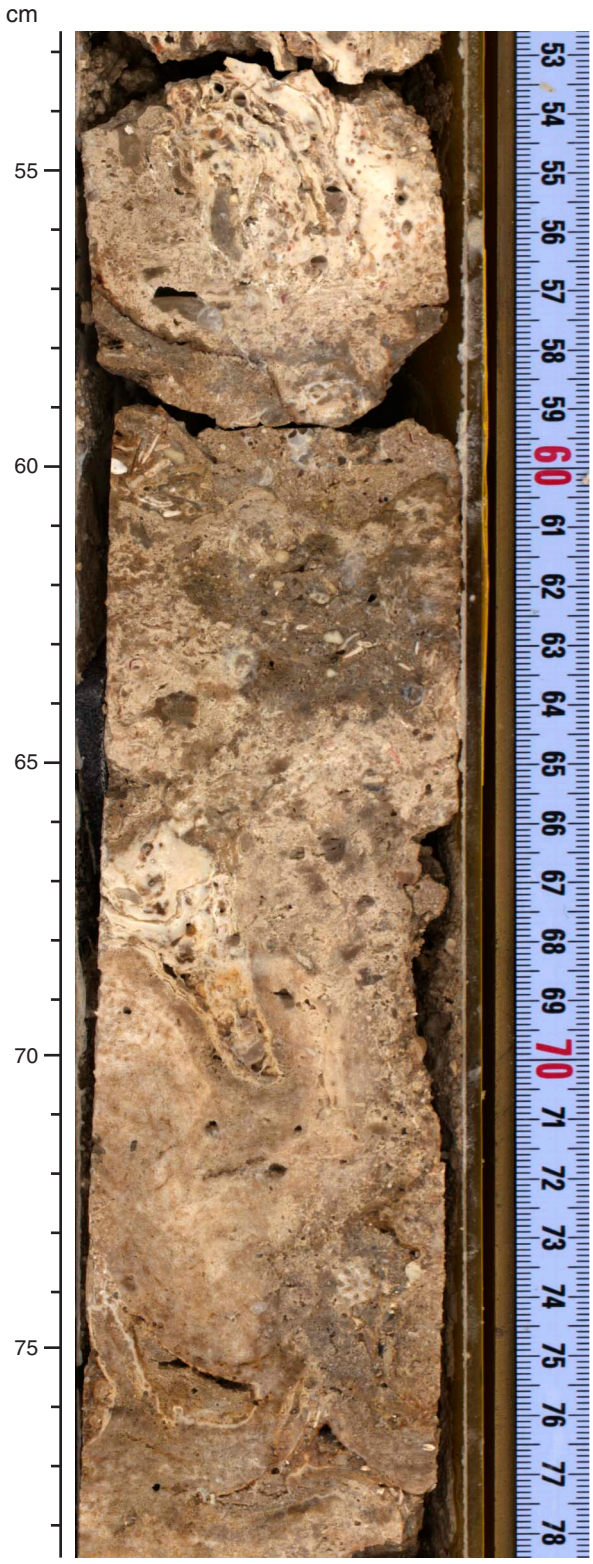

Figure F75. High-resolution line scan image of bioclastic packstone with *Halimeda* (interval 325-M0055A-5R-1, 9–14 cm).

Figure F76. High-resolution line scan image of thick coralline algal crusts beneath a massive *Porites* (in situ?) (interval 325-M0055A-5R-1, 27–37 cm).

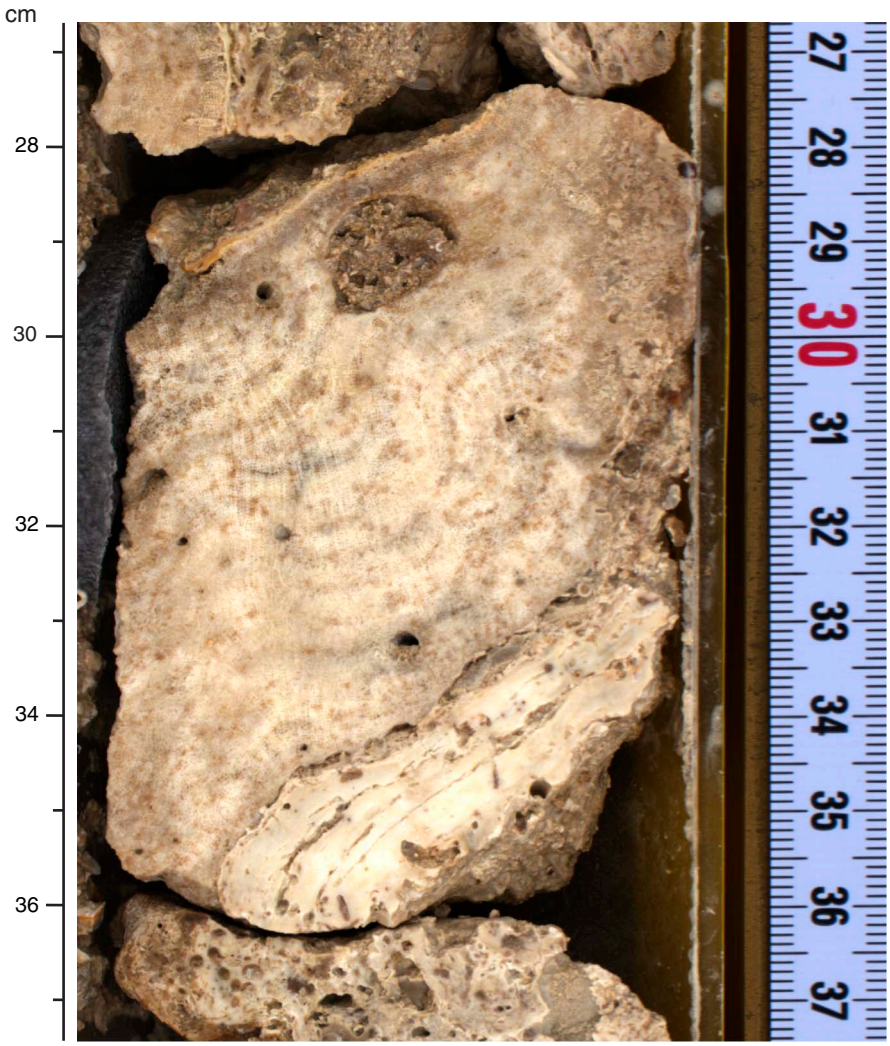

Figure F77. High-resolution line scan image of a massive Faviidae covered by a thick coralline algal crust (interval 325-M0055A-5R-1, 1–10 cm).

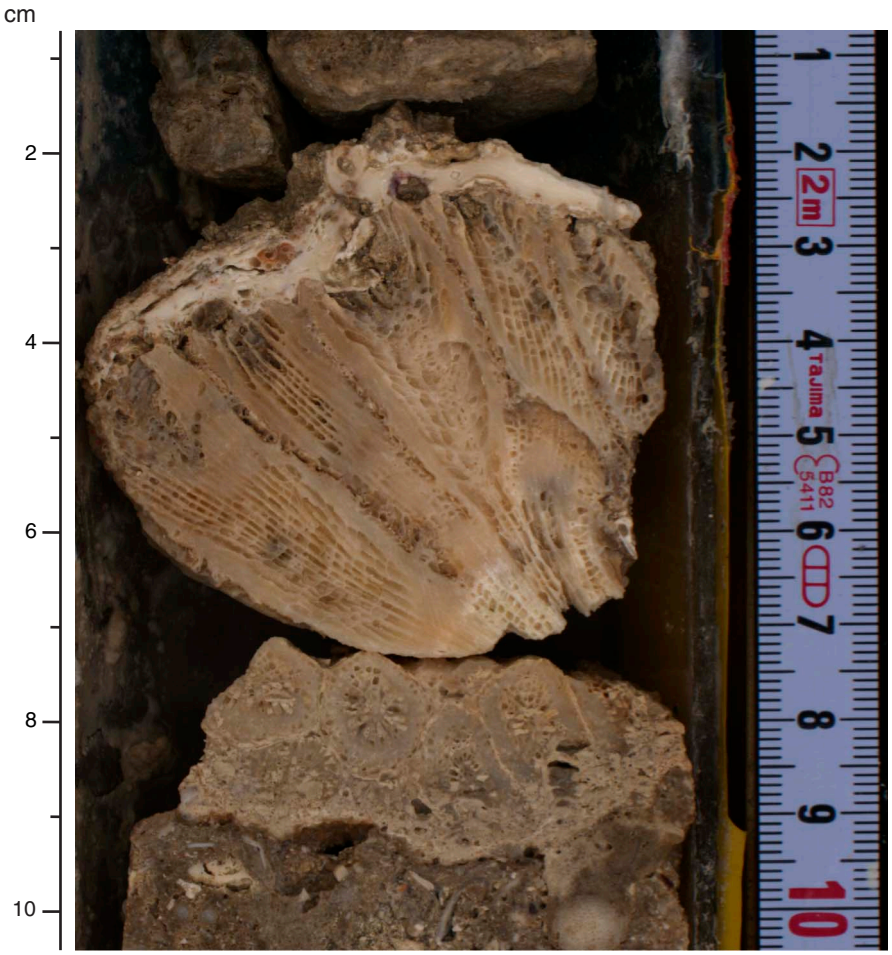

Figure F78. High-resolution line scan image of coralgal boundstone with a thick coralline algal crust (interval 325-M0055A-5R-2, 8–34 cm).

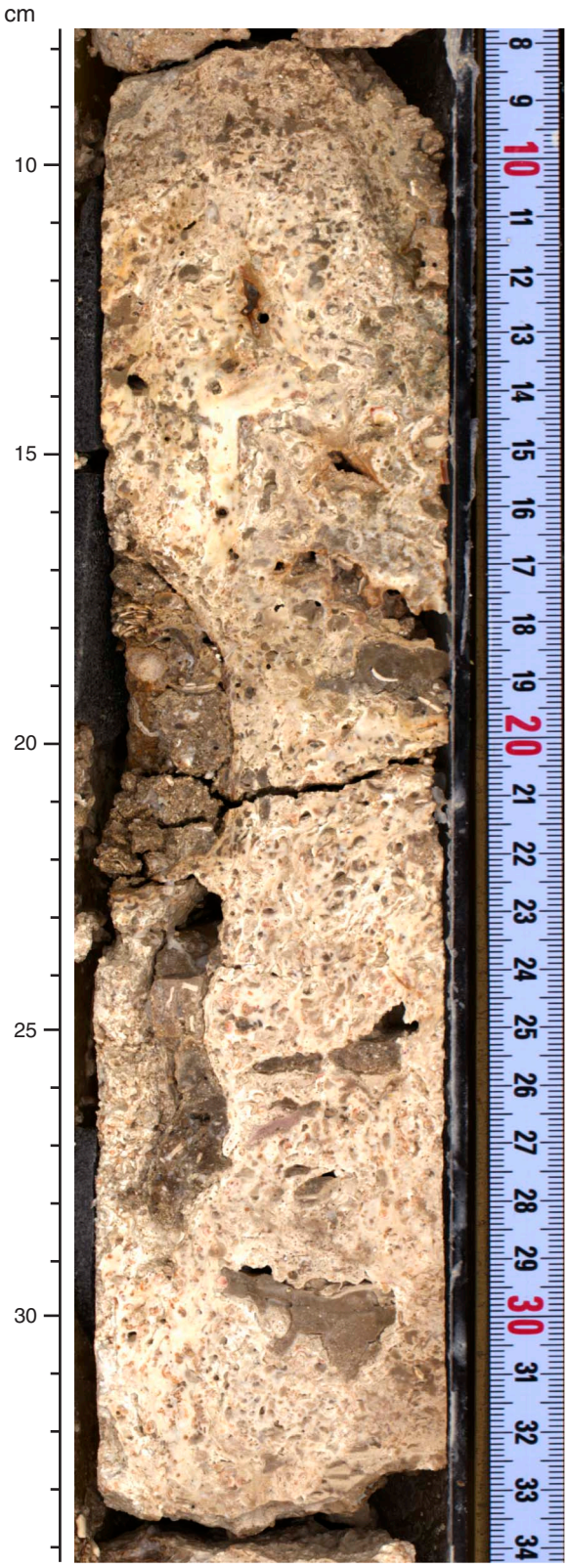

Figure F79. High-resolution line scan image of a massive coral with signs of dissolution (interval 325-M0055A-6R-1, 66–77 cm).

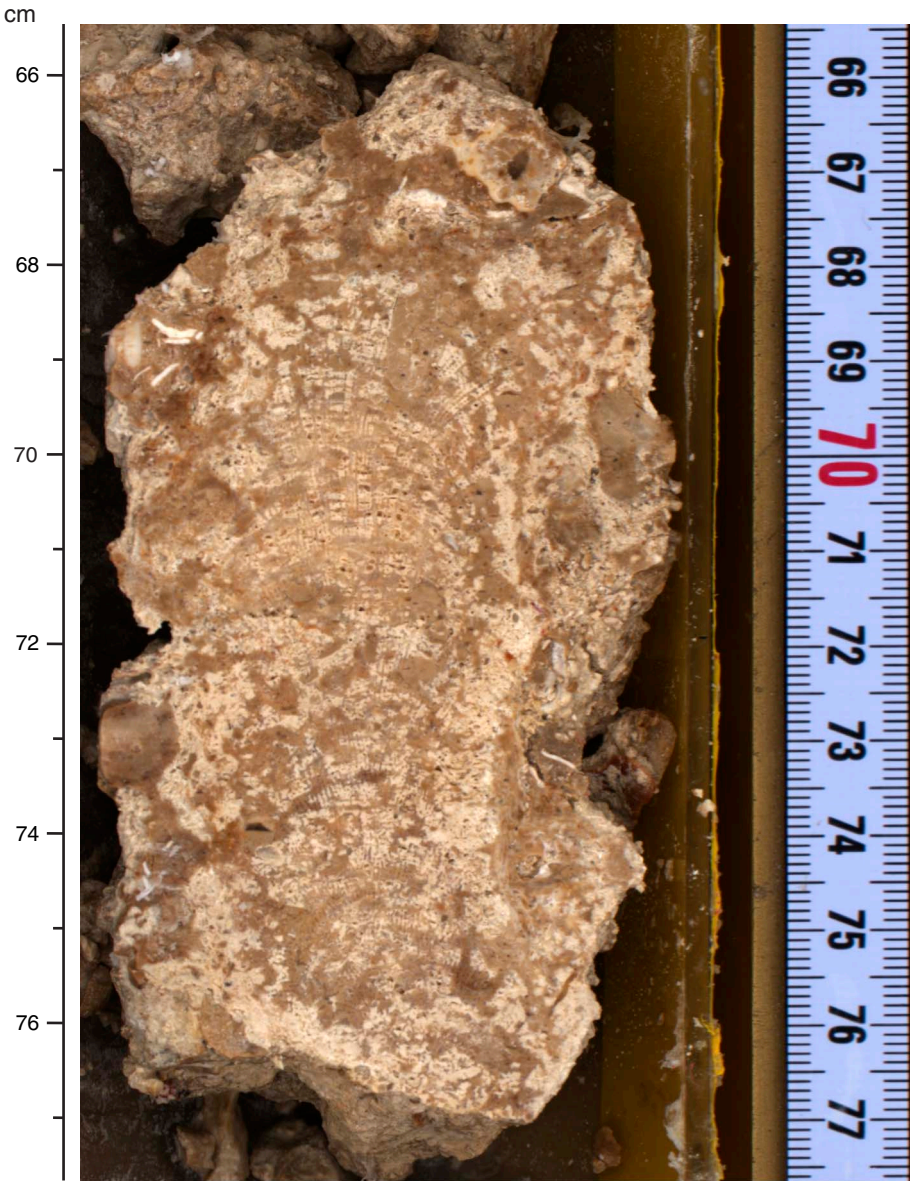

Figure F80. High-resolution line scan image of grainstone interlayered with boundstone (interval 325-M0055A-5R-2, 34–49 cm).

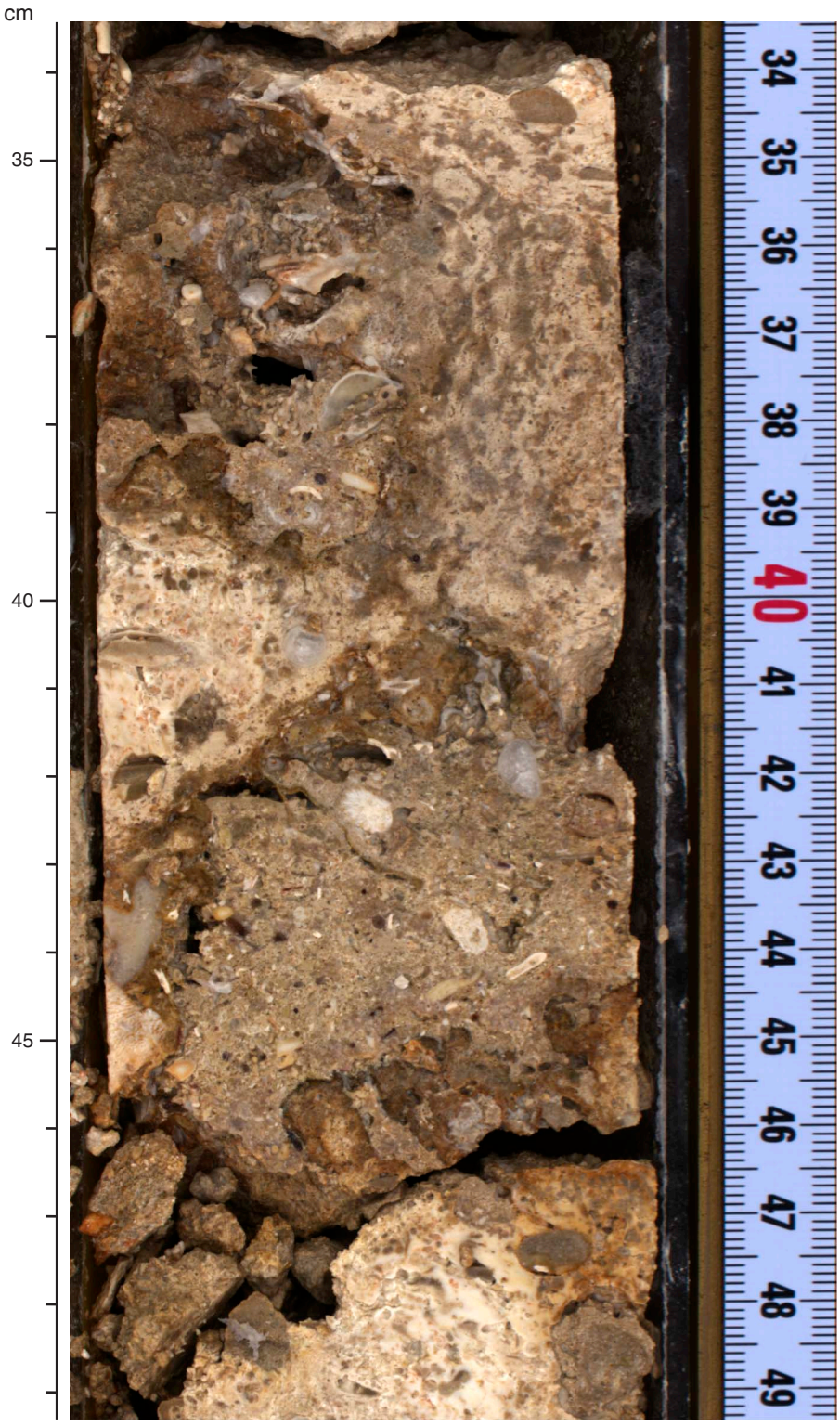

Figure F81. High-resolution line scan image of a robust branching Pocilloporidae in boundstone (interval 325-M0055A-5R-2, 63–74 cm).

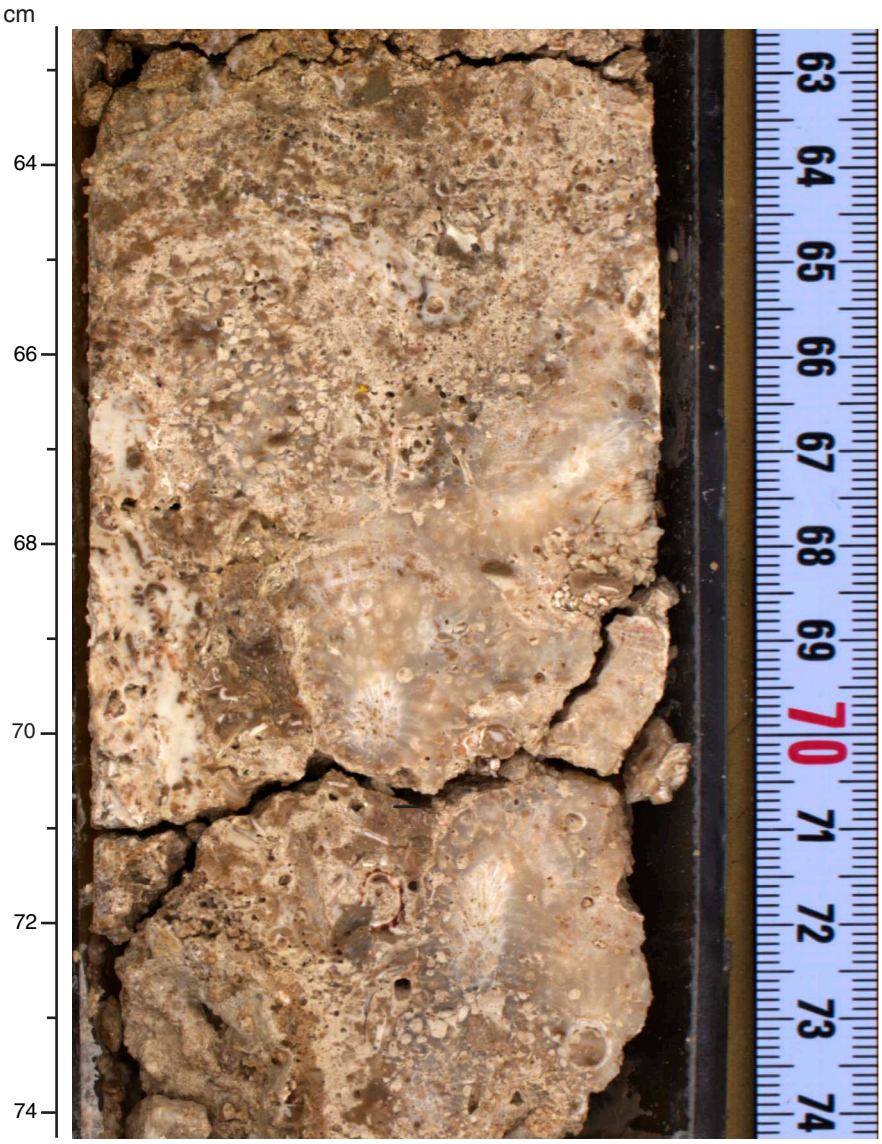

Figure F82. High-resolution line scan image of grainstone with *Halimeda,* coral, and mollusks (interval 325-M0055A-7R-1, 11–17 cm).

Figure F83. Summary diagram showing data collected on whole cores using the MSCL, Hole M0055A.

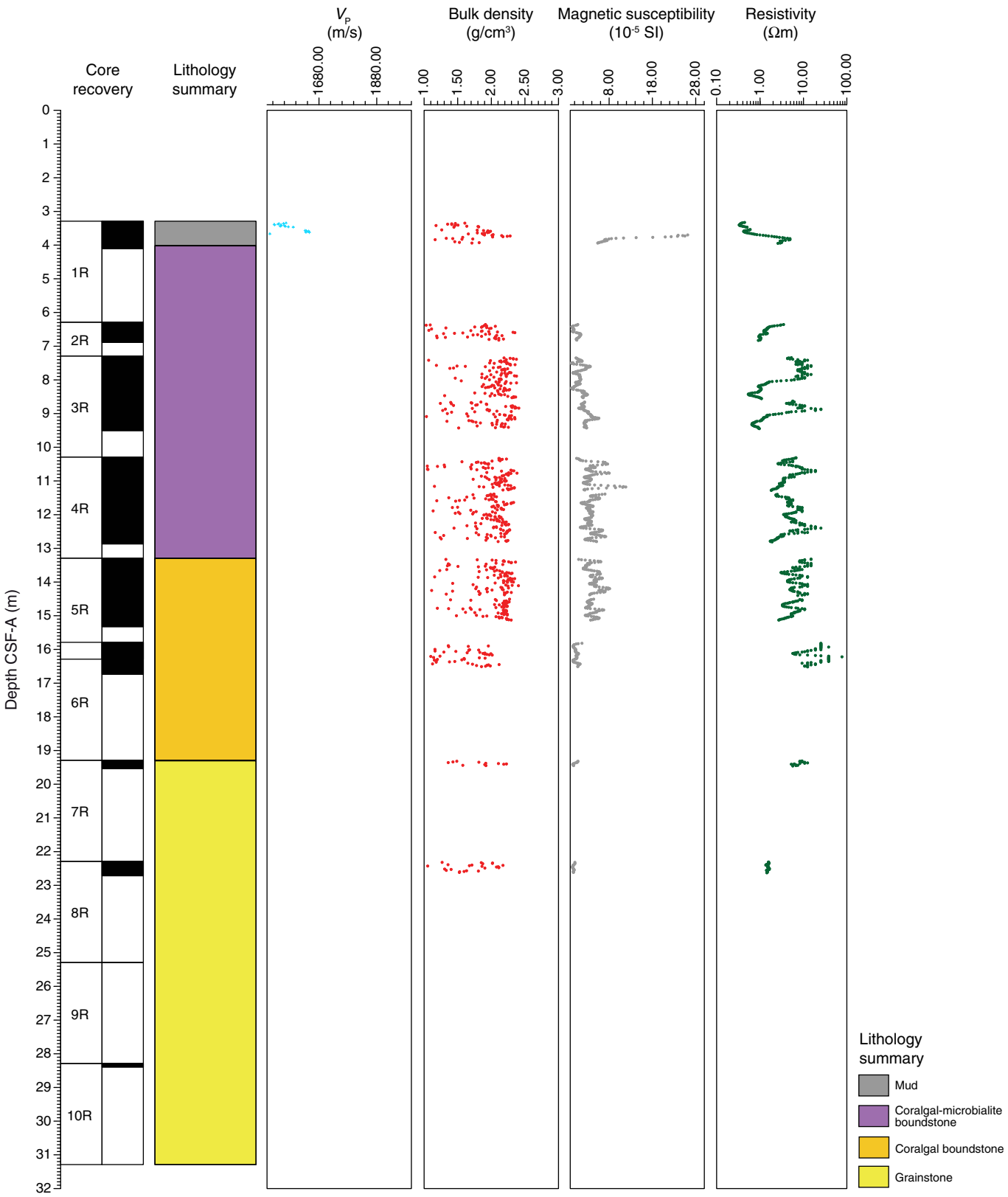

Figure F84. Petrophysical measurements obtained from discrete samples with a pycnometer, Hole M0055A. Bulk density measured on whole cores with the MSCL is shown in red on the bulk density plot.

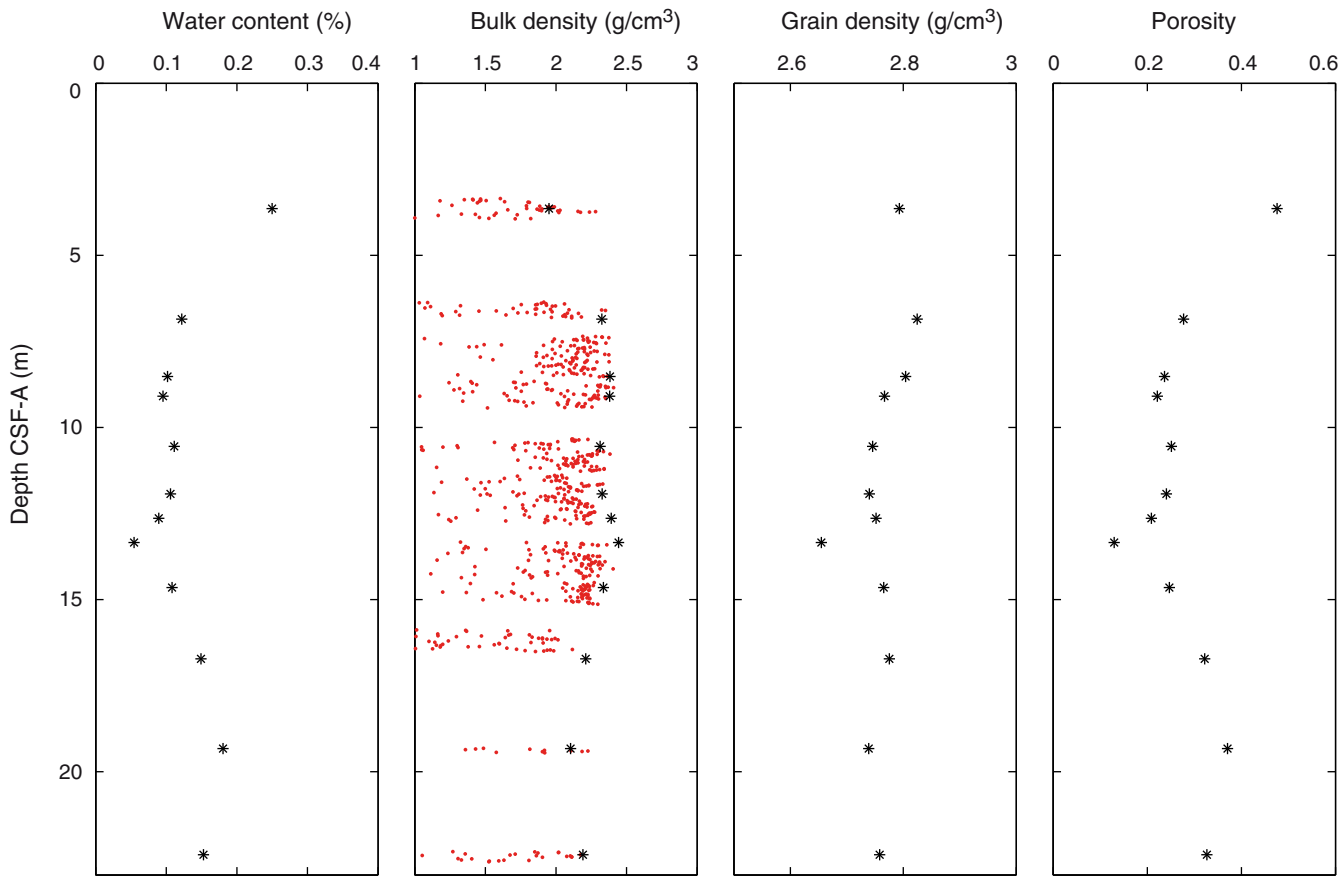

Figure F85. *P*-wave velocity data, Hole M0055A. **A.** Plot of initial, dry, and resaturated *P*-wave velocity measurements on discrete samples vs. depth. Three measurements were taken at each depth and are denoted by a dot. Average values are plotted as an open triangle. **B.** Plot showing discrete *P*-wave velocity vs. discrete bulk density.

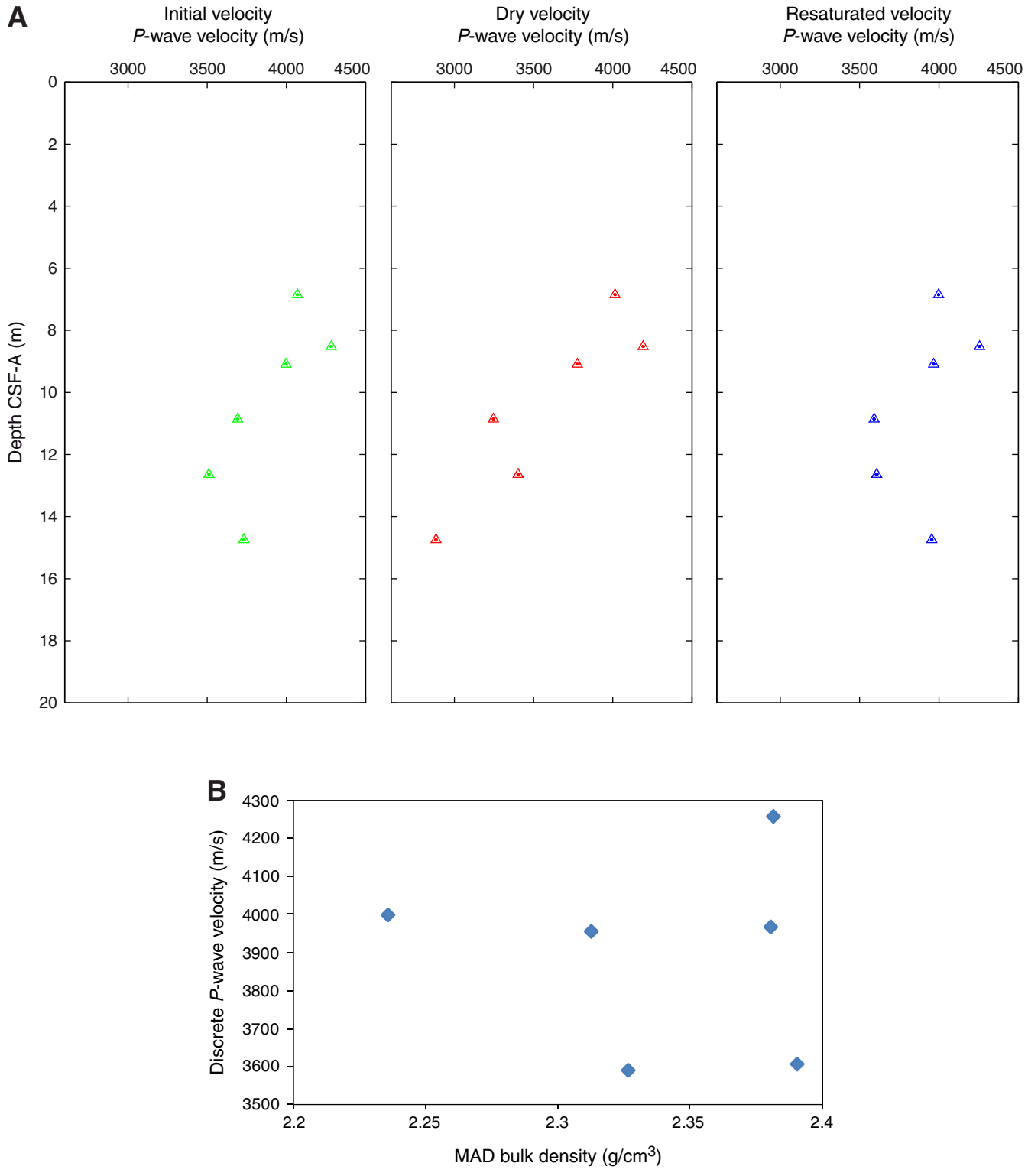

Figure F86. Values of reflectance (L*), green to red (a*), and blue to yellow (b*) indexes, along with ratio a*/b* for Hole M0055A.

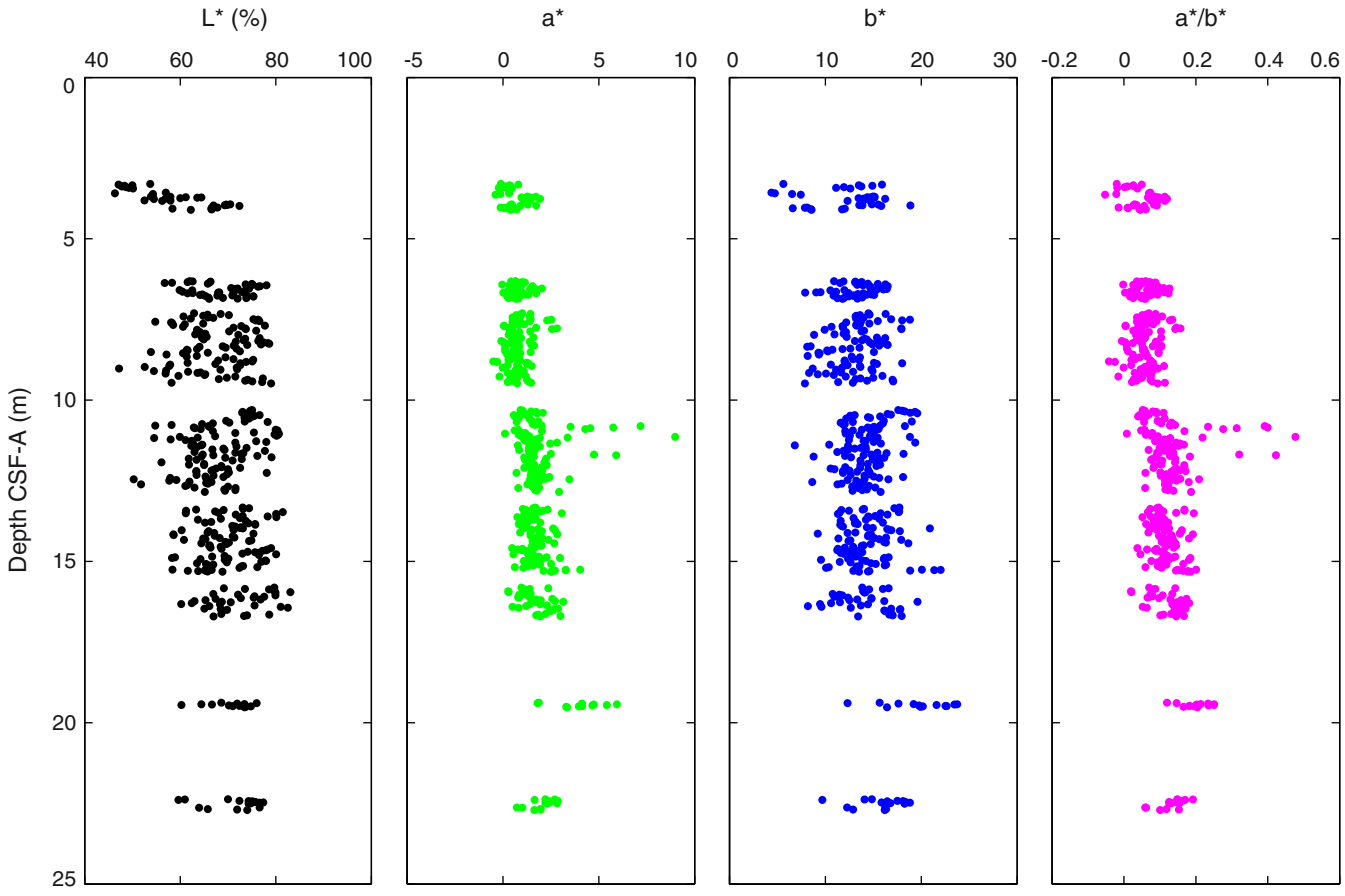

Figure F87. Magnetic susceptibility record for Hole M0055A. Water depth = 87.33 m (LAT).

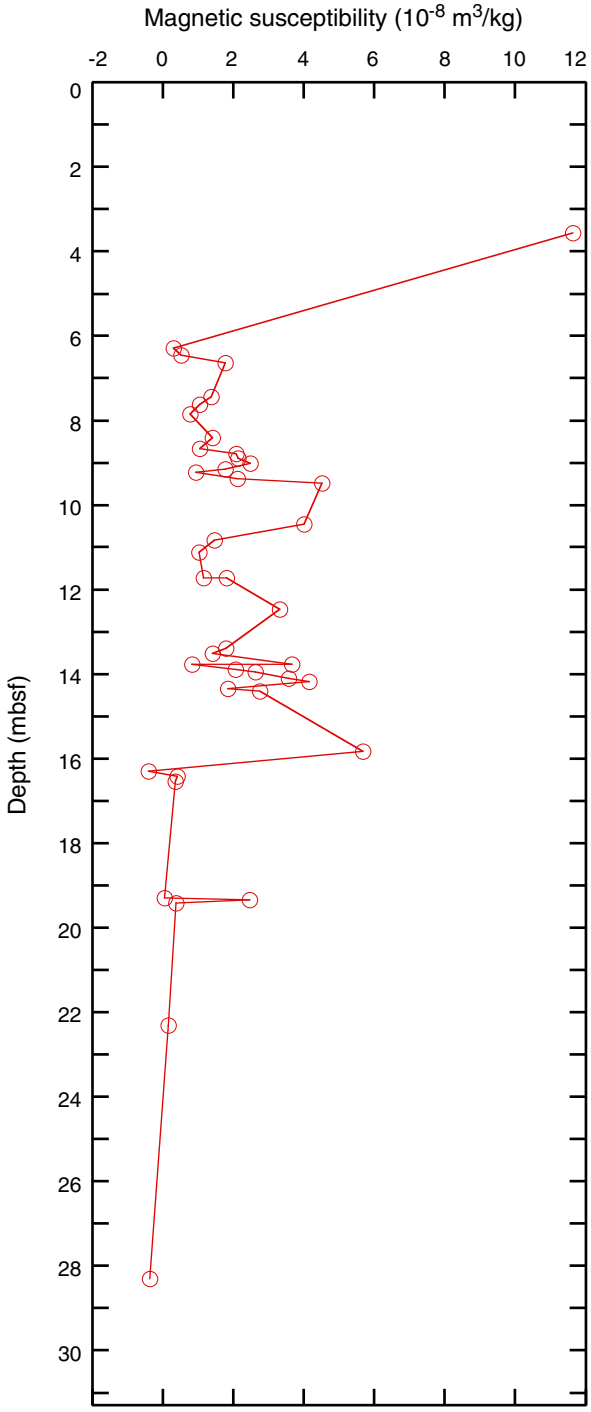

Figure F88. Preliminary chronology for Hole M0055A. Radiocarbon data are presented as graphs with the uncalibrated radiocarbon age and uncertainty shown as the red normal distribution on the ordinate axis and the probability distribution of the calibrated age shown in gray on the abscissa. The marine09 calibration curve is shown in blue. Horizontal bars indicate portions of the age distribution that are significant at the 95.4% confidence interval and the mean age (white circle ±1 standard deviation) used for the purposes of the preliminary dating. All ages are presented as thousands of calendar years BP (1950 AD). See Table **T10** in the "Methods" chapter. (See Bronk Ramsey [2009], as well as Bronk Ramsey [2010] at **c14.arch.ox.ac.uk/oxcal.html.**)

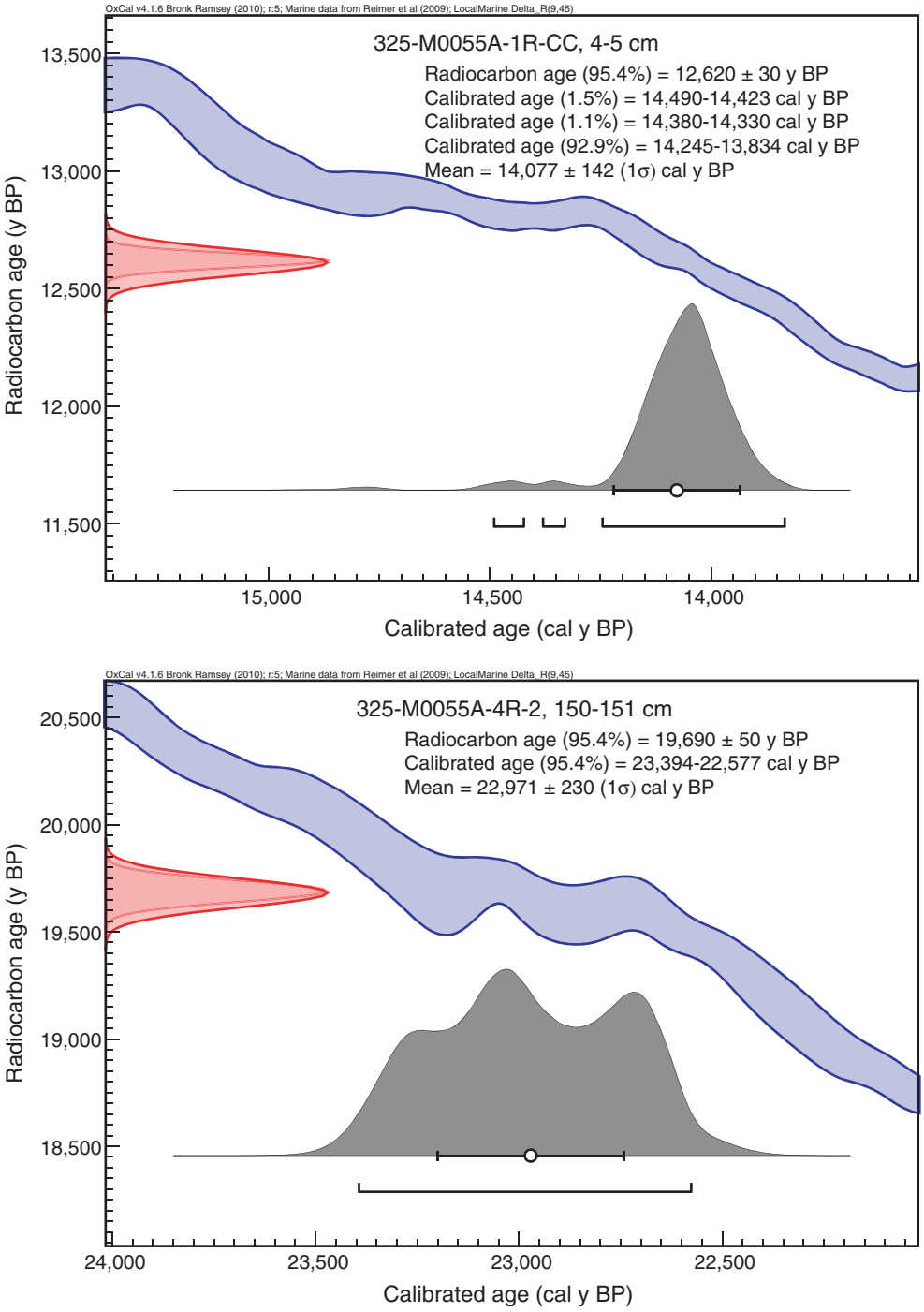

Figure F89. High-resolution line scan image of a massive *Cyphastrea* encrusted by thin coralline algae (interval 325-M0056A-2R-1, 23–37 cm).

Figure F90. High-resolution line scan image of branching coralline algae with encrusting benthic foraminifera and encrusting *Montipora* (interval 325-M0056A-2R-1, 49–68 cm).

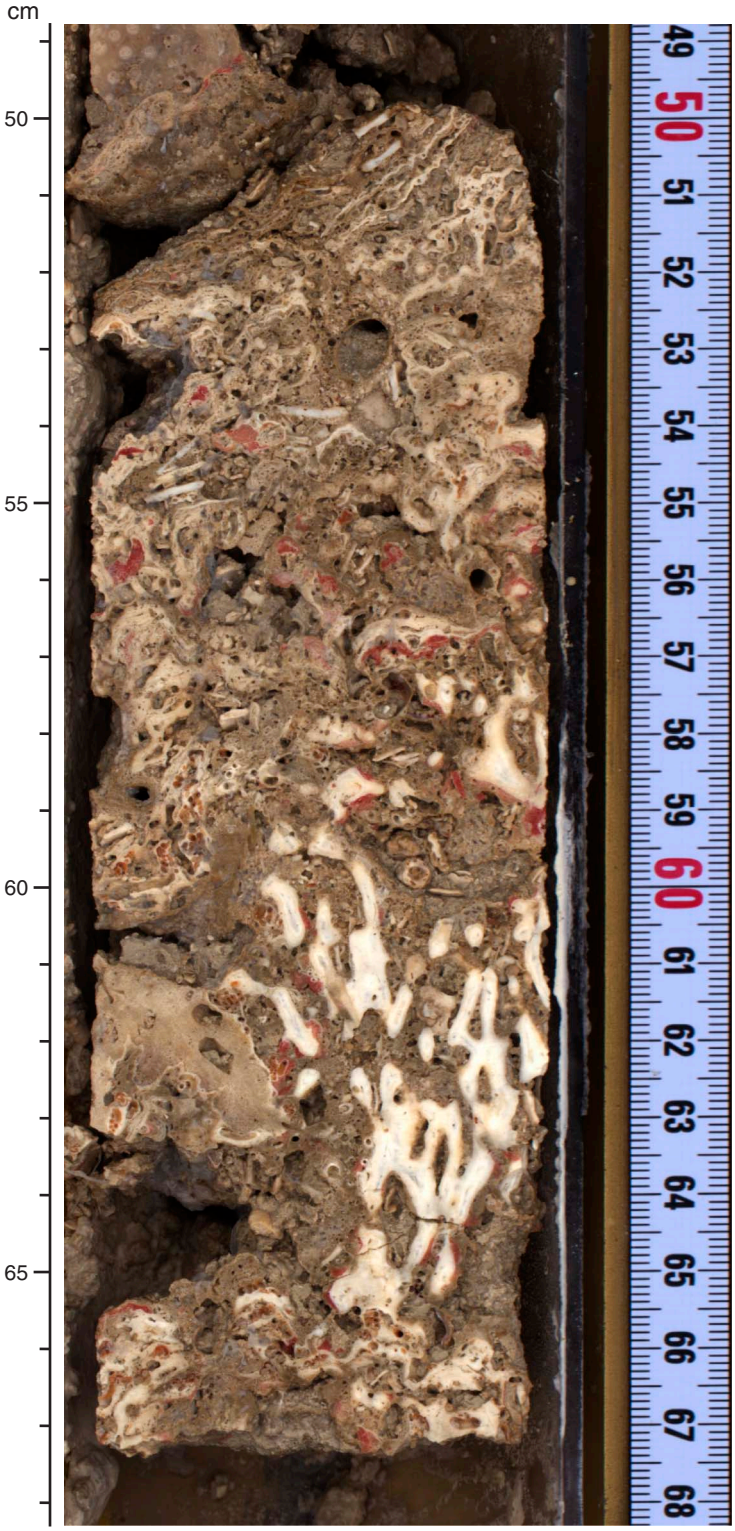

Figure F91. High-resolution line scan image of a coralgal boundstone with massive corals (Faviidae) and coralline algae (interval 325-M0056A-2R-1, 81–98 cm).

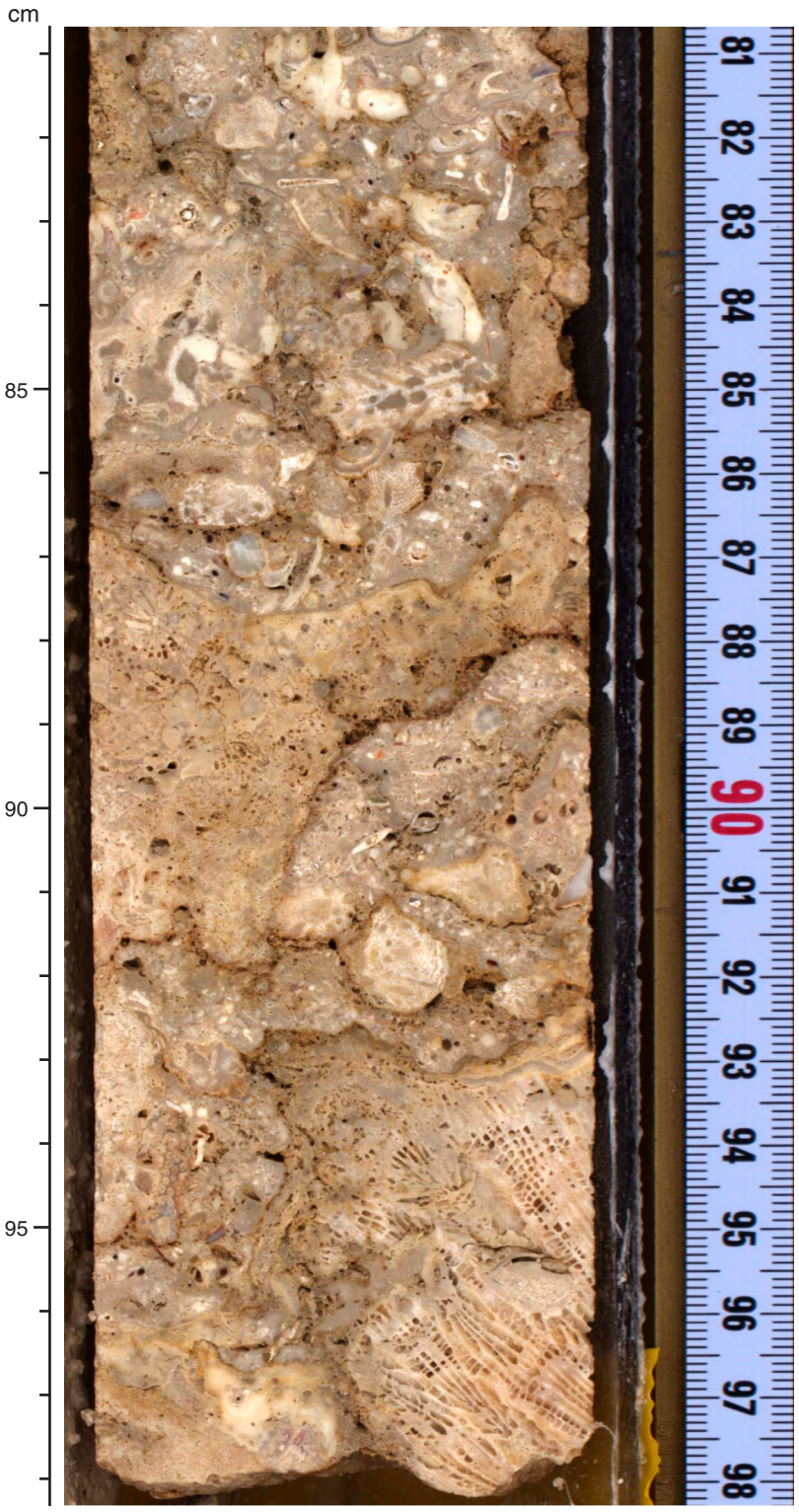

Figure F92. High-resolution line scan image of a massive Faviidae over a bioclastic packstone (interval 325-M0056A-2R-1, 121–135 cm).

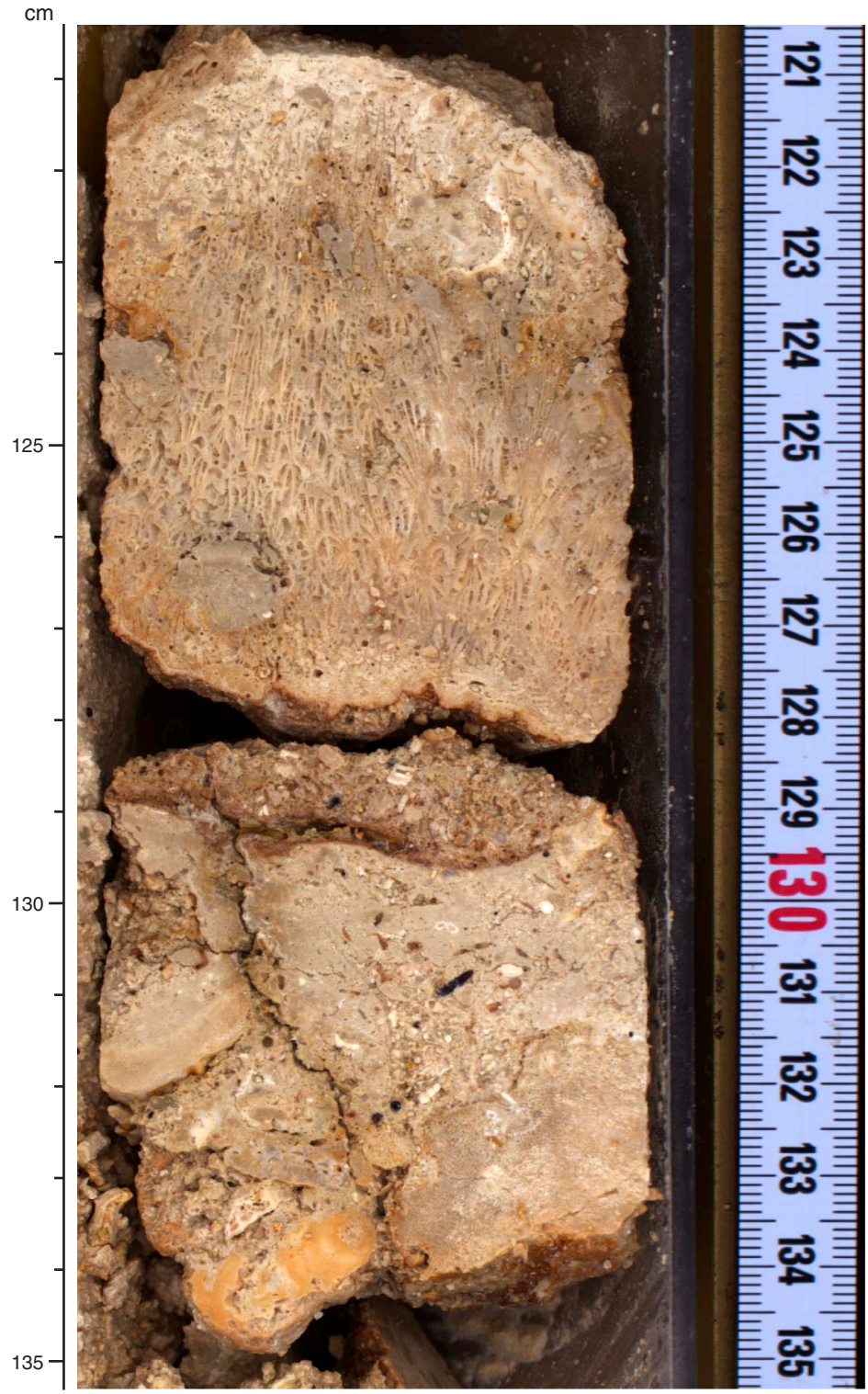

Figure F93. High-resolution line scan image of a massive *Cyphastrea* encrusted by thick coralline algae (interval 325-M0056A-2R-1, 11–22 cm).

Figure F94. High-resolution line scan image of a Faviidae(?) in a bioclastic grainstone with brown stains (interval 325-M0056A-4R-1, 127–140 cm).

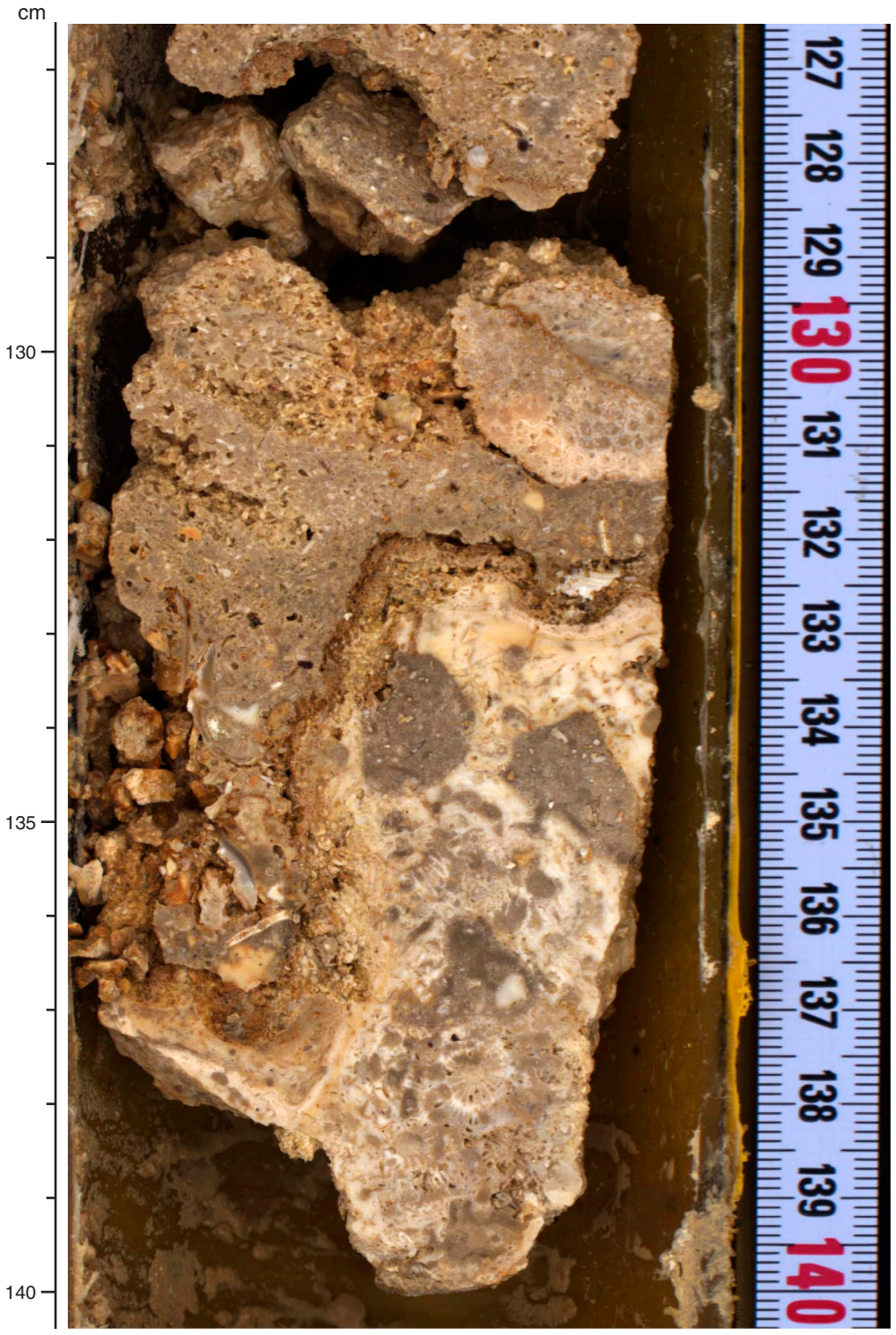

Figure F95. High-resolution line scan image of packstone with mollusks and *Halimeda* moldic porosity (interval 325-M0056A-7R-1, 30–47 cm).

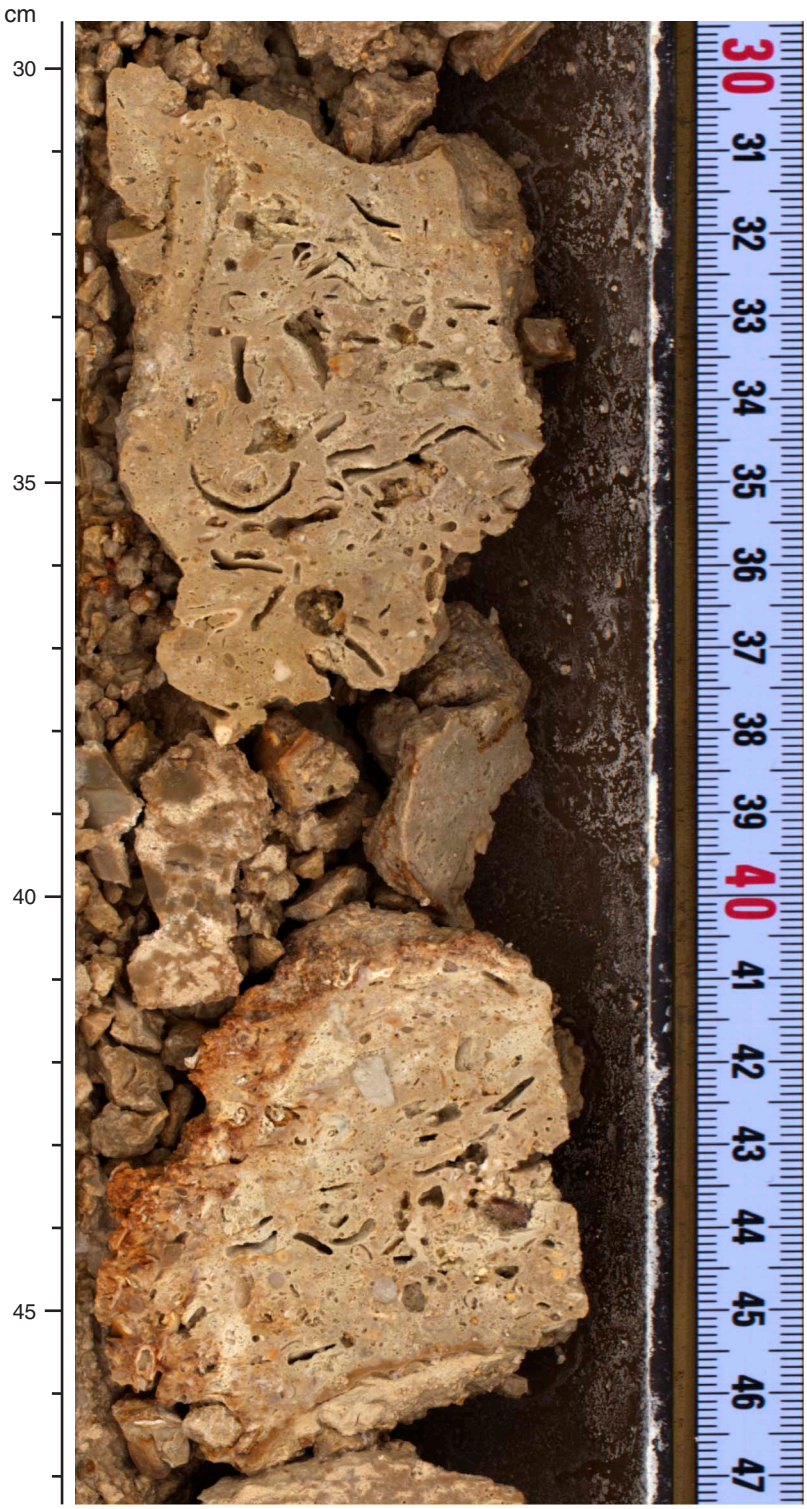

Figure F96. High-resolution line scan image of a coralgal-microbialite boundstone with encrusting *Montipora*(?) and massive *Porites* (interval 325-M0056A-8R-1, 39–61 cm). Abundant secondary porosity filled with fine internal sediment that, in some instances, forms geopetal fabrics.

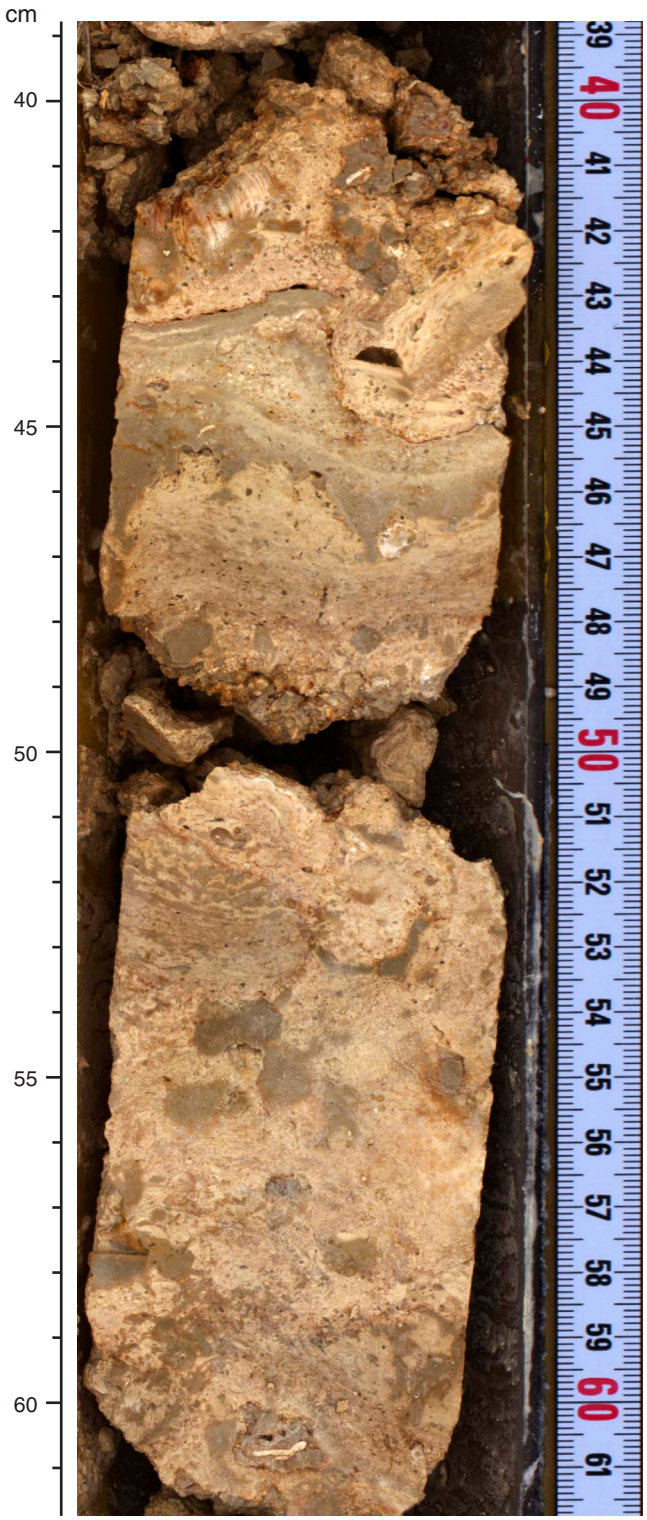

Figure F97. High-resolution line scan image of a coralgal-microbialite boundstone with secondary porosity (interval 325-M0056A-8R-2, 4–27 cm).

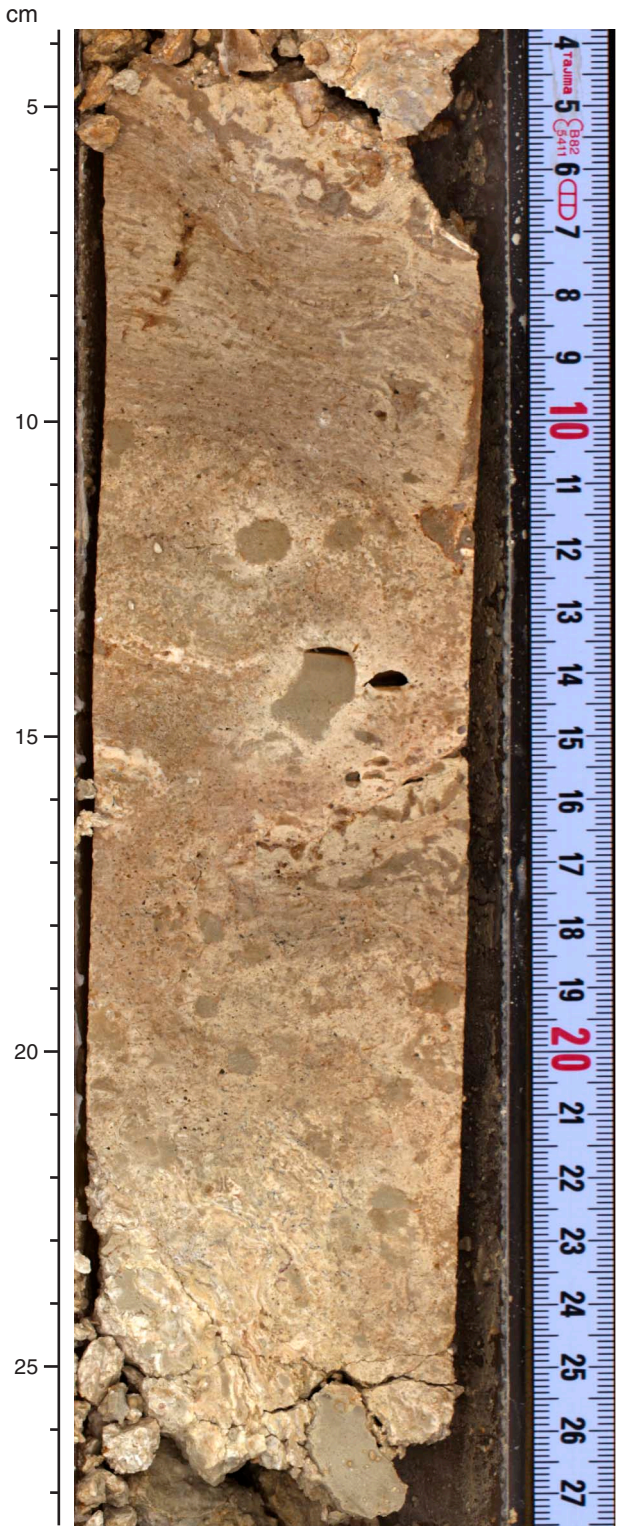

Figure F98. High-resolution line scan image of coralgal-microbialite boundstone with secondary porosity fully or partially infilled in places to form geopetal fabrics (interval 325-M0056A-9R-1, 6–17 cm).

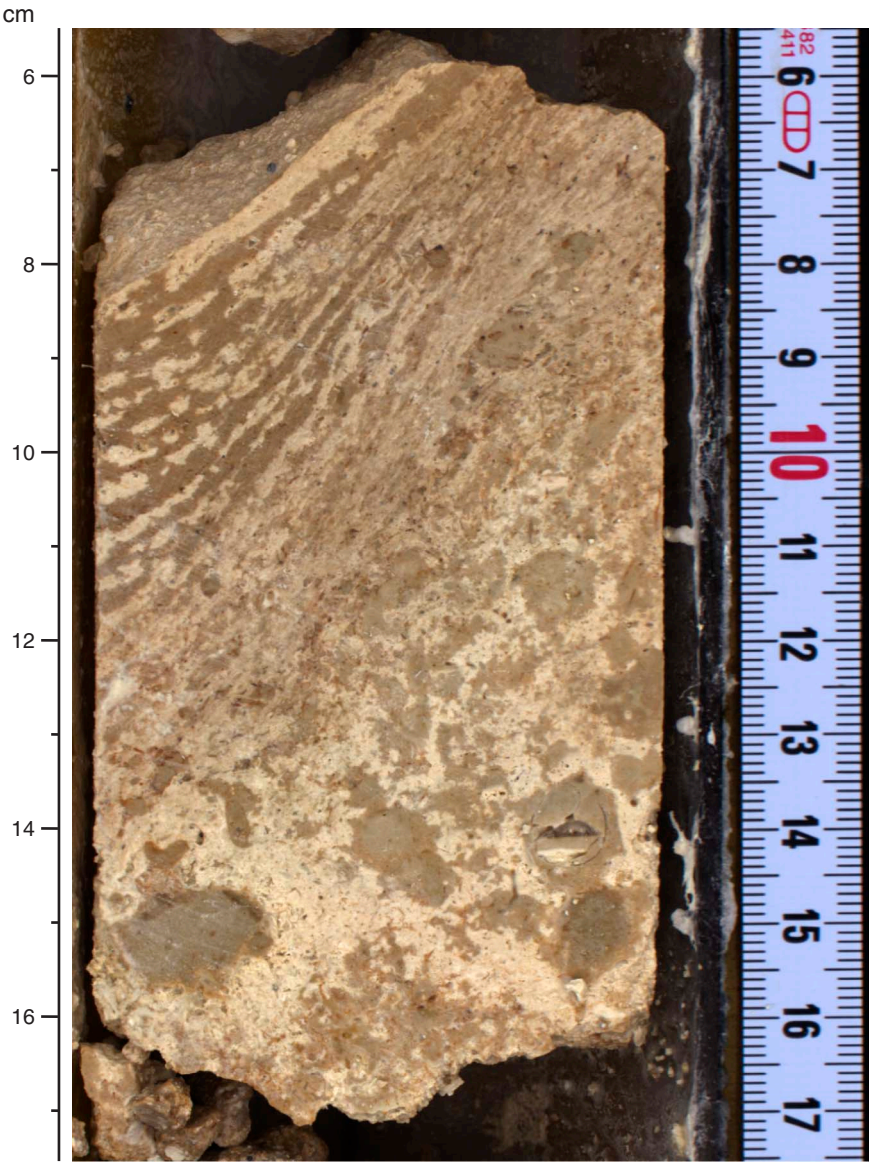

Figure F99. High-resolution line scan image of a coralgal-microbialite boundstone with thick coralline algae encrusted by microbialite and brown stains (interval 325-M0056A-8R-2, 41–52 cm).

Figure F100. High-resolution line scan image of a coralgal boundstone with massive Faviidae and encrusting *Montipora*(?) or *Porites*(?) (interval 325-M0056A-8R-1, 88–105 cm).

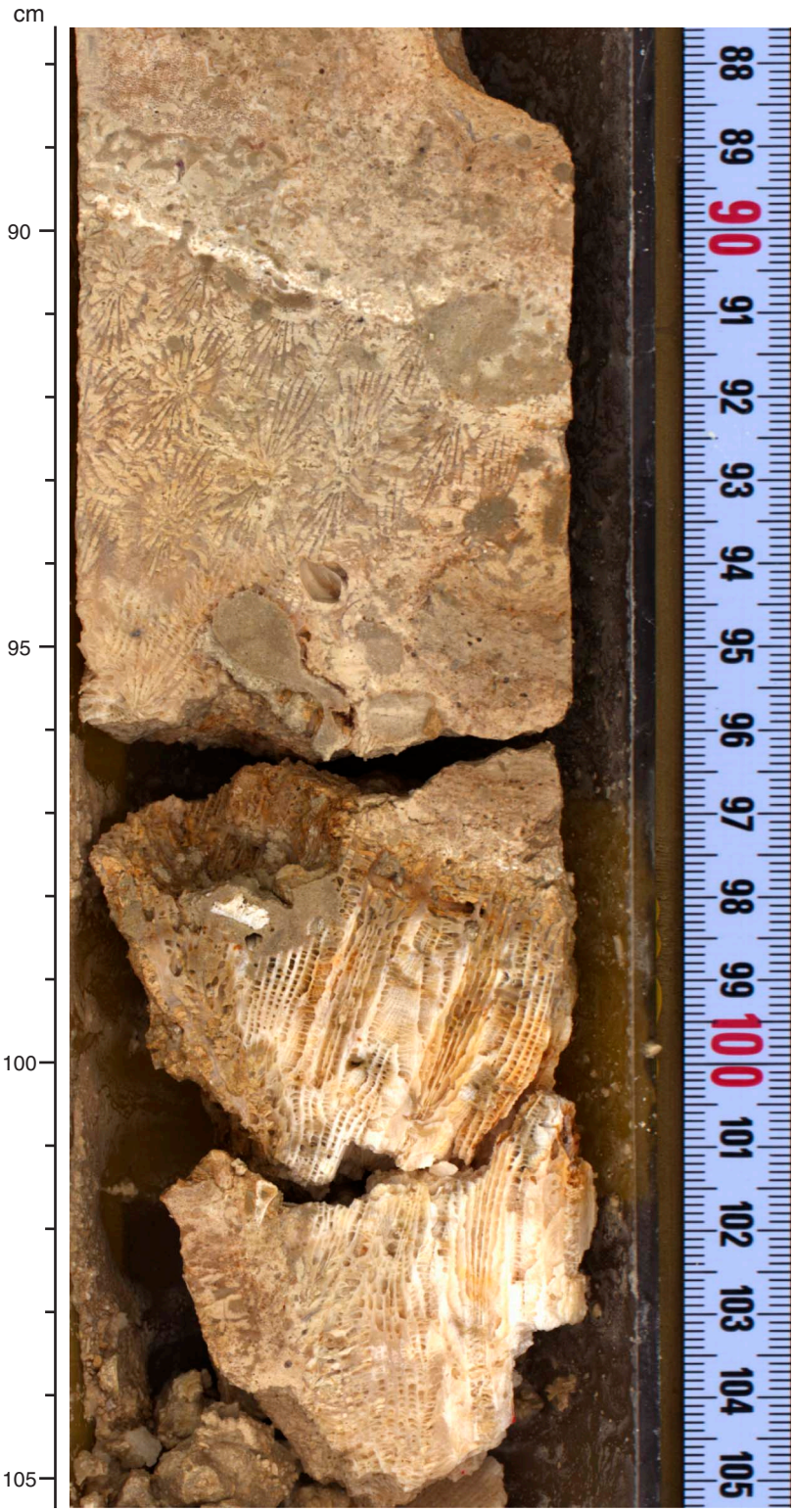

Figure F101. High-resolution line scan image of a packstone with mollusks, corals, larger foraminifera, and *Halimeda,* with moldic porosity (interval 325-M0056A-11R-1, 55–71 cm).

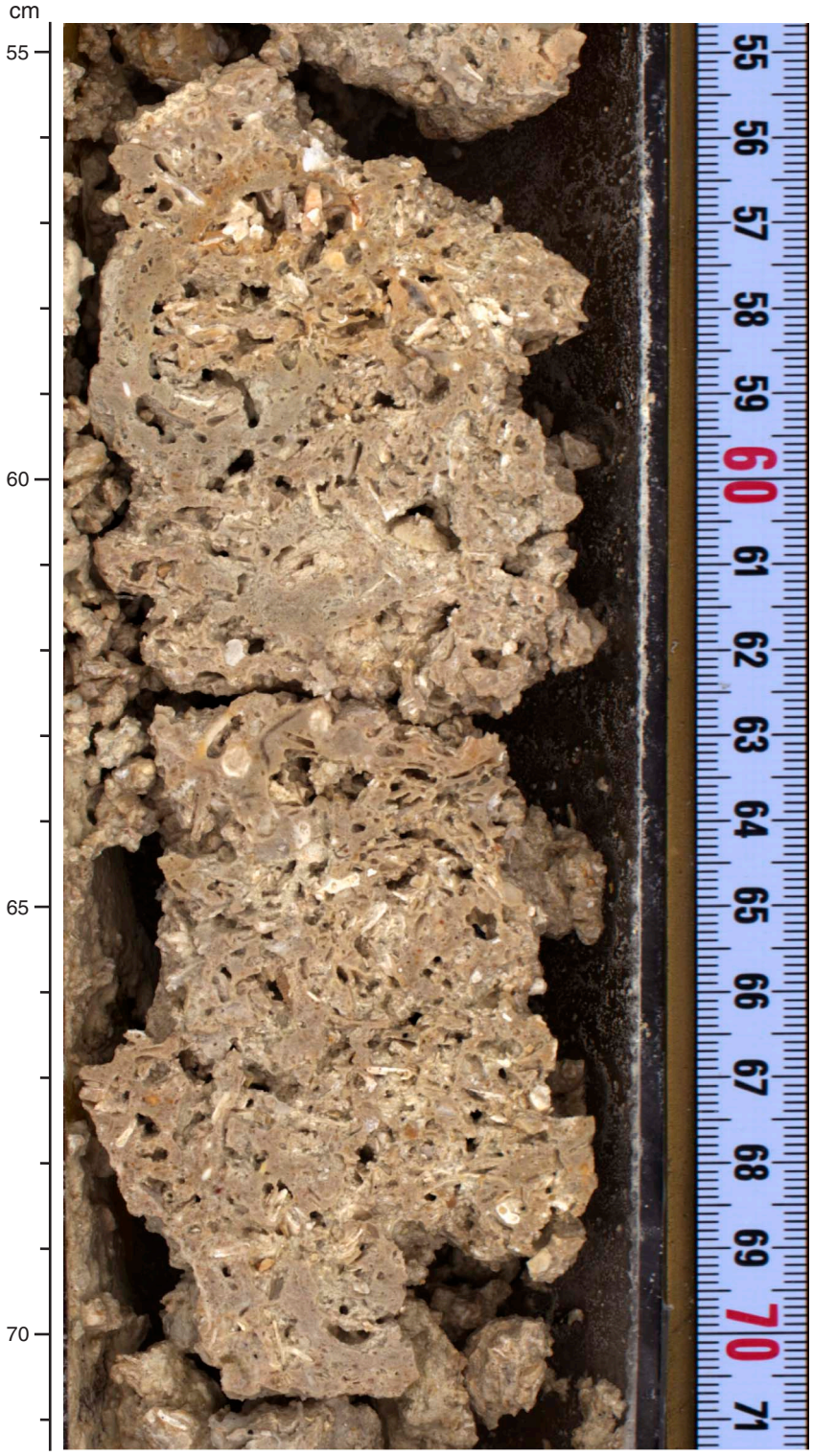

Figure F102. High-resolution line scan image of a packstone with mollusks, corals, larger foraminifera, and *Halimeda,* with moldic porosity (interval 325-M0056A-11R-1, 0–13 cm).

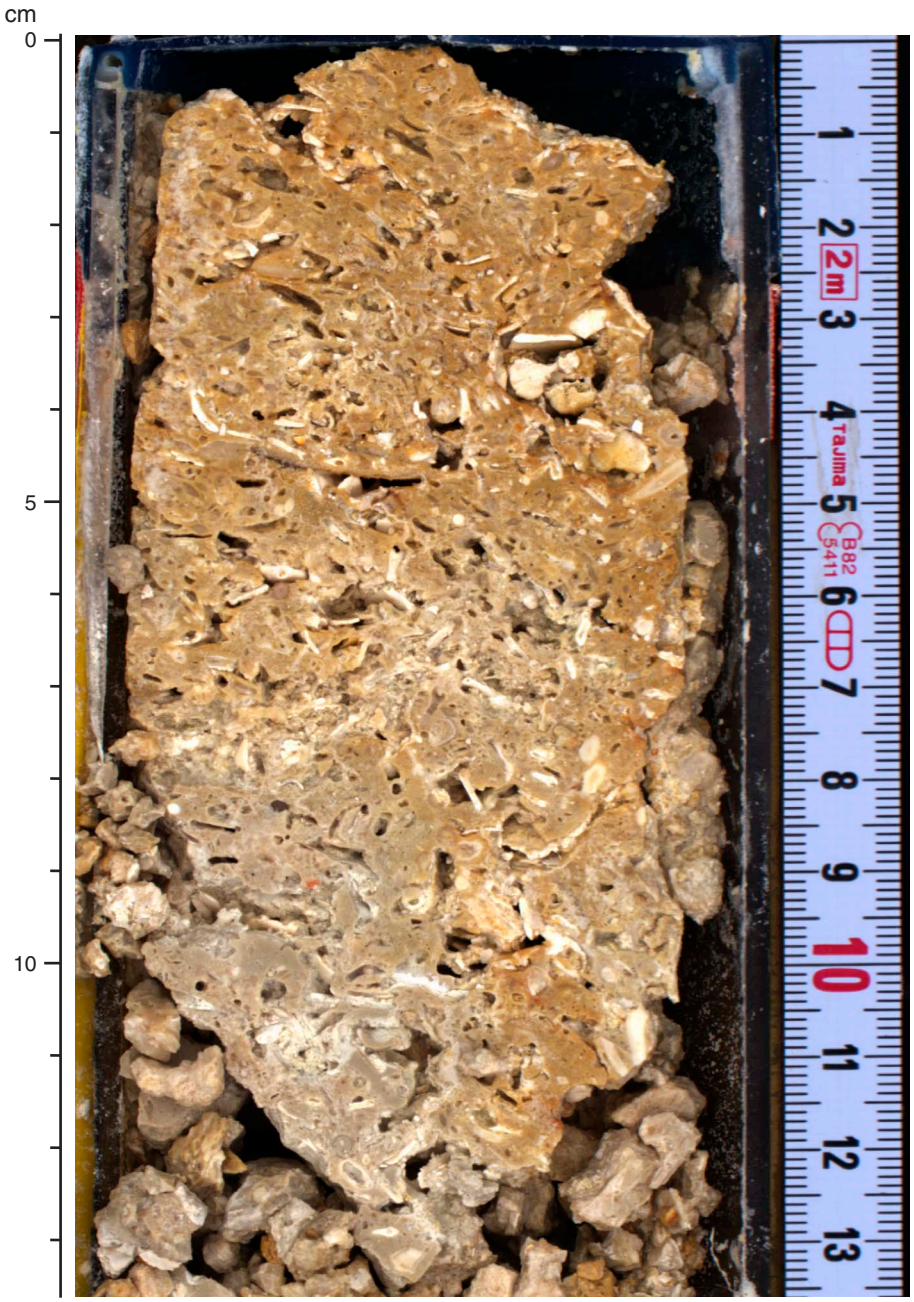

Figure F103. High-resolution line scan image of a packstone with *Halimeda,* mollusks and corals (interval 325-M0056A-16R-CC, 1–8 cm).

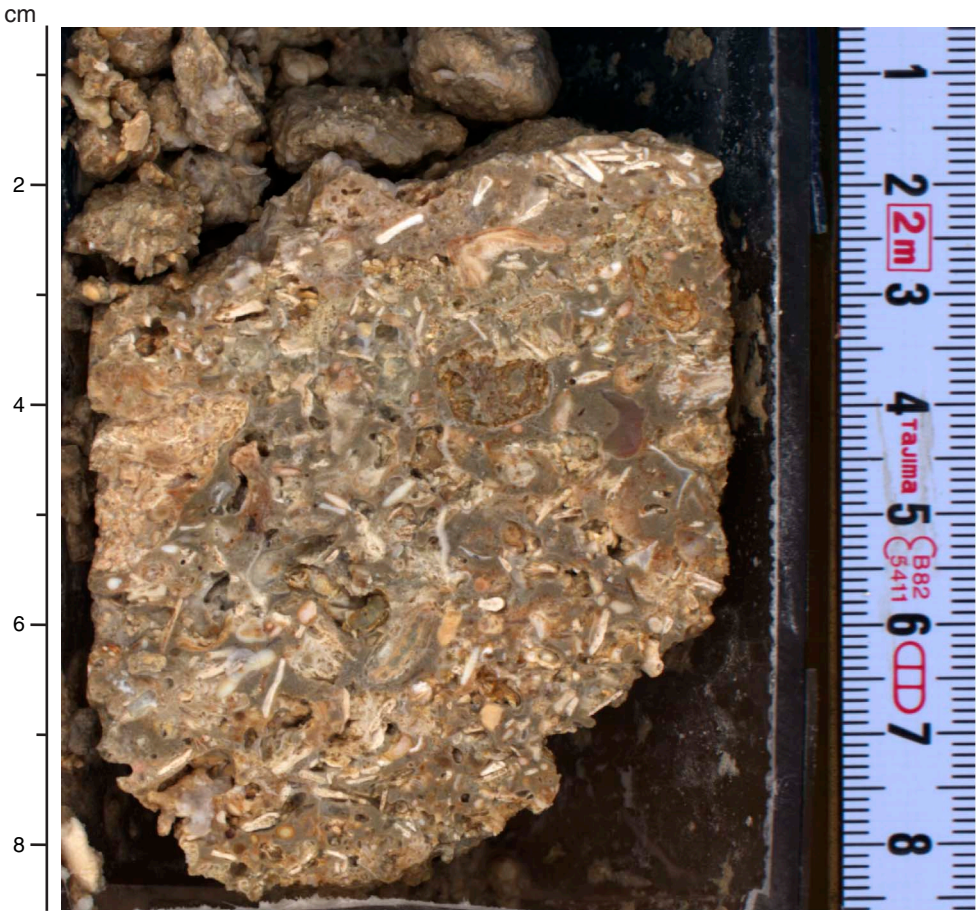

Figure F104. Summary diagram showing data collected on whole cores using the MSCL, Hole M0056A.

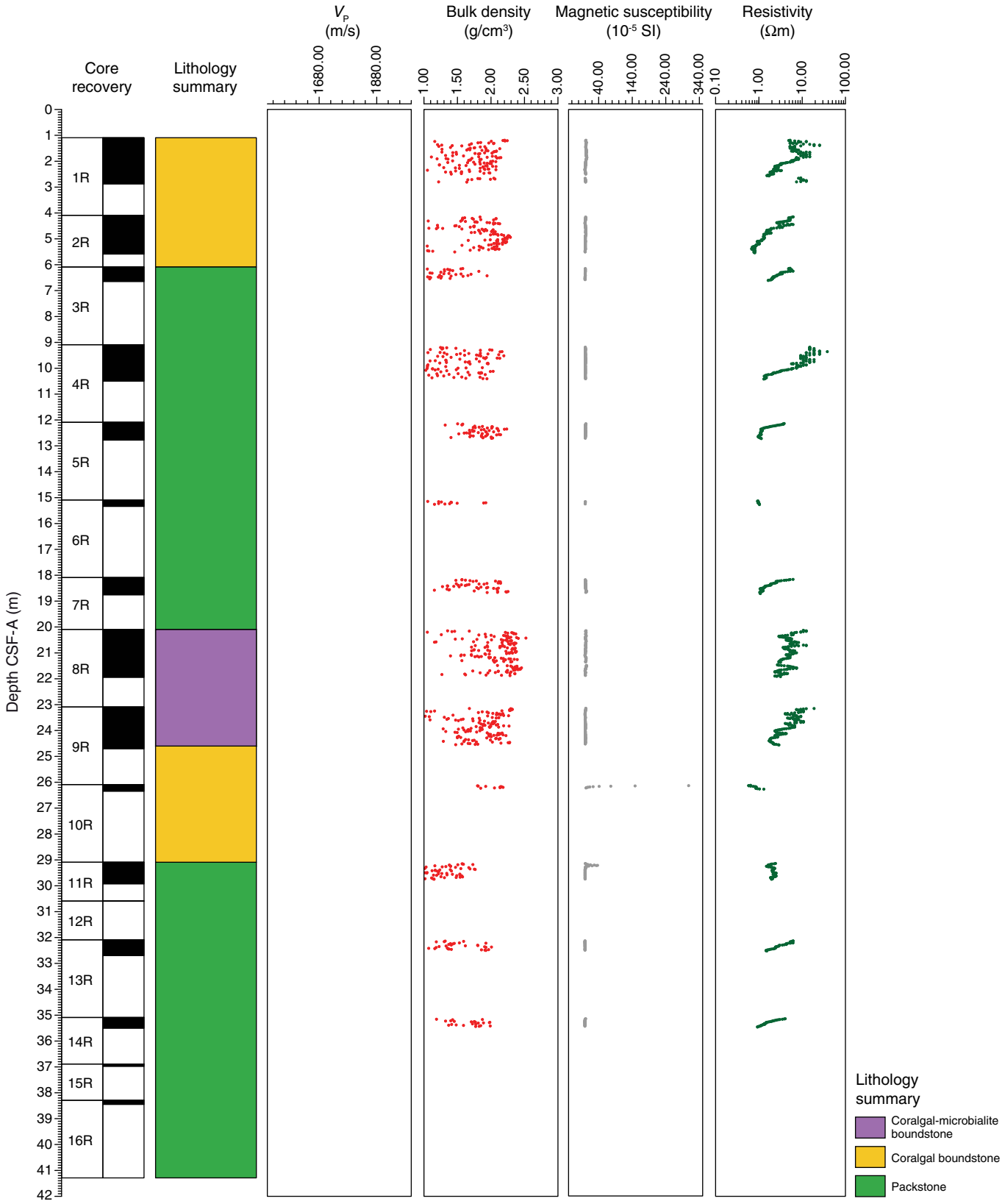

Figure F105. Petrophysical measurements obtained from discrete samples with a pycnometer, Hole M0056A. Bulk density measured on whole cores with the MSCL is shown in red on the bulk density plot.

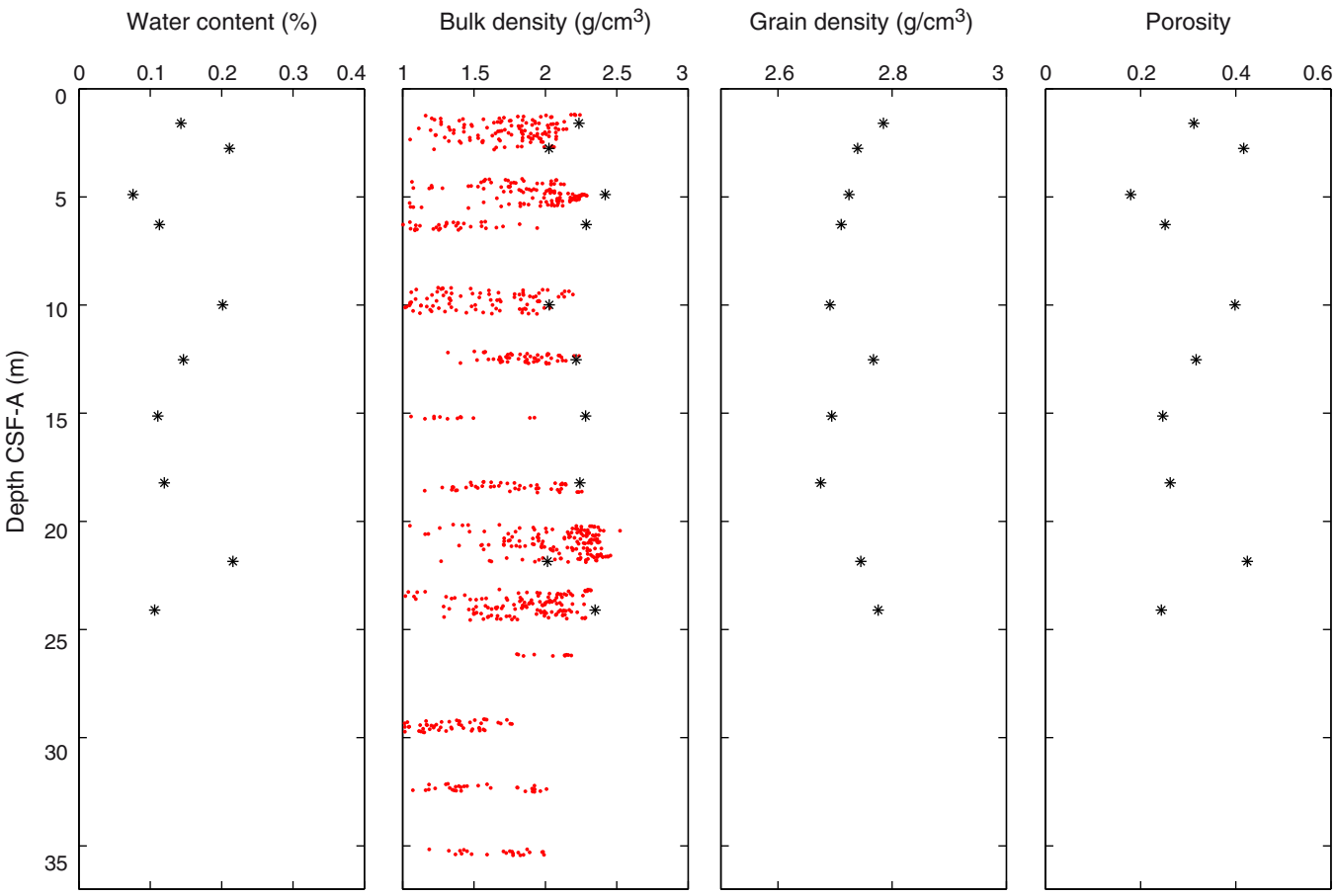

Figure F106. *P*-wave velocity data, Hole M0056A. **A.** Plot of initial, dry, and resaturated *P*-wave velocity measurements on discrete samples vs. depth. Three measurements were taken at each depth and are denoted by a dot. Average values are plotted as an open triangle. **B.** Plot showing discrete *P*-wave velocity vs. discrete bulk density.

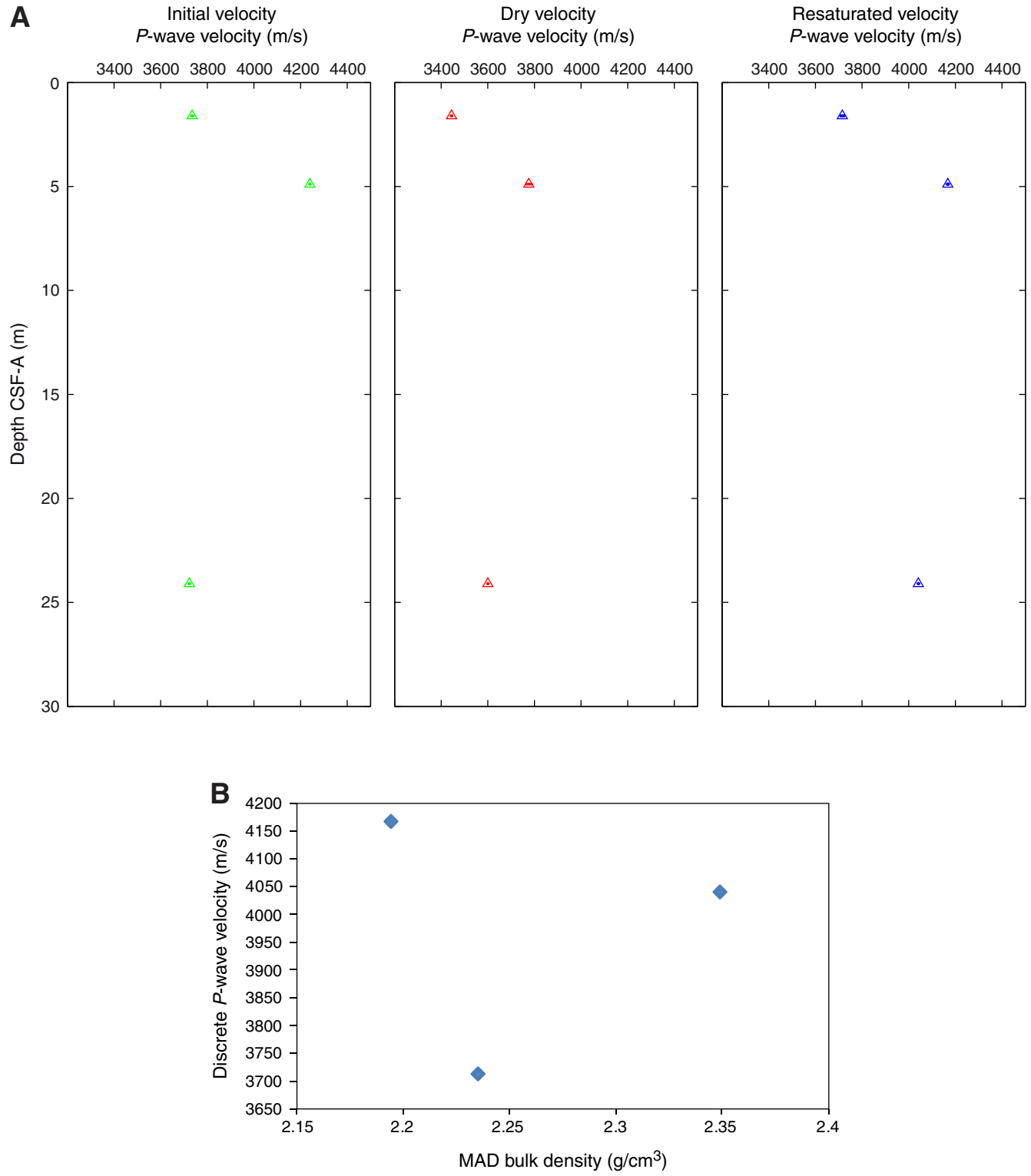

Figure F107. Values of reflectance (L*), green to red (a*), and blue to yellow (b*) indexes, along with ratio a*/b* for Hole M0056A.

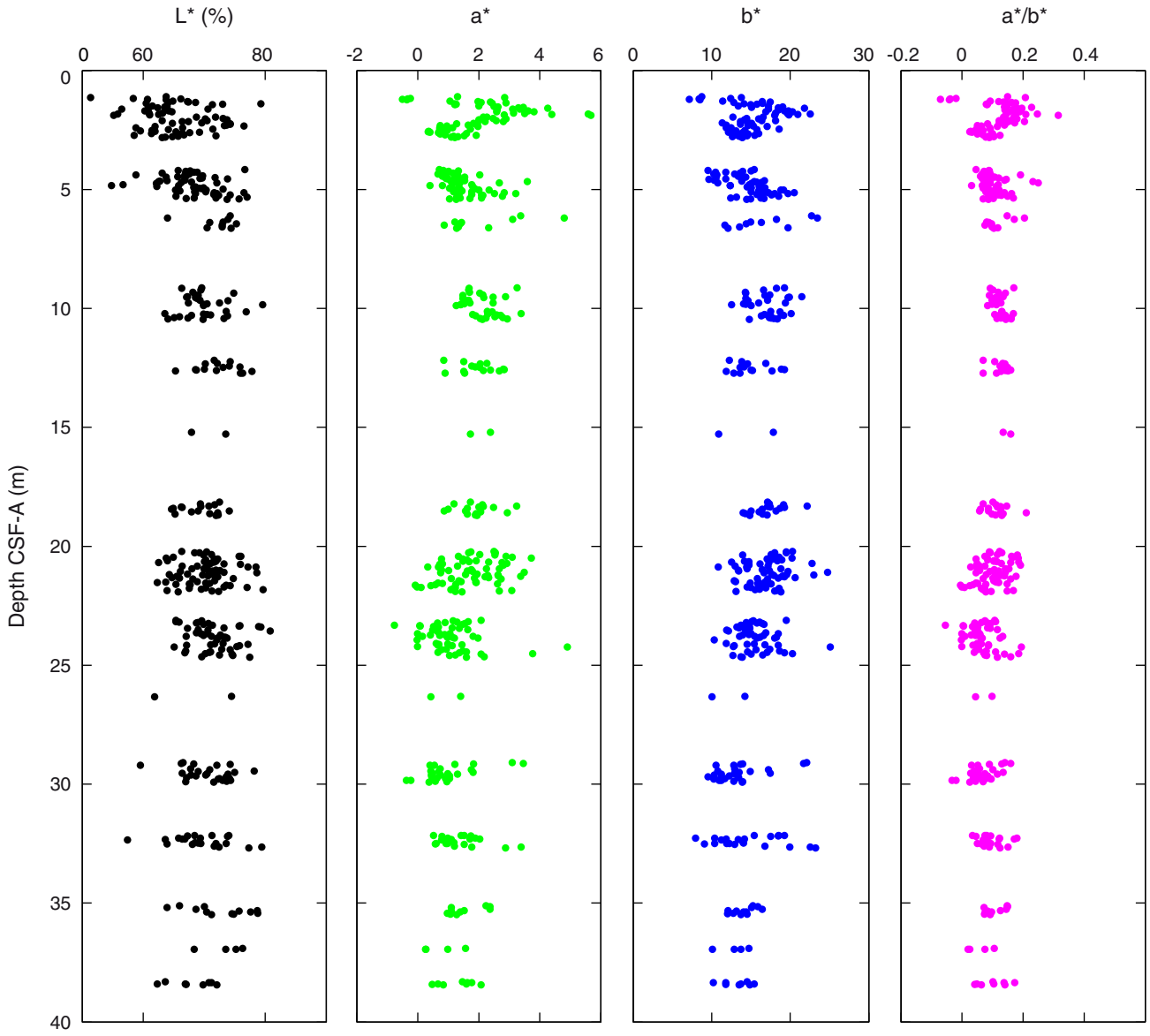

Figure F108. Magnetic susceptibility record for Hole M0056A. Water depth = 81.22 m (LAT).

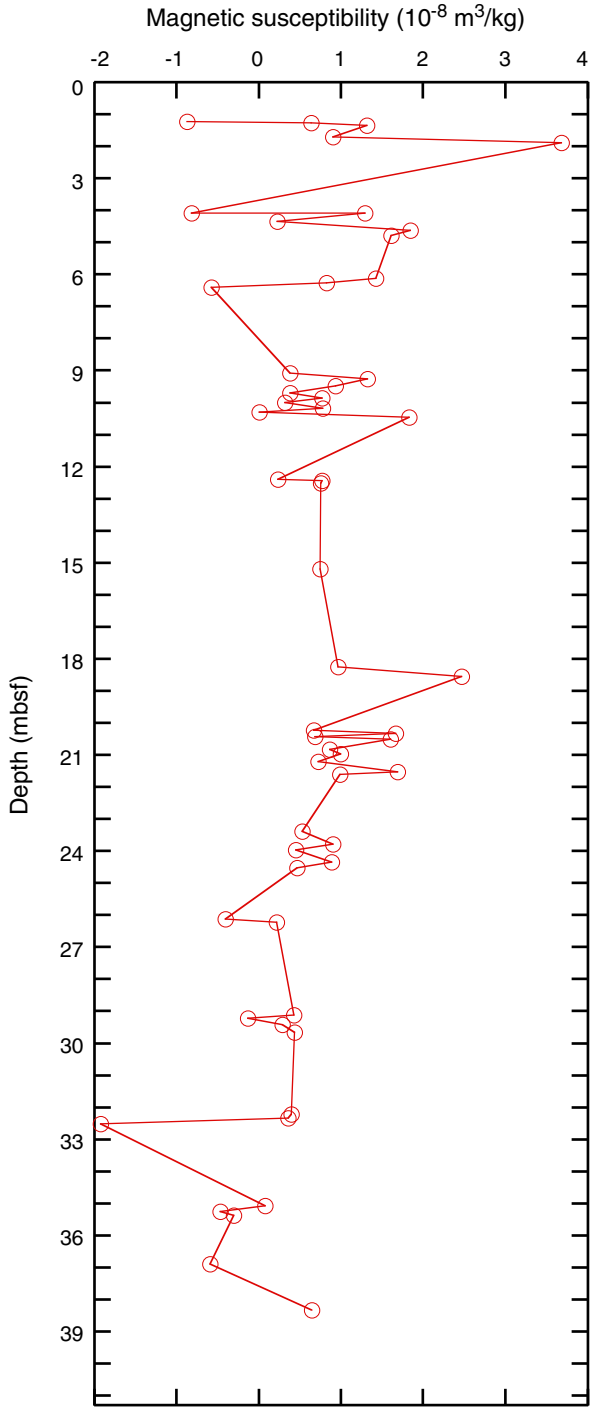

Figure F109. Preliminary chronology for Hole M0056A. Radiocarbon data are presented as graphs with the uncalibrated radiocarbon age and uncertainty shown as the red normal distribution on the ordinate axis and the probability distribution of the calibrated age shown in gray on the abscissa. The marine09 calibration curve is shown in blue. Horizontal bars indicate portions of the age distribution that are significant at the 95.4% confidence interval and the mean age (white circle ±1 standard deviation) used for the purposes of the preliminary dating. All ages are presented as thousands of calendar years BP (1950 AD). See Table **T10** in the "Methods" chapter. (See Bronk Ramsey [2009], as well as Bronk Ramsey [2010] at **c14.arch.ox.ac.uk/oxcal.html.**)

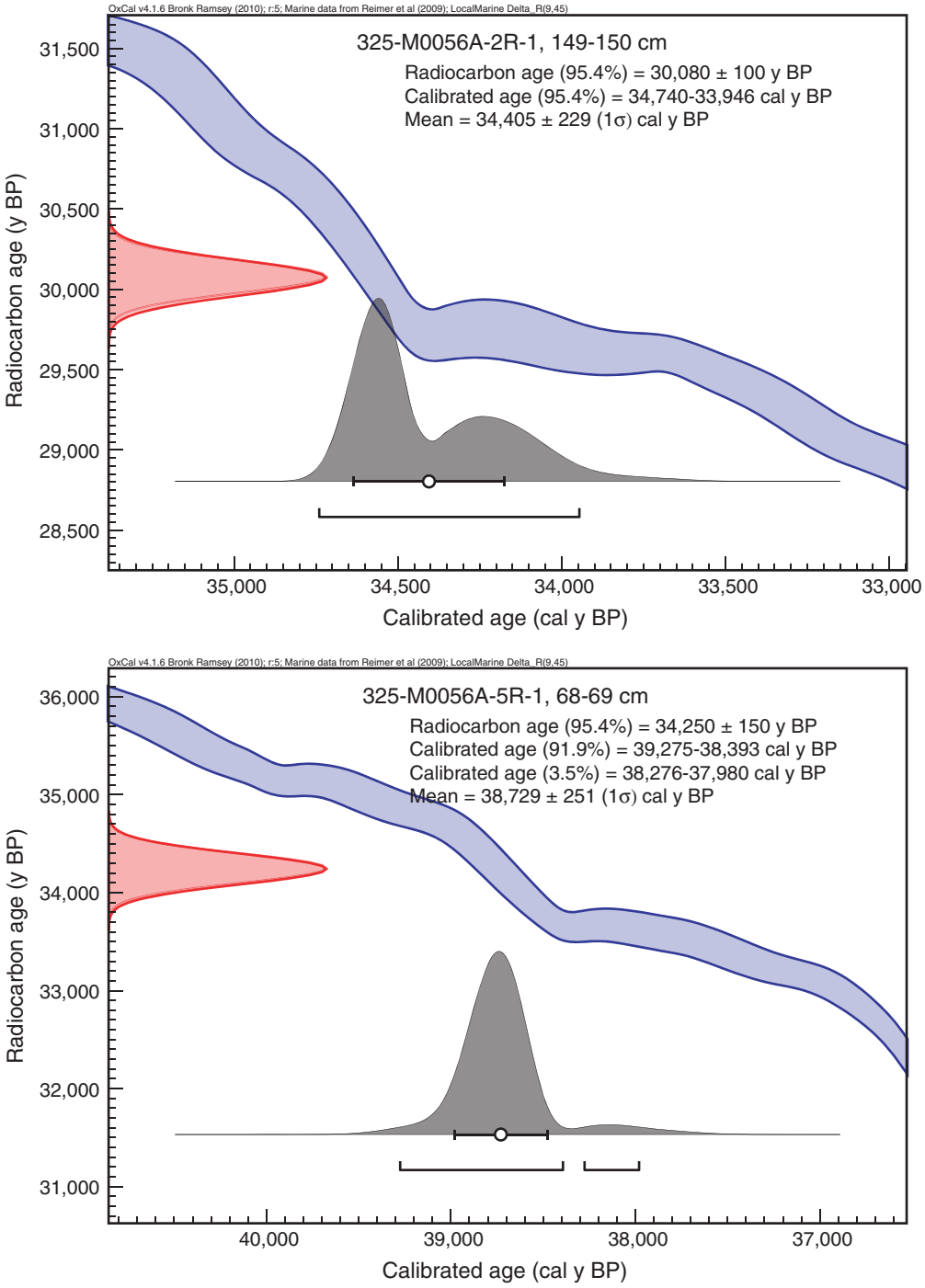

Figure F110. High-resolution line scan image of a massive *Isopora* (in situ) covered by a thick coralline algal crust containing vermetids (interval 325-M0057A-5R-1, 11–48 cm).

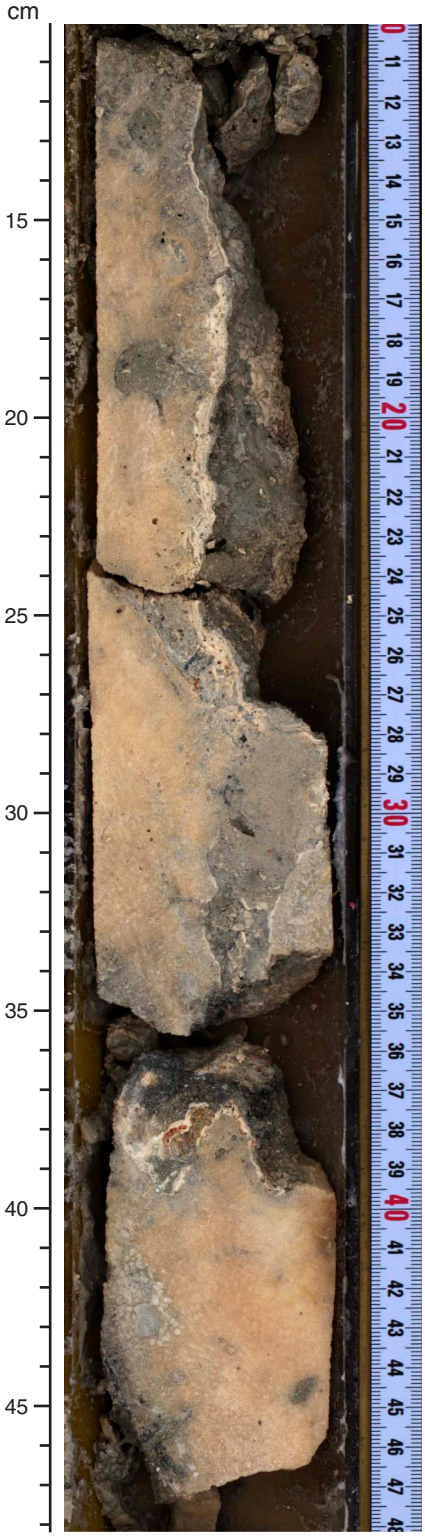

Figure F111. High-resolution line scan image of a tabular *Acropora* encrusted by thick coralline algae (interval 325-M0057A-3R-1, 6–16 cm).

Figure F112. High-resolution line scan image of a submassive *Montipora* (in situ?) encrusted by thick, foliose coralline algae and locally bored (interval 325-M0057A-1R-1, 1–14 cm).

Figure F113. High-resolution line scan image of a massive *Isopora* encrusted by thick coralline algae with protuberances and microbialites (interval 325-M0057A-4R-1, 74–88.5 cm).

Figure F114. High-resolution line scan image of a bioeroded massive *Montipora* encrusted by thick coralline algae (interval 325-M0057A-2R-1, 63–91 cm).

Figure F115. High-resolution line scan image of a medium branching *Acropora* (interval 325-M0057A-4R-1, 101–113 cm).

Figure F116. High-resolution line scan image of a branching *Isopora* encrusted by thick coralline algae and microbialites and infilled with *Halimeda*-rich internal sediment (interval 325-M0057A-6R-2, 1–38 cm).

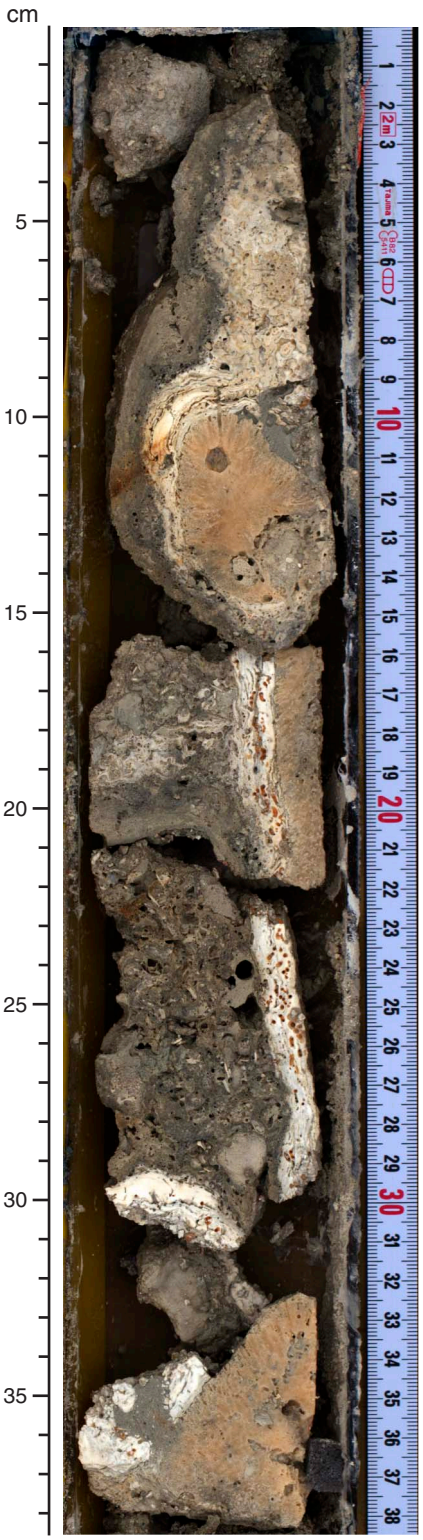

Figure F117. High-resolution line scan image of lumps of *Halimeda* rudstone with muddy matrix and borings infilled by a grainstone (interval 325-M0057A-7R-1, 121–137 cm). Coral fragments of thick *Pocillopora* and fine to medium branching *Acopora* are also visible.

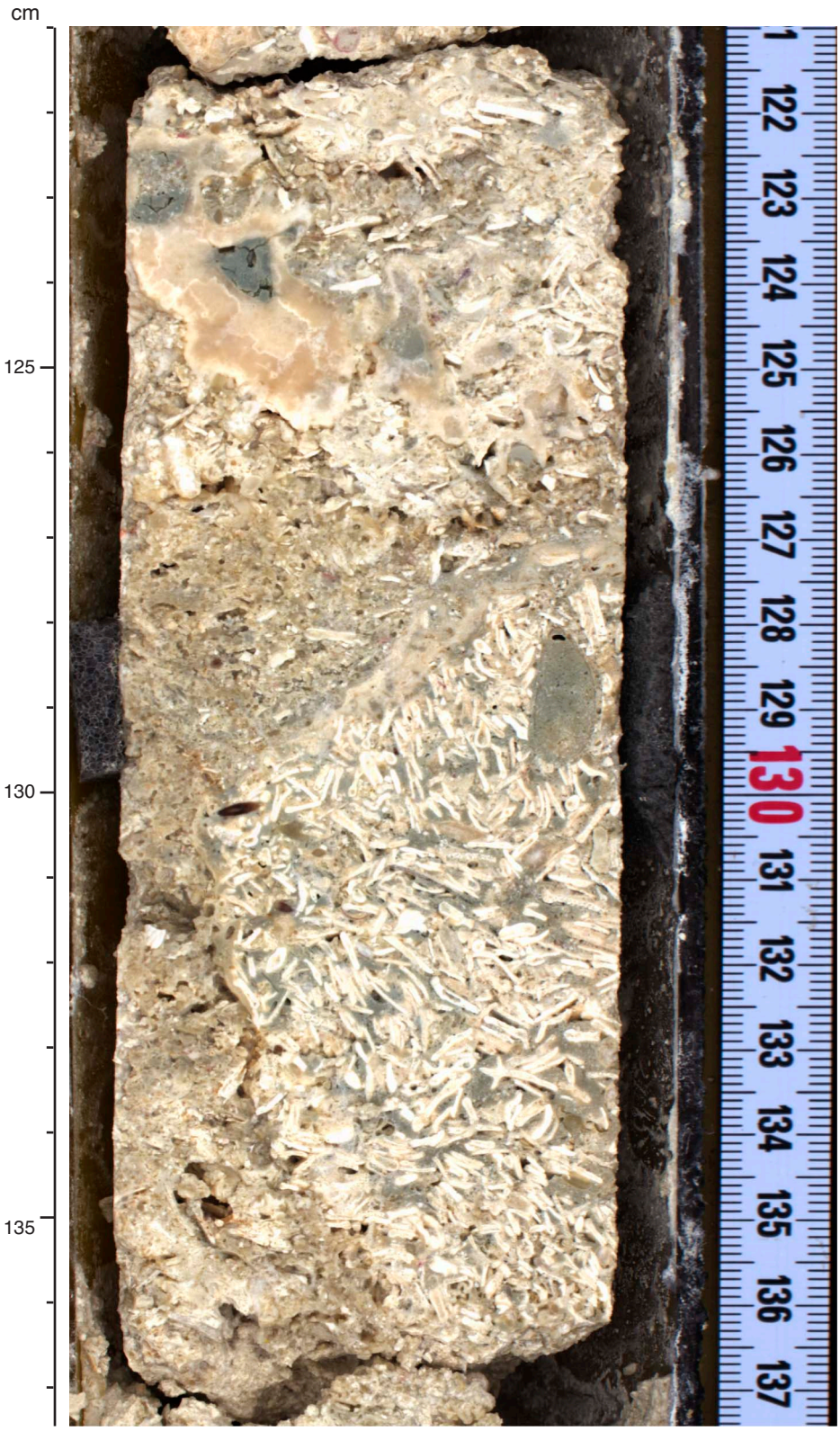

Figure F118. High-resolution line scan image of a massive *Montastrea curta* with *Halimeda*-rich internal sediment (interval 325-M0057A-8R-1, 0–9 cm).

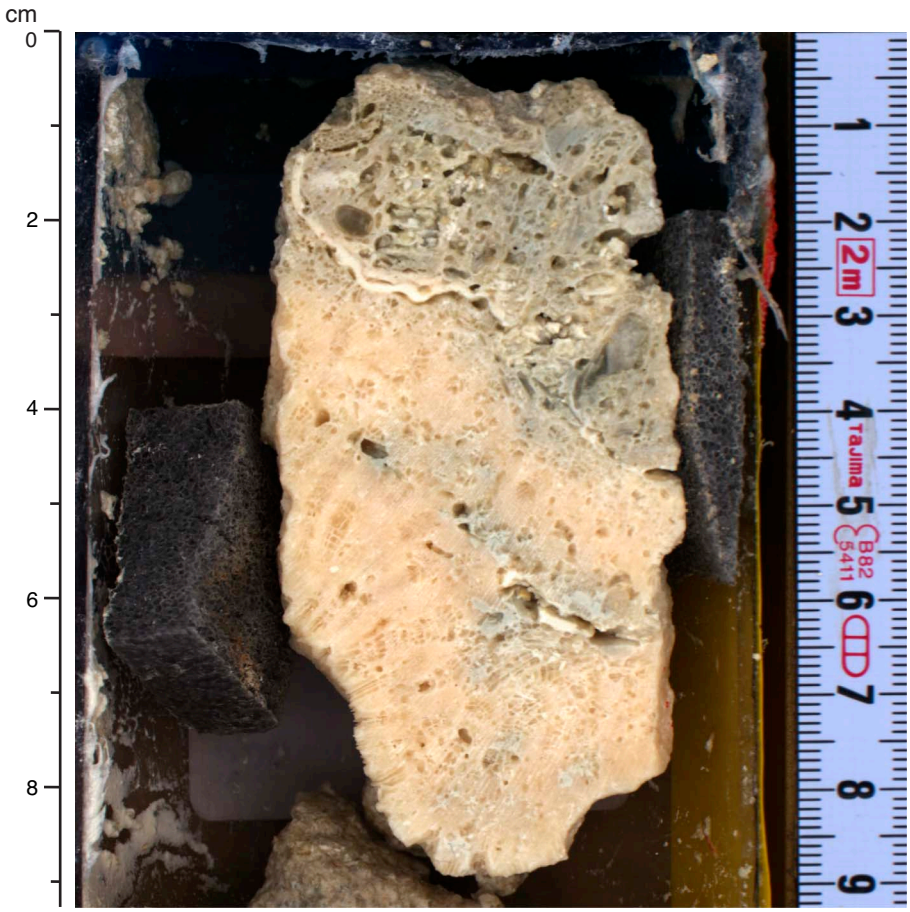

Figure F119. High-resolution line scan image of *Halimeda* grainstone to rudstone with partial dissolution of originally aragonitic components and an irregular brown stained surface (interval 325-M0057A-7R-1, 38–51 cm).

Figure F120. High-resolution line scan image of a massive *Platygyra* encrusted by coralline algae (interval 325-M0057A-7R-2, 40–59 cm). Internal sediment is a *Halimeda*-rich rudstone.

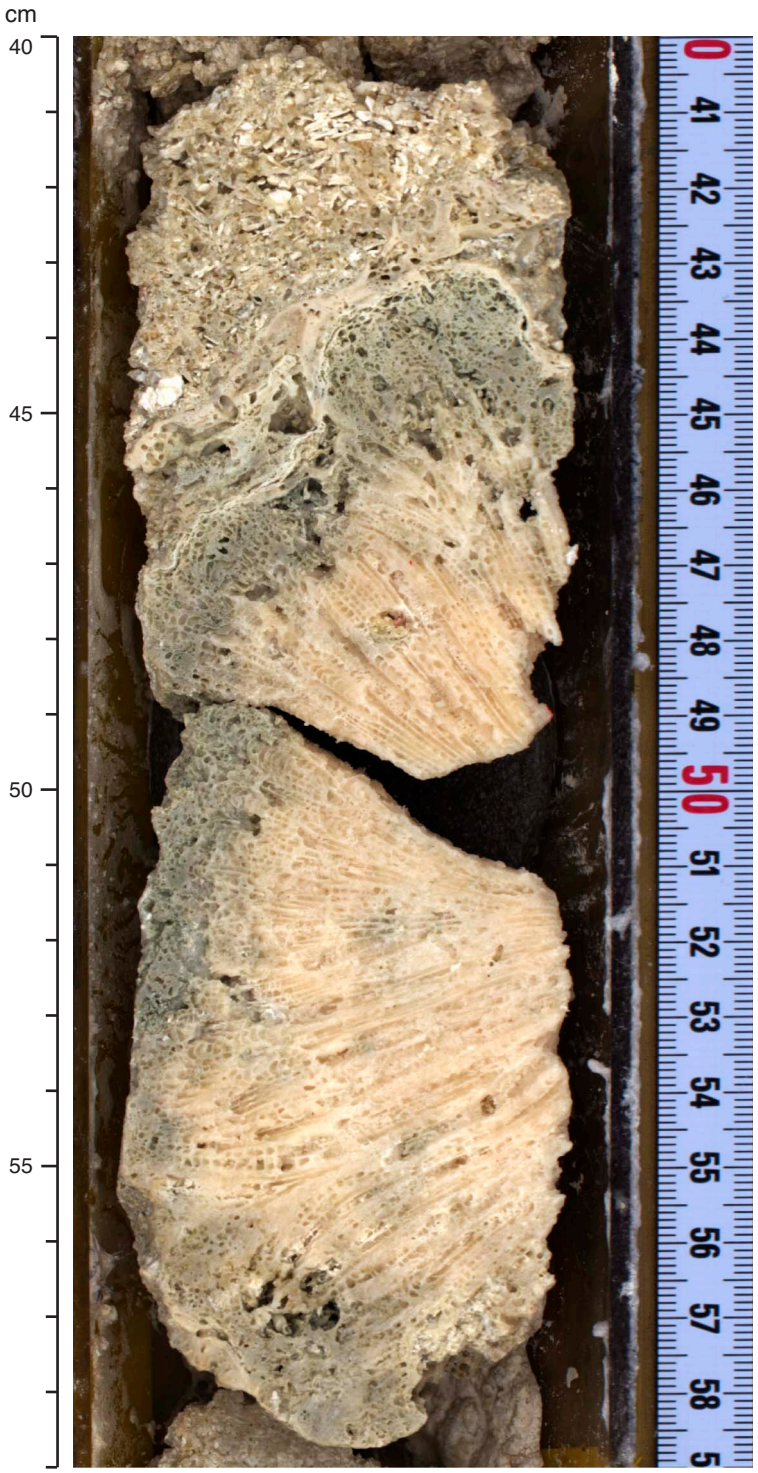

Figure F121. High-resolution line scan image of a solitary discoid Fungiidae (interval 325-M0057A-8R-1, 46–50 cm).

Figure F122. High-resolution line scan image of an altered massive *Montipora* and thick coralline algal crust (interval 325-M0057A-10R-1, 56–70 cm).

Figure F123. High-resolution line scan image of a rudstone affected by dissolution with red staining (interval 325-M0057A-10R-1, 44–51 cm).

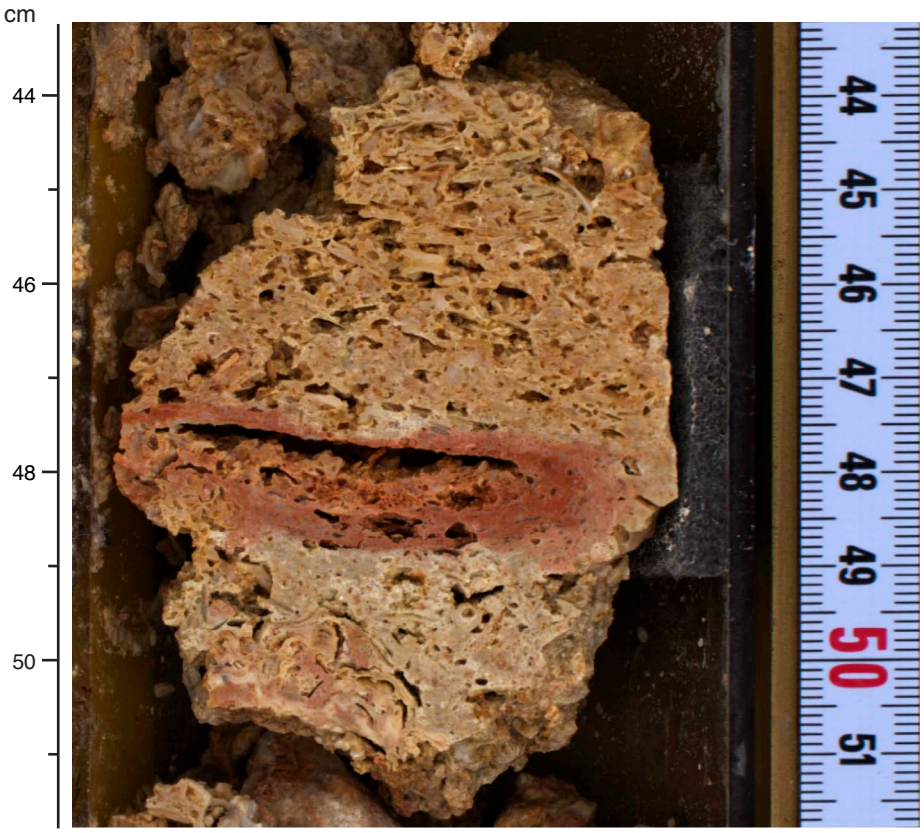

Figure F124. High-resolution line scan image of a massive *Symphillia* (interval 325-M0057A-11R-1, 38–53 cm).

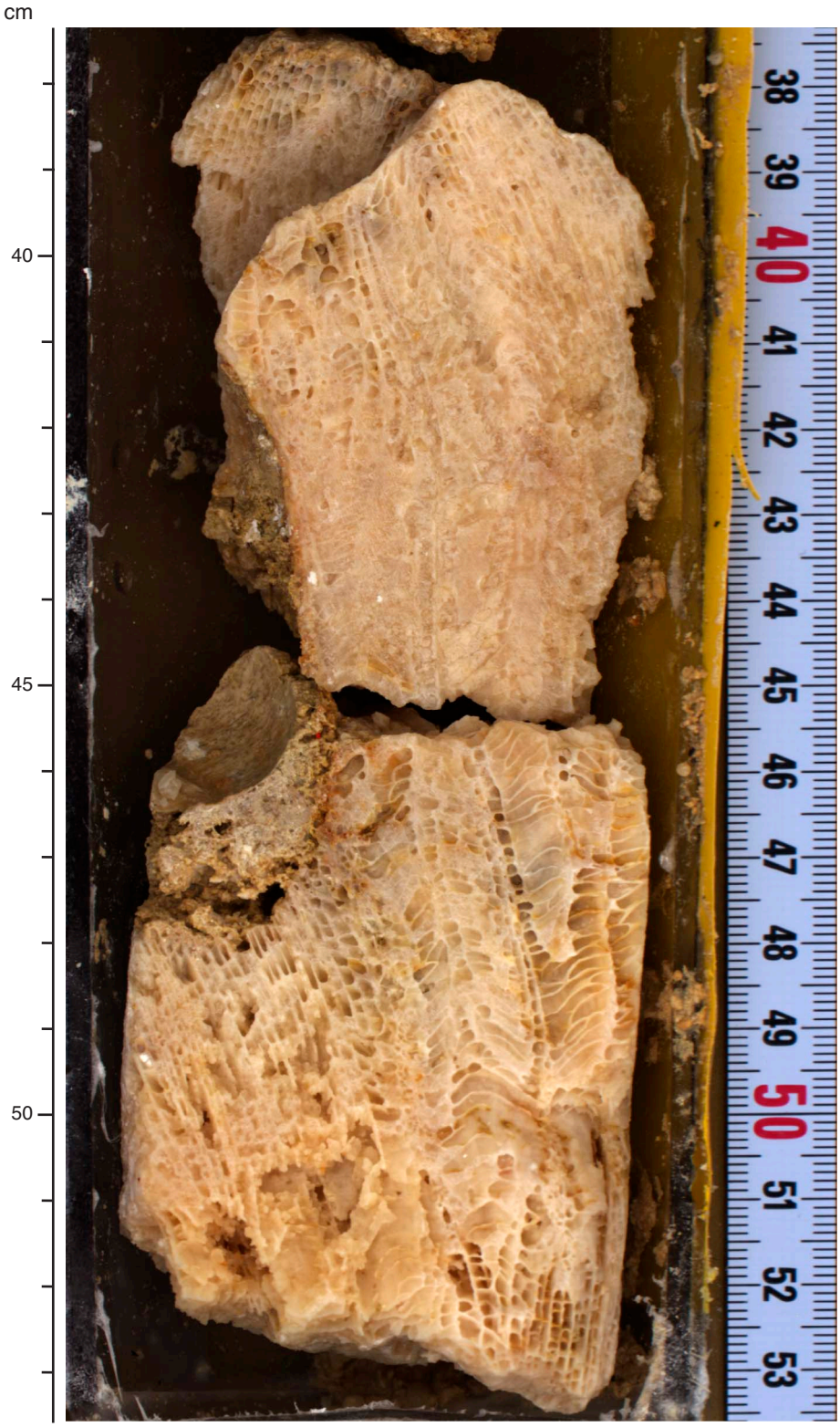

Figure F125. High-resolution line scan image of a massive *Porites* (in situ?) with red staining on top (interval 325-M0057A-10R-1, 75.5–95 cm).

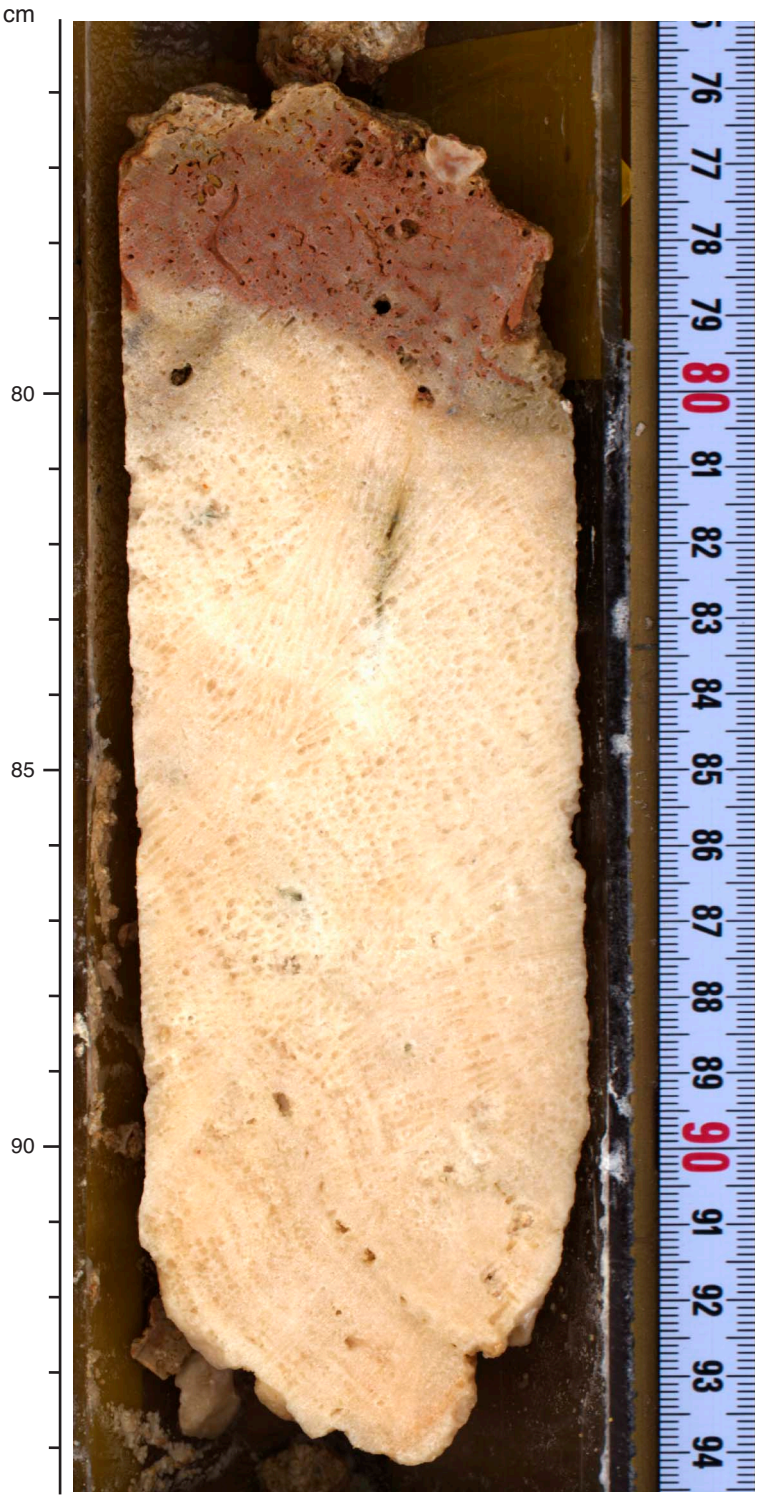

Figure F126. High-resolution line scan image of a framework of encrusting and submassive *Montipora* and fine branching undetermined corals encrusted by thick coralline algae and affected by dissolution (interval 325-M0057A-14R-1, 0–18 cm). Dissolution cavities have brown coatings.

Figure F127. High-resolution line scan image of a submassive *Porites* and Agariciidae encrusted by thick coralline algae, with brown staining at the top (interval 325-M0057A-13R-1, 40–46 cm).

Figure F128. High-resolution line scan image of a coral framework of bioeroded (by sponges) and partially dissolved encrusting and submassive *Pachyseris* encrusted by thick coralline algae (interval 325-M0057A-15R-1, 90–106 cm).

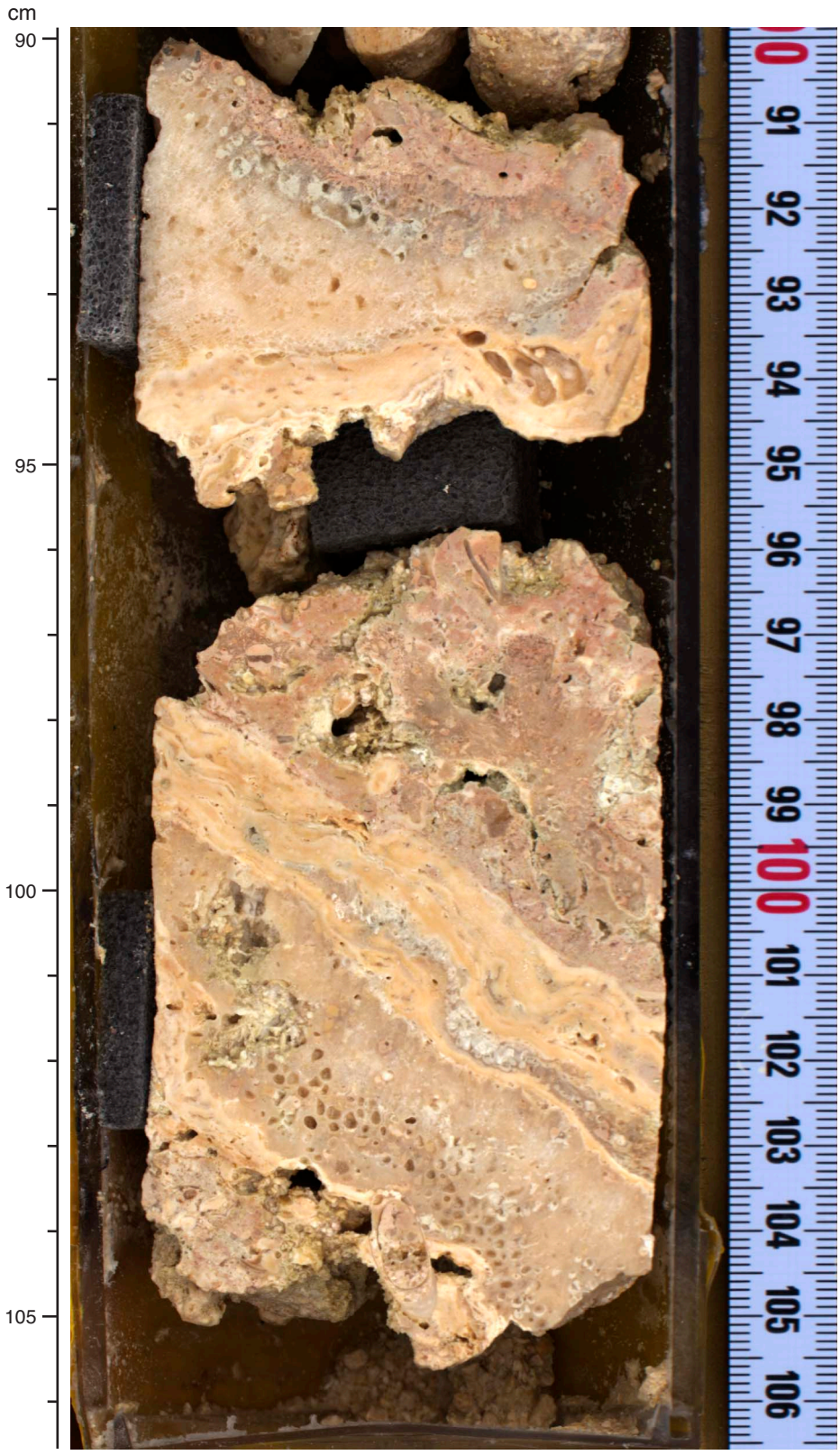

Figure F129. High-resolution line scan image of an in situ Faviidae (possibly *Favites*) encrusted by thick coralline algae and affected by dissolution (interval 325-M0057A-15R-1, 34–48 cm).

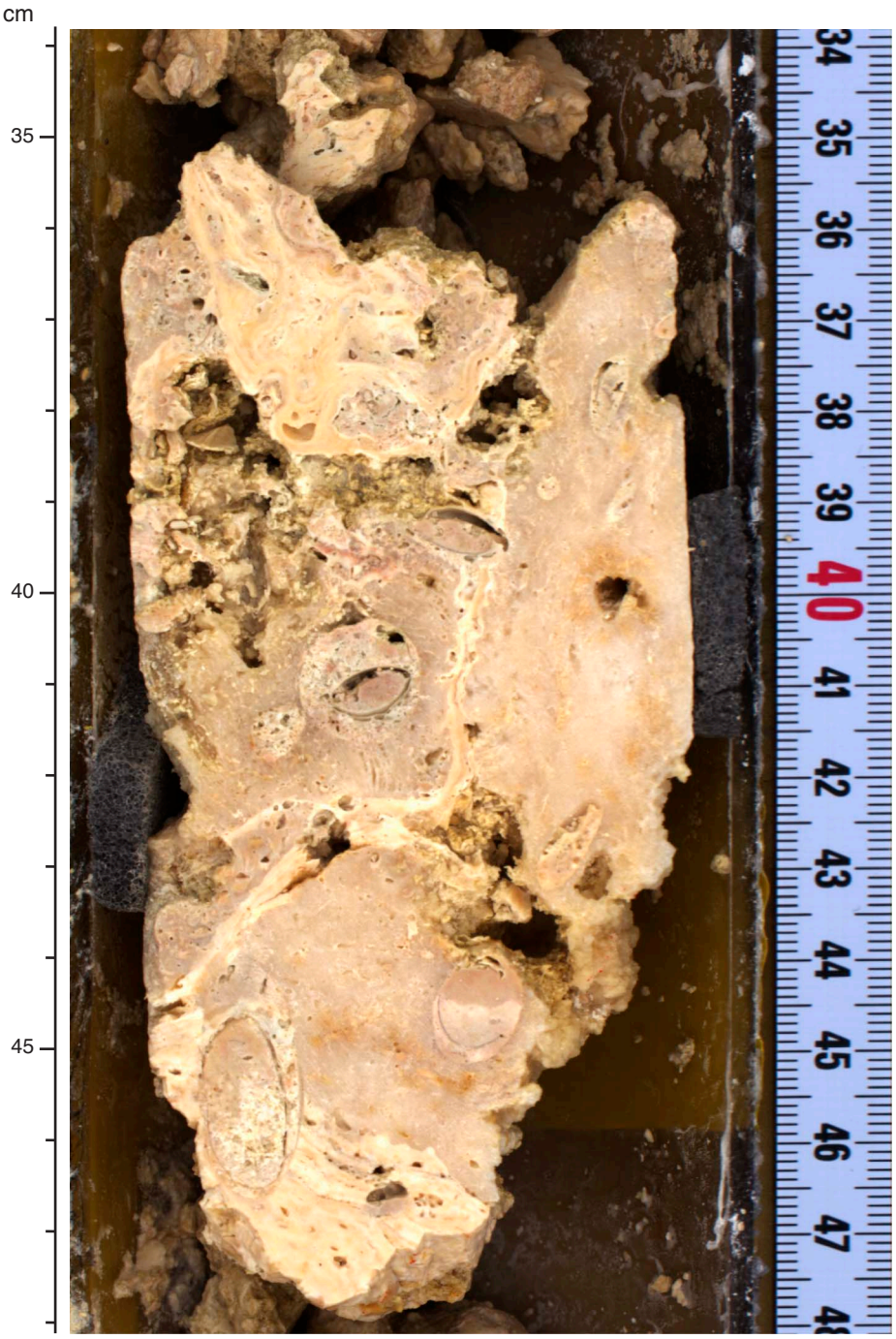

Figure F130. High-resolution line scan image of a coral boundstone containing encrusting or foliaceous Agariciidae(?), fine branching coral, and *Porites* or *Montipora* infilled with packstone internal sediment (interval 325-M0057A-14R-2, 49–70 cm). Dissolution features include red to brown staining and dissolution cavities.

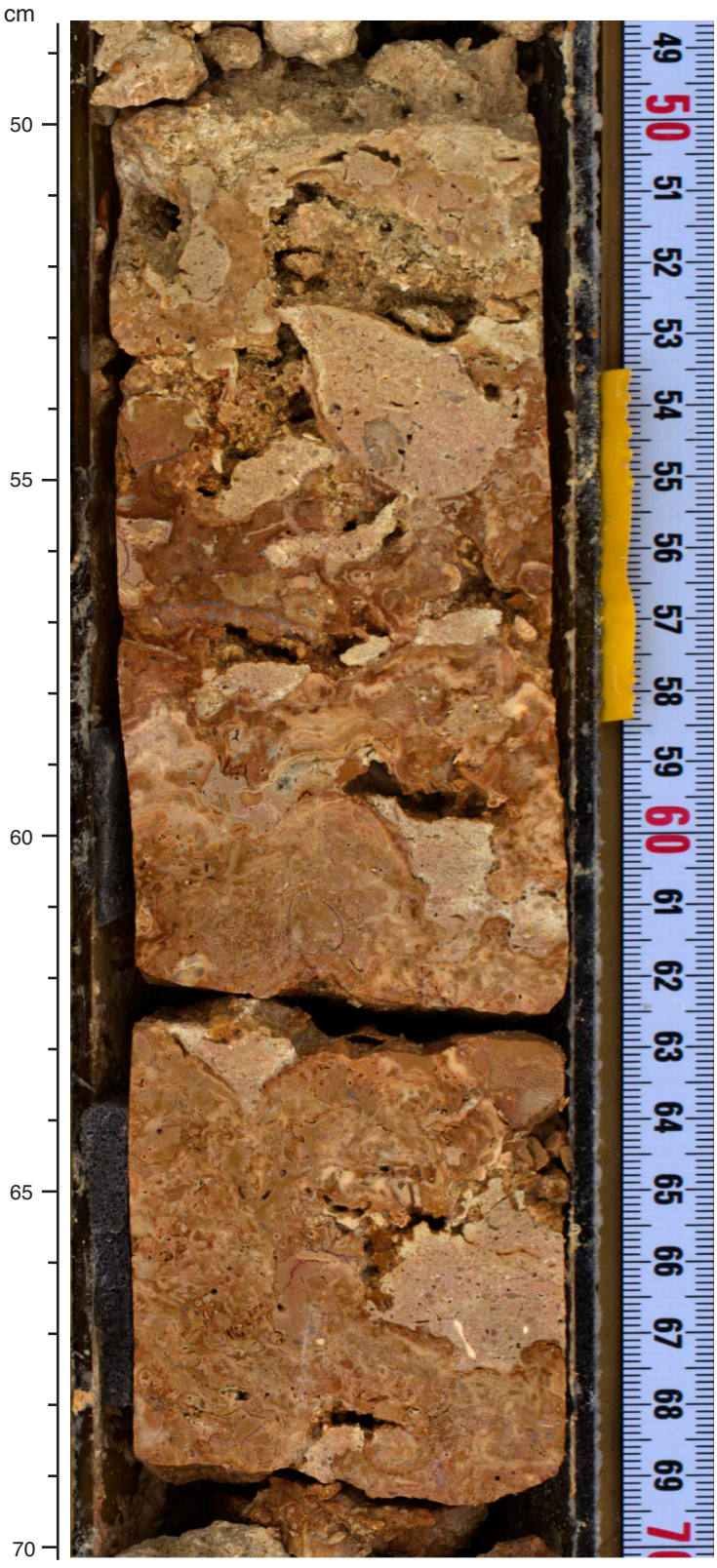

Figure F131. High-resolution line scan image of internal sediment consisting of grainstone with coral, coralline algae, gastropods, and bivalve fragments (interval 325-M0057A-16R-1, 84–91 cm).

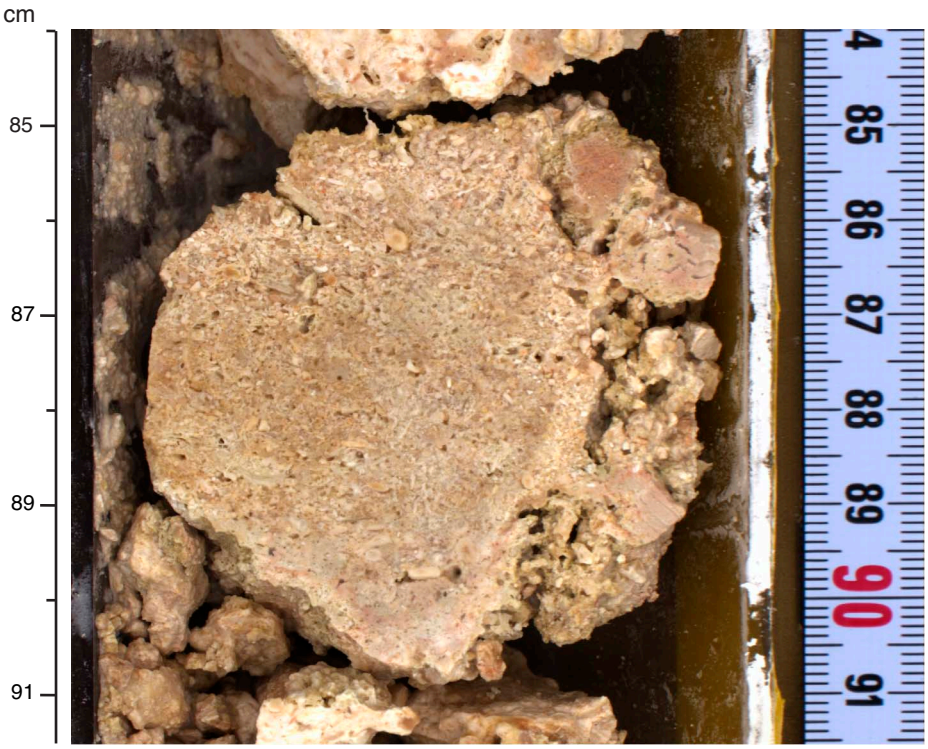

Figure F132. High-resolution line scan image of a framework of encrusting to submassive *Pachyseris* and encrusting Agariciidae covered by thick coralline algal crusts and containing dissolution cavities (interval 325-M0057A-15R-2, 63–76 cm).

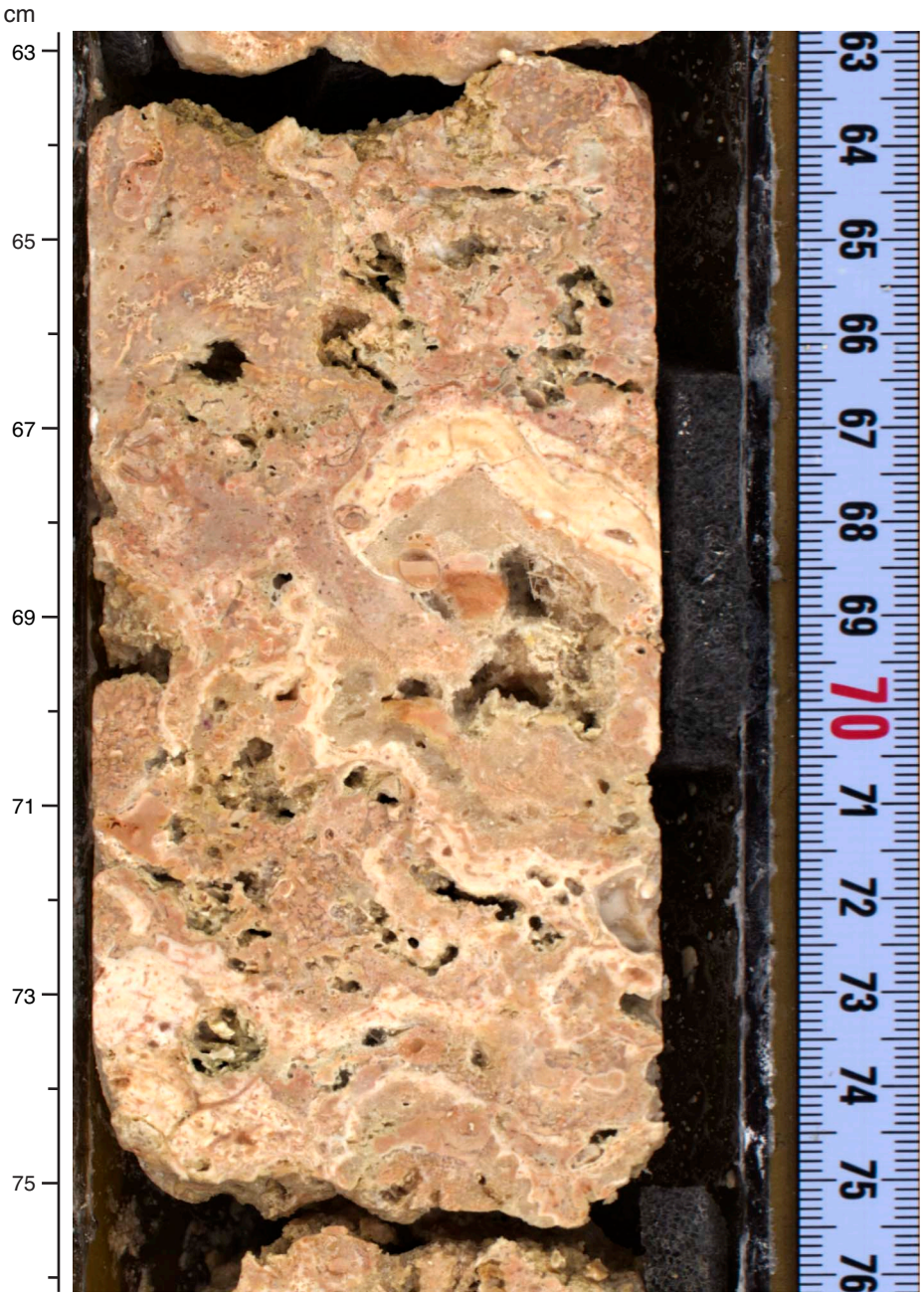

Figure F133. Summary diagram showing data collected on whole cores using the MSCL, Hole M0057A.

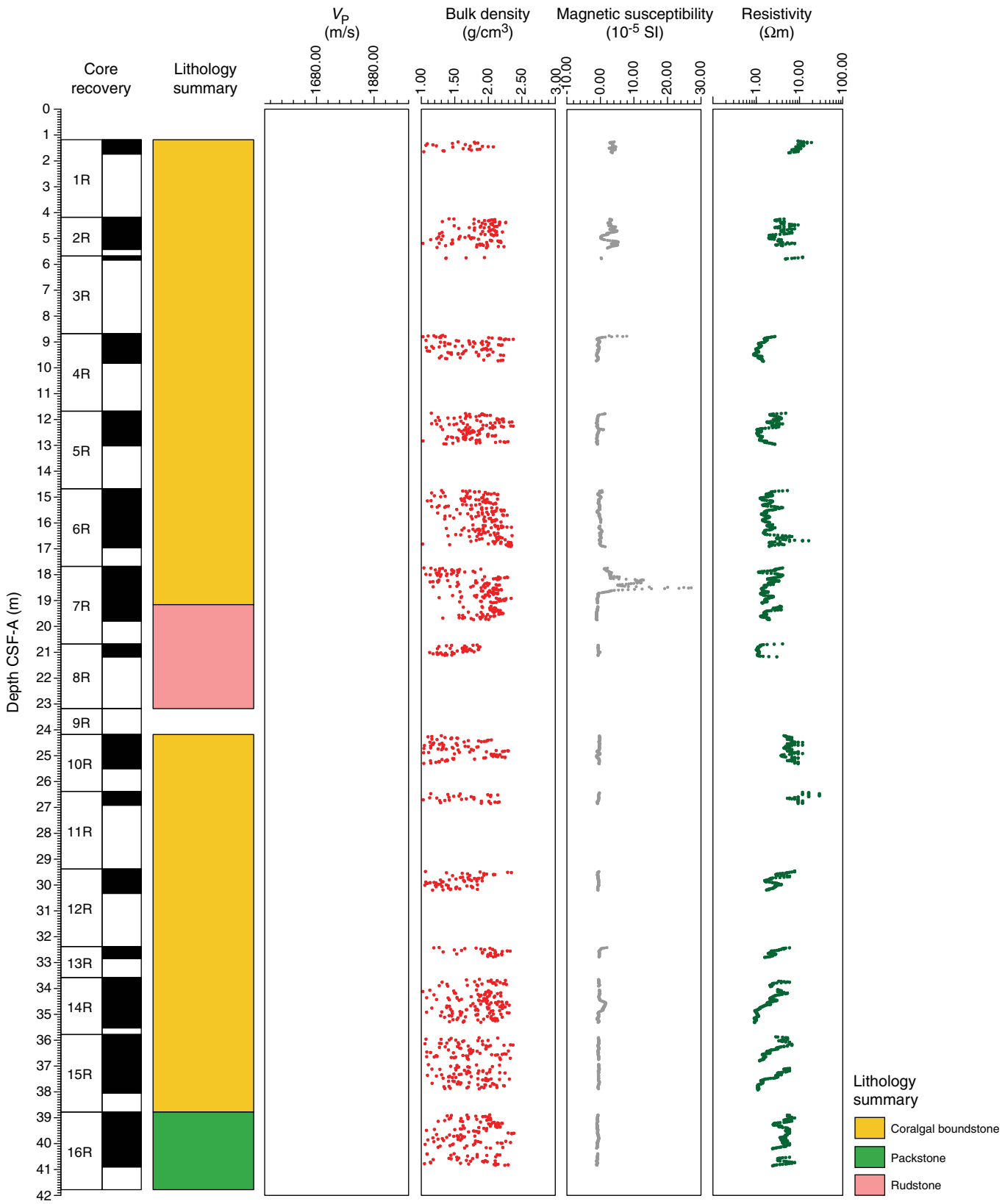

Figure F134. Petrophysical measurements obtained from discrete samples with a pycnometer, Hole M0057A. Bulk density measured on whole cores with the MSCL is shown in red on the bulk density plot.

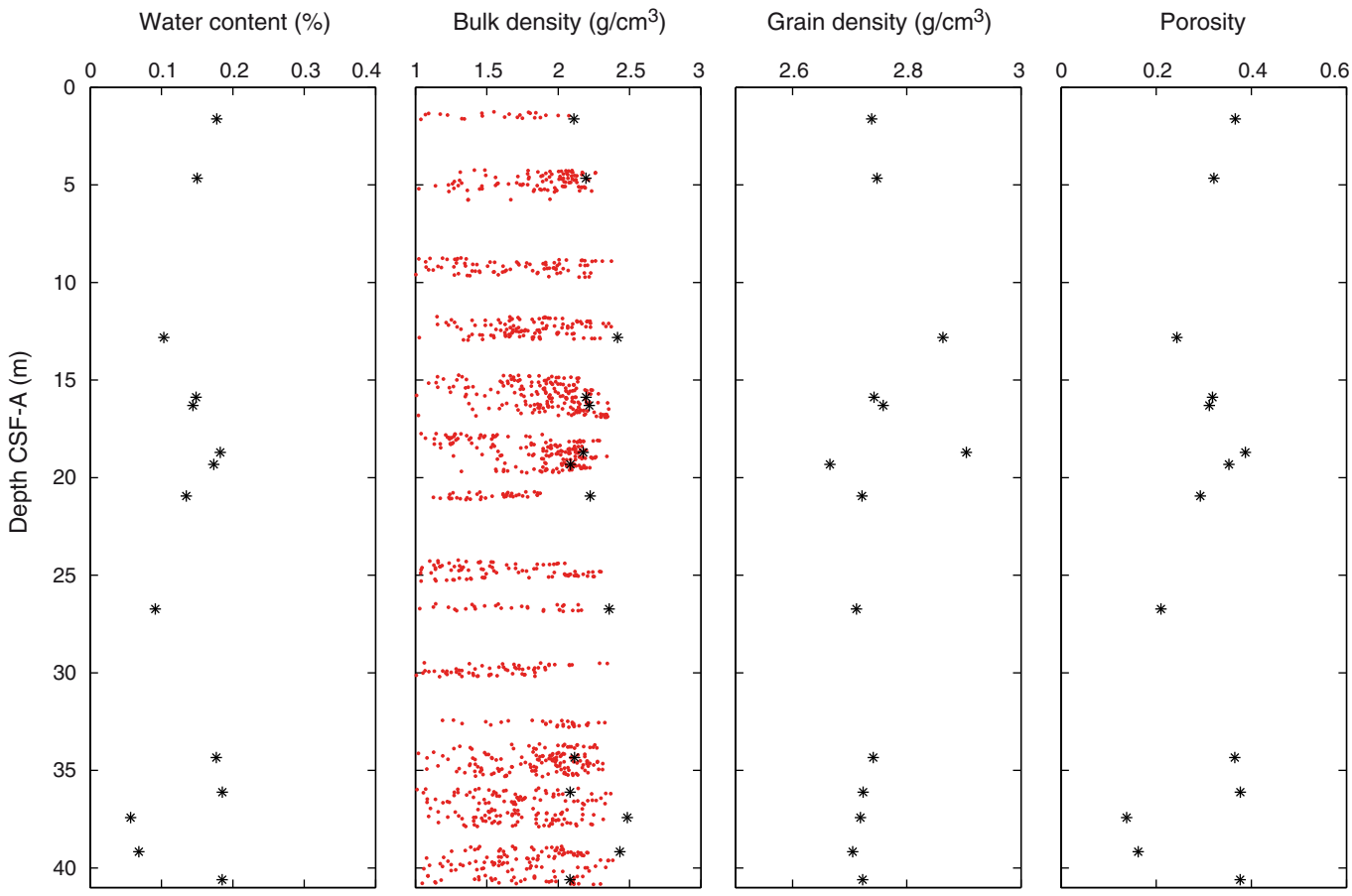

Figure F135. *P*-wave velocity data, Hole M0057A. **A.** Plot of initial, dry, and resaturated *P*-wave velocity measurements on discrete samples vs. depth. Three measurements were taken at each depth and are denoted by a dot. Average values are plotted as an open triangle. **B.** Plot showing discrete *P*-wave velocity vs. discrete bulk density.

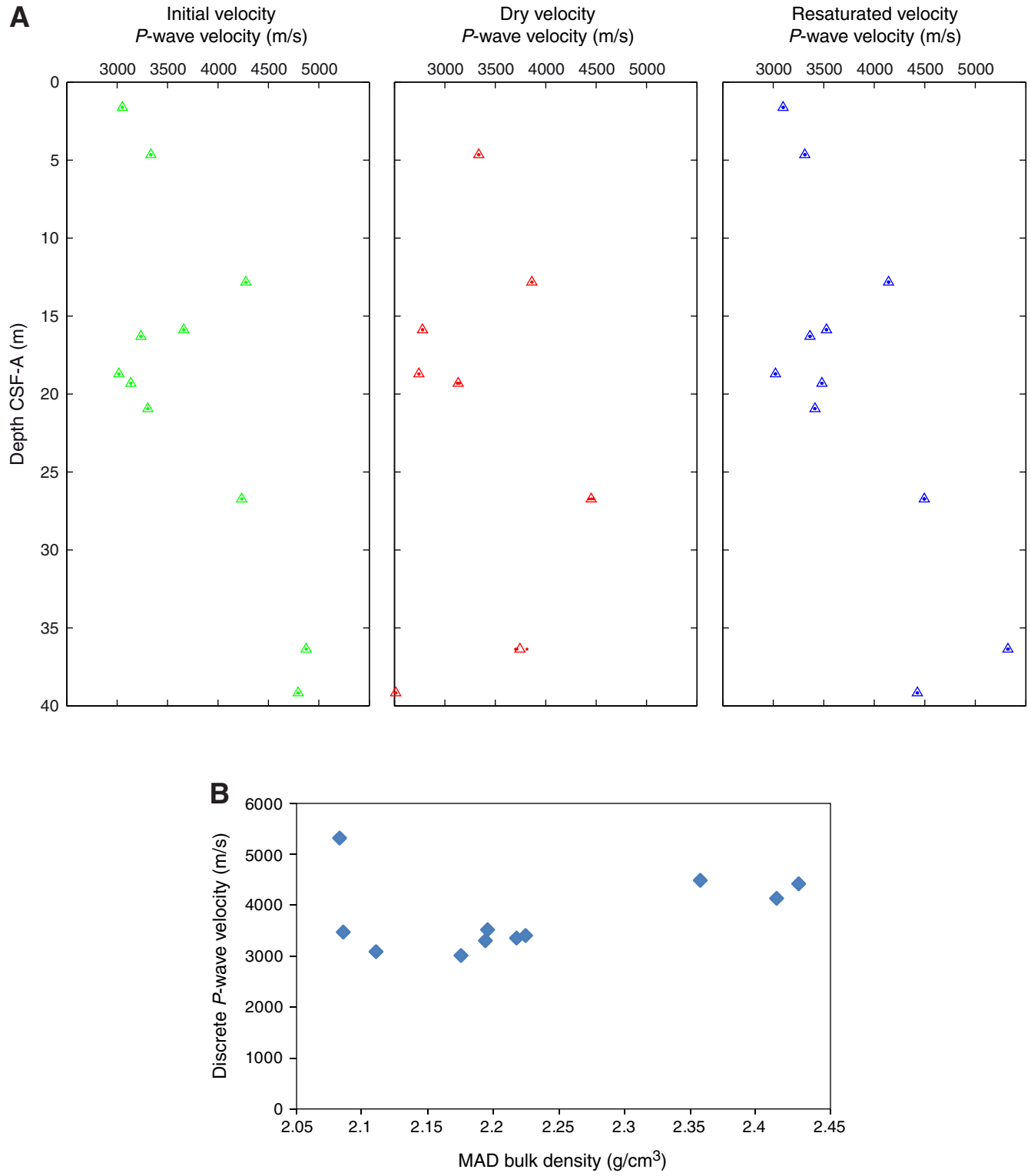

Figure F136. Values of reflectance (L*), green to red (a*), and blue to yellow (b*) indexes, along with ratio a*/b* for Hole M0057A.

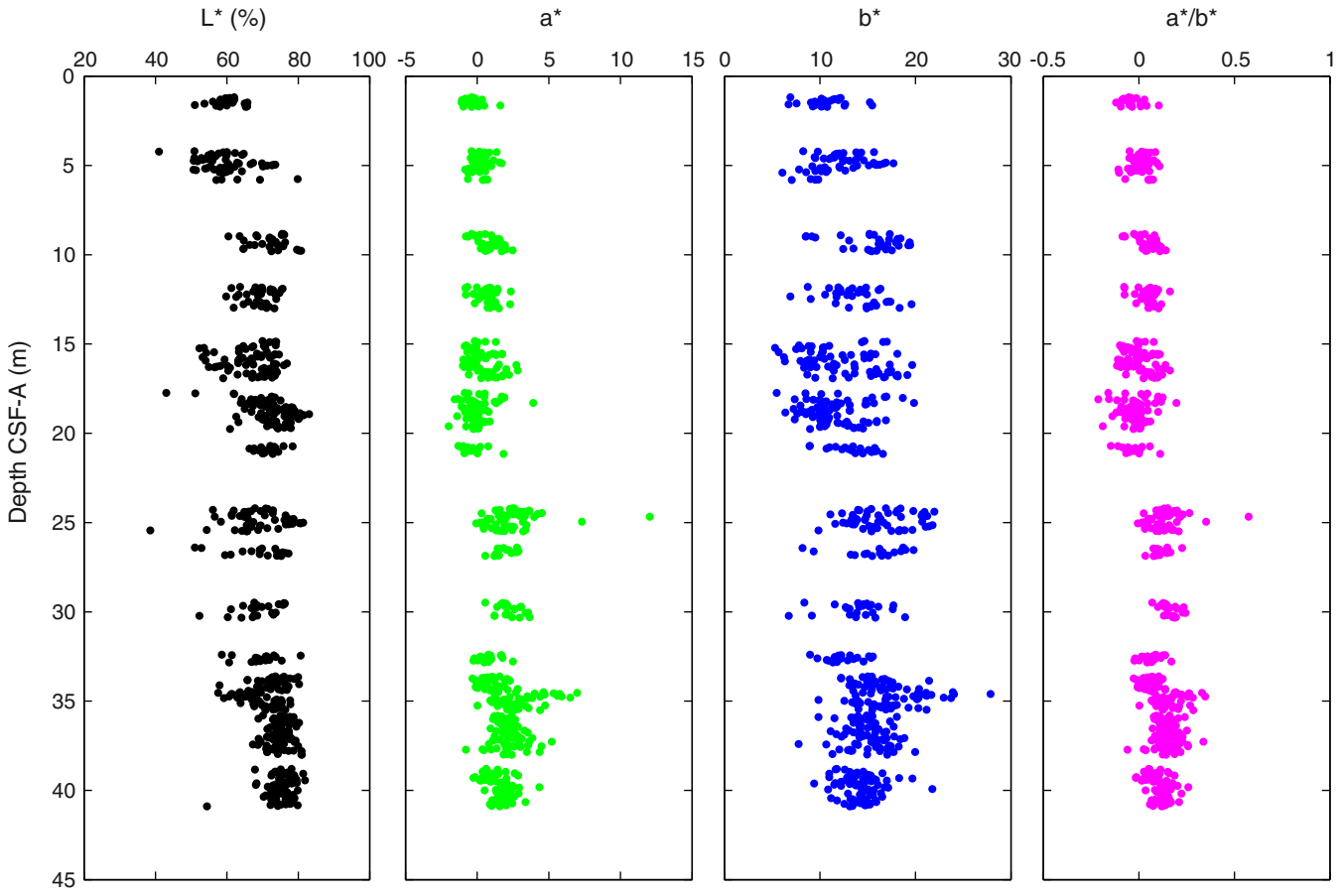

Figure F137. Magnetic susceptibility record for Hole M0057A. Water depth = 42.27 m (LAT).

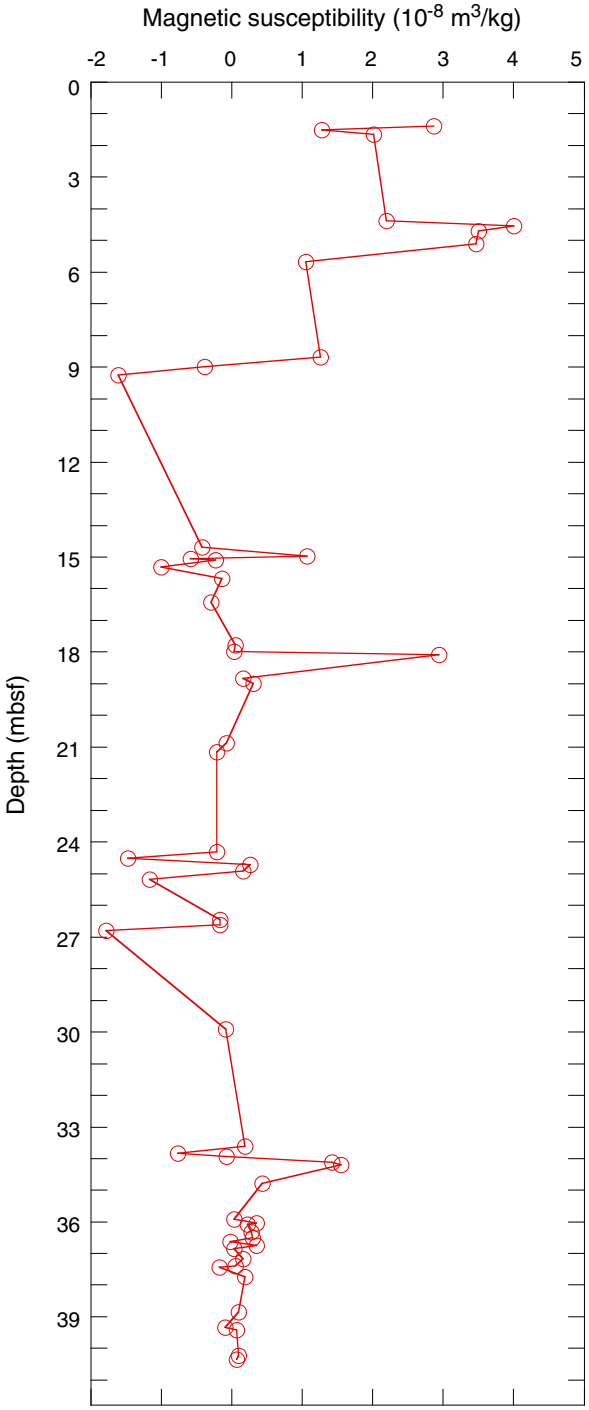

Figure F138. Preliminary chronology for Hole M0057A. Radiocarbon data are presented as graphs with the uncalibrated radiocarbon age and uncertainty shown as the red normal distribution on the ordinate axis and the probability distribution of the calibrated age shown in gray on the abscissa. The marine09 calibration curve is shown in blue. Horizontal bars indicate portions of the age distribution that are significant at the 95.4% confidence interval and the mean age (white circle ±1 standard deviation) used for the purposes of the preliminary dating. All ages are presented as thousands of calendar years BP (1950 AD). See Table **T10** in the "Methods" chapter. (See Bronk Ramsey [2009], as well as Bronk Ramsey [2010] at **c14.arch.ox.ac.uk/oxcal.html.**)

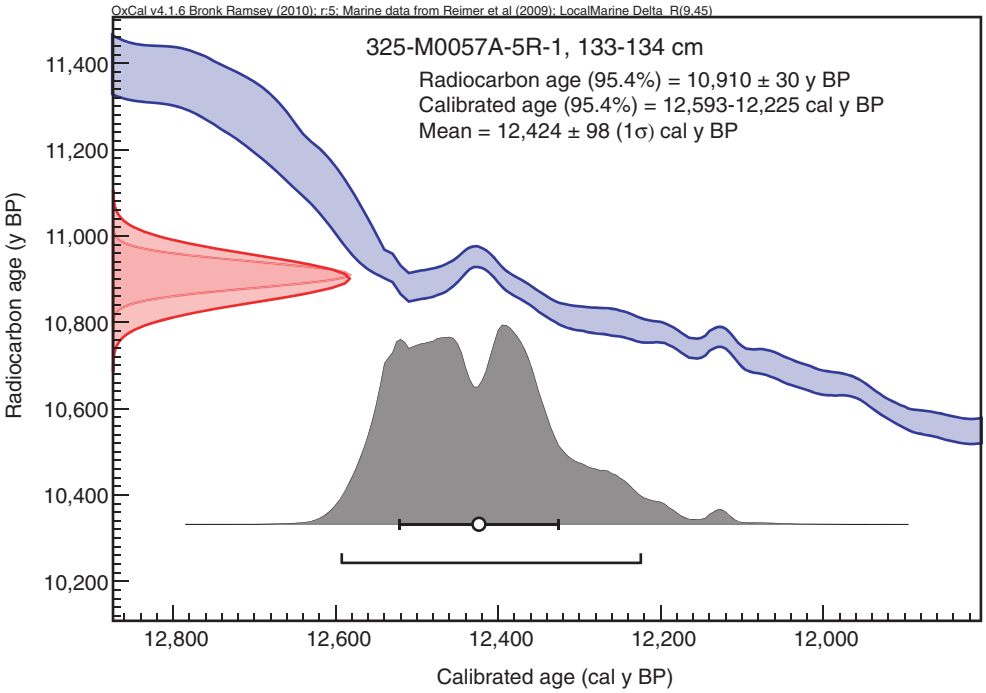

Figure F139. High-resolution line scan image of homogeneous green mud without layering or bioturbation but containing small benthic and planktonic foraminifera and a few sponge spicules (interval 325-M0058A-1X-1, 20–50 cm).

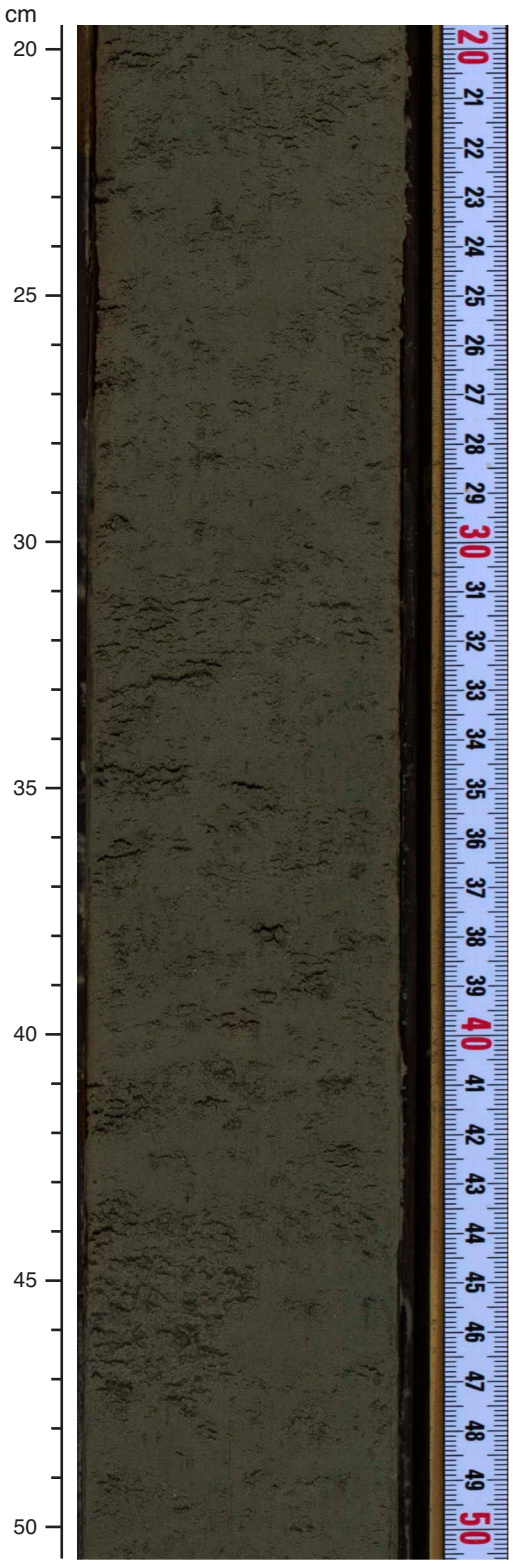

Figure F140. High-resolution line scan image of fine to medium sand with larger foraminifera (interval 325-M0058A-3X-1, 135–149 cm).

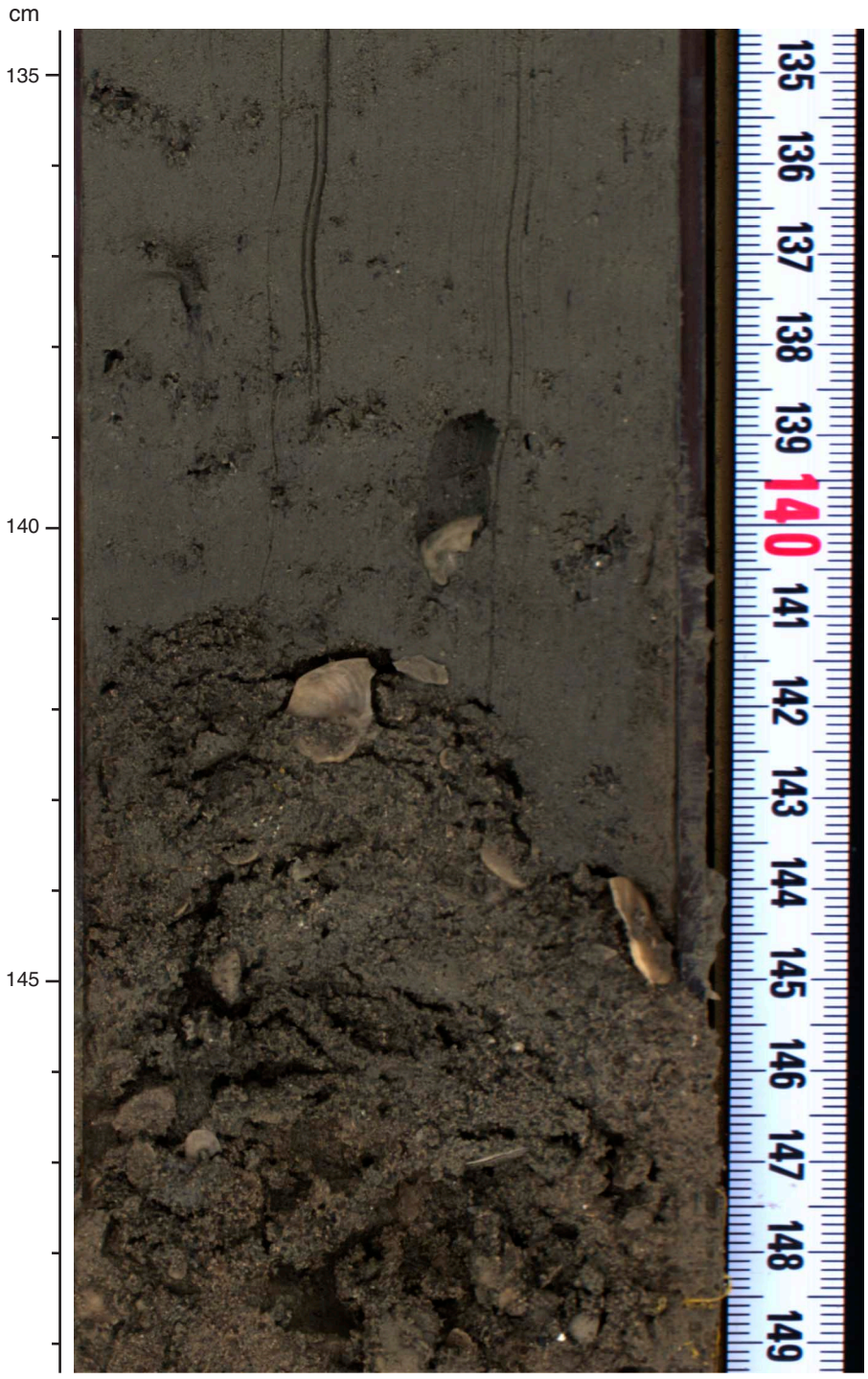

Figure F141. High-resolution line scan image of a grainstone with larger foraminifera, mollusks, and *Halimeda* (interval 325-M0058A-4X-1, 94–111 cm).

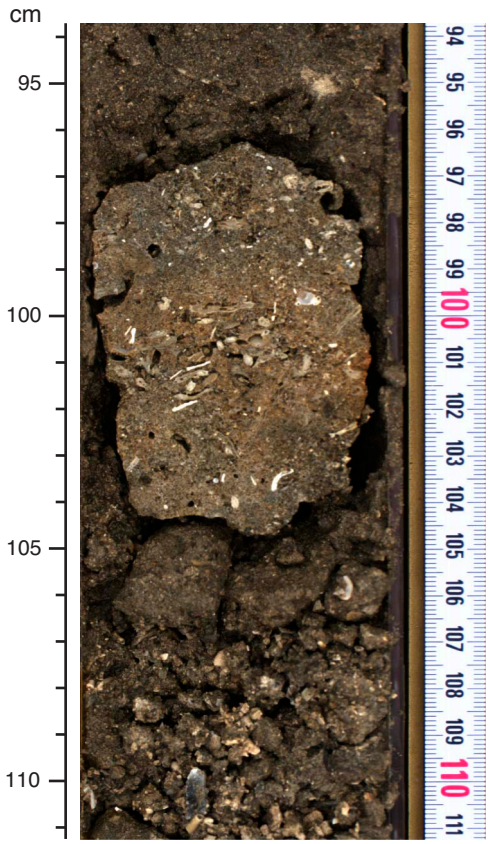

Figure F142. High-resolution line scan image of green mud without layering or bioturbation but containing small benthic foraminifera, a few small mollusk fragments, and planktonic foraminifera (interval 325-M0058A-8X-1, 60–90 cm).

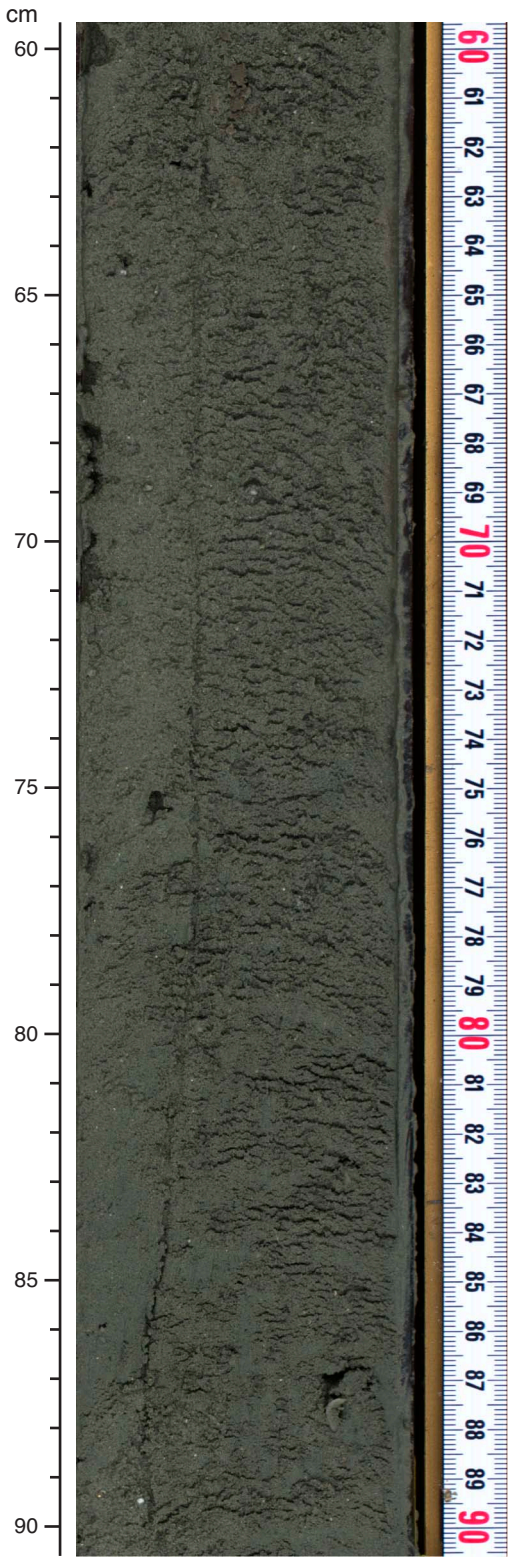

Figure F143. High-resolution line scan image of green mud without layering or bioturbation but containing small benthic foraminifera, fragments of shells, and agglutinated worm tubes (34–38 cm) (interval 325-M0058A-9X-1, 20–50 cm).

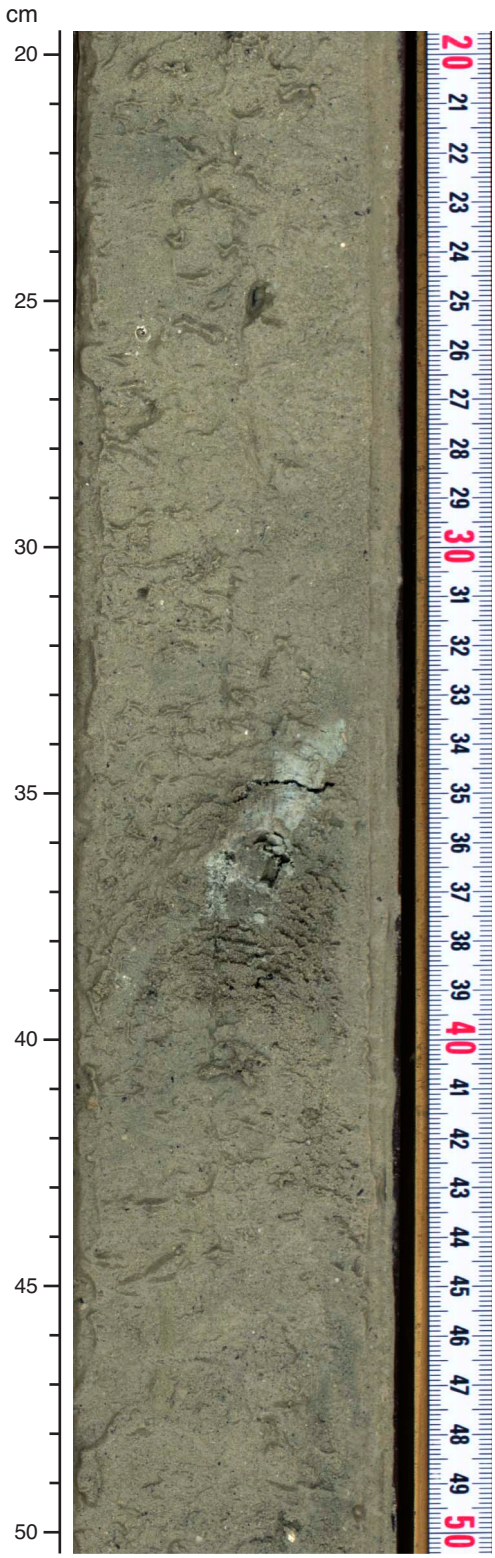

Figure F144. High-resolution line scan image of bioturbated green mud (interval 325-M0058A-11X-2, 20–30 cm).

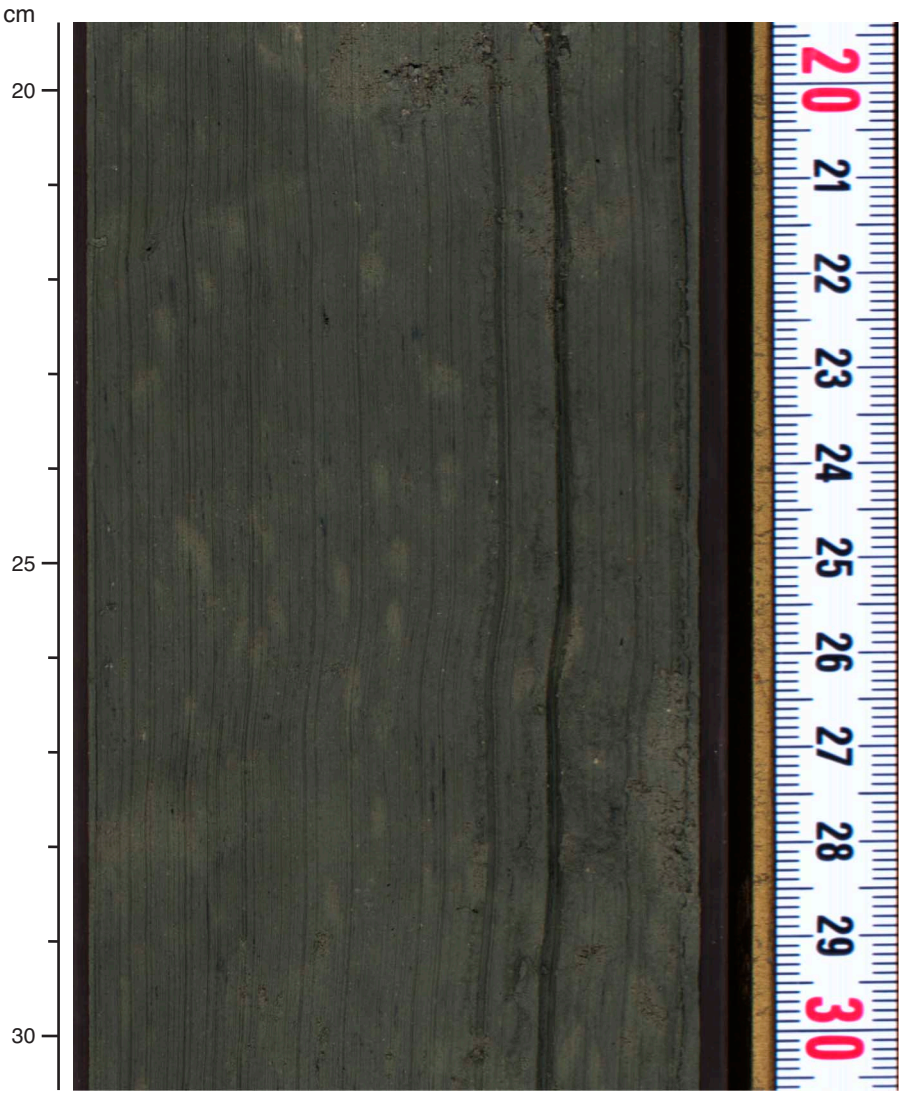

Figure F145. High-resolution line scan image of green mud above fine-medium sand with small fragments of mollusk shells, bryozoans, and small benthic foraminifera (interval 325-M0058A-11X-3, 41–58 cm).

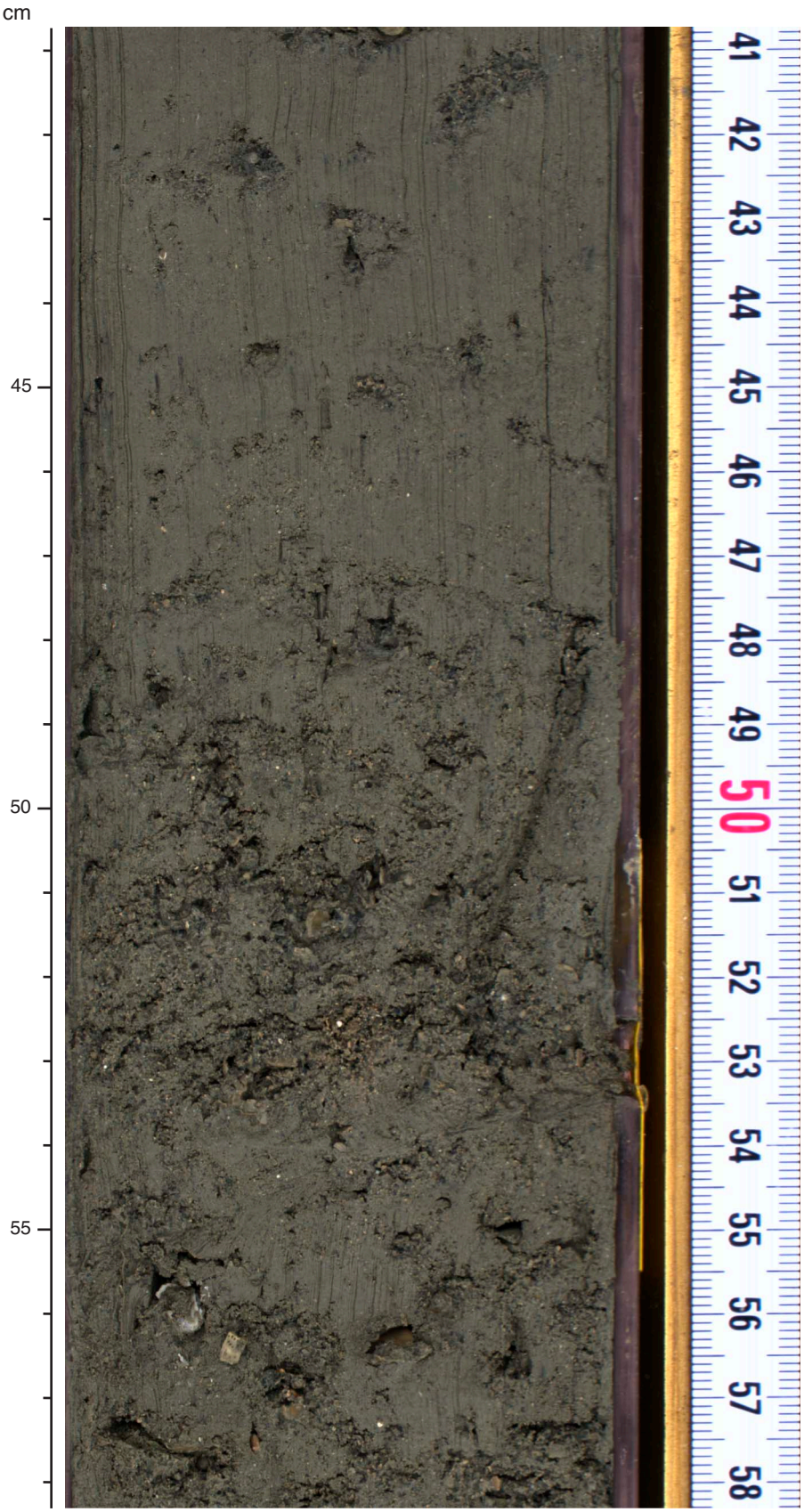

Figure F146. High-resolution line scan image of bioturbation in green mud, including centimeter diameter burrows filled with fine-medium sand (interval 325-M0058A-13X-1, 48–72 cm).

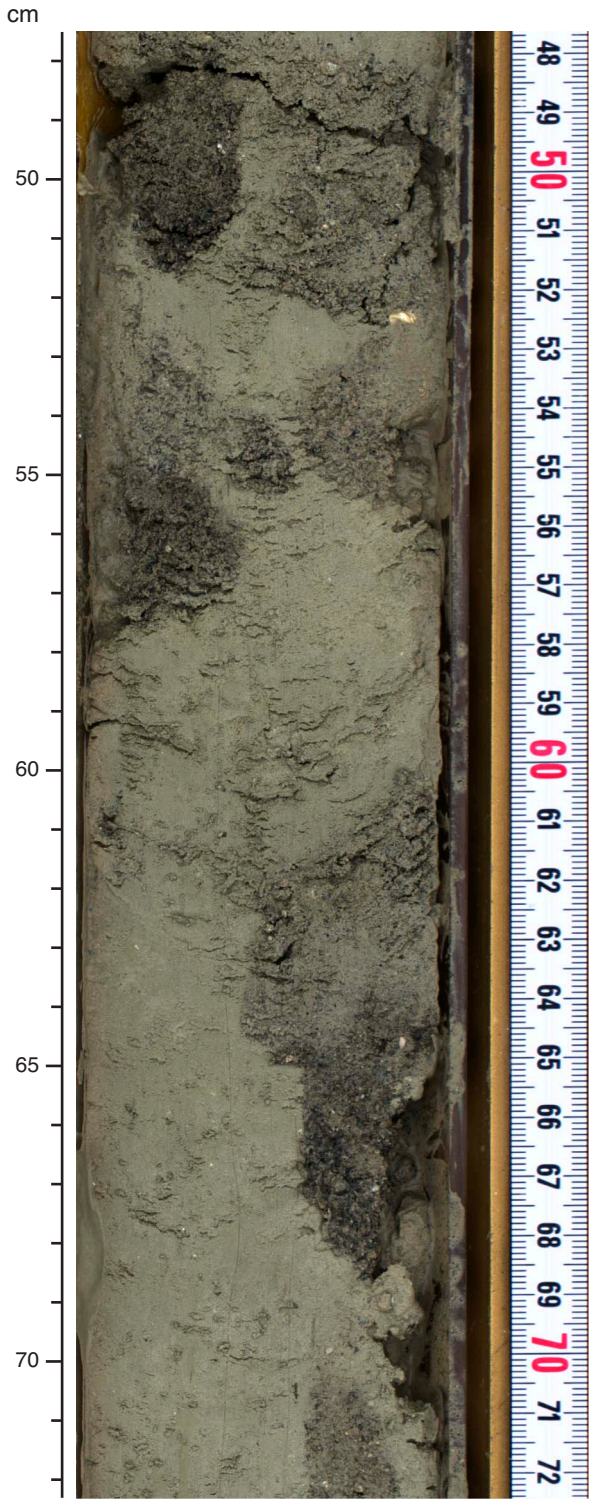

Figure F147. Summary diagram showing data collected on whole cores using the MSCL, Hole M0058A.

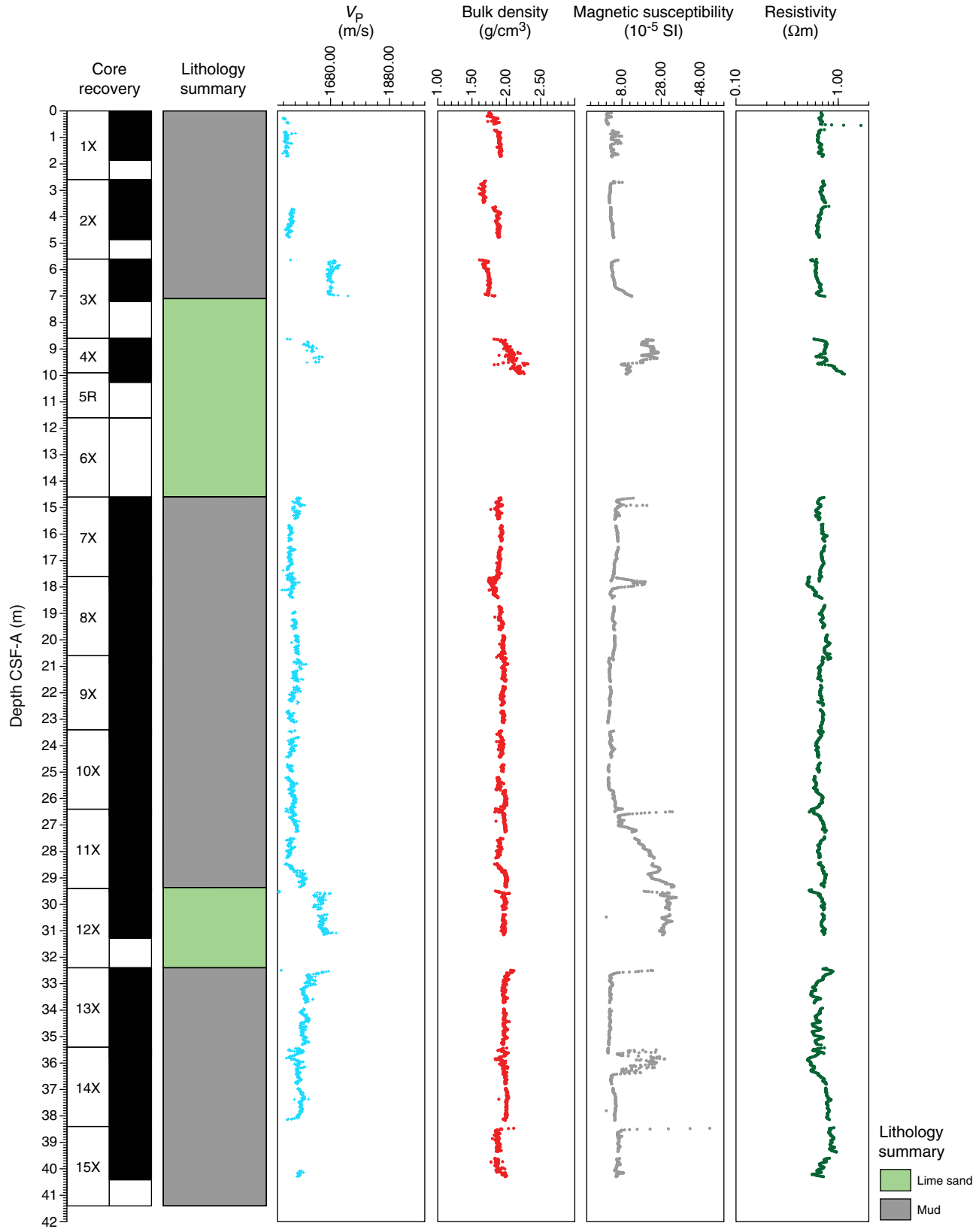

Figure F148. Petrophysical measurements obtained from discrete samples with a pycnometer, Hole M0058A. Bulk density measured on whole cores with the MSCL is shown in red on the bulk density plot.

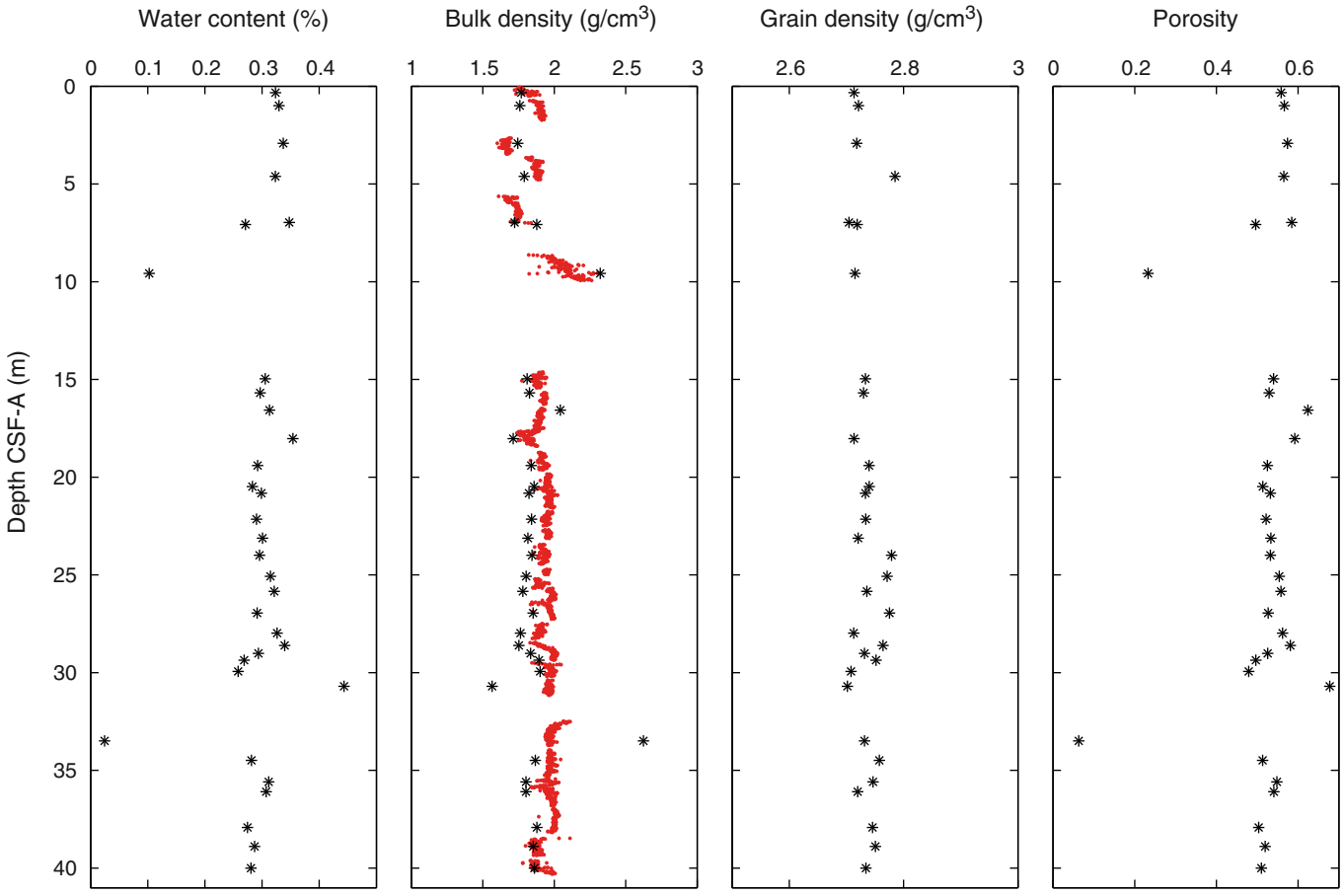

Figure F149. *P*-wave velocity data, Hole M0058A. **A.** Plot of initial *P*-wave velocity measurements on discrete samples vs. depth. Three measurements were taken at each depth and are denoted by a circle. Average values are plotted as an open triangle. **B.** Plot showing discrete *P*-wave velocity vs. discrete bulk density.

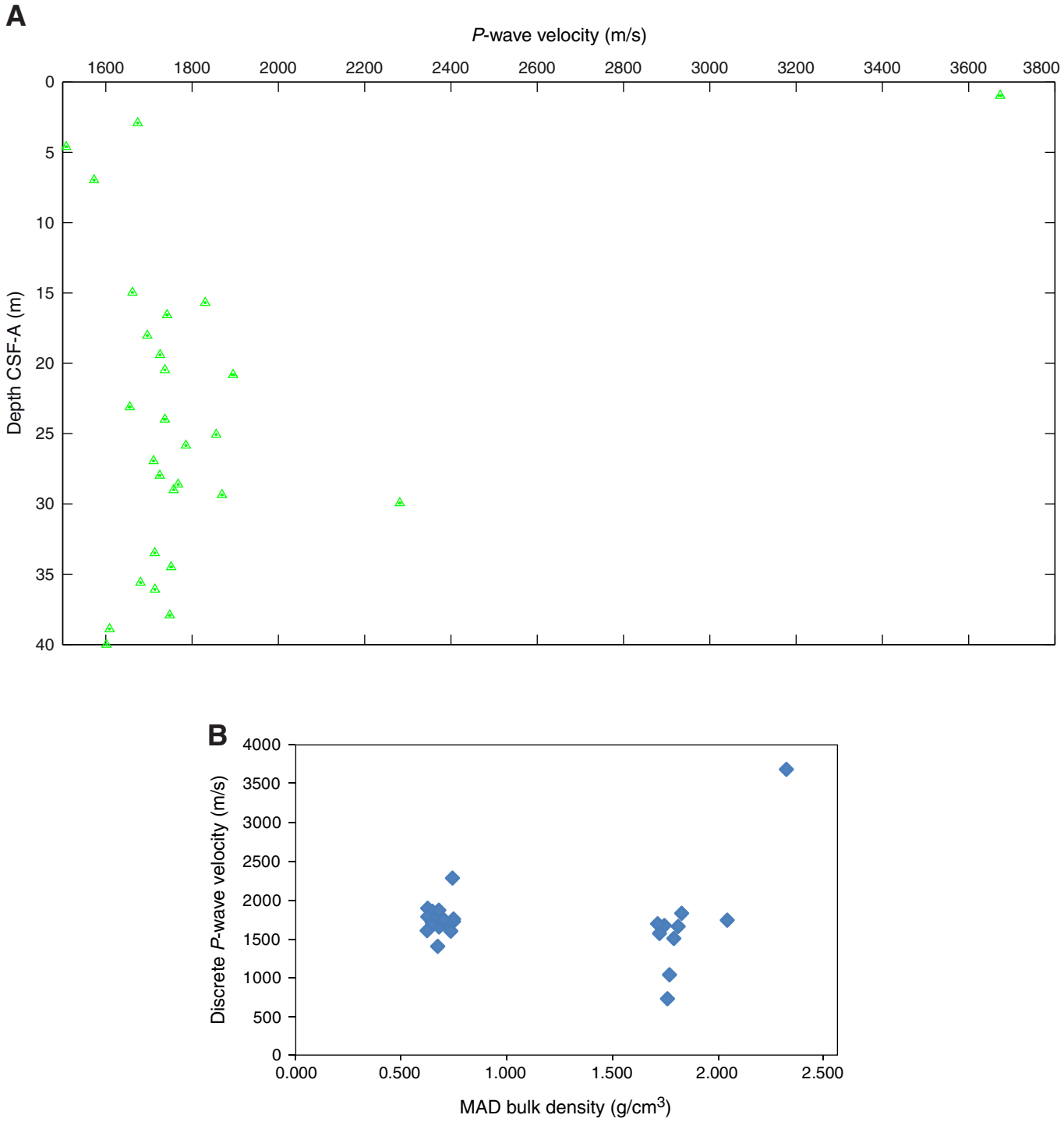

Figure F150. Values of reflectance (L*), green to red (a*), and blue to yellow (b*) indexes, along with ratio a*/b* for Hole M0058A.

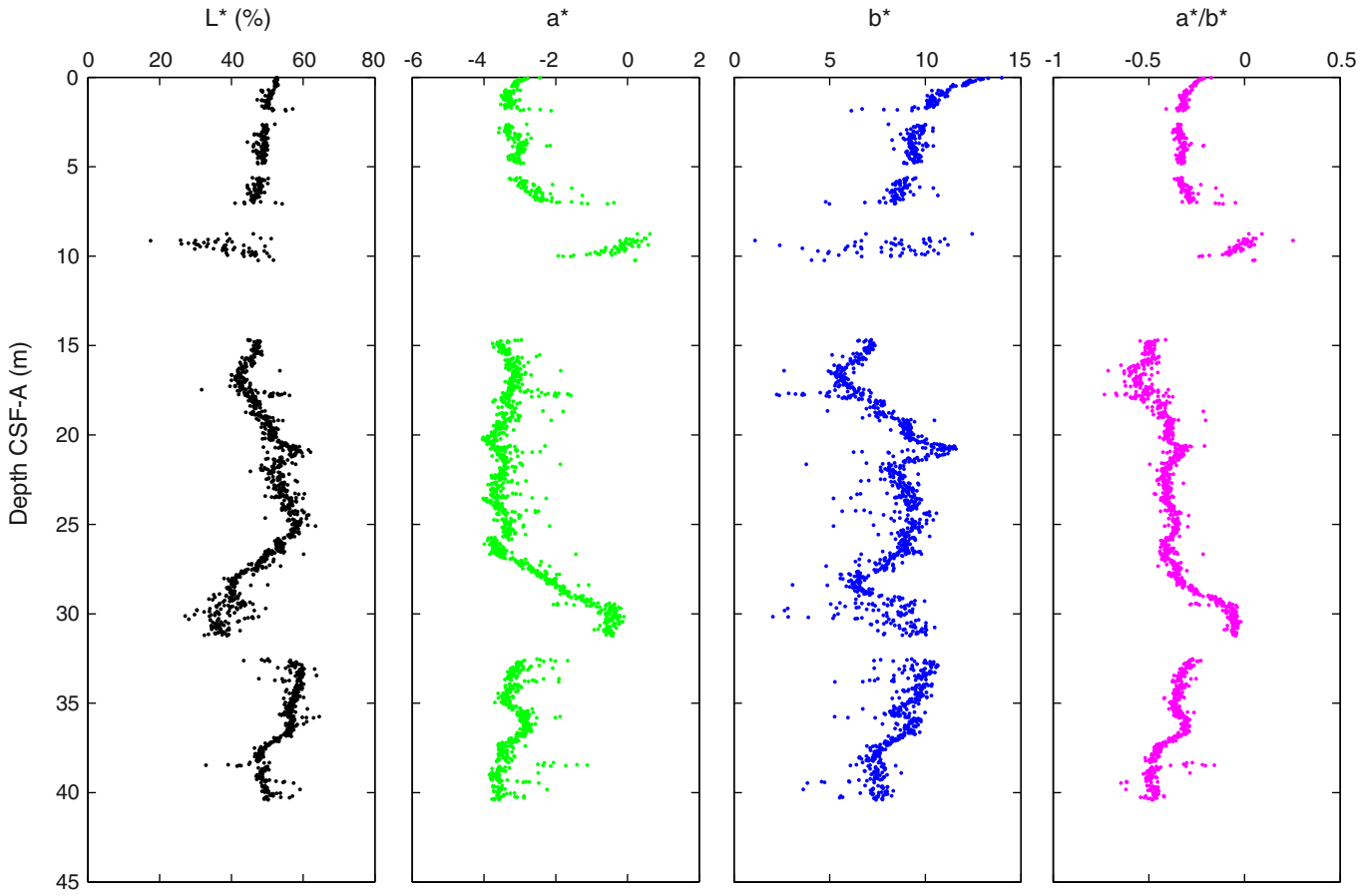

Figure F151. Plot of thermal conductivity vs. depth, Hole M0058A. Error bars indicate the standard deviation.

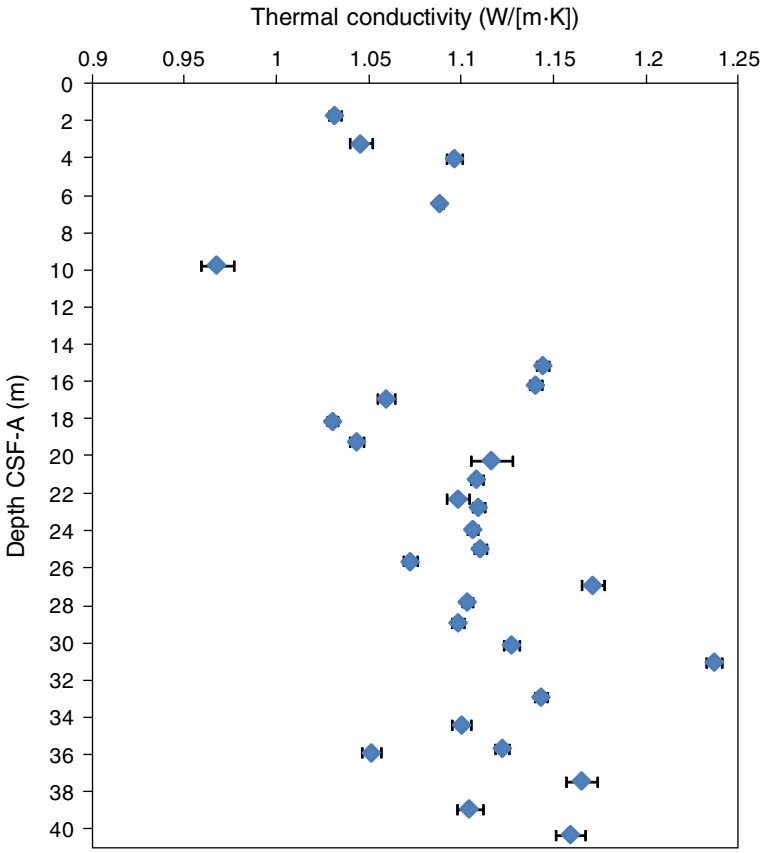

Figure F152. Values of color reflectance (L*), discrete paleomagnetic measurements (magnetic susceptibility), and multisensor core logger (MSCL) magnetic susceptibility measurements, Hole M0058A.

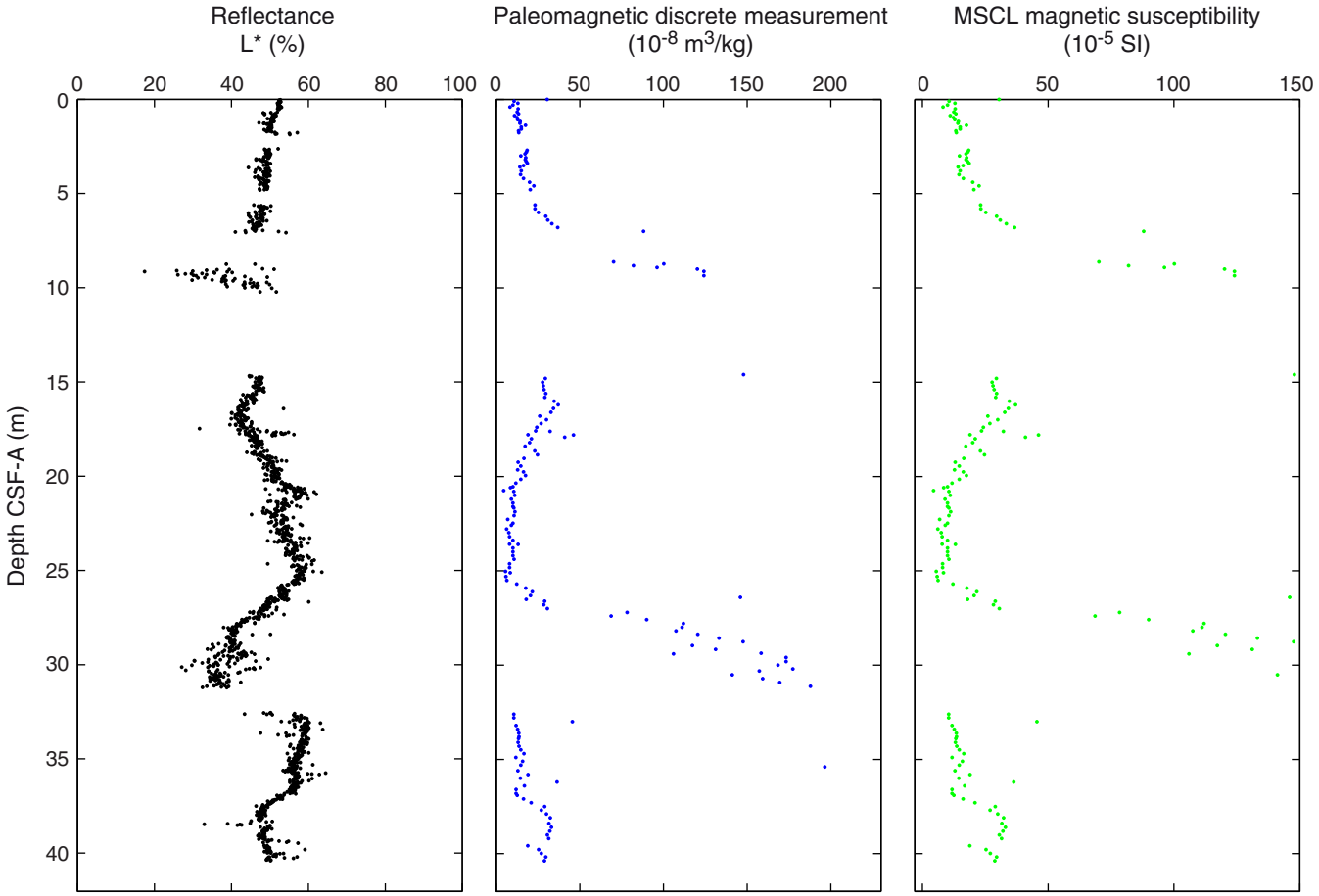

Figure F153. Magnetic susceptibility record for Hole M0058A. Water depth = 167.14 m (LAT).

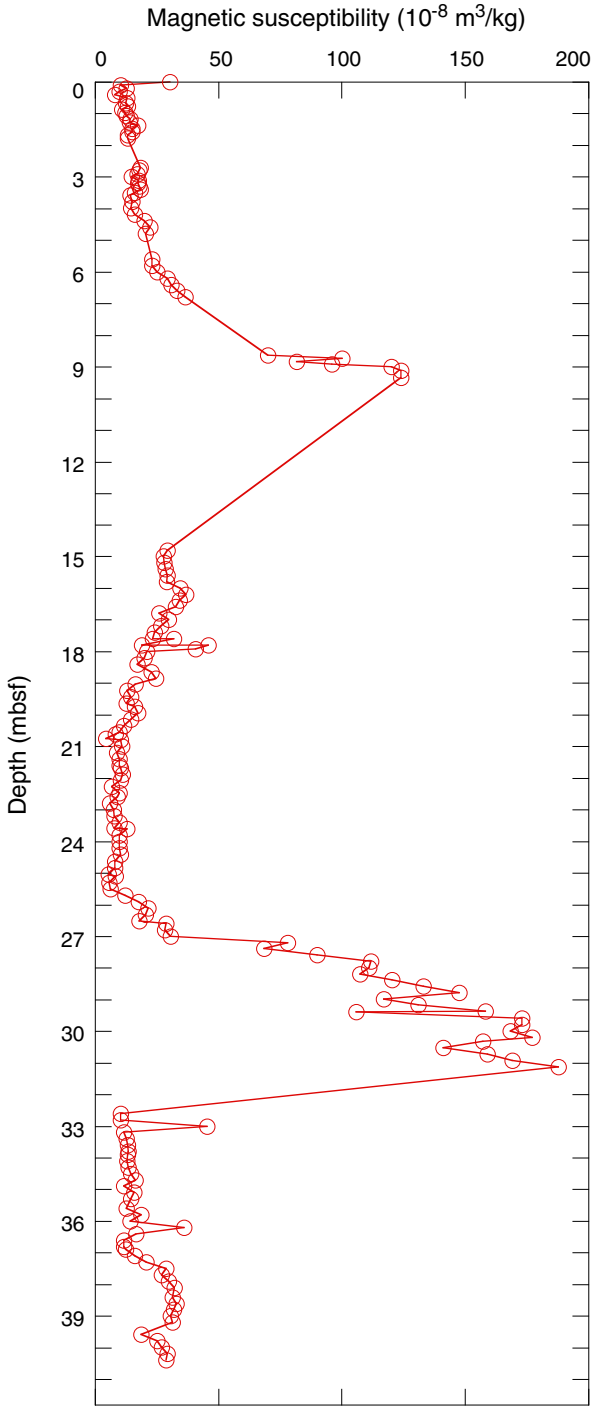

Figure F154. Preliminary chronology for Hole M0058A. Radiocarbon data are presented as graphs with the uncalibrated radiocarbon age and uncertainty shown as the red normal distribution on the ordinate axis and the probability distribution of the calibrated age shown in gray on the abscissa. The marine09 calibration curve is shown in blue. Horizontal bars indicate portions of the age distribution that are significant at the 95.4% confidence interval and the mean age (white circle ±1 standard deviation) used for the purposes of the preliminary dating. All ages are presented as thousands of calendar years BP (1950 AD). See Table **T10** in the "Methods" chapter. (See Bronk Ramsey [2009], as well as Bronk Ramsey [2010] at **c14.arch.ox.ac.uk/oxcal.html.**)

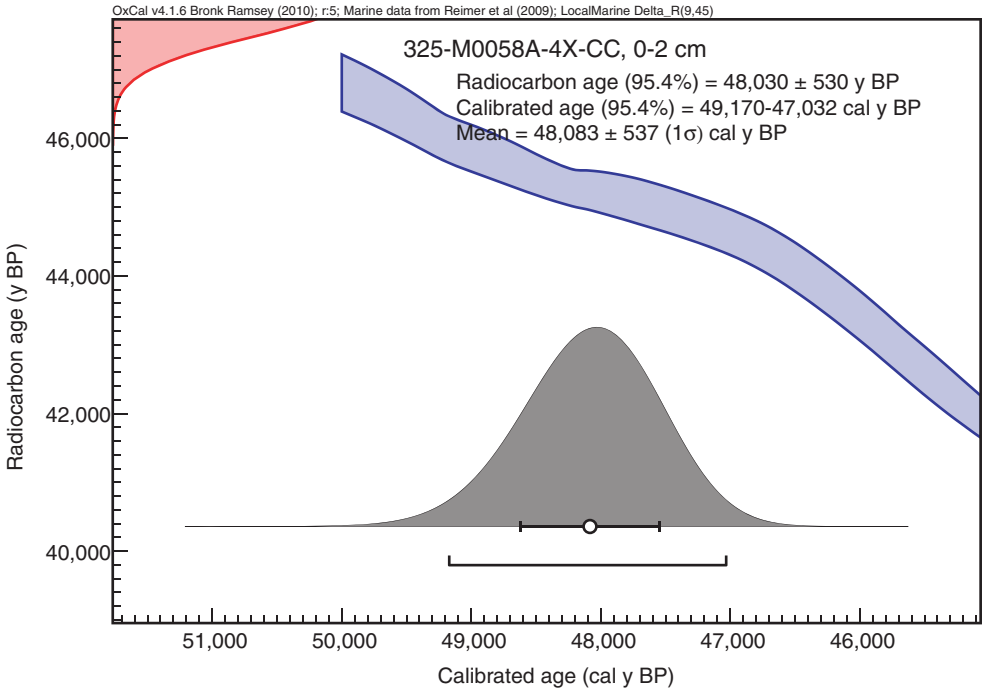

Warning! Date out of range - 48030+/-530BP

Figure F155. Transect summary of recovery and main lithostratigraphic units as interpreted for transect NOG-01B. Holes are plotted against present-day sea level (LAT taken from corrected EM300 multibeam bathymetry). Distances between holes are indicated on the diagram but are not drawn to horizontal scale.

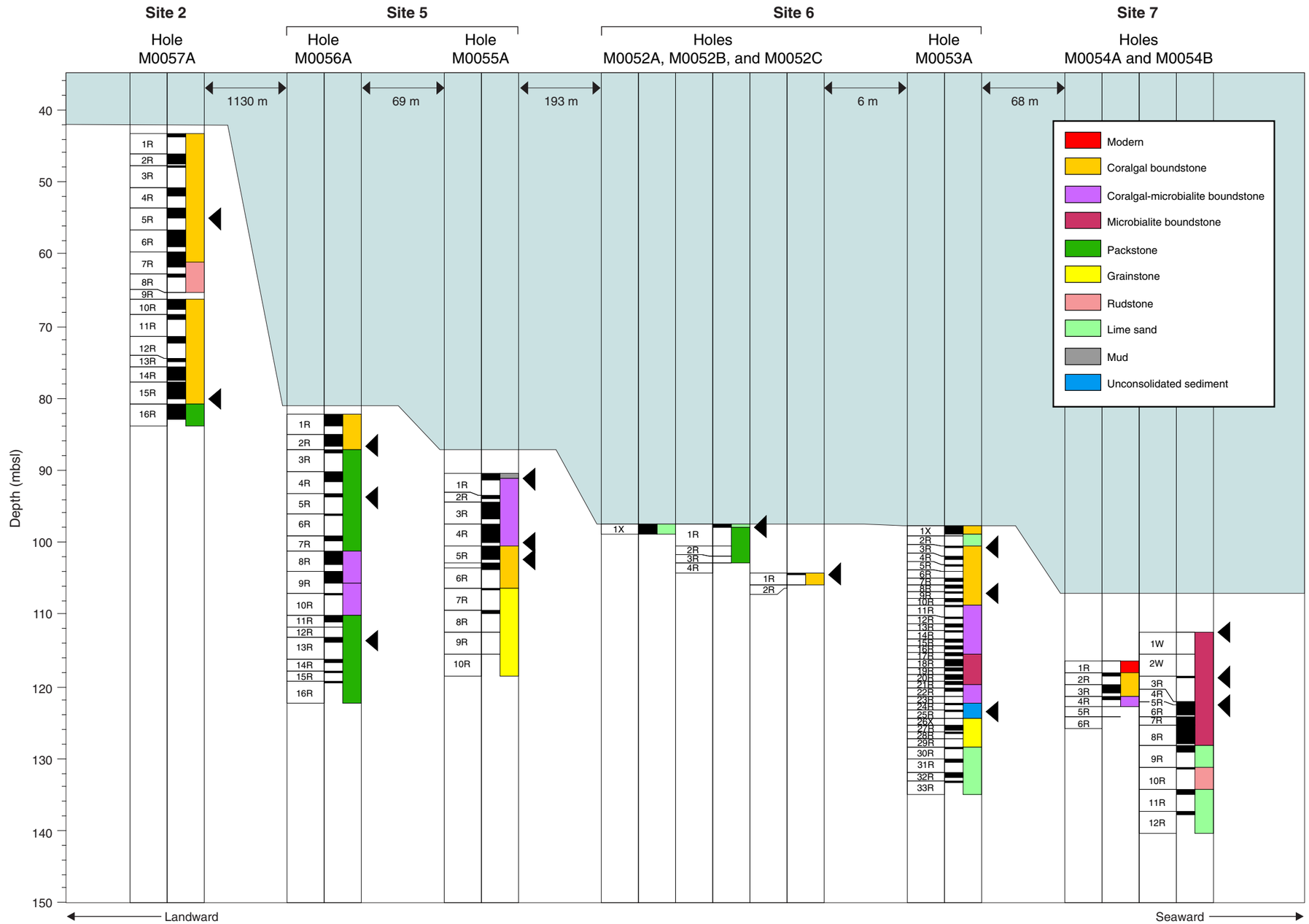

Figure F156. Porosity of discrete samples for all holes measured in transect NOG-01B in order from shallow water to deep water (left to right).

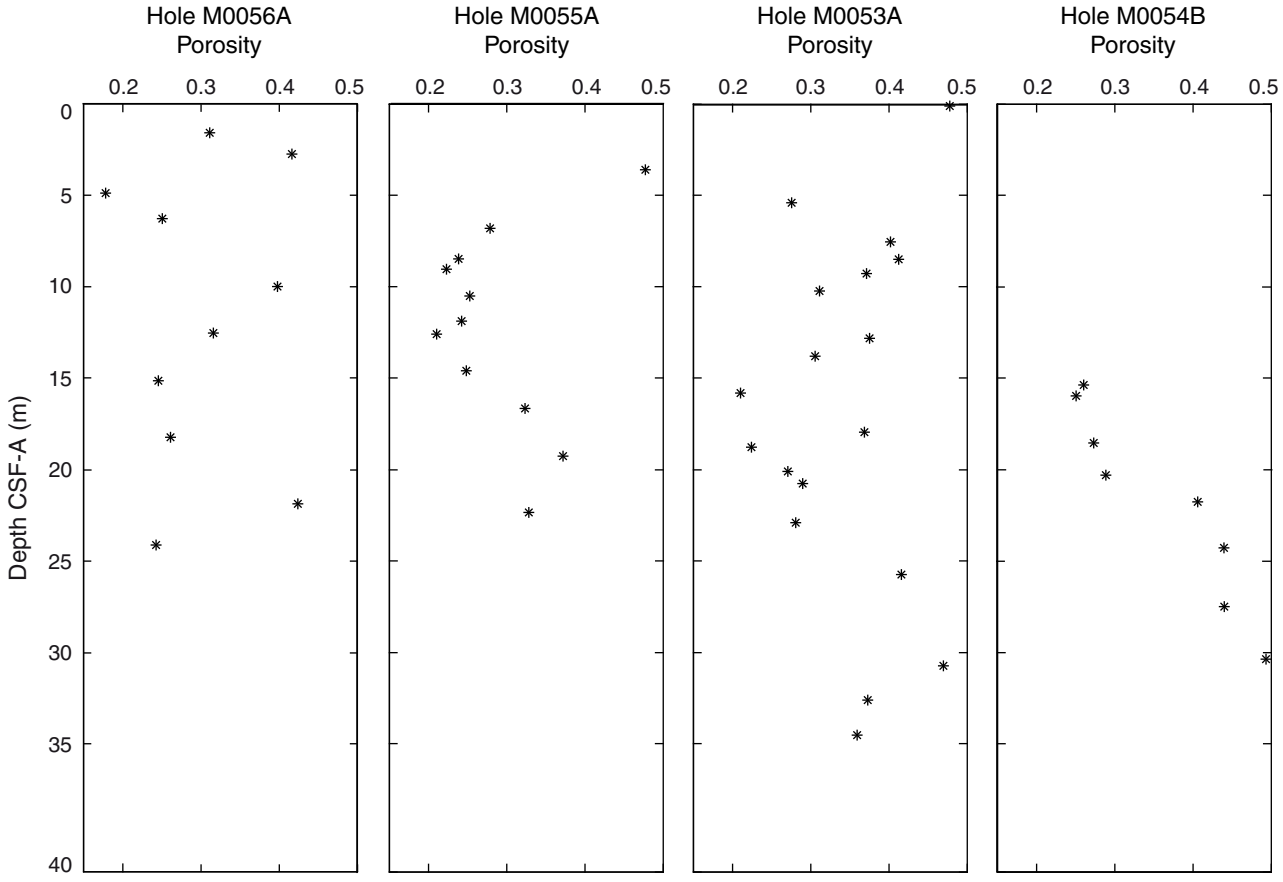

Figure F157. Plot showing porosity vs. bulk density measured in discrete samples from transect NOG-01B.

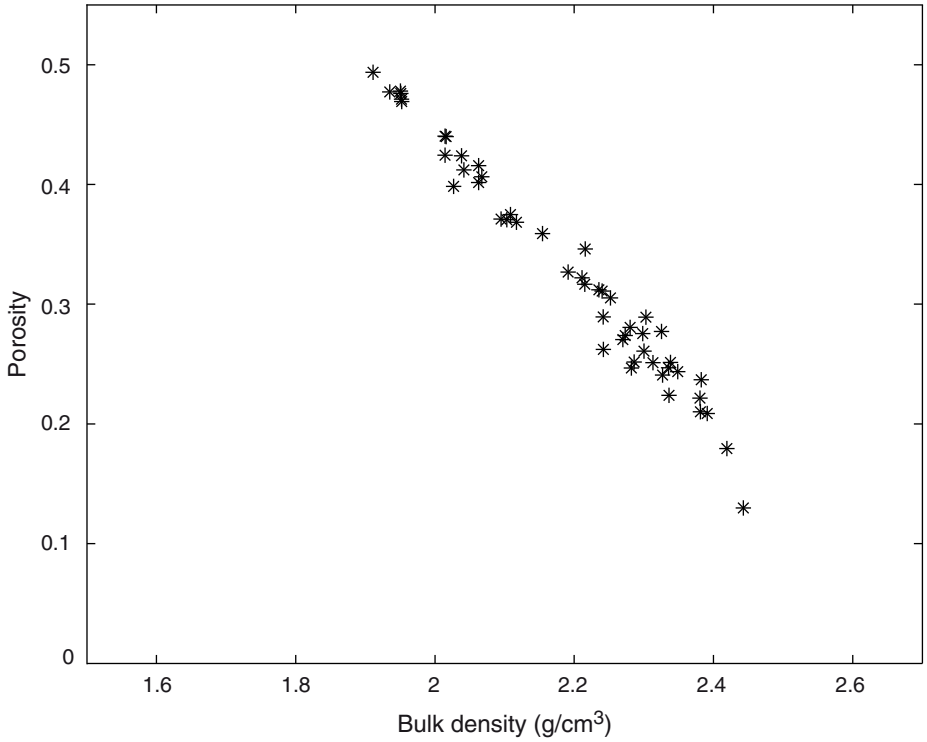

Figure F158. Plot of all porosity and *P*-wave velocity measurements from discrete samples analysis from all transect NOG-01B holes.

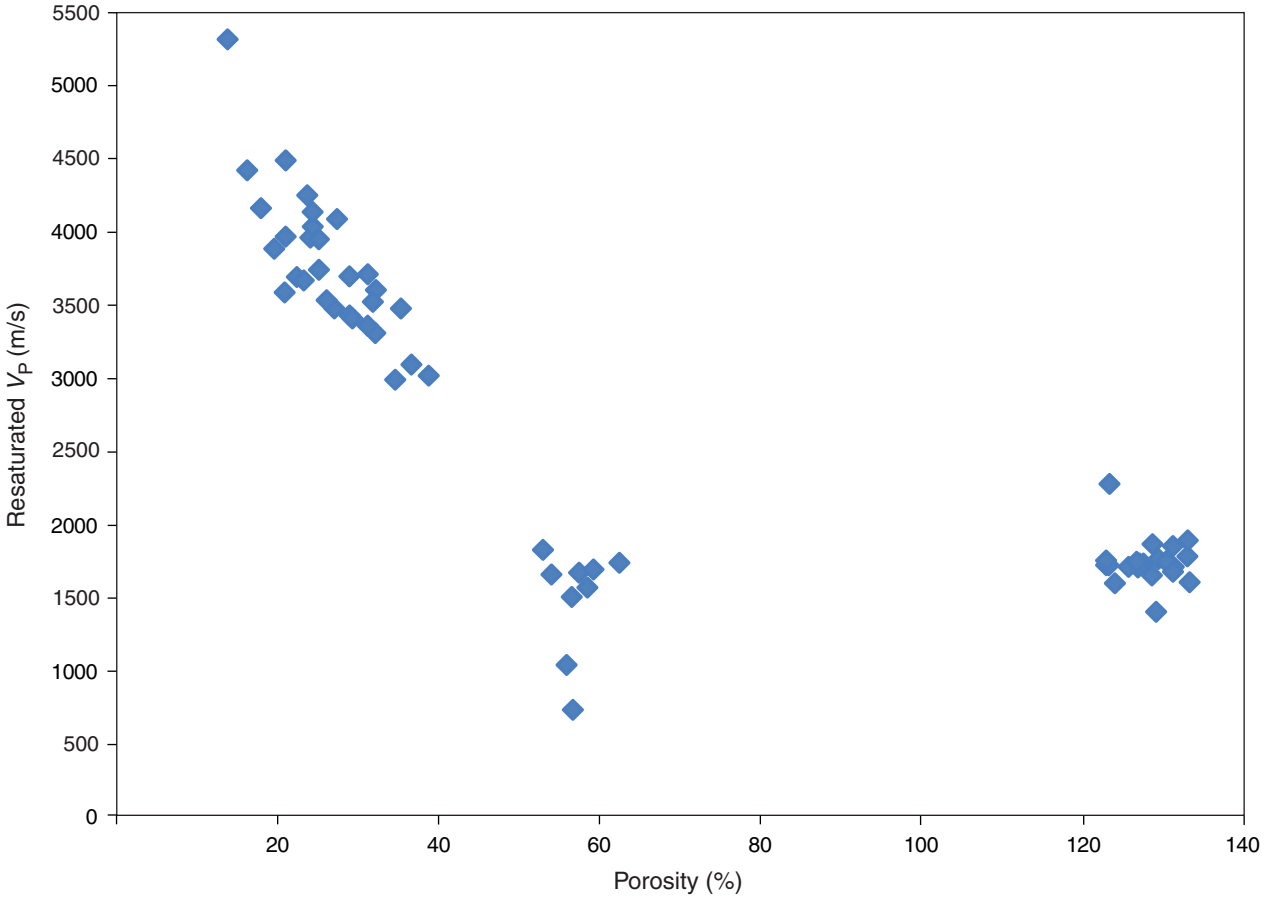

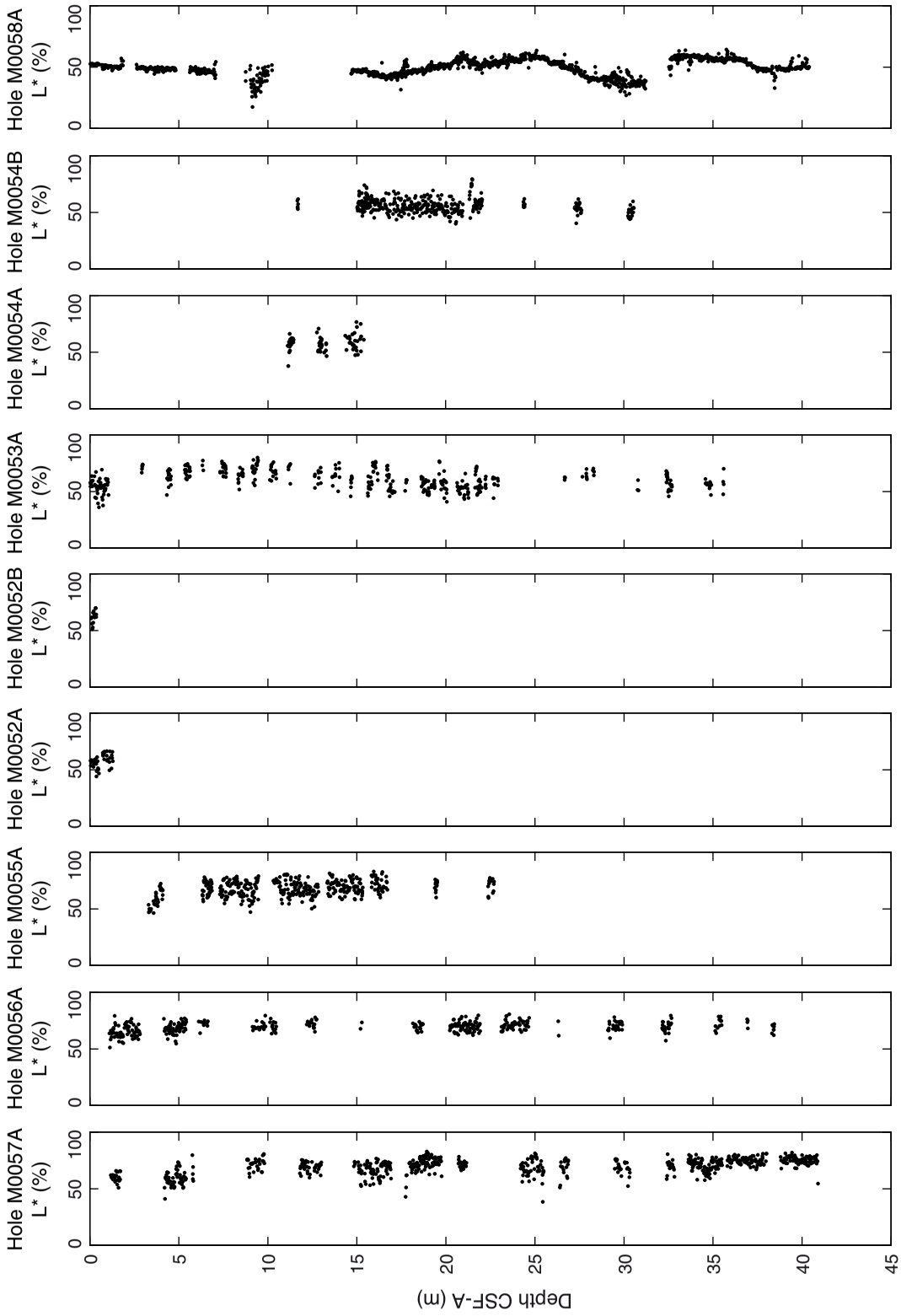

Figure F159. Color reflectance (L*) for all transect NOG-01B holes in order from shallow water to deep water (left to right).

Figure F160. Chemical components in interstitial water samples collected from Hole M0058A.

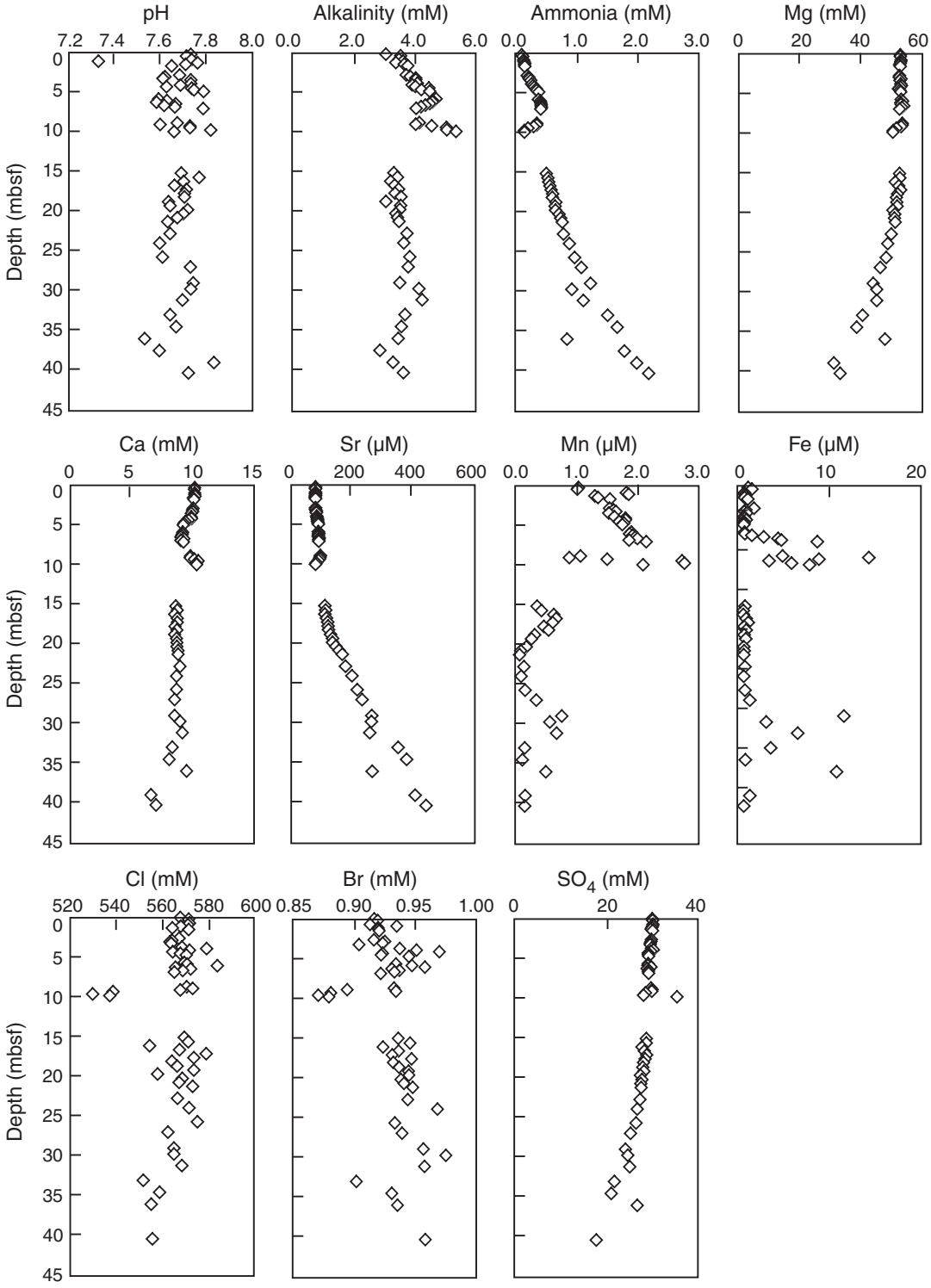

Figure F161. Composition-depth profiles of mineral content in sediments from Hole M0058A. Horizontal gray bars denote discrete coarse-grained units.

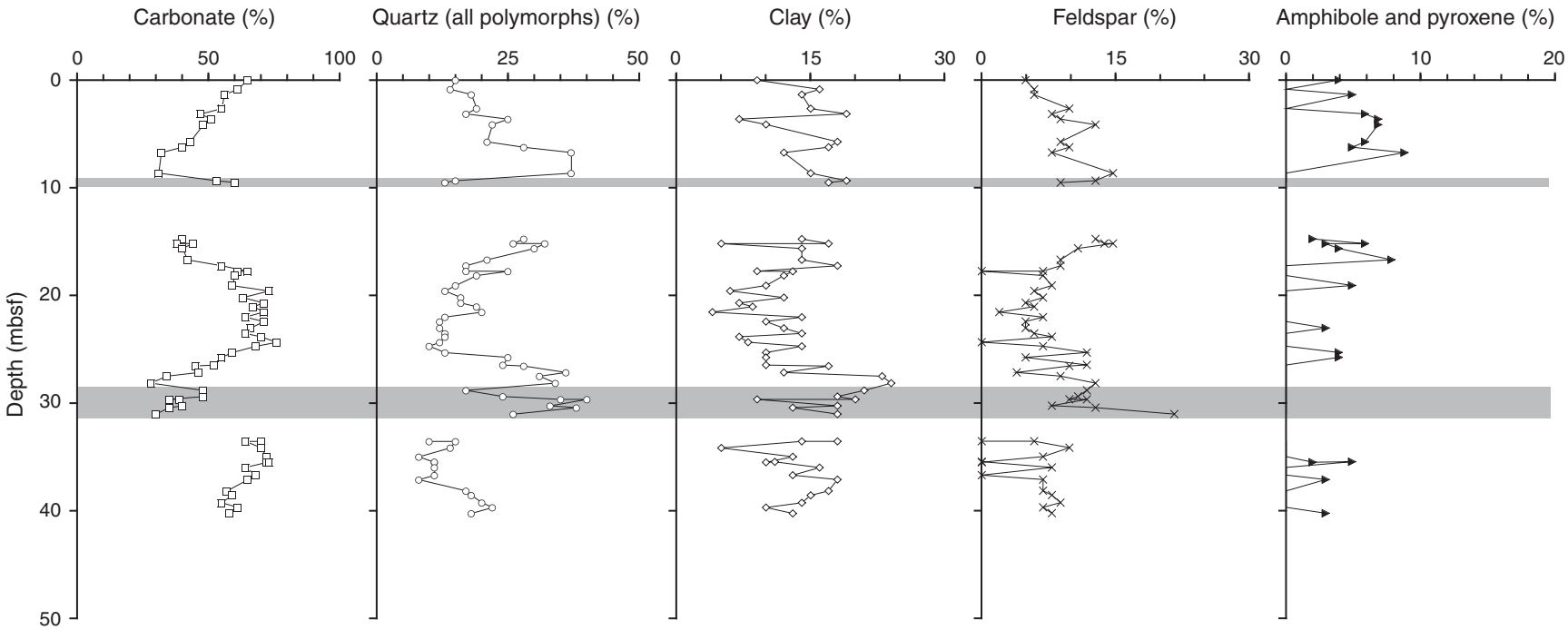

Figure F162. Depth profiles of relative abundance ratio of mineral phases in sediments from Hole M0058A. Horizontal gray bars denote discrete coarse-grained units.

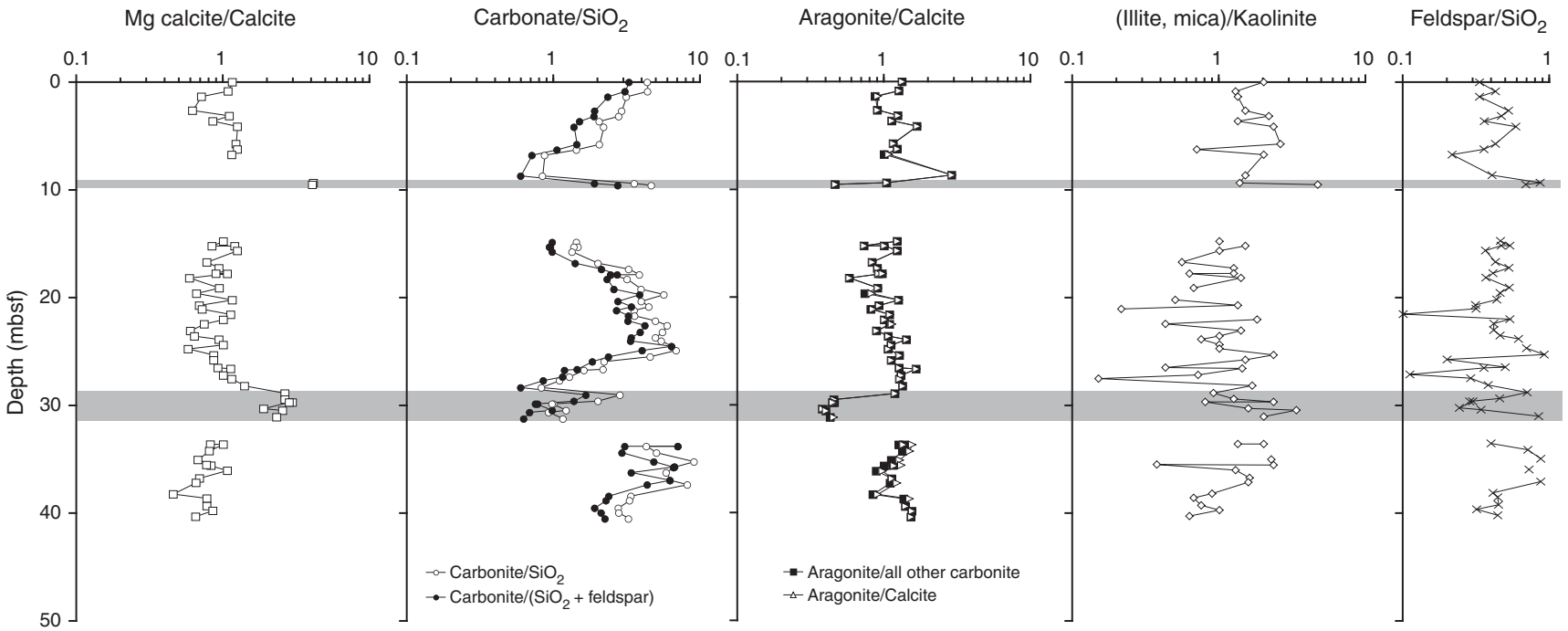

Figure F163. Depth profiles of total carbon (TC), total inorganic carbon (TIC), and total organic carbon (TOC) contents in sediments from Hole M0058A. Horizontal gray bars denote discrete coarse-grained units.

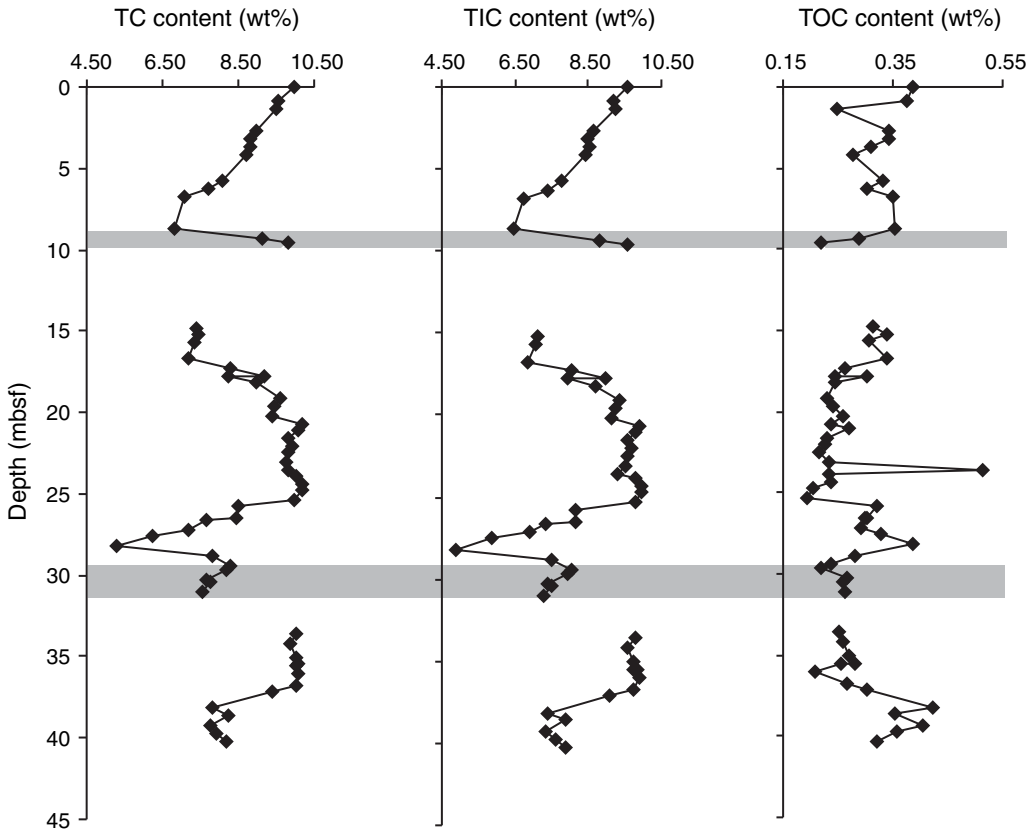

Figure F164. Composite illustrating the detail acquired by the ABI40 tool and 3D virtual borehole, transect NOG-01B. 3D Borehole = 3D borehole visualization. ABI40 traveltime image is overlain by total gamma ray (TGR). OH = open hole.

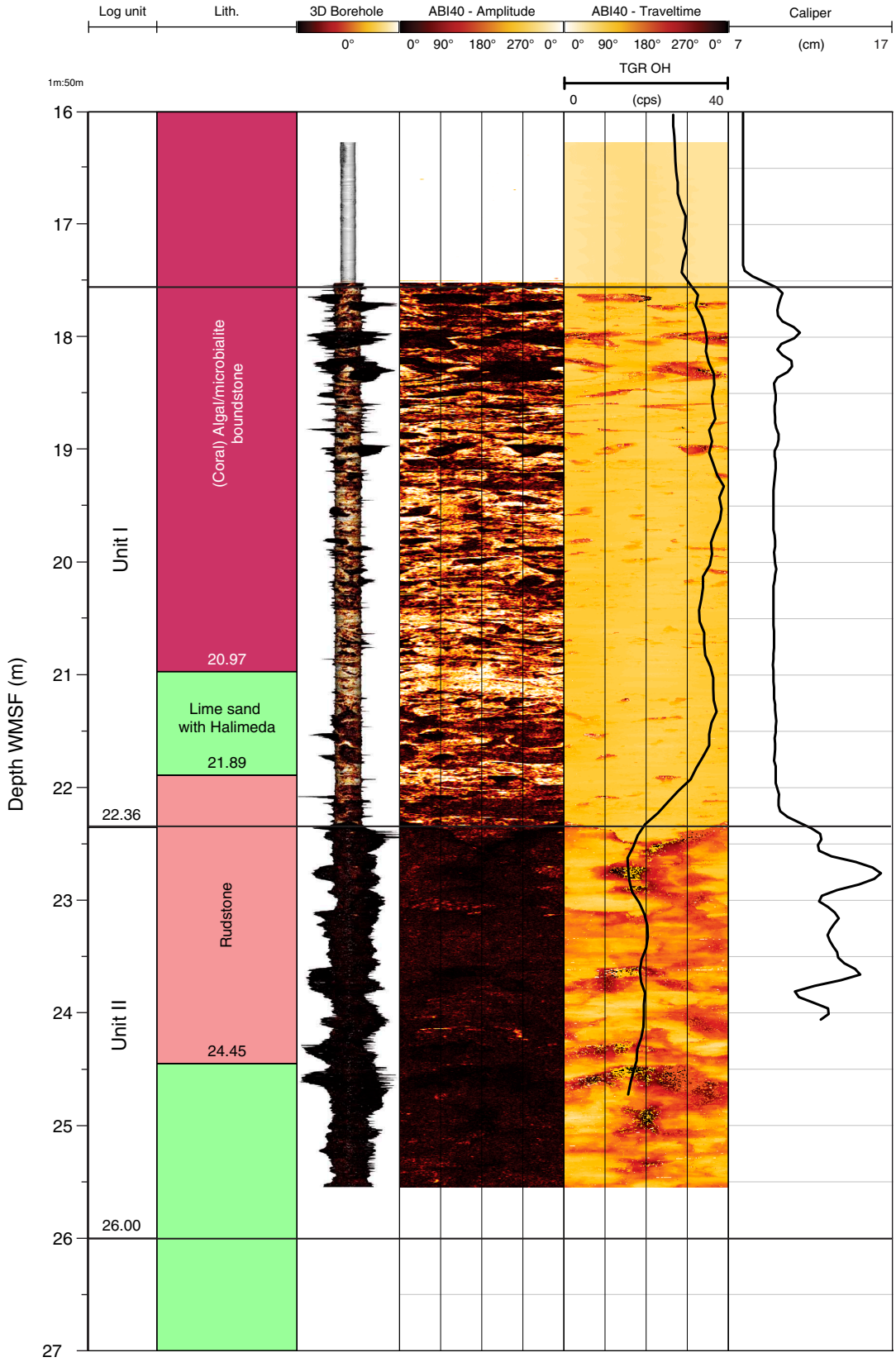

Table T1. Coring summary, transect NOG-01B. (See table note.) (Continued on next two pages.)

Core	Date (2010)	Time (UTC)	Depth (mbsf) Top	Depth (mbsf) Bottom	Length (m) Cored	Length (m) Recovered	Recovery (%)	Comments
325-M0052A-								
1X	27 Mar	0030	0	1.4	1.4	1.3	92.86	Liner crushed, bit broken. Vessel heave lifted pipe out of the hole.
325-M0052B-								
1R	27 Mar	0200	0	3	3	0.45	15.00	Hole collapses back to 1 m depth.
2R	27 Mar	0250	3	4.5	1.5	0	0.00	Weather pushing working limit.
3R	27 Mar	0340	4.5	5.4	0.9	0.01	1.11	
4R	27 Mar	0745	5.4	6.9	1.5	0	0.00	Barrel stuck. Pipe had to be recovered—bit bent.
325-M0052C-								
				*****Drilled from 0.0 to 6.9 mbsf*****				
1R	27 Mar	1020	6.9	8.4	1.5	0.1	6.67	
2R	27 Mar	1130	8.4	8.8	0.4	0	0.00	Recover barrel—bit completely sheared off.
325-M0053A-								
1X	28 Mar	0210	0	1.4	1.4	1.21	86.43	Harder after 1 m coring—three teeth chipped off EXN bit.
2R	28 Mar	0325	1.4	2.9	1.5	0.01	0.67	Occasional large swell causing bit to "bounce" slightly.
3R	28 Mar	0430	2.9	4.3	1.4	0.1	7.14	
4R	28 Mar	0515	4.3	5.3	1	0.3	30.00	
5R	28 Mar	0620	5.3	6.3	1	0.34	34.00	Bad vibration through drill string.
6R	28 Mar	0700	6.3	7.3	1	0.09	9.00	Bad vibration through drill string.
7R	28 Mar	0745	7.3	8.3	1	0.37	37.00	
8R	28 Mar	0820	8.3	9.1	0.8	0.33	41.25	
9R	28 Mar	0910	9.1	10.1	1	0.38	38.00	
10R	28 Mar	0950	10.1	11.1	1	0.39	39.00	
11R	28 Mar	1050	11.1	12.6	1.5	0.21	14.00	
12R	28 Mar	1130	12.6	13.6	1	0.4	40.00	
13R	28 Mar	1220	13.6	14.6	1	0.45	45.00	
14R	28 Mar	1300	14.6	15.6	1	0.13	13.00	
15R	28 Mar	1350	15.6	16.6	1	0.58	58.00	
16R	28 Mar	1440	16.6	17.6	1	0.54	54.00	
17R	28 Mar	1540	17.6	18.6	1	0.33	33.00	
18R	28 Mar	1630	18.6	19.6	1	0.78	78.00	
19R	28 Mar	1720	19.6	20.6	1	0.54	54.00	
20R	28 Mar	1820	20.6	21.6	1	0.67	67.00	
21R	28 Mar	1920	21.6	22.6	1	0.5	50.00	
22R	28 Mar	1955	22.6	23.6	1	0.42	42.00	
23R	28 Mar	2030	23.6	24.6	1	0.07	7.00	
24R	28 Mar	2100	24.6	25.6	1	0.12	12.00	
25R	28 Mar	2140	25.6	26.6	1	0.24	24.00	
26X	28 Mar	2215	26.6	27.6	1	0.1	10.00	
27R	28 Mar	2245	27.6	28.6	1	0.74	74.00	
28R	28 Mar	2330	28.6	29.6	1	0.14	14.00	
29R	29 Mar	0000	29.6	30.6	1	0.02	2.00	
30R	29 Mar	0030	30.6	32.3	1.7	0.35	20.59	
31R	29 Mar	0130	32.3	34.3	2	0.42	21.00	
32R	29 Mar	0210	34.3	35.3	1	0.61	61.00	
33R	29 Mar	0250	35.3	37.3	2	0.3	15.00	
325-M0054A-								
				*****Drilled from 0.0 to 9.42 mbsf*****				Drill down to set API.
1R	29 Mar	1915	9.42	11.02	1.6	0.01	0.63	Crossover sub joint popped after coring 1.5 m—switched out crossover and saver subs.
2R	29 Mar	2100	11.02	12.72	1.7	0.44	25.88	
3R	29 Mar	2140	12.72	14.22	1.5	1.2	80.00	
4R	29 Mar	2245	14.22	15.72	1.5	0.58	38.67	
5R	29 Mar	2315	15.72	17.22	1.5	0	0.00	
6R	29 Mar	2355	17.22	18.72	1.5	0	0.00	
325-M0054B-								
				*****Drilled from 0.0 to 5.36 mbsf*****				Reenter same location.
1W	30 Mar	0915	5.36	8.4	3.04	0.07	2.30	Infill due to tripping HQ pipe in Hole M0054A.
2W	30 Mar	1000	8.4	11.6	3.2	0	0.00	Infill due to tripping HQ pipe in Hole M0054A.
3R	30 Mar	1045	11.6	15	3.4	0.11	3.24	Fresh material cored in last 1 m of this run
4R	30 Mar	1130	15	15.4	0.4	0.56	140.00	Excessive mud pressure stopped run—due to picking up core from previous run?
5R	30 Mar	1150	15.4	15.5	0.1	0.18	180.00	Short run, high pressure and bit blocked. Assumed due to rapid heave being too quick for compensators to react, causing core to twist off.
6R	30 Mar	1250	15.5	17	1.5	1.4	93.33	
7R	30 Mar	1320	17	18.2	1.2	1.17	97.50	
8R	30 Mar	1510	18.2	21.2	3	2.77	92.33	

Table T1 (continued). (Continued on next page.)

Core	Date (2010)	Time (UTC)	Depth (mbsf) Top	Depth (mbsf) Bottom	Length (m) Cored	Length (m) Recovered	Recovery (%)	Comments
9R	30 Mar	1600	21.2	24.2	3	0.77	25.67	
10R	30 Mar	1650	24.2	27.2	3	0.25	8.33	
11R	30 Mar	1750	27.2	30.2	3	0.59	19.67	
12R	30 Mar	1910	30.2	33.2	3	0.38	12.67	
325-M0055A-								
				*****Drilled from 0.0 to 3.29 mbsf*****				Wash down to set API.
1R	1 Apr	2015	3.29	6.29	3	0.82	27.33	
2R	1 Apr	2045	6.29	7.29	1	0.6	60.00	
3R	1 Apr	2215	7.29	10.29	3	2.22	74.00	
4R	1 Apr	2340	10.29	13.29	3	2.58	86.00	
5R	2 Apr	0120	13.29	16.29	3	2.04	68.00	
6R	2 Apr	0220	15.79	19.29	3.5	0.95	27.14	Top 0.5 m is infill due to hole collapse.
7R	2 Apr	0300	19.29	22.29	3	0.25	8.33	
8R	2 Apr	0400	22.29	25.29	3	0.43	14.33	
9R	2 Apr	0450	25.29	28.29	3	0	0.00	
10R	2 Apr	0540	28.29	31.29	3	0.11	3.67	
325-M0056A-								
				*****Drilled from 0.0 to 1.09 mbsf*****				Wash down to set API.
1R	2 Apr	1450	1.09	4.09	3	1.79	59.67	
2R	2 Apr	1600	4.09	6.09	2	1.5	75.00	
3R	2 Apr	1700	6.09	9.09	3	0.56	18.67	
4R	2 Apr	1800	9.09	12.09	3	1.41	47.00	
5R	2 Apr	1915	12.09	15.09	3	0.69	23.00	
6R	2 Apr	2000	15.09	18.09	3	0.25	8.33	
7R	2 Apr	2050	18.09	20.09	2	0.67	33.50	Replace API-HQ crossover and saver sub as weld failed after run.
8R	2 Apr	2250	20.09	23.09	3	1.86	62.00	
9R	2 Apr	2350	23.09	26.09	3	1.62	54.00	
10R	3 Apr	0050	26.09	29.09	3	0.26	8.67	
11R	3 Apr	0140	29.09	30.59	1.5	0.84	56.00	
12R	3 Apr	0230	30.59	32.09	1.5	0	0.00	
13R	3 Apr	0345	32.09	35.09	3	0.61	20.33	
14R	3 Apr	0425	35.09	36.89	1.8	0.42	23.33	
15R	3 Apr	0505	36.89	38.29	1.4	0.09	6.43	
16R	3 Apr	0620	38.29	41.29	3	0.16	5.33	
325-M0057A-								
				*****Drilled from 0.0 to 1.18 mbsf*****				Wash down to set API.
1R	3 Apr	1545	1.18	4.18	3	0.56	18.67	
2R	3 Apr	1645	4.18	5.68	1.5	1.25	83.33	
3R	3 Apr	1715	5.68	8.68	3	0.16	5.33	Hole collapsing—required pumping after the run.
4R	3 Apr	1900	8.68	11.68	3	1.14	38.00	
5R	3 Apr	1950	11.68	14.68	3	1.34	44.67	
6R	3 Apr	2100	14.68	17.68	3	2.28	76.00	
7R	3 Apr	2230	17.68	20.68	3	2.12	70.67	
8R	3 Apr	2350	20.68	23.18	2.5	0.51	20.40	Run stopped after 2.5 m because of twist off between top pipe and crossover sub.
9R	4 Apr	0140	23.18	24.18	1	0	0.00	
10R	4 Apr	0255	24.18	26.38	2.2	1.33	60.45	
11R	4 Apr	0340	26.38	29.38	3	0.54	18.00	
12R	4 Apr	0425	29.38	32.38	3	0.95	31.67	Mud leak at crossover sub. Requires pipe trip of three rods after run. Partial hole collapse during repair necessitates open hole drilling back to previous depth of 32.38 mbsf.
13R	4 Apr	0800	32.38	33.58	1.2	0.47	39.17	
14R	4 Apr	0930	33.58	35.78	2.2	1.95	88.64	
15R	4 Apr	1100	35.78	38.78	3	2.27	75.67	
16R	4 Apr	1230	38.78	41.78	3	2.13	71.00	
325-M0058A-								
1X	5 Apr	0230	0	2.6	2.6	1.87	71.92	Fluorescent microspheres.
2X	5 Apr	0320	2.6	5.6	3	2.27	75.67	Fluorescent microspheres—bag did not burst.
3X	5 Apr	0400	5.6	8.6	3	1.61	53.67	Fluorescent microspheres.
4X	5 Apr	0440	8.6	9.9	1.3	1.67	128.46	Fluorescent microspheres.
5R	5 Apr	0540	9.9	11.6	1.7	0	0.00	Fluorescent microspheres.
6X	5 Apr	0620	11.6	14.6	3	0.01	0.33	Fluorescent microspheres.
7X	5 Apr	0700	14.6	17.6	3	3.37	112.33	Fluorescent microspheres.
8X	5 Apr	0740	17.6	20.6	3	3.31	110.33	Fluorescent microspheres.
9X	5 Apr	0840	20.6	23.4	2.8	3.09	110.36	Fluorescent microspheres.
10X	5 Apr	0915	23.4	26.4	3	3.27	109.00	Fluorescent microspheres.
11X	5 Apr	0945	26.4	29.4	3	3.15	105.00	Fluorescent microspheres.

Table T1 (continued).

Core	Date (2010)	Time (UTC)	Depth (mbsf) Top	Depth (mbsf) Bottom	Length (m) Cored	Length (m) Recovered	Recovery (%)	Comments
12X	5 Apr	1040	29.4	32.4	3	1.88	62.67	Fluorescent microspheres.
13X	5 Apr	1320	32.4	35.4	3	3.4	113.33	Fluorescent microspheres.
14X	5 Apr	1400	35.4	38.4	3	2.96	98.67	Fluorescent microspheres.
15X	5 Apr	1515	38.4	41.4	3	2.02	67.33	Fluorescent microspheres.

Note: UTC = Universal Time Coordinated, EXN = extended nose corer, API = American Petroleum Institute.

Table T2. Physical properties summary, transect NOG-01B. (See table notes.)

Hole	Value	*P*-wave MSCL (m/s)	*P*-wave saturated discrete samples (m/s)	Magnetic susceptibility MSCL ($\times 10^{-5}$ SI)	Electrical resistivity MSCL (Ωm)	Bulk density MSCL (g/cm^3)	Bulk density discrete sample (g/cm^3)	Porosity (%)	Grain density (g/cm^3)	Thermal conductivity (W/[m·K])	L* (D65)	a* (D65)	b* (D65)	a*/b*
M0052A	Min	—	—	3.16	1.12	1.85	1.95	42	2.78	—	44.06	–1.13	5.5	–0.12
	Max	—	—	6.06	1.40	2.23	2.04	47	2.78	—	66.39	0.84	15.64	0.07
	Mean ± SD	—	—	4.63 ± 0.78	1.23 ± 0.07	2.08 ± 0.09	2.00 ± 0.06	45 ± 3	2.78 ± 0.00	—	58.00 ± 5.74	–0.37 ± 0.61	9.80 ± 2.02	–0.04 ± 0.06
M0052B	Min	—	—	1.79	0.96	1.06	1.95	48	2.80	—	51.24	–1.17	7.5	–0.13
	Max	—	—	4.32	1.49	1.98	1.95	48	2.80	—	69.91	1.94	14.76	0.13
	Mean ± SD	—	—	2.87 ± 0.81	1.20 ± 0.16	1.65 ± 0.29	—	—	—	—	61.88 ± 5.46	0.43 ± 0.76	11.20 ± 1.82	0.03 ± 0.07
M0052C	Min	—	—	—	—	—	—	—	—	—	73.61	0.56	11.94	0.05
	Max	—	—	—	—	—	—	—	—	—	75.14	0.61	13.12	0.05
	Mean ± SD	—	—	—	—	—	—	—	—	—	74.38 ± 1.08	0.59 ± 0.04	12.53 ± 0.83	0.05 ± 0.00
M0053A	Min	1525	3434	–1.64	0.52	1.01	1.94	21	2.72	0.94	35.96	–0.77	2.12	–0.23
	Max	1830	3973	69.26	31.28	2.34	2.38	48	2.80	1.15	79.95	2.89	21.18	0.27
	Mean ± SD	1616 ± 91	3646 ± 246	5.47 ± 7.09	2.97 ± 4.43	1.86 ± 0.30	2.17 ± 0.13	34 ± 8	2.76 ± 0.03	1.05 ± 0.11	60.57 ± 8.61	0.62 ± 0.65	10.86 ± 3.86	0.05 ± 0.06
M0054A	Min	—	2994	0.21	0.93	1.01	2.22	20	2.76	1.055	39.63	–0.21	5.64	–0.03
	Max	—	3890	43.95	66.18	2.22	2.42	35	2.85	1.055	77.13	2.04	15.05	0.14
	Mean ± SD	—	3442 ± 634	4.79 ± 4.94	10.87 ± 11.94	1.65 ± 0.33	2.32 ± 0.14	27 ± 10	2.80 ± 0.06	—	59.20 ± 6.59	0.65 ± 0.43	10.22 ± 2.01	0.06 ± 0.04
M0054B	Min	1502	3538	–1.09	0.56	1.02	1.91	25	2.74	—	40.12	–0.79	3.26	–0.14
	Max	1678	4093	22.91	25.28	2.37	2.34	49	2.82	—	79.36	3.5	19.61	0.36
	Mean ± SD	1570 ± 62	3770 ± 234	9.39 ± 6.03	7.22 ± 5.21	1.94 ± 0.31	2.15 ± 0.17	38 ± 10	2.78 ± 0.03	—	55.93 ± 6.19	0.70 ± 0.62	10.34 ± 2.88	0.06 ± 0.05
M0055A	Min	1510	3591	–0.84	0.33	1.00	1.95	13	2.66	—	46.36	–0.5	4.37	–0.05
	Max	1647	4256	395.32	77.41	2.41	2.44	48	2.83	—	83.07	8.98	23.74	0.48
	Mean ± SD	1580 ± 47	3896 ± 255	11.30 ± 46.23	6.80 ± 7.24	1.94 ± 0.33	2.28 ± 0.14	28 ± 9	2.76 ± 0.04	—	68.22 ± 7.14	1.46 ± 1.07	13.96 ± 2.87	0.10 ± 0.06
M0056A	Min	—	3715	–1.22	0.58	1.00	2.02	18	2.68	—	51.4	–0.76	7.15	–0.07
	Max	—	4168	308.18	38.20	2.52	2.42	42	2.79	—	80.83	5.68	25.1	0.31
	Mean ± SD	—	3975 ± 233	1.55 ± 11.49	4.66 ± 4.31	1.78 ± 0.37	2.21 ± 0.14	31 ± 8	2.73 ± 0.04	—	69.32 ± 4.79	1.61 ± 0.95	15.45 ± 3.02	1.10 ± 0.05
M0057A	Min	—	3022	–1.27	0.87	1.00	2.08	14	2.67	—	38.56	–1.98	5.3	–0.21
	Max	—	5322	27.09	28.91	2.38	2.49	39	2.90	—	83.03	12.05	27.87	0.58
	Mean ± SD	—	3782 ± 718	0.32 ± 2.52	3.52 ± 2.98	1.77 ± 0.34	2.23 ± 0.14	30 ± 8	2.75 ± 0.06	—	69.84 ± 7.12	1.14 ± 1.44	13.97 ± 3.36	0.07 ± 0.09
M0058A	Min	1504	1508	–0.22	0.50	1.60	1.57	6	2.70	0.97	17.46	–4.04	1.1	–0.73
	Max	1739	2281	52.74	1.68	2.32	2.62	68	3.73	1.24	64.48	0.63	13.99	0.25
	Mean ± SD	1574 ± 40	1729 ± 150	7.80 ± 8.74	0.68 ± 0.08	1.92 ± 0.09	1.86 ± 0.18	52 ± 11	2.77 ± 0.18	1.10 ± 0.05	49.56 ± 6.46	–2.87 ± 0.96	8.38 ± 1.62	–0.35 ± 0.13

Notes: MSCL = multisensor core logger. SD = standard deviation. — = no measurement taken. In Hole M0058A for the *P*-wave velocity values only initial values were used. Calculation of the mean discounted the one anomalous value, as described in the text.

Table T3. Larger foraminifera observed in cores from transect NOG-01B. (**See table note.**)

Core, section, interval (cm)	Abundance	Preservation	*Alveolinella*	*Amphistegina*	*Baculogypsina*	*Calcarina*	*Cycloclypeus*	Elphidiidae	*Gypsina*	*Heterostegina*	*Homotrema*	*Lenticulina*	*Marginopora*	Miliolida	*Operculina*	*Planorbulinella*	*Planostegina*	Rotallida	Soritinae	*Sphaerogypsina*	Textulariida
325-																					
M0052A-1X-2, 30–35	C	Good	×	×																	
M0052B-1R-1, 10–15	C	Good	×	×																×	
M0053A-1X-1, 60–65	C	Good	×	×						×									×		
M0053A-24R-CC, 6–11	R	Good/fragmented		×							×										
M0053A-27R-1, 40–45	R	Good/fragmented		×																	
M0053A-30R-1, 15–20	A	Abraded/fragmented/stained		×	×	×									×						
M0053A-32R-1, 20–25	C	Fragmented		×	×			×							×						
M0053A-33R-CC, 5–10	C	Fragmented	×	×	×										×						
M0054B-9R-1, 45–50	R	Good		×																	
M0054B-12R-1, 10–15	C	Fragmented		×		×									×						
M0055A-1R-1, 10–15	Ab																				
M0057A-5R-1, 70–75	Ab																				
M0057A-6R-1, 130–135	Ab																				

Note: Abundance: A = abundant, C = common, R = rare, Ab = absent.

Table T4. Geochemical data relating to interstitial water collected from transect NOG-01B. This table is available in an **oversized format.**

Table T5. Mineralogy of nonclay components based on Highscore analysis I/I_c, Hole M0058A. (**Continued on next page.**)

Core, section, interval (cm)	Top depth (mbsf)	Carbonates (wt%)					SiO_2 (wt%)			Feldspars (wt%)			Evaporites (wt%)		
		Aragonite	Calcite	Mg calcite		Minor carbonates	Quartz	Tridymite	Cristobalite	Albite	Other feldspars		Gypsum	Halite	Koninckite
325-M0058A-															
1X-1, 4–5	0.04	37	13	15			15			5				2	
1X-2, 22–23	0.89	34	13	14			14				6	Anorthite	2	2	
1X-2, 72–73	1.39	26	17	12	1	Siderite	17		1	6				1	
2X-1, 8–9	2.68	26	18	11			19				10	Anorthite	1		
2X-1, 58–59	3.18	26	10	11			17			8				2	
2X-2, 7–8	3.66	27	13	11			24		1	9				2	
2X-2, 58–59	4.17	30	8	10			22			13					
3X-1, 17–18	5.77	23	9	11			20		1	9				2	
3X-1, 67–68	6.27	22	8	10			28			10					
3X-1, 117–118	6.77	16	7	8	1	Siderite	37			8				1	
4X-1, 8–9	8.68	23	8				35	2		10	5	K-feldspar		2	
4X-1, 78–79	9.38	27	5	21			15			6	7	K-feldspar			
4X-1, 95–96	9.55	19	8	33			13			9					
7X-1, 19–20	14.79	22	9	9			28			13			2	1	
7X-1, 62–63	15.22	16	12	10			26			13	1	K-feldspar			
7X-1, 62–63	15.22	22	10	12			32			15				2	
7X-2, 7–8	15.67	22	8	10			30			11				1	
7X-3, 34–35	16.73	19	13	10			21			9				2	
7X-3, 89–90	17.28	26	15	14			16		1	9				2	
7X-3, 139–140	17.78	31	18	16			16		1	7				2	
8X-1, 19–20	17.79	30	15	16			25								
8X-1, 59–60	18.19	22	24	14			14	4	1	7				2	
8X-2, 48–49	19.12	28	16	15			15			8				2	
8X-2, 98–99	19.62	31	23	15	4	Eitelite	13			6				2	
8X-3, 48–49	20.23	35	13	15			16			7				2	
8X-3, 98–99	20.73	34	22	15			15		1	5				2	
9X-1, 48–49	21.08	30	21	15	1	Kutnohorite	19			6				2	
9X-1, 98–99	21.58	37	16	18			20			2				2	
9X-2, 38–39	22.05	32	16	16			13			7				2	
9X-2, 79–80	22.46	37	19	14	1	Kutnohorite	12			5				2	
9X-3, 48–49	23.07	31	22	13			12			5				2	
9X-3, 98–99	23.57	33	19	12			10	3		6				2	
10X-1, 48–49	23.88	41	15	14			11		2	8				2	
10X-1, 98–99	24.38	40	18	18			12							2	
10X-2, 12–13	24.75	35	21	12			9		1	7				2	
10X-3, 23–24	25.34	33	14	12			13			12				2	
10X-3, 68–69	25.79	29	14	12			24		1	5				2	
10X-3, 139–140	26.5	29	12	11			23		1		12	Anorthite		2	
11X-1, 19–20	26.59	28	8	9			28			10				1	
11X-1, 79–80	27.19	26	10	10			35		1		4	K-feldspar		1	
11X-2, 14–15	27.53	19	7	8			31			9			2		
11X-2, 79–80	28.18	16	5	7			34			13				1	
11X-3, 49–50	28.86	26	6	16			17			12				1	
11X-3, 105–106	29.42	15	9	24			24			11					
12X-1, 29–30	29.69	11	6	18			35			10					
12X-1, 29–30	29.69	12	7	20			40			12					
12X-1, 89–90	30.29	11	10	19			33			8					
12X-2, 14–15	30.46	10	7	18			38			10	3	K-feldspar			
12X-2, 74–75	31.06	9	6	14	1	Ankerite	26			10	12	K-feldspar			4

Table T5 (continued).

Core, section, interval (cm)	Top depth (mbsf)	Carbonates (wt%)					SiO_2 (wt%)			Feldspars (wt%)			Evaporites (wt%)		
		Aragonite	Calcite	Mg calcite		Minor carbonates	Quartz	Tridymite	Cristobalite	Albite	Other feldspars		Gypsum	Halite	Koninckite
13X-1, 119–120	33.59	39	16	13	2	Ankerite	10							2	
13X-1, 119–120	33.59	37	12	12	3	Ankerite	14		1	6					
13X-2, 29–30	34.19	40	15	12	3	Kutnohorite	13		1	10				2	
13X-2, 112–113	35.02	38	18	12	4	Ankerite	8			7					
13X-3, 14–15	35.54	36	17	14	2, 3	Ankerite, kutnohorite	11							2	
14X-1, 9–10	35.49	39	17	13	3, 1	Kutnohorite, otavite	9		2						
14X-1, 62–63	36.02	30	15	16	3	Kutnohorite	11			8				2	
14X-1, 133–134	36.73	36	19	13			11							2	
14X-2, 24–25	37.14	34	17	11	3	Kutnohorite	8				7	Anorthite			
14X-2, 129–130	38.19	26	20	9	2	Vaterite	17			7				1	
15X-1, 19–20	38.59	34	13	10	2	Kutnohorite	18				8	Anorthite			
15X-1, 89–90	39.29	32	13	10			20			9			1		
15X-2, 14–15	39.72	37	13	11			21		1	7					
15X-2, 69–70	40.27	35	14	9			17		1	8					

Table T6. Mineralogy of clay groups based on Highscore analysis of I/I_C, Hole M0058A.

Core, section, interval (cm)	Top depth (mbsf)	Muscovite (wt%)	Muscovite/ Illite group clays (wt%)		Kaolinite (wt%)	Kaolin group clays (wt%)		Amphiboles + pyroxenes (wt%)		Other minerals (wt%)	
325-M0058A-											
1X-1, 4–5	0.04	6			3			4	Amphibole	1	Grimaldiite
1X-2, 22–23	0.89		9	Illite	7						
1X-2, 72–73	1.39	8			6			5	Amphibole	1	Rutile
2X-1, 8–9	2.68	9			6						
2X-1, 58–59	3.18		13	Illite	6			6	Amphibole		
2X-2, 7–8	3.66	4			3			7	Amphibole		
2X-2, 58–59	4.17	7			3			7	Amphibole		
3X-1, 17–18	5.77		13	Illite	5			6	Amphibole	1	Almandine
3X-1, 67–68	6.27	7			5	5	Dickite	5	Amphibole		
3X-1, 117–118	6.77	8			4			9	Amphibole		
4X-1, 8–9	8.68	9			6						
4X-1, 78–79	9.38	11			8						
4X-1, 95–96	9.55	14			3					1	Rutile
7X-1, 19–20	14.79	7			7			2	Amphibole		
7X-1, 62–63	15.22				5	12	Halloysite	6	Amphibole		
7X-1, 62–63	15.22					2	Nacrite	3	Amphibole		
7X-2, 7–8	15.67	7	3	Glauconite	7			4	Amphibole		
7X-3, 34–35	16.73	5			7	2	Clinochrysotile	8	Cordierite	3	Clinoptilolite (zeolite)
7X-3, 89–90	17.28	10			8						
7X-3, 139–140	17.78		5	Glauconite	4						
8X-1, 19–20	17.79	5			8						
8X-1, 59–60	18.19		7	Lepidolite	5						
8X-2, 48–49	19.12	4			6			5	Pyroxene		
8X-2, 98–99	19.62				6						
8X-3, 48–49	20.23	4			8						
8X-3, 98–99	20.73	4			3						
9X-1, 48–49	21.08		1.5	Illite	7						
9X-1, 98–99	21.58				4					1	Anatase
9X-2, 38–39	22.05	9				5	Nacrite				
9X-2, 79–80	22.46	3			7					1	Pyrolusite
9X-3, 48–49	23.07		7	Illite	5			3	Amphibole		
9X-3, 98–99	23.57	7			7						
10X-1, 48–49	23.88	3			4						
10X-1, 98–99	24.38	4			4					2	Jackobsite
10X-2, 12–13	24.75	7			7						
10X-3, 23–24	25.34	7			3			4	Pyroxene		
10X-3, 68–69	25.79	6			4			4	Pyroxene		
10X-3, 139–140	26.5	3			7						
11X-1, 19–20	26.59		10	Zinnwaldite	7						
11X-1, 79–80	27.19	5			7						
11X-2, 14–15	27.53				7	13	Halloysite				
11X-2, 79–80	28.18	15			9						
11X-3, 49–50	28.86		10	Taeniolite	11						
11X-3, 105–106	29.42	10			8						
12X-1, 29–30	29.69	8	6	Glauconite	6						
12X-1, 29–30	29.69		4	Lepidolite	5						
12X-1, 89–90	30.29	11			7						
12X-2, 14–15	30.46	10				3	Nacrite				
12X-2, 74–75	31.06	12			6						
13X-1, 119–120	33.59		9, 3	Illite, talc	6						
13X-1, 119–120	33.59	8			6					2	Titanomagnetite
13X-2, 29–30	34.19				3	2	Dickite				
13X-2, 112–113	35.02		9	Illite	4						
13X-3, 14–15	35.54	7			3			2	Amphibole	3	Zircon
14X-1, 9–10	35.49	3			8			5	Pyroxene		
14X-1, 62–63	36.02	9			7						
14X-1, 133–134	36.73	8				5	Nacrite			6	Heulandite (zeolite)
14X-2, 24–25	37.14	11			7			3	Amphibole		
14X-2, 129–130	38.19	8			7	2	Lizardite				
15X-1, 19–20	38.59	5	1	Bementite	9						
15X-1, 89–90	39.29	6			8						
15X-2, 14–15	39.72		5	Glauconite		5	Nacrite				
15X-2, 69–70	40.27		5	Phlogopite	8			3	Amphibole		

Table T7. Mineral group weight percents, Hole M0058A. (**Continued on next page.**)

Core, section, interval (cm)	Top depth (mbsf)	Combined mineral groups (wt%)						Ratios of wt% mineral and mineral groups						
		Carbonates	All SiO_2	All feldspars	All clays	(Illite, mica)	Kaolinite	Mg calcite/ Calcite	Carbonates/ SiO_2	Carbonates/ Feldspar + SiO_2	Aragonite/Other carbonates	Aragonite/ Both calcites	(Illite, mica)/ Kaolinite	Feldspars/ SiO_2
325-M0058A-														
1X-1, 4–5	0.04	65	15	5	9	6	3	1.15	4.33	3.25	1.32	1.32	2.00	0.33
1X-2, 22–23	0.89	61	14	6	16	9	7	1.08	4.36	3.05	1.26	1.26	1.29	0.43
1X-2, 72–73	1.39	56	18	6	14	8	6	0.71	3.11	2.33	0.87	0.90	1.33	0.33
2X-1, 8–9	2.68	55	19	10	15	9	6	0.61	2.89	1.90	0.90	0.90	1.50	0.53
2X-1, 58–59	3.18	47	17	8	19	13	6	1.10	2.76	1.88	1.24	1.24	2.17	0.47
2X-2, 7–8	3.66	51	25	9	7	4	3	0.85	2.04	1.50	1.13	1.13	1.33	0.36
2X-2, 58–59	4.17	48	22	13	10	7	3	1.25	2.18	1.37	1.67	1.67	2.33	0.59
3X-1, 17–18	5.77	43	21	9	18	13	5	1.22	2.05	1.43	1.15	1.15	2.60	0.43
3X-1, 67–68	6.27	40	28	10	17	7	10	1.25	1.43	1.05	1.22	1.22	0.70	0.36
3X-1, 117–118	6.77	32	37	8	12	8	4	1.14	0.86	0.71	1.00	1.07	2.00	0.22
4X-1, 8–9	8.68	31	37	15	15	9	6		0.84	0.60	2.88	2.88	1.50	0.41
4X-1, 78–79	9.38	53	15	13	19	11	8	4.20	3.53	1.89	1.04	1.04	1.38	0.87
4X-1, 95–96	9.55	60	13	9	17	14	3	4.13	4.62	2.73	0.46	0.46	4.67	0.69
7X-1, 19–20	14.79	40	28	13	14	7	7	1.00	1.43	0.98	1.22	1.22	1.00	0.46
7X-1, 62–63	15.22	38	26	14	17	0	17	0.83	1.46	0.95	0.73	0.73	0.00	0.54
7X-1, 62–63	15.22	44	32	15	5	3	2	1.20	1.38	0.94	1.00	1.00	1.50	0.47
7X-2, 7–8	15.67	40	30	11	14	7	7	1.25	1.33	0.98	1.22	1.22	1.00	0.37
7X-3, 34–35	16.73	42	21	9	14	5	9	0.77	2.00	1.40	0.83	0.83	0.56	0.43
7X-3, 89–90	17.28	55	17	9	18	10	8	0.93	3.24	2.12	0.90	0.90	1.25	0.53
7X-3, 139–140	17.78	65	17	7	9	5	4	0.89	3.82	2.71	0.91	0.91	1.25	0.41
8X-1, 19–20	17.79	61	25	0	13	5	8	1.07	2.44	2.44	0.97	0.97	0.63	0.00
8X-1, 59–60	18.19	60	19	7	12	7	5	0.58	3.16	2.31	0.58	0.58	1.40	0.37
8X-2, 48–49	19.12	59	15	8	10	4	6	0.94	3.93	2.57	0.90	0.90	0.67	0.53
8X-2, 98–99	19.62	73	13	6	6	0	6	0.65	5.62	3.84	0.74	0.82	0.00	0.46
8X-3, 48–49	20.23	63	16	7	12	4	8	1.15	3.94	2.74	1.25	1.25	0.50	0.44
8X-3, 98–99	20.73	71	16	5	7	4	3	0.68	4.44	3.38	0.92	0.92	1.33	0.31
9X-1, 48–49	21.08	67	19	6	8.5	1.5	7	0.71	3.53	2.68	0.81	0.83	0.21	0.32
9X-1, 98–99	21.58	71	20	2	4	0	4	1.13	3.55	3.23	1.09	1.09	0.00	0.10
9X-2, 38–39	22.05	64	13	7	14	9	5	1.00	4.92	3.20	1.00	1.00	1.80	0.54
9X-2, 79–80	22.46	71	12	5	10	3	7	0.74	5.92	4.18	1.09	1.12	0.43	0.42
9X-3, 48–49	23.07	66	12	5	12	7	5	0.59	5.50	3.88	0.89	0.89	1.40	0.42
9X-3, 98–99	23.57	64	13	6	14	7	7	0.63	4.92	3.37	1.06	1.06	1.00	0.46
10X-1, 48–49	23.88	70	13	8	7	3	4	0.93	5.38	3.33	1.41	1.41	0.75	0.62
10X-1, 98–99	24.38	76	12	0	8	4	4	1.00	6.33	6.33	1.11	1.11	1.00	0.00
10X-2, 12–13	24.75	68	10	7	14	7	7	0.57	6.80	4.00	1.06	1.06	1.00	0.70
10X-3, 23–24	25.34	59	13	12	10	7	3	0.86	4.54	2.36	1.27	1.27	2.33	0.92
10X-3, 68–69	25.79	55	25	5	10	6	4	0.86	2.20	1.83	1.12	1.12	1.50	0.20
10X-3, 139–140	26.50	52	24	12	10	3	7	0.92	2.17	1.44	1.26	1.26	0.43	0.50
11X-1, 19–20	26.59	45	28	10	17	10	7	1.13	1.61	1.18	1.65	1.65	1.43	0.36
11X-1, 79–80	27.19	46	36	4	12	5	7	1.00	1.28	1.15	1.30	1.30	0.71	0.11
11X-2, 14–15	27.53	34	31	9	23	3	20	1.14	1.10	0.85	1.27	1.27	0.15	0.29
11X-2, 79–80	28.18	28	34	13	24	15	9	1.40	0.82	0.60	1.33	1.33	1.67	0.38
11X-3, 49–50	28.86	48	17	12	21	10	11	2.67	2.82	1.66	1.18	1.18	0.91	0.71
11X-3, 105–106	29.42	48	24	11	18	10	8	2.67	2.00	1.37	0.45	0.45	1.25	0.46
12X-1, 29–30	29.69	35	35	10	20	14	6	3.00	1.00	0.78	0.46	0.46	2.33	0.29
12X-1, 29–30	29.69	39	40	12	9	4	5	2.86	0.98	0.75	0.44	0.44	0.80	0.30
12X-1, 89–90	30.29	40	33	8	18	11	7	1.90	1.21	0.98	0.38	0.38	1.57	0.24
12X-2, 14–15	30.46	35	38	13	13	10	3	2.57	0.92	0.69	0.40	0.40	3.33	0.34
12X-2, 74–75	31.06	30	26	22	18	12	6	2.33	1.15	0.63	0.43	0.45	2.00	0.85

Table T7 (continued).

Core, section, interval (cm)	Top depth (mbsf)	Combined mineral groups (wt%)						Ratios of wt% mineral and mineral groups						
		Carbonates	All SiO_2	All feldspars	All clays	(Illite, mica)	Kaolinite	Mg calcite/ Calcite	Carbonates/ SiO_2	Carbonates/ Feldspar + SiO_2	Aragonite/Other carbonates	Aragonite/ Both calcites	(Illite, mica)/ Kaolinite	Feldspars/ SiO_2
13X-1, 119–120	33.59	70	10	0	18	12	6	0.81	7.00	7.00	1.26	1.34	2.00	0.00
13X-1, 119–120	33.59	64	15	6	14	8	6	1.00	4.27	3.05	1.37	1.54	1.33	0.40
13X-2, 29–30	34.19	70	14	10	5	0	5	0.80	5.00	2.92	1.33	1.48	0.00	0.71
13X-2, 112–113	35.02	72	8	7	13	9	4	0.67	9.00	4.80	1.12	1.27	2.25	0.88
13X-3, 14–15	35.54	72	11	0	10	7	3	0.82	6.55	6.55	1.00	1.16	2.33	0.00
14X-1, 9–10	35.49	73	11	0	11	3	8	0.76	6.64	6.64	1.15	1.30	0.38	0.00
14X-1, 62–63	36.02	64	11	8	16	9	7	1.07	5.82	3.37	0.88	0.97	1.29	0.73
14X-1, 133–134	36.73	68	11	0	13	8	5	0.68	6.18	6.18	1.13	1.13	1.60	0.00
14X-2, 24–25	37.14	65	8	7	18	11	7	0.65	8.13	4.33	1.10	1.21	1.57	0.88
14X-2, 129–130	38.19	57	17	7	17	8	9	0.45	3.35	2.38	0.84	0.90	0.89	0.41
15X-1, 19–20	38.59	59	18	8	15	6	9	0.77	3.28	2.27	1.36	1.48	0.67	0.44
15X-1, 89–90	39.29	55	20	9	14	6	8	0.77	2.75	1.90	1.39	1.39	0.75	0.45
15X-2, 14–15	39.72	61	22	7	10	5	5	0.85	2.77	2.10	1.54	1.54	1.00	0.32
15X-2, 69–70	40.27	58	18	8	13	5	8	0.64	3.22	2.23	1.52	1.52	0.63	0.44

Table T8. Total carbon, Hole M0058A. (See table notes.)

Core, section, interval (cm)	Sample ID (DIS)	Sample ID (Analysis)	TC (wt%)	TOC (wt%)	TIC (wt%)
325-M0058A-					
1X-1, 4–5	4350293	TOC 1	9.97	0.39	9.58
1X-2, 22–23	4350366	TOC 2	9.57	0.38	9.19
1X-2, 72–73	4350372	TOC 3	9.51	0.25	9.26
2X-1, 8–9	4350433	TOC 4	9.00	0.34	8.65
2X-1, 58–59	4350435	TOC 5	8.83	0.34	8.49
2X-2, 7–8	4350514	TOC 6	8.82	0.31	8.51
2X-2, 58–59	4350516	TOC 7	8.69	0.28	8.41
3X-1, 17–18	4350558	TOC 8	8.08	0.33	7.75
3X-1, 67–68	4350560	TOC 9	7.71	0.30	7.41
3X-1, 117–118	4350562	TOC 10	7.08	0.35	6.73
4X-1, 8–9	4350616	TOC 11	6.84	0.35	6.49
4X-1, 78–79	4350627	TOC 12	9.11	0.29	8.83
4X-1, 95–96	4350630	TOC 13	9.79	0.22	9.57
7X-1, 19–20	4350670	TOC 14	7.41	0.32	7.09
7X-1, 62–63	4350672	TOC 15	7.45	0.34	7.11
7X-2, 7–8	4350786	TOC 16	7.35	0.31	7.05
7X-3, 34–35	4350905	TOC 17	7.20	0.34	6.86
7X-3, 89–90	4350930	TOC 18	8.30	0.26	8.03
7X-3, 139–140	4350937	TOC 19	9.19	0.25	8.95
8X-1, 19–20	4350991	TOC 20	8.24	0.30	7.94
8X-1, 59–60	4350999	TOC 21	8.95	0.25	8.71
8X-2, 48–49	4351119	TOC 22	9.60	0.23	9.37
8X-2, 98–99	4351121	TOC 23	9.46	0.24	9.22
8X-3, 48–49	4351226	TOC 24	9.39	0.26	9.13
8X-3, 98–99	4351225	TOC 25	10.16	0.24	9.92
9X-1, 48–49	4351230	TOC 26	10.06	0.27	9.79
9X-1, 98–99	4351229	TOC 27	9.83	0.23	9.60
9X-2, 38–39	4351258	TOC 28	9.90	0.23	9.68
9X-2, 79–80	4351260	TOC 29	9.79	0.22	9.57
9X-3, 48–49	4351288	TOC 30	9.74	0.23	9.51
9X-3, 98–99	4351290	TOC 31	9.82	0.51	9.31
10X-1, 48–49	4351296	TOC 32	10.01	0.23	9.78
10X-1, 98–99	4351297	TOC 33	10.18	0.24	9.95
10X-2, 12–13	4351321	TOC 34	10.17	0.21	9.96
10X-3, 23–24	4351423	TOC 35	9.96	0.19	9.77
10X-3, 68–69	4351426	TOC 36	8.48	0.32	8.16
10X-3, 139–140	4351427	TOC 37	8.45	0.30	8.14
11X-1, 19–29	4351474	TOC 38	7.65	0.30	7.36
11X-1, 79–80	4351475	TOC 39	7.20	0.29	6.91
11X-2, 14–15	4351542	TOC 40	6.22	0.33	5.89
11X-2, 79–80	4351544	TOC 41	5.27	0.39	4.89
11X-3, 49–50	4351613	TOC 42	7.80	0.28	7.52
11X-3, 105–106	4351620	TOC 43	8.29	0.24	8.05
12X-1, 29–30	4351691	TOC 44	8.18	0.22	7.96
12X-1, 89–90	4351693	TOC 45	7.66	0.27	7.40
12X-2, 14–15	4351754	TOC 46	7.77	0.26	7.51
12X-2, 74–75	4351765	TOC 47	7.54	0.26	7.28
13X-1, 24–25	4351823	TOC 48			
13X-1, 119–120	4351821	TOC 49	10.03	0.25	9.77
13X-2, 29–30	4351860	TOC 50	9.86	0.26	9.60
13X-2, 112–113	4351858	TOC 51	10.00	0.27	9.74
13X-3, 14–15	4351871	TOC 52	10.02	0.28	9.74
14X-1, 9–10	4351934	TOC 53	10.10	0.26	9.85
14X-1, 62–63	4351940	TOC 54	10.09	0.21	9.88
14X-1, 133–134	4351944	TOC 55	10.00	0.27	9.74
14X-2, 24–25	4351976	TOC 56	9.39	0.30	9.09
14X-2, 129–130	4351978	TOC 57	7.79	0.42	7.37
15X-1, 19–20	4352009	TOC 58	8.26	0.35	7.90
15X-1, 89–90	4352007	TOC 59	7.74	0.41	7.34
15X-2, 14–15	4352032	TOC 60	7.94	0.36	7.59
15X-2, 69–70	4352034	TOC 61	8.20	0.32	7.88

Notes: Total organic carbon (TOC) content was determined on bulk ground samples (1 g of sample) using a LECO CS-125 analyzer. The analytical precision is about ±0.02% absolute. TC = total carbon, TIC = total inorganic carbon. Not comprehensible; probably a mix-up with one of double samples XRD48 (325-M0058A-13X-1, 119–120 cm) + XRD49 (325-M0058A-13X-1, 119–120 cm) during sampling.